



**HAL**  
open science

# Influence of flowability improvement of powders on its dust generation capacity

Maria Camila Jiménez Garavito

► **To cite this version:**

Maria Camila Jiménez Garavito. Influence of flowability improvement of powders on its dust generation capacity. Chemical and Process Engineering. Université de Lorraine, 2023. English. NNT : 2023LORR0138 . tel-04513197

**HAL Id: tel-04513197**

**<https://hal.univ-lorraine.fr/tel-04513197>**

Submitted on 20 Mar 2024

**HAL** is a multi-disciplinary open access archive for the deposit and dissemination of scientific research documents, whether they are published or not. The documents may come from teaching and research institutions in France or abroad, or from public or private research centers.

L'archive ouverte pluridisciplinaire **HAL**, est destinée au dépôt et à la diffusion de documents scientifiques de niveau recherche, publiés ou non, émanant des établissements d'enseignement et de recherche français ou étrangers, des laboratoires publics ou privés.



**UNIVERSITÉ  
DE LORRAINE**

**BIBLIOTHÈQUES  
UNIVERSITAIRES**

## AVERTISSEMENT

Ce document est le fruit d'un long travail approuvé par le jury de soutenance et mis à disposition de l'ensemble de la communauté universitaire élargie.

Il est soumis à la propriété intellectuelle de l'auteur. Ceci implique une obligation de citation et de référencement lors de l'utilisation de ce document.

D'autre part, toute contrefaçon, plagiat, reproduction illicite encourt une poursuite pénale.

Contact bibliothèque : [ddoc-theses-contact@univ-lorraine.fr](mailto:ddoc-theses-contact@univ-lorraine.fr)  
*(Cette adresse ne permet pas de contacter les auteurs)*

## LIENS

Code de la Propriété Intellectuelle. articles L 122. 4

Code de la Propriété Intellectuelle. articles L 335.2- L 335.10

[http://www.cfcopies.com/V2/leg/leg\\_droi.php](http://www.cfcopies.com/V2/leg/leg_droi.php)

<http://www.culture.gouv.fr/culture/infos-pratiques/droits/protection.htm>

# THÈSE

Présentée par

**Maria Camila JIMÉNEZ GARAVITO**

pour l'obtention du grade de

**Docteur de l'Université de Lorraine**

**Spécialité : Genie des Procédés, des Produits et des Molécules**

**Influence of flowability improvement of powders on its  
dust generation capacity**

*Incidence de l'amélioration de l'écoulement d'une poudre  
sur sa capacité à générer un empoussièrment*

Thèse soutenue publiquement le 16 juin 2023 devant le jury :

**Rapporteurs :**

Diego BARLETTA

Professeur associé à l'Université de Salerne

Eberhard SCHMIDT

Professeur à l'Université de Wuppertal

**Examineurs :**

Thierry RUIZ

Professeur à l'Université de Montpellier (président)

Véronique FALK

Professeur à l'Université de Lorraine (directrice de thèse)

Maria Graciela CARES-PACHECO

MDC à l'Université de Lorraine (co-directrice de thèse)

Fabien GERARDIN

Responsable laboratoire PROCEP à l'INRS (co-encadrant de thèse)



# Acknowledgments

---

I would like to express my heartfelt gratitude to all those who have supported and guided me throughout this journey. Completing my PhD would not have been possible without their invaluable contributions and encouragement.

First, I would like to thank my advisors, Véronique FALK, Maria-Graciela CARES-PACHECO, and Fabien GERARDIN for their mentorship, patience, rigor, and commitment to my professional and personal growth. Graciela, thank you for all the countless hours you have dedicated to this work and the time we have shared together beyond the professional relationship. Véronique, thank you for your guidance, especially during times when I was stressed out; you always had the right words to make me feel better and refocused on the right path. Fabien, thanks for all the support during these three and a half years, through the ups and downs.

I am grateful to the members of my dissertation committee, Diego BARLETTA, Eberhard SCHMIDT and Thierry RUIZ, for their valuable insights, critical feedback, constructive suggestions and enriching discussion that significantly enhanced the quality of this thesis.

During my PhD, I conducted my research at the Institut National de Recherche et de Sécurité (INRS) and the Laboratoire Réactions et Génie des Procédés (LRGP), where I had the privilege to share my daily life with amazing human beings.

From INRS, I extend my gratitude to Flo, Steph M, Maxime, Hubert, Steph P, Julien, Matthieu, Audrey, Jean Pierre, and Eric for your unwavering support and smiles during challenging times. I am also thankful to Sebastian, Raph, Véro, and Olivier W who taught me all about dustiness and that helped me through the experimentation. Thanks to Olivier R and Davy which introduce me to the amazing world of electron microscopy, making me love it, passing countless hours in front of the SEM and TEM.

I would like to thank also to all the members of the LRGP, particularly the EMMAD team, for the time we spent together. A special thank you goes to Philippe for his guidance whenever needed and Maud for your good energy and technical assistant. Thanks to David for his help in constructing the free-flow instrument during the final stages of my thesis, thank you for your patience and dedication.

---

I am grateful for the laughter and memorable moments shared with the Bureau de Jeunes Chercheurs members and my LRGP friends: Diego, Felipe, Andres, Matteo, Stephanie, Margarita, Adilson, and Juan David. Special thanks to Fatima and Andrea for the countless hours we spent in our offices, talking, working, and supporting one another. I must also express my heartfelt thanks to all my friends from ENSIC: Andresito, Chechito, Juli, Boliche, Lau, Andre, Diegui, Vale, Cick, and Juan P.

To my friends who are not in Nancy, I extend a massive thank you for your support from afar (Hillary, Silvia, Pachi, Angara, Ale, Alicat, Ellen, K, Moya, Abril, Sofi S, Meli, Angela, Sofi H and Maria). Your presence, despite the distance, meant a lot to me. Special thanks to Javier for telling me about this PhD opportunity; none of this would have happened without you.

From the bottom of my heart, I want to thank my closest friends. Piñi, thank you for the endless hours of laughter, dancing, and simply being together, along with Michi. Pau, you arrived like an angel during the toughest times, thank you for the amazing meals you cooked for me. Your support was truly indispensable. I love you all.

Finalmente, muchas gracias a mis papas y a mi hermana por su apoyo y amor incondicional, este logro es de ustedes. Gracias también a toda mi familia que siempre ha estado pendiente de mi apoyándome desde lejos. Los amo.

*Maria Camila Jiménez Garavito*  
12 September, 2023

# Contents

<b>General Introduction</b>	<b>7</b>
<b>1 State of the art</b>	<b>11</b>
1. Introduction	11
2. General definitions	11
3. Powders in motion	12
4. Powder properties	14
4.1. Particle size distribution and shape	14
4.2. Particle and powder density	15
5. Interparticle interactions	15
5.1. Van der Waals forces	15
5.2. Capillary forces	16
5.3. Electrostatic forces	17
6. Flow behaviour - dense flow regime	17
6.1. Factors influencing powder flow behaviour	18
6.1.1. Particle intrinsic properties	18
6.1.2. Relative humidity	18
6.1.3. Flow additives	19
6.1.4. Temperature	19
6.2. Flowability measuring techniques	19
6.2.1. Static measures: Angle of repose	21
6.2.2. Quasi-static measures	23
6.2.2.1. Densification measures	23
6.2.2.2. Shear tests	25
6.2.3. Dynamic measures	28
6.2.3.1. Flow rate through an orifice	28
6.2.3.2. Dynamic angle of repose	29
6.2.3.3. Fluidized bed	30
7. Dustiness	31
7.1. Factors influencing powder dustiness	33
7.1.1. Particle size and shape	33
7.1.2. Relative humidity	34
7.2. Dustiness measuring methods	35
7.2.1. Dustiness methodologies development	35
7.2.2. Standard methods	36
7.2.2.1. Rotating drum (RD) - NF 15051-2	36
7.2.2.2. Continuous drop (CD) - NF 15051-3	37
7.2.2.3. Vortex shaker - NF 17199-5	40
7.2.2.4. Small rotating drum - NF 17199-4	41

8.	Flowability and dustiness: what do we know?	42
9.	Conclusions	42
<b>2</b>	<b>Materials and methods</b>	<b>45</b>
1.	Introduction	45
2.	Powders	45
2.1.	Microcrystalline cellulose	45
2.2.	Wheat flour	46
2.3.	Joint filler	46
2.4.	Glass beads	46
2.5.	Lactose	46
3.	Silica nanoparticles	47
4.	Powders mixtures and surface coverage	47
4.1.	Water activity and conditioning	50
5.	Materials physical characterisation	51
5.1.	Particles shape	51
5.2.	Particle size distribution	52
5.3.	Specific surface	53
5.4.	Pycnometric density	54
5.5.	Behaviour towards water	55
5.6.	Surface energy	56
6.	Motion characterisation techniques	57
6.1.	Flowability	57
6.1.1.	Densification	57
6.1.2.	Shear test - plastic failure	59
6.1.3.	Flow through an orifice	60
6.2.	Dustiness	61
7.	Conclusion	62
<b>3</b>	<b>Flow behavior and densification</b>	<b>65</b>
1.	Introduction	67
2.	Materials and methods	70
2.1.	Powder Materials	70
2.2.	Powders physical characterisation techniques	71
2.3.	Granular compaction devices	71
3.	Results & Discussions	74
3.1.	Physical characterisation	74
3.2.	Dynamics of compaction under free surface conditions	76
3.3.	From compressibility to flowability, an energetic approach	79
4.	Conclusions	86
5.	Host powders densification characterisation	87
<b>4</b>	<b>Surface coverage and flowability</b>	<b>91</b>
1.	Introduction	93
2.	Experimental Design: Materials and methods	96
2.1.	Factors	97
2.2.	Responses: flow characterisation in the quasi-static regime	100
2.3.	Physical powder characterisation techniques	101
3.	Results & Discussions	101
3.1.	Physical characterisation	101

3.2.	Experimental Design . . . . .	104
3.3.	Why, how and how much? . . . . .	108
4.	Conclusions . . . . .	112
5.	Annex . . . . .	114
6.	Flow factor and interparticle forces: An attempt to go further in the reflexion	116
<b>5</b>	<b>Dustiness and glidants</b>	<b>121</b>
1.	Introduction . . . . .	122
2.	Materials and methods . . . . .	126
2.1.	Materials . . . . .	126
2.2.	Physical characterisation . . . . .	126
2.3.	Surface energy . . . . .	126
2.4.	Preparation of mixtures . . . . .	127
2.5.	Dustiness . . . . .	128
2.5.1.	The rotating drum (RD) . . . . .	128
2.5.2.	The vortex shaker (VS) . . . . .	129
3.	Results and discussion . . . . .	131
3.1.	Physical characterisation . . . . .	131
3.2.	Dustiness of Host Powders and SIPERNAT D10 . . . . .	133
3.3.	Influence of relative humidity on the dustiness of HP . . . . .	134
3.4.	Influence on dustiness when adding Sipernat D10 . . . . .	137
3.5.	Dustiness real-time analysis . . . . .	139
3.6.	Surface energy analysis: Dustiness and interparticles forces . . . . .	140
4.	Conclusions . . . . .	142
5.	Surface properties a deeper insight . . . . .	143
<b>6</b>	<b>The relationship between flowability and dustiness</b>	<b>147</b>
1.	Introduction . . . . .	147
2.	Experimental approach . . . . .	147
3.	Flowability . . . . .	148
4.	Quasi-static regime . . . . .	148
5.	Dynamic regime . . . . .	151
6.	Dustiness . . . . .	155
7.	Are flowability and dustiness related? . . . . .	156
8.	Conclusion . . . . .	161
	<b>Conclusion and perspectives</b>	<b>163</b>
	<b>Nomenclature</b>	<b>168</b>
	<b>List of figures</b>	<b>173</b>
	<b>List of tables</b>	<b>176</b>
	<b>Bibliography</b>	<b>193</b>
<b>7</b>	<b>Résumé en français des travaux menés et des résultats obtenus</b>	<b>195</b>
1.	Contexte . . . . .	195
2.	Principaux résultats obtenus . . . . .	199
2.1.	Coulabilité . . . . .	200
2.2.	Pulvéulence . . . . .	201

2.3.	Rélation coulabilité-pulvérulence . . . . .	202
3.	Perspectives . . . . .	203

# General Introduction

---

Nowadays, granular materials are ubiquitous in daily life, whether they are processed or are a part of the natural environment (i.e. seeds, sand, and pollen). According to archaeological tools, food powder production was developed about 50,000 years ago (upper Paleolithic) by grinding seeds, plants and nuts between millstones [1, 2]. Since, powder manufacture and employment have arisen and developed, becoming the second most handled material after water [3]. Powders are used and handled in numerous industries, such as construction, pharmaceuticals, food, and cosmetics. It is difficult to estimate how much powder is produced and consumed worldwide. However, it is estimated that half of the end-use products, and three-quarters of raw materials, in the chemical industry are in divided solid form [4]. In an effort to quantify the amount of raw powders produced in France, a market study of powders from various industries was done. The results of this study revealed that the mass production of powders exceeds 40 million tons per year (Fig.1). Despite, it is likely to be an underestimation of the real amount since data from pharmaceutical, cosmetic, and other industries are not publicly available. This statistic offers a glimpse into the true scale of powder handling and the associated challenges faced by the countless individuals who work with these materials on a daily basis.

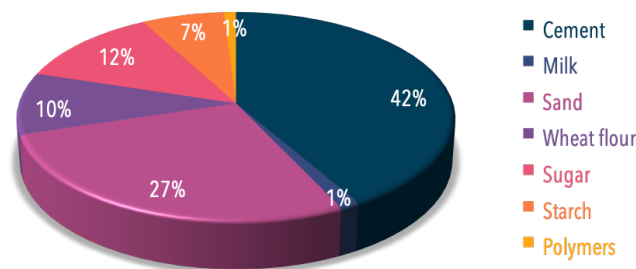


**Figure 1.** Granular materials production in France (40 million tons/year)[5–13].

Even if powders are widely used, their processing still presents several complications (Fig.2). For instance, storage in hoppers, silos and bins exhibits problems like blockage, arching, ratholes and segregation [14]. These problems cause difficulties during transfer of powders requiring clumsy hand scooping or hammering the storage equipment, being harmful to the workers and damaging the facilities. Powder compaction can produce certain complications on transfer operations. Moreover, specific operations such as dosage, encounter inconsistent results which are problematic in all kind of products, like

pharmaceuticals that require a precise quantity of active principals.



**Figure 2.** Powder handling clumsy and dangerous operations due to poor flowability and dustiness.

All of these problems are commonly dictated by the poor flowability of powders. Powder flowability can be improved by:

1. Facility modification, such as adding vibration feeders widely used for fertilizers [15]. However, this is seldom a universal solution since the flow behaviour might worsen for finer powders.
2. Powder fluidization, which has been shown to enhance the flow behaviour of powders with large particles. Nevertheless, for finer pharmaceutical powders, this process requires the addition of other mechanisms, such as magnetic assistance [16], which increases process complexity and costs [17].
3. Adding flow additives, which is considered the most effective solution with the best benefit/cost ratio and the most frequently adopted solution in industries. Based on trial and error -industrial “*savoir-faire*”- the amount of flow additives added to formulations is around 0.5–2% wt. [18].

One of the most used flow additives is amorphous silica nanoparticles (S-NP). This formulation ingredient is Generally Recognized As Safe (GRAS) by the United States Food and Drug Administration (FDA), limiting its use to 2% wt. in food products. Still, suggests to add an “amount not in excess of the reasonably needed quantity required to produce an anticaking effect” [19]. In contrast, the European Food Safety Authority (EFSA) established an acceptable daily intake as “not specified”, implying that S-NP does not represent any hazard to health [20]. Even if both regulation entities, FDA and EFSA, consider S-NP safe for food use, their toxicity is still controversial. These regulation entities focus their resolutions on the toxic effects of S-NP ingestion, where high doses have been shown to be tolerated [21]. However and surprisingly, occupational inhalation exposure is not

considered. A recent review revealed that at high exposure levels, for both crystalline and amorphous silica, had similar toxic effects, with the exception of causing silicosis disease which is only attributed to the crystalline form [22]. In addition, *in vitro* and *in vivo* studies showed an increase on pro-inflammatory responses with nanometric silica exposure in comparison to micrometric one [21, 23]. Although some studies suggest that there may be potential toxicity associated with the use of S-NP, it is still not well established. Regulatory entities do not always operate under the principle of precaution, which can be associated with the increased of S-NP use on industry despite potential risks [24].

In addition to poor flow complications, mechanical operations such as sieving, conveying, and granulation, as well as manual operations like pouring and weighting, are prompt to emit dust clouds. Dust emission can cause problems during powders processing, resulting in cross-contamination, filter clogging, and product loss, as well as increasing the risk of inhalation, explosions and fires [25] (Fig.2). Dust emission has been strongly linked to occupational risk due to its dangerous consequences. Over the years studies have mostly focused on the characterisation of pure powders, testing a wide variety of materials on different testing methods. However, focusing on pure powders overlooks the dust emission of most powder products, which are composed of several ingredients.

This thesis was conducted between the Reactions and Chemical Engineering Laboratory (LRGP) and the National Institut of Research and Safety (INRS), the reference organism of occupational safety and risk prevention in France. This collaboration aimed to relate powders' **flowability** to **dustiness**. Nowadays, S-NP are added systematically to powder products to ensure process feasibility—good flowability. Surprisingly, to the best of our knowledge, the relation between flowability and dustiness has never been directly studied. Therefore, this work **aims** to evaluate the effects of the addition of S-NP on dust emission. The understanding of the S-NP mechanism of action on flowability might provide a guide to reduce their use and occupational exposure.

This manuscript consists of six chapters, which present the background of the research work and the results, which are reported through three publications and a final results chapter. Each publication-chapter include a synthesis of the most significant findings, followed by additional results not included in the published work.

The **first chapter** explores the interest in studying powders, providing relevant definitions and introducing the complex behaviour of powders and their properties. In addition, powders' flowability and dustiness are introduced, along with their respective characterisation methods. Finally, the first insights into the correlation between flowability and dustiness are presented.

The **second chapter** focuses on the material and methods used in the study. The

reasoning behind the selection of powder samples is thoroughly explained, as well as the methods. The first part presents the selection of powders, flow additives and the formulation protocol followed by the physicochemical characterisation of the powders and formulations. The flowability and dustiness characterisation techniques are also thoroughly described.

The results of this work are presented from chapter 3 to 6. Chapters 3 and 4 focus on flowability results, while chapter 5 presents dustiness results. Finally, chapter 6 discusses the relationship between these two end-use properties.

In the **third chapter**, the initial findings on flowability are discussed. This chapter aims to identify an appropriate flowability measuring device based on the amount of energy applied to the sample. Furthermore, this chapter presents the impact of flow additives on pharmaceutical excipients.

**Publication I:** Effects of humidity and glidants on the flowability of pharmaceutical excipients. An experimental energetical approach during granular compaction. M.-G. Cares Pacheco, M.-C. Jiménez Garavito, A. Ober, F. Gerardin, E. Silvente and V. Falk. Int.J.Pharm. 2021. DOI: [10.1016/j.ijpharm.2021.120747](https://doi.org/10.1016/j.ijpharm.2021.120747)

In the **fourth chapter** the discussion of flowability results is carried forward with a deeper focus on comprehending the factors that contribute to the flow behaviour of powders. Additionally, this section evaluates the action mechanism of flow additives on powder flowability.

**Publication II:** Silica nanoparticles as glidants for industrial processing: a statistical approach. M.-C. Jiménez Garavito, M.-G. Cares Pacheco, F. Gerardin and V. Falk. 2022. DOI: [10.1021/acs.iecr.2c02455](https://doi.org/10.1021/acs.iecr.2c02455)

**Chapter five** presents the results of the influence of adding flow additives on powders' dust emission. This shows the importance of adhesive interactions between the powders and the nano additives allowing to deepen the understanding of the propensity to emit dust.

**Publication III:** The effect of silica nanoparticles on the dustiness of industrial powders. M.-C. Jiménez Garavito, M.-G. Cares Pacheco, F. Gerardin, S. Bau, O. Witschger and V. Falk. DOI: [10.1016/j.appt.2023.104105](https://doi.org/10.1016/j.appt.2023.104105)

The final chapter of the manuscript, **chapter six**, explores the relationship between flowability and dustiness. The first part presents the results of flowability tests conducted using different devices to evaluate the effects of different formulations. Then, the results of dust emission are presented, followed by an analysis of the different behaviours of dust generation according to the sample and the formulation. Finally, the correlation between flowability and dustiness is assessed, seeking to find models that could allow the prediction of these two end-use properties.

Finally, a general **conclusion** is presented, highlighting the main findings and contributions of this study. Furthermore, some future work **perspectives** are proposed.

# 1

## State of the art

---

### 1. Introduction

This chapter aims to describe concepts that will serve as a basis for understanding the factors influencing flowability and dustiness as end-use properties. The first part of the chapter covers the basic definitions of powders and their complex behaviour. Then, the powder properties and the interactions between particles that govern their motion are discussed. The second and third parts of the chapter focus on the state-of-the-art research on flowability and dustiness, respectively. Each part includes an introductory section defining the end-use property, followed by a discussion of the factors influencing each property and the techniques used to characterise them. Finally, the last part of the chapter presents the state-of-the-art on the relationship between powder flowability and dustiness, highlighting the lack of studies in this area and the relevance of the present work.

### 2. General definitions

What is the difference between granular matter, bulk solid or powder? Are sand, coffee, flour and corn seeds in the same category? Are all of them powders? Well, in daily life, no one would ever refer to corn seeds as powder. However, the definition is not well established and varies according to the scientific community. Some authors differentiate granular matter from powders [26, 27], while others use these terms as synonyms [3, 4, 28]. Granular matter is often defined as an assembly of individual/discrete particles in close contact with each other [4, 28]. This term varies depending on the particle size, whether below 1 mm [29], above 1  $\mu m$  [3] or all sizes are considered. A more detailed definition of granular matter was proposed by Richards and Brown in 1970, where they classified bulk solids into three main categories based on the size of the particles (Fig.1.1) [27]. Herein, the term **powder** will be used as a synonym of granular materials to designate "granular powders" and "granular solids".

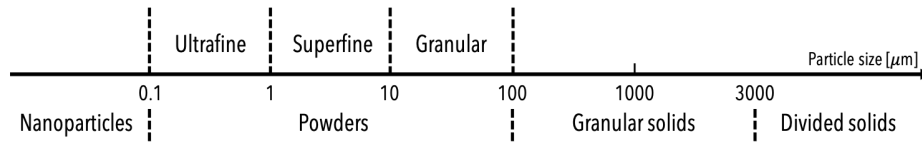
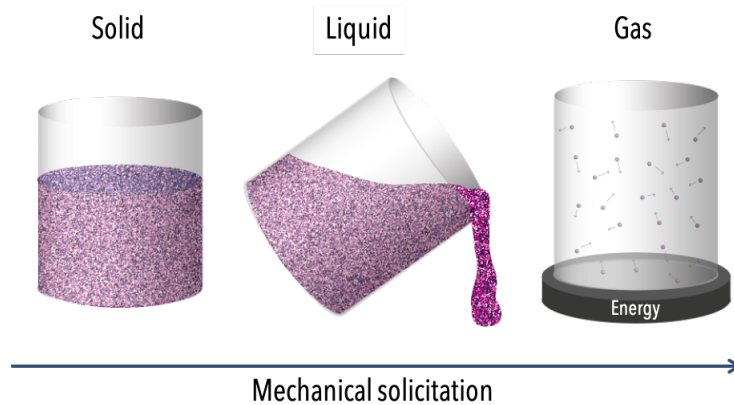


Figure 1.1. Richards and Brown bulk solids definition [27].

Unlike powders, nanoparticles (NP) have been thoroughly described by international standards and regulatory entities. For instance, the ISO 17200 [30] standard defines NP as a “*nano-object with all external dimensions in the nanoscale where the lengths of the longest and the shortest axes of the nano-object do not differ significantly*”. The nanoscale refers to sizes between 1 and 100 nm according to the standard ISO/TS 80004-1 [31]. The European Commission has a more detailed definition stating that: “*a nanomaterial (NM) is a natural, incidental or manufactured material consisting of solid particles that are present, either on their own or as identifiable constituent particles in aggregates or agglomerates, and where 50% or more of these particles in the number-based size distribution fulfil at least one of the following conditions: (a) one or more external dimensions of the particle are in the size range 1 nm to 100 nm; (b) the particle has an elongated shape, such as a rod, fibre or tube, where two external dimensions are smaller than 1 nm and the other dimension is larger than 100 nm; (c) the particle has a plate-like shape, where one external dimension is smaller than 1 nm and the other dimensions are larger than 100 nm*” [32]. Besides, in the previous legislation of 2011 [33], materials with specific surface area by volume (VSSA) above  $60 \text{ m}^2/\text{cm}^3$  were considered NM, while the new one (2022) states that materials with a VSSA of below  $6 \text{ m}^2/\text{cm}^3$  shall not be considered NM [32], without directly implying that materials above  $6 \text{ m}^2/\text{cm}^3$  are NM. The NM definition is well established in the European community because the use of NM must be clearly indicated on food and cosmetic products labels (EU 1169/2011).

### 3. Powders in motion

The state of matter to which granular materials are known to belong is difficult to define, and it is commonly admitted that they behave like any of the three states [34], solid, liquid and gas, as depicted in figure 1.2. While matter phase transitions are generally governed by thermodynamic modifications [35], in the case of granular materials, the change in their behaviour is attributed to mechanical forces. Thus, we refer to these behaviours as solid, liquid, and gaseous regimes [36]. The transition between these regimes is determined by the intrinsic properties of the granular material, environmental conditions, and the magnitude of mechanical forces. For transition between regimes, the interparticle interaction forces must be overcome.



**Figure 1.2.** Powders behaviour regimes solid, liquid and gas.

Solid, liquid-fluid and gaseous regimes can co-exist during industrial powder handling operations such as, silos discharge as schematized in shown in figure 1.3. The solid regime is characterised by particles in constant contact with one another. In this regime, the particles exhibit organized structures determined by the action of interparticle interaction forces that keep this static state equilibrium. This behaviour is seen in storage and transport, where powders tend to compact. The solid regime of granular media is often described using soil plasticity models. The liquid regime could be defined as an intermediate regime between the quasi-static and the fluid regime, also called dense flow regime. A decrease in the interparticle forces network by a mechanical solicitation let the particles space and flow in a fluid-like way, **flowability**. The characterisation of this regime is still misunderstood and complex to measure. This behaviour is observed in transfer operations in dense phase or hopper, silos and bins discharge. The gaseous regime occurs when grains are subjected to strong mechanical forces, causing them to collide and disperse like a gas, **dustiness**. In contrast to molecular gases, this regime's stability depends on the solicitation level, as collisions between particles dissipate energy, ultimately determining their stability. This phenomenon can be described by the kinetic theory using the Boltzmann inelastic gas equation for two identical particles.

From the perspective of powder behaviour, flowability and dustiness can be related to the transition of the liquid/gas regimes. The following sections will discuss these phenomena, along with the powder properties and particle interactions that intervene and influence them.

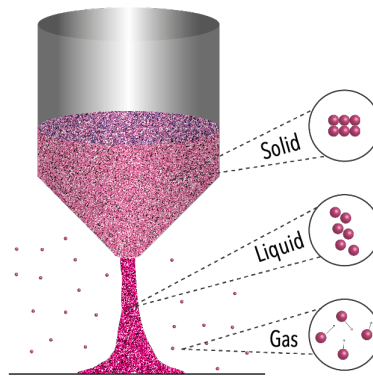


*Figure 1.3. Solid, liquid and gas powder regimes co-existing in an industrial process.*

## 4. Powder properties

### 4.1. Particle size distribution and shape

Powders' behaviour is influenced by the physical and physicochemical properties of their primary particles. Most powders are composed of non spherical particles with non-smooth surfaces and polydisperse size distribution. These heterogeneities influence their behaviour in comparison to monodispersed spherical powders. Then, their characterisation is commonly made by the comparison with spheres. For example, one of the most often used methods to characterise particle size and distribution is light diffraction. This technique characterises particles by their equivalent diameter, which is the diameter of a sphere with the same volume (surface, specific surface...) as the measured particle [37]. It is important to note that the assumption of spherical particle shape may not always accurately describe the particle size distribution of certain powders, such as those with fibrous or flake-like shapes. To ensure accurate measurements, it is recommended to verify the results obtained through laser diffraction by comparing them with morphology characterisations of the particles.

Particle size distribution (PSD) classes the different sizes of particles according to their volume or number fraction. The PSD is often presented in a lognormal distribution indicating the  $d_{10}$ ,  $d_{50}$ , and  $d_{90}$ .  $d_{10}$  represents the diameter for when 10% of the sample is smaller and represents the smaller sizes. The median diameter,  $d_{50}$ , indicates that 50% of the particles are smaller than the  $d_{50}$  size, while  $d_{90}$  corresponds to 90% of the particles, showing the larger particles. Besides the normal distribution diameters, the De Brouckere mean diameter,  $d_{4,3}$ , and the Sauter mean diameter,  $d_{3,2}$ , are widely used to express a mean value of the PSD diameters. The  $d_{4,3}$  is better for characterising big particles, as its measurement is based on the mass/volume, while  $d_{3,2}$  identifies better the smaller particles by relating to the specific surface.

Particle shape can be intended or not according to the manufacturing method. The shape

is generally described qualitatively using terms like: "flaky, rod-like, spherical, fibrous" [37] as their forms are far from geometrical shapes. One of the most used parameters to characterise shape is sphericity, proposed by Wadell in 1935, defined as the ratio of the surface area of an equal volume sphere to the surface area of the particle [38].

#### 4.2. Particle and powder density

Density is defined as the ratio of mass to volume. The powders volume could vary due to the evolution empty spaces between particles. Then, we have different definitions of densities. The true density is the mass of a powder bed over the volume occupied by the particles without the voids (inter and intra particular). Its measure consists of introducing a small quantity of powder into a vessel with a known volume, which is then vacuumed. Helium molecules are then used to fill the empty spaces. The difference between the vessel's volume and the helium injected volume provides the actual volume of the powder. The pycnometry density,  $\rho$ , of the sample can then be calculated using the powder measured volume and the mass added to the vessel. In contrast, bulk density,  $\rho_b$ , measures the volume occupied by a powder bed, including voids and particle porosity.

### 5. Interparticle interactions

Gravity mainly governs the motion of objects [39]. In the case of granular materials, this motion depends on the type of interaction between the particles with gravity forces influence decrease with particle size. Physicists often work with particles greater than 100  $\mu\text{m}$  (glass beads and sand) which interactions are mainly governed by friction and collision. For heterogeneous cohesive powders, other interparticle interactions such as van der Waals and capillary forces govern their motion. In this section, these interparticle interactions are described in detail.

#### 5.1. Van der Waals forces

The van der Waals forces ( $F_{vdW}$ ) are attractive electrical forces between atoms and molecules, composed by three interaction types [39]:

- *Keesom forces* are dipole-dipole interactions between polar molecules.
- *Debye forces* are dipole - induced-dipole interactions between a polar molecule that induce a non-polar molecule, a dipole.
- *London forces* are dispersive forces between non-polar molecules producing a temporary induced-dipole – induced-dipole interaction.

From these interactions, the strongest ones are the Keesom forces, and the weakest are the London forces. All of these, called van der Waals forces, are inversely proportional to the distance between two molecules. As the distance between the molecules increases, the

strength of the van der Waals forces decreases. This is because the fluctuating dipoles that give rise to the van der Waals forces become weaker and less able to interact with each other as the distance between the molecules increases. Therefore, van der Waals forces are typically only significant when the molecules are within a few nanometers of each other.

Van der Waals forces are usually determined from Hamaker model [40] presented in equation 1.1.

$$F_{vdW} = \frac{A}{12d^2} \left( \frac{D_1 D_2}{D_1 + D_2} \right) \quad (1.1)$$

where  $F_{vdW}$  refers to van der Waals forces [N],  $A$  is the Hamaker constant, which is material dependent with values around  $10^{-19}$  [J],  $d$  is the distance between particles [m] and  $D_i$  is the diameter of the particle/s [m].

## 5.2. Capillary forces

Capillary forces are attractive forces between particles or a particle and a surface due to the presence of liquid (Fig.1.4). The capillary force of two spherical particles can be determined by equation 1.2. The first term of the equation is the axial component of the surface force at the solid/liquid/gas interphase, and the second one is the force due to the reduced hydrostatic pressure in the bridge [41].

$$F_{cap} = 2\pi r_2 \gamma + \pi r_2^2 \Delta P \quad (1.2)$$

where  $\gamma$  is the liquid surface tension [N/m],  $\Delta P$  is pressure differential between the inner and the external part of the meniscus (Eq.1.3) and,  $r_1$  and  $r_2$  are the inner and external meniscus radii, respectively (see figure 1.4).

$$\Delta P = \gamma \left[ \frac{1}{r_1} - \frac{1}{r_2} \right] \quad (1.3)$$

These forces, as well as  $F_{vdW}$ , become stronger as the distance between particles decreases. Furthermore, the surface tension between the grain and the liquid is important in this interaction because their adhesive forces are greater, and materials with high surface tensions have stronger capillary forces. As a result, the geometry and topography of the particle surface have an impact on this interaction.

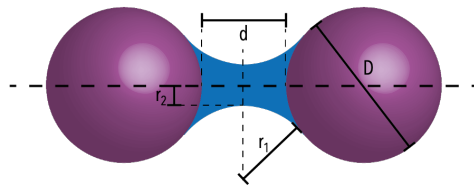


**Figure 1.4.** Liquid bridge between two spherical particles [41].

### 5.3. Electrostatic forces

Electrostatic forces arise between charged particles due to their electric charges being either attractive or repulsive. For two spherical particles of the same size, these forces can be determined using the Coulomb's law [42], presented in equation 1.4.

$$F_{elec} = \frac{q_1 q_2}{4\pi a^2 \varepsilon_r \varepsilon_0} \quad (1.4)$$

where  $q_1$  and  $q_2$  are the electric charges [ $\mu C/m^2$ ],  $a$  is the distance between the particles,  $\varepsilon_r$  is the relative permittivity [F/m] and  $\varepsilon_0$  is the vacuum permittivity [F/m].

Particles can charge during collisions that generally occur during powder handling operations, such as pneumatic conveying, transfer and mixing. These forces play a significant role in how the particles behave and interact, which can lead to agglomerates formation, poor flow and dust emission. This latter can cause sparks, which may result in fire and explosions, affecting the workers' safety, the installations and the operations performance [43]. The powders' electrostatic charging mechanism is still poorly understood, making its prediction and control challenging [44]. One of the main solutions adopted in industries are the addition of fine powders to coarse particles, which have been shown to decrease the powder charge and to ground the powder handling equipment.

## 6. Flow behaviour - dense flow regime

One of the most studied phenomena of granular media is its flow behaviour since this property is essential in product manufacture in many industries. Despite its relevance, to this day, no constitutive law describes how powders flow, as in the case of liquids with the Navier-Stokes equation [36]. Like other terms in the area of granular media, flowability is not well-defined and has several definitions. The standard ISO 1719-9 [45] defines it as "*the time for a mass of powder to pass through a specified funnel*". Similarly, ISO 3252 [46] describe flowability as "*the behaviour of a powder when flowing through a funnel of defined dimensions*". These standards associates flow behaviour to a defined measurement, which has been proposed by other authors [26, 47, 48]. In contrast, ISO 16559 [49] provides a more general and simplified definition, referring to flowability as the "*ability of a solid bulk material to flow*".

Prescott and Barnum states that flowability definitions may vary according to the domain [14]. For instance, formulators relate flowability to products while engineers link it to the process. These authors also emphasize that flowability cannot be expressed as a single value pointing out the complexity of the powders' flow behaviour which is influenced by multiple factors. Moreover, Don McGlinchey introduces the term "*handleability*" as a synonym for flowability, referring to the ease or difficulty of dealing with bulk materials

[29].

The presented definitions describe the powder's ability to flow on a specific device or attribute flowability to a powder property. This latter definition oversimplifies flow behaviour which is not an intrinsic property of powders. Thus, the same powder may exhibit excellent flow under certain conditions but behave as cohesive if conditions change. For instance, Saker et al. [50] demonstrated that the flowability classification of food and pharmaceutical powders could differ depending on employed the measuring device. Therefore, two terms may be considered when referring to powder flow behaviour. The first is "powder flow", which is a global observation, and the second, "flowability", as the ability to flow in a device under specific mechanical conditions [51].

## 6.1. Factors influencing powder flow behaviour

Powder flowability is influenced by powders' intrinsic properties, environmental, mechanical (energy supplied by a characterisation device) conditions and by the addition of flow additives. In this section this factors will be discussed.

### 6.1.1. Particle intrinsic properties

Particle size distribution (PSD) is the most studied and characterised powder property [18, 50–65]. Particle size has an effect on interparticle interactions, smaller particles have a greater specific surface which increases the number of possible contacts, increasing at the same time van der Waals forces. As a result, theoretically speaking, the finner a powder is, the more cohesive is, which leads to poor flowability. Studies on ibuprofen [62], pharmaceutical granulated [59], and food powders [65] have shown that powders with smaller PSD presented poorer flow than those with greater size. Besides, Liu et al. [62] showed that materials with narrow PSD and bigger particles presented a better flow. In addition, shape influence has also been studied in lactoses[57] and 3D printing powders [64], showing that highly spherical powders, with few fine and larger particles, had a better flow.

### 6.1.2. Relative humidity

Relative humidity (RH) is an environmental parameter that influences flowability in different ways and strongly depends on the sample behaviour towards water. In general, it can be stated that at high RH, above 60% - 80%, liquid bridges form, increasing capillary forces and worsening flow behaviour [47]. Besides, RH alter conductivity, which has two known effects on granular materials [66]. At low RH, the conductivity decreases, which reduces the strength of electric forces. Conversely, at high RH, the conductivity increases, having the opposite effect. RH effect on powders has been widely studied, mostly founding that its increase decreases the powder flow behaviour. Studies with lactose [66–68], pectin, maltodextrin and starch [69], flour, wheat and tea [70] have presented this effect.

Some other studies have found that RH influence on flowability depends on the powder, founding mixed effects according to the sample [51, 71, 72]. Although the impact of relative humidity (RH) on powder flowability is significant, it is often neglected in research studies [57, 73–75]. While it is true that controlling RH in industrial settings can be challenging and expensive, it seems essential to control RH in research studies. This practice avoids water's influence on other parameters, leading to more accurate and representative results.

### 6.1.3. Flow additives

In industry, one of the main solutions to assess poor flowability is the addition of flow additives—or glidants such as stearates, talc and NP, such as amorphous silica NP (S-NP) [18, 76]. The effect of S-NP on flow behaviour has been widely studied. Some authors have found that hydrophobic S-NP improved flowability more effectively compared to hydrophilics. [51, 77–79]. Several studies have shown that the ideal concentration of glidants ranges between 0.1-2% wt, with better performance near the upper limit [80–86]. Notwithstanding, other studies have reported that increasing glidant concentration does not always enhance flowability and could even worsen it [50, 83, 87, 88]. Why do flow additives enhance flow behaviour? This question is extensively treated in chapter 4.

### 6.1.4. Temperature

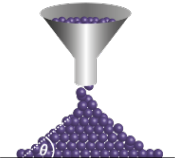
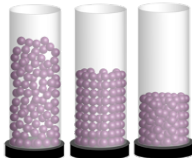
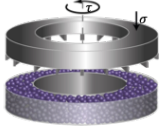
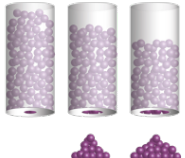
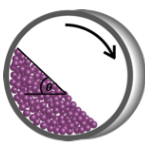
The effect of temperature on powders' flow behaviour seems to vary according to the sample, as it can act in different ways. An increase in temperature may decrease the water content, which decreases capillary forces, enhancing flowability. In contrast, temperature increases solubility, in presence of water, giving rise to solid bridges, increasing cohesion and reducing powder flow behaviour. Teunou and Fitzpatrick [70] studied the temperature effect on three powders (whey, tea and flour), founding out that two of them decrease their flow behaviour when temperature increases due to the action of solubility and plasticity of the powers. On the other hand, the third powder (flour) improved its flow behaviour with an increase in temperature. In this case, the authors explain that it should be due to a reduction in moisture in the sample. Tomasetta et al. [89] found no significant effect of temperature on the flowability of an FCC powder and corundum, while glass beads' cohesion increased with temperature. This latter result is in agreement with studies made from the same research group, where two samples of titanium dioxide [90] and five ceramics [74] increased their cohesion with temperature (20°C to 500°C) increase.

## 6.2. Flowability measuring techniques

Measuring powders' flowability is as varied as their behaviour. There is a wide variety of techniques which are generally associated with a powder handling operation. Therefore, selecting an appropriate technique often depends on the specific application of the powder in question, based on industrial savoir-faire [91, 92]. Some classifications can be found in the scientific literature according to:

- The **stress levels** applied to the sample [93] or confined/unconfined conditions [94] these classifications are mainly adopted by powder technology groups.
- **Flow velocity** during the test [92, 95, 96]. This classification is mainly used by granular physicists in order to attribute some models used to describe the different flow regimes (solid-like, fluid-like and gas-like).

This thesis employs the latter classification, categorising the characterisation techniques as static, quasi-static and dynamic. Static measures describe flowability on powders that are not in motion or settled. Quasi-static class is intended for those techniques where powders are "relatively in motion", experiencing some kinetic energy with an almost settled sample. Dynamic methods quantify the flow behaviour of powders in motion. This classification of tests can also be associated with the state in which the powder behaves. Consequently, the static and quasi-static regimes evaluate the behaviour of granular materials in the solid and solid/liquid intermediate regimes and the dynamic methods in the liquid regime. Figure 1.5 presents a synthesis of flowability characterisation techniques using flow velocity classification. This figure offers concise and informative details about each technique, which is also a guide for the following sections.

Regime	Static	Quasi-static		Dynamic	
Method	Angle of repose 	Densification 	Shear test 	Flow through an orifice 	Dynamic angle 
Measured property	Powder pile rupture limit	Rearrangement capacity	Plastic-rigid rupture	Capacity to flow through an orifice	Powder bed instability
Flow index	<ul style="list-style-type: none"> <li>▪ Angle of repose</li> </ul>	<ul style="list-style-type: none"> <li>▪ Hausner ratio</li> <li>▪ Carr index</li> </ul>	<ul style="list-style-type: none"> <li>▪ Flow factor</li> <li>▪ Bulk adhesion</li> </ul>	<ul style="list-style-type: none"> <li>▪ Critical diameter</li> <li>▪ <math>C_{BV}</math> parameter</li> </ul>	<ul style="list-style-type: none"> <li>▪ Dynamic angle</li> </ul>
Industrial application	Pharmaceuticals, food and cosmetics	Pharmaceuticals, food, cosmetics and metals	Pharmaceuticals and silos sizing	Pharmaceuticals and metals	Pharmaceuticals, food, cosmetics, metals and cement
Devices	<ul style="list-style-type: none"> <li>▪ PT-X</li> <li>▪ Granuheap</li> </ul>	<ul style="list-style-type: none"> <li>▪ PT-X</li> <li>▪ Granupack</li> <li>▪ Densitap</li> <li>▪ FT4</li> </ul>	<ul style="list-style-type: none"> <li>▪ RST-XS Schulze</li> <li>▪ Brookfield PFT</li> <li>▪ FT4</li> <li>▪ Sevilla PT</li> <li>▪ Evolution PT</li> </ul>	<ul style="list-style-type: none"> <li>▪ Granuflow</li> <li>▪ Hall flowmeter</li> <li>▪ Flowdex</li> </ul>	<ul style="list-style-type: none"> <li>▪ Rotating drum</li> <li>▪ Revolution PT</li> <li>▪ Granudrum</li> </ul>
Standards	<ul style="list-style-type: none"> <li>▪ NF 12047:1997</li> <li>▪ ISO 8398:1989</li> <li>▪ ISO 4324:1977</li> <li>▪ ISO 902:1976</li> </ul>	<ul style="list-style-type: none"> <li>▪ NF 1237:1995</li> <li>▪ ISO/ASTM 52925</li> <li>▪ ISO 9161:2021</li> <li>▪ ISO 23145-2:2016</li> </ul>	<ul style="list-style-type: none"> <li>▪ ASTM D7891-15</li> </ul>	<ul style="list-style-type: none"> <li>▪ ISO 14629:2016</li> <li>▪ ISO 4490:2018</li> <li>▪ ISO 13517</li> </ul>	-

**Figure 1.5.** Synthesis of several flowability characterisation techniques.

These methods are presented in more detail in the following section; they were chosen based on their widespread use in industry and research.

### 6.2.1. Static measures: Angle of repose

The angle of repose (AoR) is the angle formed between the horizontal axis and the slope of a stable powder pile produced by pouring a free and uncompacted granulated material [97]. It is also defined as the highest possible slope of a settled pile of powder without collapsing [98]. During the pile formation, two angles are formed,  $\theta$ , being the maximum angle of the pile before the particles start moving (Fig.1.6a) and  $\alpha$ , which is produced after the pile avalanche (Fig.1.6b) [99].

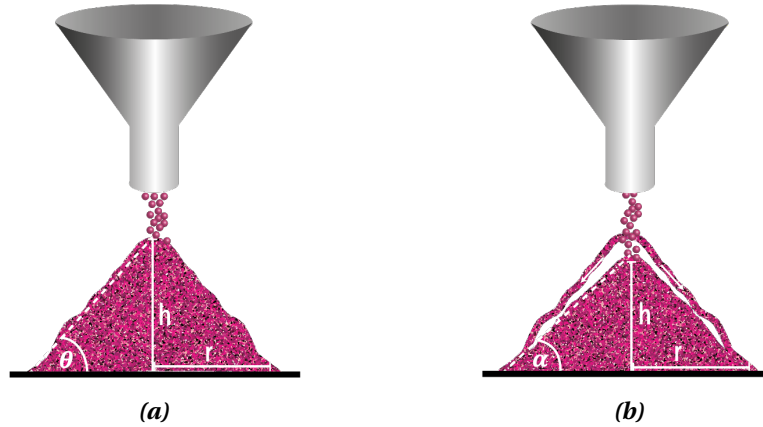


**Figure 1.6.** Angle of repose variation. a)  $\theta$  refers to the maximum angle of the pile before avalanche and b)  $\alpha$ , the angle produced after avalanche.  $h$  represents the height and  $r$  the radii of the pile.

The AoR measure varies between these two angles and it is calculated with the following expression:

$$AoR = \tan^{-1} \left( \frac{h}{r} \right) \quad (1.5)$$

The AoR measurement provides an estimate of flowability by representing the resistance of a moving powder due to the frictional force between the particles [100]. Figure 1.7 shows the forces acting on a particle on the powder pile's outer layer.

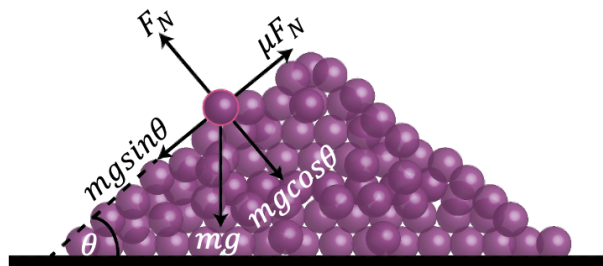


**Figure 1.7.** Forces acting on a particle on a pile of powder.  $F_N$  is the normal force,  $m$  is the mass of the particle,  $\mu$  is the friction coefficient,  $g$  is the gravitational acceleration and  $\theta$  is the angle of repose.

To produce an avalanche, the tangential component of the weight,  $mg \sin(\theta)$ , must overcome the friction force, which is defined as the product of the friction coefficient,  $\mu$  and the normal force,  $mg \cos(\theta)$ :

$$mgsin(\theta) \leq \mu \cdot mgcos(\theta) \quad (1.6)$$

where  $m$  is the mass of the particle in [kg],  $g$  is the gravitational acceleration [ $m/s^2$ ], and  $\theta$  is the angle of repose [ $^\circ$ ].

The equation 1.7 is the result of clearing up the terms in both sides of equation 1.6. This expression shows that the stability of the AoR depends on the friction interaction between particles. The AoR is measured when  $\tan(\alpha) = \mu$ , meaning that all particles are still.

$$\tan(\theta) \leq \mu \quad (1.7)$$

Several authors have defined a classification of powder flowability according to the AoR [27, 29, 48]. Regardless of the classification, powders that form angles below  $25^\circ$  are considered free-flowing, while those above  $45^\circ$  present a poor flow. Table 1.1 shows the flowability classification proposed by Carr in 1965 [48]. In the AoR, the action of cohesive/adhesive forces is not considered. In the case of cohesive powders, the measure of the AoR might be challenging since a perfect heap is not achieved, even though it tends to create greater AoR following the classification the Carr classification.

**Table 1.1.** Angle of repose flowability classification [48]

Flowability	Angle of repose [ $^\circ$ ]
Excellent	25 - 30
Good	31 - 35
Fair	36 - 40
Acceptable	41 - 45
Poor	46 - 55
Very poor	55 - 65
Very, very poor	> 66

A wide variety of AoR measuring devices exist, some of which are presented in figure 1.8. This measure is strongly influenced by many factors, such as powder properties (e.g. PSD and roughness) and device related (e.g. falling distance, type of device) that limit the technique, making it less reproducible and operator-dependent [97, 101, 102]. Despite these limitations, it remains one of the most widely used devices in the industry due to its ease of use and quick application [97]. It may not be the most reproducible measure, but it still allows for a rough comparison of the flow behaviour of different samples, making it useful in various industries such as agriculture, pharmaceuticals, geology, and food processing [95, 101].

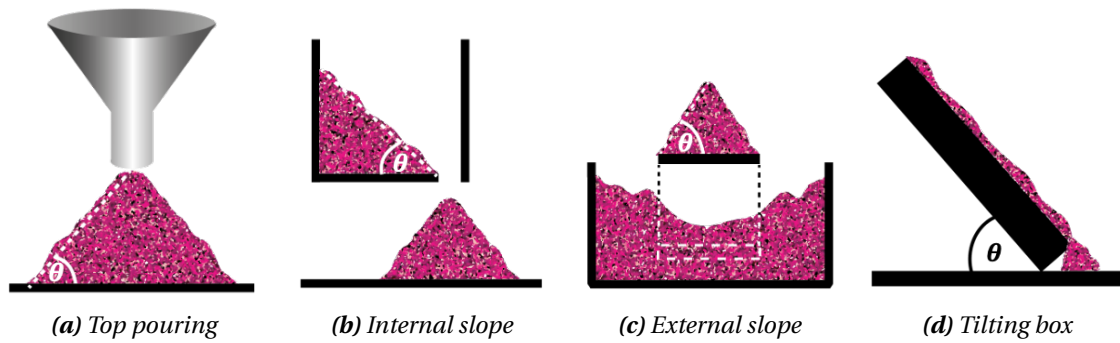


**Figure 1.8.** Angle of repose measuring techniques.  $\theta$  refers to the angle of repose

## 6.2.2. Quasi-static measures

### 6.2.2.1. Densification measures

As explained in section 4.2., powder density can be quantified in several ways. The bulk density,  $\rho_b$ , is the volume occupied by a mass of powder simply poured into a container. The particles' arrangement in the container varies according to interparticle interactions and bulk density increases by supplying energy to the container through vibrations. These motions make the powder particles move and fill the initial void spaces, decreasing the powder-bed volume, as shown in figure 1.9. The resulting density is called the tapped density,  $\rho_t$ .

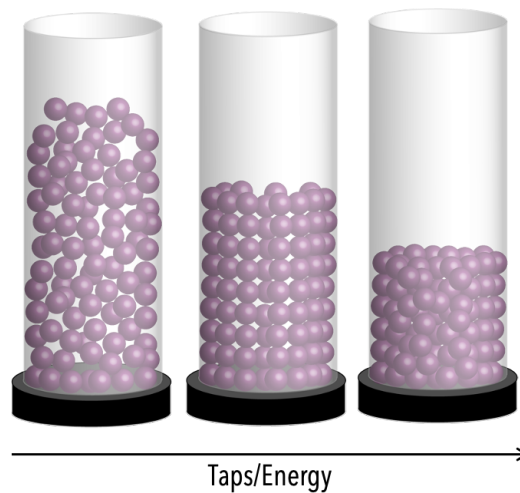


**Figure 1.9.** Densification of granular materials.

Powder densification is related to their flow behaviour by their easiness of densifies. For instance, in 1965, Carr stated, "It is obvious that compressibility is a very important flow characteristic... the more compressible a material is, the less flowable it will be". Therefore, he proposed the first flowability classification based on powder densification (table 1.2) [48]. The Carr index (CI) is defined as follows:

$$CI = 100 \left( \frac{\rho_t - \rho_b}{\rho_t} \right) \quad (1.8)$$

In 1967, Henry Hausner proposed another flowability classification based on powder densification of metallic powders [103]. According to Hausner, "high friction between particles results in low  $\rho_b$  and with decreasing friction, it increases." He also stated that "while tapping, the particles are forced to jump, losing contact with each other for a moment during which there is no friction between particles". Based on this observation, he introduced the Hausner ratio (HR), which is the ratio of tapped density to bulk density:

$$HR = \frac{\rho_t}{\rho_b} \quad (1.9)$$

Both flowability indices classifications are presented in table 1.2. Free-flowing powders have lower CI and HR, while the higher values represent poor-flowing.

**Table 1.2.** Densification flowability classifications [48]

Flowability	Carr index [%]	Hausner ratio [-]
Excellent	5 - 10	1.00 - 1.11
Good	11 - 15	1.12 - 1.18
Fair	16 - 20	1.19 - 1.25
Acceptable	21 - 25	1.26 - 1.34
Poor	26 - 31	1.35 - 1.45
Very poor	32 - 37	1.46 - 1.59
Very, very poor	>38	>1.60

Several densification measurement protocols are presented in the standards [104–106]. All of them share the device specification, which consists of a tapping device producing  $250 \pm 15$  taps per minute from a height of 3 mm (Fig.1.10a). The graduated cylinder size, the amount of sample and the number of taps varies according to the standard. For instance, the French standard NF 1237 [104] employs 2500 taps to estimate the tapped density of solid fertilizers. The standard ASTM D8176-18 [105] is intended to characterise activated charcoal, using 100 mL of sample and making a series of 1000 taps til the volume stabilizes. The standard ASTM D4164-13 [106] preconises 1000 taps for catalytic samples of 240 - 250 mL. The United States and the European pharmacopoeia recommend measuring the volume of the powder at 10, 500 and 1250 taps [107]. If the difference between the last two volume readings exceeds 2 mL, an additional set of 1250 taps is conducted until the difference between the last two series of taps is less than 2 mL. This characterisation is commonly simplified to fixed number of taps (e.g. 500 taps [50]) by industrials. Nonetheless, this measurement may not accurately evaluate the powder flowability at its maximal densification state and may assess it at a mid-stage, leading to less precise comparisons between samples. Further discussion on this subject can be found in Chapter 3.

Besides tapping devices, densification measurements can be performed in particle dampers (Fig.1.10b). These devices are characterised by applying harmonically driven vibrations to powders with sinusoidal waves, which differs from tapping devices' highly energetic shock waves [50, 108]. Particle dampers allow varying the amplitude and the frequency of the waves and, therefore, the supplied energy. Saker et al. [50] have shown that powder densification depends on the supplied energy to the powder, achieving different densification states according to the energy.

The way in which granular materials rearrange and compact is dependent to the amount of compaction dynamic and the energy supplied. Consequently a same sample might not have the same tapped density at 1000 taps than at 5000 taps. Granular materials reach their maximal densification state at different number of taps and energy because of interparticle interactions.

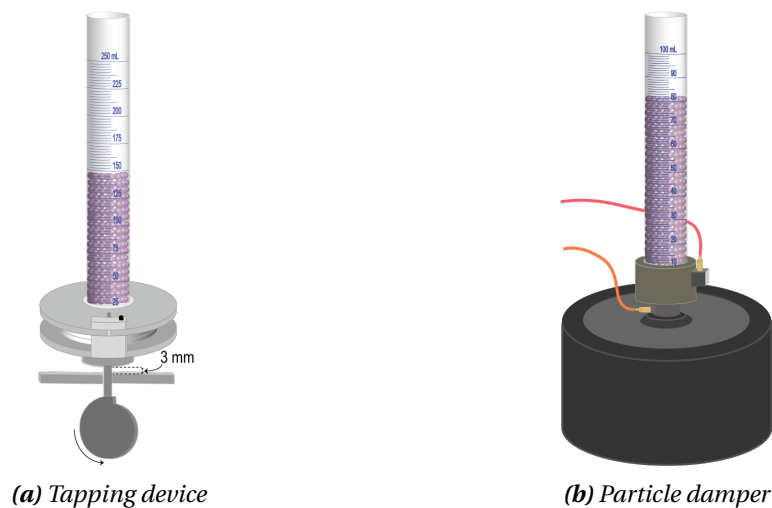


**Figure 1.10.** Densification devices.

#### 6.2.2.2. Shear tests

Based on the fact that interparticle interaction forces govern powder motion, quantifying them may allow a better understanding of their flow behaviour. The bulk adhesive forces of a powder can be characterised by a shear test, which measures the forces involved in a powder-bed plastic-failure, on the quasi-static regime.

Proposed by Coulomb in 1773, when studying the weight that a masonry pillar could withstand [109], the rigid-plastic analysis looks for the angle of the failure plain of a material submitted to normal stress. Coulomb's yield criterion is the theoretical basis of shear tests (Eq.1.10), and it relates the resistance—friction and cohesion—to the movement as follows:

$$|\tau| = \mu\sigma + c \quad (1.10)$$

where  $\tau$  is the shear stress,  $\mu$  is the friction coefficient,  $\sigma$  is the normal stress and  $c$  are the bulk adhesive interactions. Figure 1.11 depicts the plastic-rigid rupture of a granular material exposed to pre-consolidation stress ( $\sigma_{ps}$ ) which is then divided into two rigid blocks when experiencing  $\sigma_c$ .

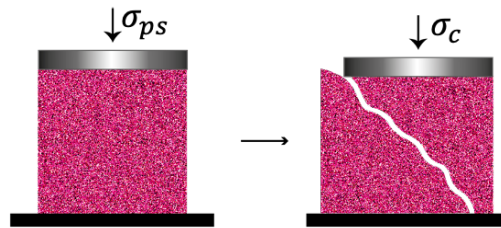


Figure 1.11. Powder rigid plastic failure: pre-shear normal stress,  $\sigma_{ps}$ , and shear normal to failure stress,  $\sigma_c$ .

Granular materials plastic-rigid analysis is characterised by multiple plastic-rigid failures, as shown in figure 1.12. Each failure, known as a failure point, corresponds to a specific couple of  $\sigma$  and  $\tau$ . The usual way to represent this state of stress is by Mohr circles. In Figure 1.12, the left side illustrates the steps of a shear test, while the right side represents the rupture points and corresponding Mohr circles.

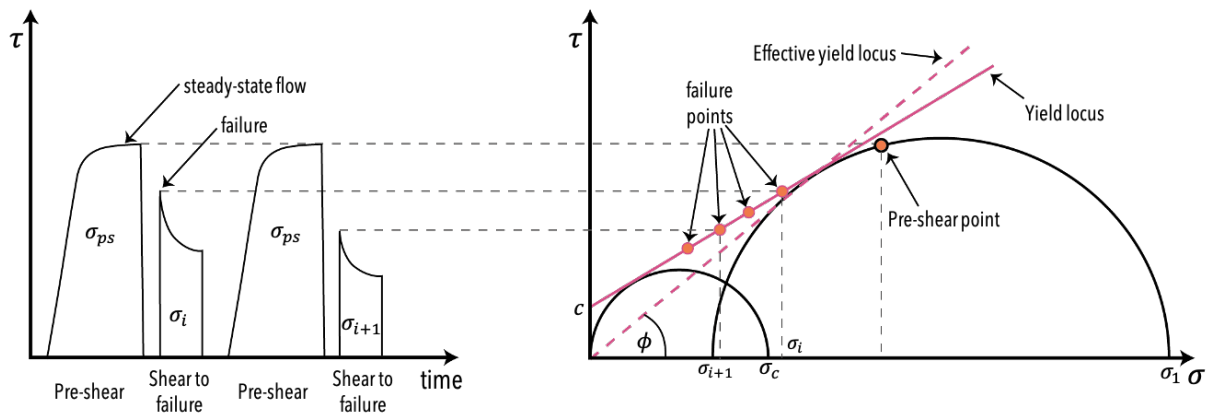


Figure 1.12. Shear test graphical representations. The left plot illustrates the shear stress ( $\tau$ ) applied overtime during the shear test. The  $\tau$  values are associated with the right graph to construct the Mohr circles, with the normal stress ( $\sigma$ ), through the failure points. The intersection of the yield locus with the y-axis represents the adhesive interactions ( $c$ ). The minor and major Mohr circle intersections with the x-axis represent the maximum compressive stress ( $\sigma_c$ ) and major principal stress ( $\sigma_1$ ).

The Mohr graphical representation is done by plotting the major Mohr circle and tracing it according to the first pre-shear,  $\tau$ , and the yield locus tangent, which is the line formed by the points of rupture. The minor circle is traced from the origin axis and the tangent of the yield locus. The point formed by the intersection of the yield locus and the y-axis represents the adhesive bulk forces,  $c$ . In addition, the right intersections of each Mohr

circle and the x-axis define the maximum compressive stress  $\sigma_c$  and major principal stress  $\sigma_1$ . The Coulomb yield criterion coupled with the Mohr circles representation is often called the Mohr-Coulomb failure model.

In 1961, Jenike [47] proposed a method to describe the behaviour of powder flow by introducing a dimensionless parameter called the flow factor,  $ff$ , as shown in Eq.1.11. This parameter has been largely used to determine the outlet dimensions for hoppers.

$$ff = \frac{\sigma_1}{\sigma_c} \quad (1.11)$$

To classify the powder flowability, the  $ff$  of a powder sample should be estimated at different consolidation states to plot the flow function (Fig.1.13). This function classifies the flowability of the powder according to the region where the flow function is placed. A powder with a flow function with high values flows better than one with lower values.

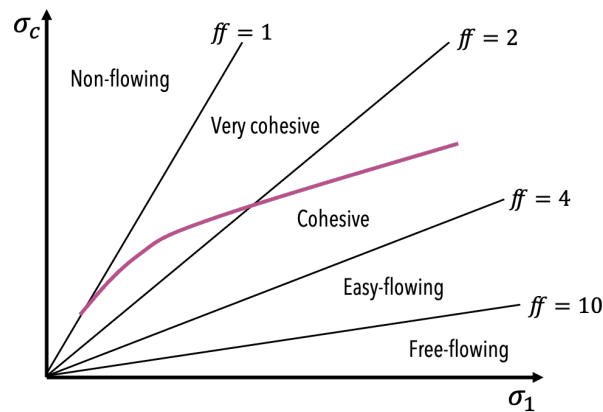


Figure 1.13. Flowability classification according to the flow function.

Since Jenike works [110], other devices [47, 75] have been developed to perform shear tests. Figure 1.14 illustrates three geometries of shear cells: translational Jenike cell, uniaxial cell, and ring cell, widely used on measuring devices.

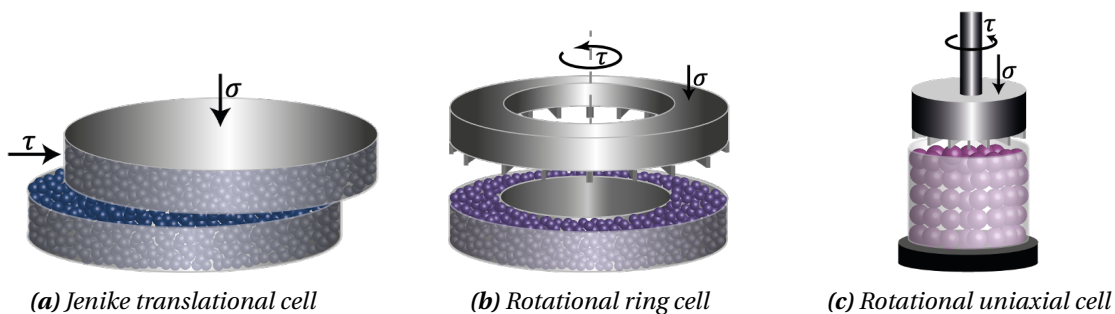


Figure 1.14. Shear test cells.

The flow behaviour classification analysis of granular materials using a shear tester measurement may be limited. For instance, the translational cells (Fig.1.14a) are limited to

the cell dimensions and unable to test samples that cannot achieve a steady state within the travel limit of the cell. In addition, Koynov et al. [60] have pointed out that shear cells are less for characterising the flow behaviour of free-flowing powders due to their high variability compared to cohesive powders. On the other hand, Cares-Pacheco and Falk [111] have suggested that highly cohesive powders may not follow the Coulomb yield criterion because the fine particles tend to agglomerate strongly. Therefore, it is difficult to achieve the steady-state flow (Fig.1.12), resulting in an inaccurate flow characterisation.

### 6.2.3. Dynamic measures

#### 6.2.3.1. Flow rate through an orifice

The powder flow rate through an orifice measures the mass of powder that flows through a specific opening over a given period. The measuring devices generally consist of a flat-ended cylinder where the outlet orifice can be interchanged, as shown in figure 1.15. This characterisation technique is intended to evaluate the flowability of powders to assess a system's efficiency and/or to ensure that powders flow through a specific equipment.

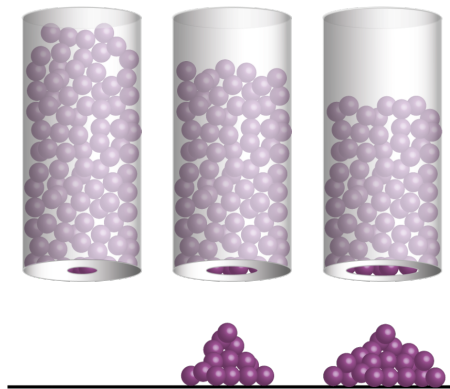


**Figure 1.15.** Flow behaviour through different orifices diameters.

Powder's flow rate can be described by the Beverloo correlation [112], an empirical equation describing the relationship between the flow rate and the orifice diameter (Eq.1.12).

$$W = C\rho_b g^{1/2} (D_o - kd)^{5/2} \quad (1.12)$$

where  $W$  is the flow rate [kg/s],  $C$  is a dimensionless function of friction, which is generally taken as 0.58,  $g$  is the gravity acceleration [ $m/s^2$ ],  $D_o$  is the diameter of the orifice [m],  $d$  is the diameter of the particles [m] and  $k$  is a dimensionless empirical coefficient. The correlation can be simplified (Eq.1.13) if the difference between  $D_o$  and  $d$  is very large, as  $(D_o - kd) \rightarrow D_o$ , then the term  $kd$  could be neglected [4].

$$W = C\rho_b g^{1/2} D_o^{5/2} \quad (1.13)$$

Several standards (ISO14629, ISO4490, ISO13517) describe this technique, most of which

use funnels with a specific orifice diameter to characterise free-flowing ceramic and metallic powders [113–115]. In contrast, commercial devices, are designed to handle larger powder samples since the orifice sizes can be modified allowing cohesive powders to flow. It is important to note that the flow ratio obtained through an orifice does not provide a flowability index for a given powder material. Instead, it serves as a means of comparing the flow behaviour of different powder samples and assessing their behaviour through each orifice.

### 6.2.3.2. Dynamic angle of repose

The dynamic angle of repose is the slope of a granular material placed in a slowly rotating cylinder with a horizontal axis and transparent walls (Fig.1.16) [29]. During rotation, the bulk reaches a maximum slope in where the particles near the surface experience a tangential force that exceeds the frictional force, for non-cohesive samples, breaking the equilibrium, inducing motion and resulting in an avalanche.

Different angles are formed by the powder-bed inside the drum during the measurement, as shown in figure 1.16a. The upper angle,  $\beta$ , is formed just when the avalanche starts to occur, and the lower angle,  $\alpha$ , is formed when the avalanche ends. For this measurement, there is a time interval between avalanches. Figure 1.16b shows the angle of repose,  $\theta$ , formed by faster rotations than the previous ones, where the gaps between avalanches are smaller, so a quasi-stable angle is obtained with a continuously flowing powder. Liu et al. [116] showed that the angles  $\alpha$  and  $\beta$  are dependent on each other, and that  $\theta$  is the average of the two. This behaviour can be compared to the variation of the static angle of repose, which also has a maximum and minimum angle.

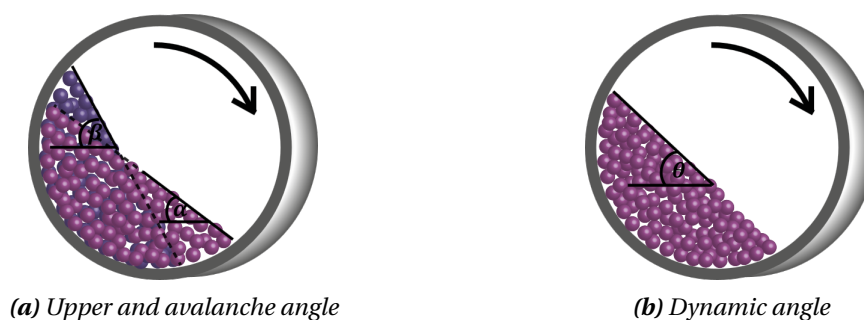


Figure 1.16. Dynamic angle measurement.

The classification of powder flowability differs from the static angle because the values of the angle categories are lower. The dynamic angle of repose seems to provide values between 3 and 10 degrees lower than the static version [101]. Still, the classification of dynamic and static angles indicates lower angles for fluid granular materials and higher angles for cohesive ones. Similarly to the static angle of repose, the lower angles indicate free-flowing materials, while the higher ones correspond to cohesive ones. In general,

both angles of repose, dynamic and static, are not intrinsic powder properties of the bulk solid. For instance, the dynamic angle of repose depends on the revolving speed and the degree of air inside the drum that might fluidize the powder-bed [47].

### 6.2.3.3. Fluidized bed

Powder fluidization is the process of suspending particles in a fluid (usually a gas) by passing the fluid through the powder bed at a velocity sufficient to overcome the weight forces and cause the particles to behave like a fluid. This process is widely used in the powder handling industry to improve powders' flowability and facilitate the handling, mixing, and storage of powders [117].

In 1973 Geldart [118] proposed a powder classification based on their fluidization behaviour. It groups powders into four categories: A, B, C and D, according to their particle size and the difference between the particle density,  $\rho_s$ , and the fluidisation fluid density,  $\rho_f$  (Fig.1.17). Type A are aerated powders with diameters varying from 40 to 100  $\mu m$ . These powders have good fluidization behaviour, expand considerably, and collapse slowly when the gas is cut off. Type B powders are coarse powders with a diameter between 40 to 2000  $\mu m$  with an intermediate fluidization behaviour, small bed expansion, and rapid collapse. Type C are cohesive powders, typically with a diameter of less than 20  $\mu m$ , with poor fluidization behaviour. C-type powders are extremely difficult to fluidize and tend to be lifted as a consolidated solid or present channelling. Type D powders are large and dense particles which need a high gas velocity for fluidization. These powders tend to deaerate fast [47].

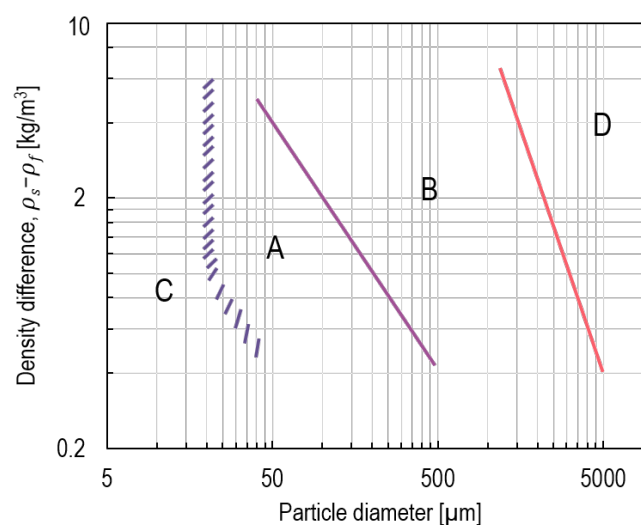


**Figure 1.17.** Geldart powder classification according to their fluidisation [118].  $\rho_s$  is the particle density,  $\rho_f$  is the fluidisation fluid density.

This "flow behaviour" section presents the main influencing factors on powder flowability and some of the most commonly used methods to evaluate it. Powder flow behaviour is critical for handling powders, but it remains poorly understood. Unlike liquids, no universal law could describe their powder flow behaviour. Therefore, it is essential to continue studying it to deepen our understanding. This state-of-the-art provides a starting point for the present, which aims to deepen the understanding of the factors that influence flow behaviour and improve it through flow additives.

## 7. Dustiness

Before defining dustiness, some terms should be defined. What is dust? According to the World Health Organization (WHO) [119], dust is composed of solid particles with sizes below  $100\ \mu\text{m}$  that can be dispersed in the air—airborne particles—also known as aerosols [120]. Unlike flowability dustiness definition is well established. The standard EN 1540 defines it as “the propensity of materials to produce airborne dust during handling” [120].

In industrial granular matter processing, airborne particles are released during industrial processes such as granular materials extraction, transport, mixing, sieving, or any operation involving mechanical solicitation [121]. Schneider et al. [122] established four exposure sources specific to nano-objects dust release that could also be applied to powders. The first is synthesis, which produces powders from raw materials or chemical reactions. The second and third involve handling manufactured bulk materials and intermediate products. The fourth one specifies the handling of finished products covered by nanomaterials. These exposure sources show that airborne particle emission can be found throughout the entire production chain during powder handling.

From a technological point of view, dustiness can be seen as an end-use property because it leads to process feasibility issues such as cross-contamination, product loss, filter clogging and process safety issues such as the risk of fire and explosion. However, dustiness is commonly related to occupational exposure and most dustiness indexes—the ratio of the mass of emitted particles in [mg] and sample mass in [kg]—are based on the region where the particles are deposited in the respiratory system. As shown in figure 1.18.a, each fraction indicates where the airborne particles are deposited: the inhalable fraction is “the mass fraction of total airborne particles which is inhaled through the nose and mouth” [120]; the thoracic fraction represents the particles that penetrate the respiratory tract after the larynx; and the respirable fraction to those that reach the alveoli.

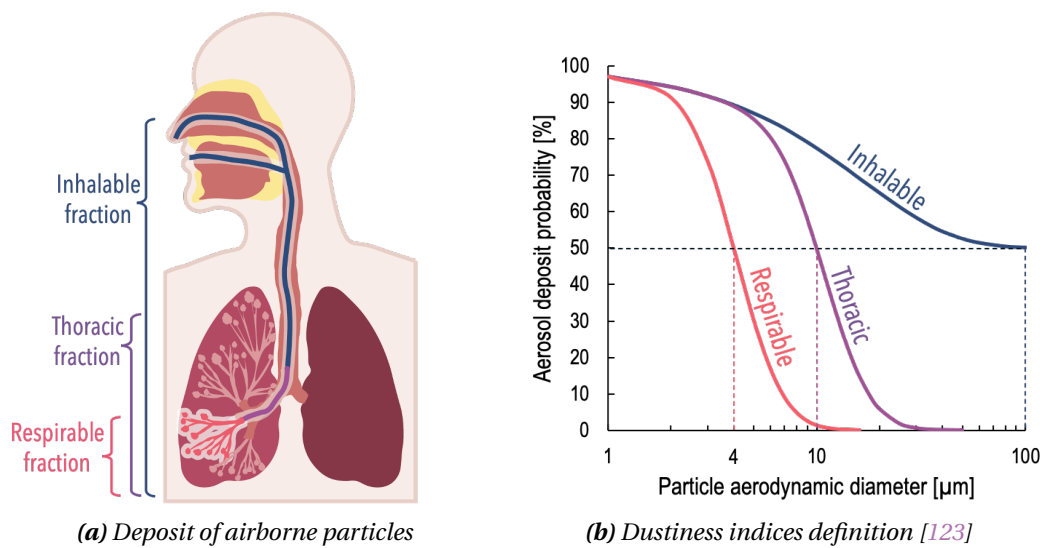


**Figure 1.18.** Dustiness fractions.

Dustiness indices also represent the average probability of airborne particles reaching a specific region of the respiratory tract. For instance, Figure 1.18b, illustrates a 50% chance of: 100  $\mu\text{m}$  particles being inhaled; 10  $\mu\text{m}$  particles being deposited in the thoracic region; and 4  $\mu\text{m}$  particles reaching the alveoli [123].

The inhalation of airborne particles can cause undesirable consequences for employees' health [124]. For example, Baker's asthma caused by the inhalation of wheat flour is the most common type of occupational asthma in France and is among the first types in most European countries [125]. This well-known disease affects 44.5% of bakers, according to a study of bakeries in Poland [126]. A similar occupational disease caused by inhalation of crystalline silica is silicosis which causes chronic inflammation and pulmonary fibrosis [127]. Other studies on occupational inhalation of industrial dust have shown that workers exposed to cement aerosols lower their lung function parameters [128]. A review that focused on reactions to food powder dusts highlighted that workers inhaling fish, seafood, soybeans, eggs, grains, and chicken, and other powdered foods, had respiratory manifestations ranging from rhinitis to asthma [129]. Studies have found that dust exposure can generate serious health consequences depending on the nature and size of the powder [25, 128–130]. Because to the health consequences, some dust exposures are regulated or the subject of strict recommendations. In France, from 2023, the average concentrations of total and respirable dust must not exceed 4 and 0.9  $\text{mg}/\text{m}^3$ , respectively [131]. In addition, there are specific limit values for some particular powders: for crystalline silica, the limit in the respirable fraction is 0.1  $\text{mg}/\text{m}^3$  while for wheat flour it is 0.5  $\text{mg}/\text{m}^3$  [132, 133]. In the case of wheat flour, a study from the United States Centers for Disease Control and Prevention (CDC) showed that the actual exposure concentration was above the limit (between 1.03 and 8.21  $\text{mg}/\text{m}^3$ ) in the inhalable fraction [132]. Despite regulations, protective measures can be insufficient to protect workers [133].

## 7.1. Factors influencing powder dustiness

### 7.1.1. Particle size and shape

The effect of particle size distribution on dustiness has been widely studied, but the conclusions are powder-related and no general conclusion can be drawn [134–137]. Some researchers show that smaller particles emit more dust than larger ones [134, 136] while others have found the opposite [135]. Plinke et al. [138] conclude that the impact of size was high for particles between 20 and 40  $\mu\text{m}$  and decreased for larger (insufficient amount of fine) and smaller (highly cohesive) particles. This behaviour was explained by the increase of cohesive forces on the smaller particles; in coarse ones, the content of the fine particles is not enough to emit airborne particles. In addition, the amount of fines in a granular material seems to increase the dust generation up to a certain level [135, 139]. In contrast, other study found no relation between dustiness and particles size distribution in some samples [136]. In addition, grains morphology has been shown to influence dustiness, where irregularly shaped particles are dustier than regular ones [137]. For instance, Hjemsted and Schneider [140] showed that flaky-shaped particles emit more dust than spherical ones.

The influence of particle size and morphology can be explained by the forces acting on particle sedimentation in laminar regime [141]. Figure 1.19 shows the forces acting on an airborne particle, allowing it to be dispersed in the air for more or less time.

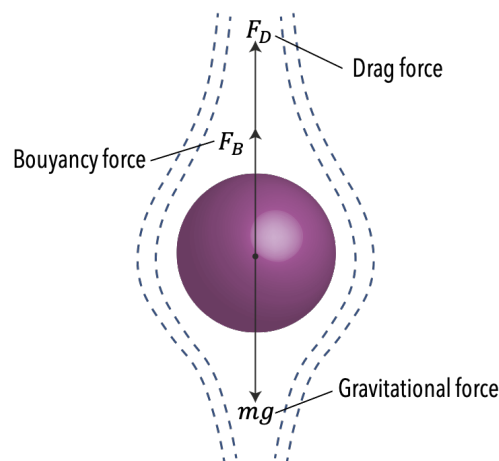


**Figure 1.19.** Forces acting on the sedimentation of an airborne particle [141].

The stability of a dispersed particle depends on its sedimentation, or falling velocity, which is described by equilibrium of the forces acting on the particle:

$$F_G = F_D + F_B \quad (1.14)$$

where  $F_G$  is the gravitational force,  $F_D$  is the drag force and  $F_B$  is the Bouyancy force. This last is often neglected since the density of the air is so much less than the particle density. Then the equation balance gives:

$$mg = 3\pi d\mu v_s \quad (1.15)$$

where  $m$  is the mass of the particle,  $g$  the gravity acceleration,  $d$  is the particle diameter,  $\mu$  is the air viscosity and  $v_s$  is the sedimentation velocity. If the mass is expressed in terms of the particle density,  $\rho$  and volume the resulting expression is:

$$\frac{\pi}{6}d^3\rho g = 3\pi d\mu v_s \quad (1.16)$$

Clearing up the sedimentation velocity:

$$v_s = \frac{d^2\rho_p g}{18\mu_{air}} \quad (1.17)$$

From equation 1.17, the influence of the size of the particle is shown because if the size of the particle decreases, the falling velocity will decrease, allowing a more stable dust cloud. For the case of morphology, the dynamic shape factor ( $\phi$ ) can be included in the equation denominator 1.17.  $\phi$  ranges from 1 for spheres to 2 for irregular particles (Table 1.3). According to the particles shape, when  $\phi$  increases, the  $v_s$  decreases. This theoretical demonstration shows the influence of particle size and morphology on dust emission. However, dust generation is a more complicated phenomenon influenced by various factors, making the experimental results vary from the theoretical ones, as already discussed above.

**Table 1.3.** Dynamic shape factor of aerosol particles (taken from [141]).

Shape/type	Shape factor $\phi$
Sphere	1.00
Fibre	1.07 - 1.32
Quartz dust	1.36
Fused alumina	1.04 - 1.49
Talc	2.04

### 7.1.2. Relative humidity

Due to its well-known impact on powder handling, the influence of RH on dustiness has been widely studied. Air humidity can act as a binder or lubricant, changing capillary forces. It can be expected that high moisture content decreases dust generation due to the formation of liquid bridges. However, the scientific literature shows that the behaviour of powders towards water depends on the powder. Some authors have found a reduction in inhalable particles emission at high RH [142, 143] while others have found the opposite [138, 144]. Lopez-Lilao et al. [145] showed an interesting powder behaviour towards water, where dustiness rose with the increase of sample RH conditioning until reaching a critical point above which the dustiness started to decrease depending on the type of powder sample.

## 7.2. Dustiness measuring methods

Dustiness methods are composed of two main steps. The first is dust generation which, generally simulate an industrial process by supplying mechanical solicitation to a powder sample. The second is sampling the generated dust which measures and recover the amount, concentration, size, and other information from the emitted particles. This section presents the dustiness measurement methods developed over the years and four standardized methods.

### 7.2.1. Dustiness methodologies development

Since 1922 dust generation characterisation has been a subject of study to predict dustiness in powder handling [146]. A plethora of devices have been developed over the years, basing dust release on the unit operation action. One of the most common simulated operations is powder pouring, used in granular materials transfer, dosage, and weighting, among others. The first dustiness measurement device was developed by Andreasen et al., [147] which consisted of a single drop tester that measured the time required for the material to fall into collection plates. The ASTM D547-41 [148], which remained in force until 1986, was the first standard to describe a dustiness method. It was a single drop test to characterise coal and coke dust emissions. This method involved recovering (weight) the emitted particles onto an upper and a downward slide to recover the fine and coarse particles. In 1989, Cowherd et al. [144] proposed the MRI tester (drop-tester), which evaluates the airborne particles emitted by a beaker filled with the sample that titles continuously. An airflow transports the aerosol, and the particles are recovered into a filter. The first rotating drum (RD) tester was proposed by Cooke et al. [149] in 1979 using a cascade impactor, to characterise dust. Twenty years later, a European project developed a single continuous drop (CD) tester connected to a RD, where dustiness was measured by the particles recovered in polyurethane foams [150].

In all methods proposed before 2005, a significant amount of powder is required. Therefore, the use of high-cost raw materials makes their dustiness measurement expensive, which is the case of many active pharmaceutical ingredients (API). Thus, Boundy et al. [151] introduced the venturi aerosolization technique, which evaluates the dust generation of 5 mg of sample. The sample is placed in a holding jar connected to a sealed chamber. An airflow passes through the tube, dispersing the particles into the chamber. The airborne particles are collected into a respirable filter attached to a cyclone and in a closed-face filter (inhalable fraction). A more recent study uses the powder rheometer FT4 to determine the amount of particles emitted during mechanical and aerated fluidization of a powder bed [152]. Airborne particle emission is determined by the change of mass in the powder bed.

### 7.2.2. Standard methods

Figure 1.20 presents a synthesis of dustiness characterisation methods that will be discussed. Although industrial powders emit dust, dustiness characterisation remains relatively uncommon in the industry, which is why the industrial applications were not included in the figure, as in the flowability one (Fig. 1.5). Typically, industrial powder dustiness is evaluated by occupational safety entities such as the French National Institute of Research and Security (INRS), where this thesis was conducted.

Regime	Dynamic			
Method	Rotating drum 	Continuous drop  53 L/min Airflow 50% RH	Vortex shaker 	Small rotating drum 
Dust generation	Avalanches	Continuous drop	Agitation	Avalanches
Dustiness index	<ul style="list-style-type: none"> <li>▪ Inhalable fraction</li> <li>▪ Thoracic fraction</li> <li>▪ Respirable fraction</li> </ul>	<ul style="list-style-type: none"> <li>▪ Inhalable fraction</li> <li>▪ Respirable fraction</li> </ul>	<ul style="list-style-type: none"> <li>▪ Respirable fraction</li> <li>▪ Size distribution</li> <li>▪ Concentration</li> <li>▪ Dust sampling</li> </ul>	<ul style="list-style-type: none"> <li>▪ Respirable fraction</li> <li>▪ Size distribution</li> <li>▪ Concentration</li> <li>▪ Dust sampling</li> </ul>
Standards	<ul style="list-style-type: none"> <li>▪ NF15051-2</li> <li>▪ NF17199-2</li> </ul>	<ul style="list-style-type: none"> <li>▪ NF15051-3</li> <li>▪ NF17199-3</li> </ul>	<ul style="list-style-type: none"> <li>▪ NF17199-5</li> </ul>	<ul style="list-style-type: none"> <li>▪ NF17199-4</li> </ul>

Figure 1.20. Synthesis of the standard dustiness characterisation methods.

The rotating drum and continuous drop method are described in the standard **NF 15051: Workplace exposure - Measurement of the dustiness of bulk materials**. Both techniques generate dust by dropping the powder sample. They differ from each other in, the dropping process intensity and duration.

#### 7.2.2.1. Rotating drum (RD) - NF 15051-2

In this method, dust generation is created by the rotational movement of a drum involving a continuous multiple dropping of the sample (Fig.1.21). The protocol consists of adding 35 cm<sup>3</sup> of sample on a 300 mm diameter stainless-steel drum with eight longitudinal vanes that enable the sample's recollection and drop. The drum rotates at 4 rpm for 60 seconds. A particle-free airflow at 38 L/min transports the airborne particles to the drum outlet [153]. The dust is recovered in two metallic foams - 20 pores per inch (ppi) and 80 ppi - and a terminal filter made of glass fibers (Figure 1.21). The weighted samples on the selective foams and filter are used to determine the sample's inhalable (Eq.1.18), thoracic (Eq.1.19), and respirable (Eq.1.20) mass fractions.

$$w_I = \frac{\Delta m_{20} + \Delta m_{80} + \Delta m_f}{m_s} \quad (1.18)$$

$$w_T = \frac{\Delta m_{80} + \Delta m_f}{m_s} \quad (1.19)$$

$$w_R = \frac{\Delta m_f}{m_s} \quad (1.20)$$

with  $w_I$  the inhalable,  $w_T$  thoracic and  $w_R$  respirable indexes expressed in [mg/kg]. The subindexes 80, 20 and  $f$  design the foam filters and glass fibre filter mass recovered in [mg], while  $m_s$  is the sample's mass in [kg].

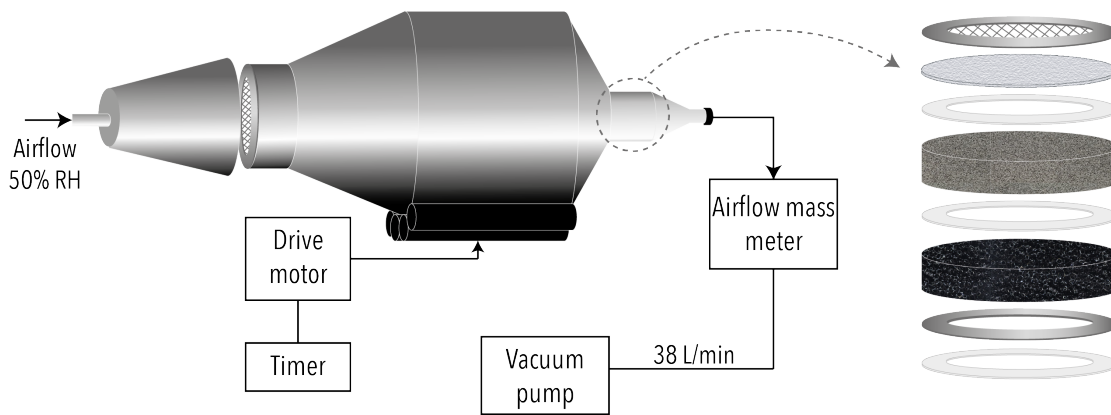


**Figure 1.21.** Rotating drum device (EN 15051-2 [154]).

The standard classifies dustiness according to four categories per fraction as shown in table 1.4. The airflow humidity during the test and the sample conditioning should be controlled at 50% RH according to the standard. The test procedure must be performed at least three times, and the relative standard deviations of their average must be <10%.

**Table 1.4.** Dustiness classification for rotating drum standard EN 15051-2 [154].

Dustiness category	Mass fractions [mg/kg]		
	Inhalable, $w_I$	Thoracic, $w_T$	Respirable, $w_R$
Very low	<300	<80	<10
Low	300 - 650	80 - 300	10 - 60
Moderate	650 - 3000	300 - 1000	60 - 210
High	>3000	>1000	>210

### 7.2.2.2. Continuous drop (CD) - NF 15051-3

This method measures the inhalable and respirable fraction of a powder sample dropped at a specific rate for a period of time. The continuous drop (CD) device is composed of a stainless-steel cylinder with an inner diameter of 150 mm. On top of it, a feeder with a

drop pipe with an inner diameter between 16 – 25 mm control the sample flow rate from 6 to 10 g/min for 10 minutes. During the powder drop, the cylinder has an upward vertical airflow of 53 L/min at 50%RH (Fig.1.22).

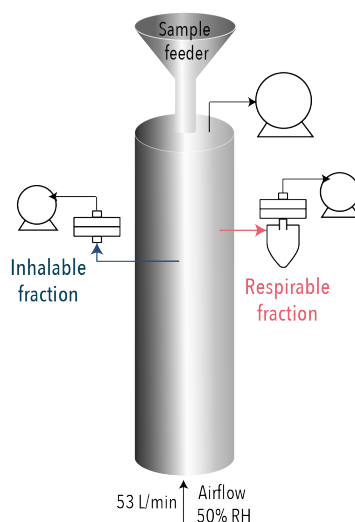


**Figure 1.22.** Continuous drop device (EN 15051-2 [155]).

The dustiness fractions are collected in different cylinder parts on preweighted filters or filter thimbles to prevent overloading. Inhalable and respirable fractions are calculated using equations 1.18 and 1.20, and their classification differs from the RD, as shown in table 1.5. The test procedure must be performed five times.

**Table 1.5.** Dustiness classification for continuous drop standard EN 15051-3 [155].

Dustiness category	Mass fractions [mg/kg]	
	Inhalable, $w_I$	Respirable, $w_R$
Very low	<1000	<20
Low	1000 - 4000	20 - 70
Moderate	4000 - 15000	70 - 300
High	>15000	>300

The standard **NF 17199: Workplace exposure - Measurement of dustiness of bulk materials that contain or release respirable NOAA and other respirable particles**, specifies the dustiness characterisation for Nano-Objects and their Aggregates and Agglomerates, also known as NOAA. NOAA size raises the question of whether the traditional way of characterising them is adequate. Therefore, in addition to quantifying the mass fractions (NF 15051 [154, 155]), real-time measurements are performed to quantify the particle concentration, size distribution, and physical aspect [156]. These measures are carried out only taking into account the respirable fraction particles, which are selected by a cyclone in the inlet of each device to remove larger particles and prevent

overloads [157].

The **number of emitted particles** during the dust generation is quantified using a condensation particle counter (CPC) [153]. This device creates an ethanol vapor that condenses into the particles' surface, making them "grow" in size to be able to identify them and counted then optically (Fig.1.23a). The CPC detects particles with a mean size between 10 nm to 1  $\mu m$  and an aerosol concentration of 0 - 100000 particles/ $cm^3$ . The particles emitted are counted for 60 seconds, and then the number-based dustiness index ( $I_{VS}$ ) is calculated as follows:

$$I_{VS} = \frac{1}{m_s} \times \sum_{t_1}^{t_1+60} C_{CPC}(t) \times Q_{VS} \times \Delta t_{CPC} \quad (1.21)$$

where  $I_{VS}$  is the number-based dustiness [ $\#/mg$ ],  $C_{CPC}$  is the particle number concentration measured by the CPC [ $\#/cm^3$ ],  $\Delta t_{CPC}$  in the measuring step [ $s$ ] and  $Q_{VS}$  the airflow rate [ $cm^3/s$ ].

The aerosol **number-based particle size distribution** ( $PSD_{ELPI}$ ) is assessed using an electrical low-pressure impactor (ELPI) [158]. This instrument charges the particles electrically and collects them into different impaction stages according to their aerodynamic diameter, as shown in figure 1.23b. The current measured at each impaction stage enables the number-based  $PSD_{ELPI}$  to be estimated. This instrument detects particles from 10 nm up to 10  $\mu m$ . The  $PSD_{ELPI}$  is calculated as follows:

$$f_n(d_i) = \frac{n_{i,VS}}{n_{tot,VS}} \times \frac{1}{\Delta \log(d_i)} \quad (1.22)$$

where  $i$  represents the channel in which the particles are counted,  $d_i$  represents the equivalent aerodynamic diameter of the  $i$ -channel,  $n_{i,VS}$  is the number of particles in the  $i$ -channel accumulated in 60 seconds,  $n_{tot,VS}$  is the total number of particles accumulated in all channels during the same 60 seconds, and  $\Delta \log(d_i)$  is the width of the  $i$ -channel of the ELPI (15 channels).

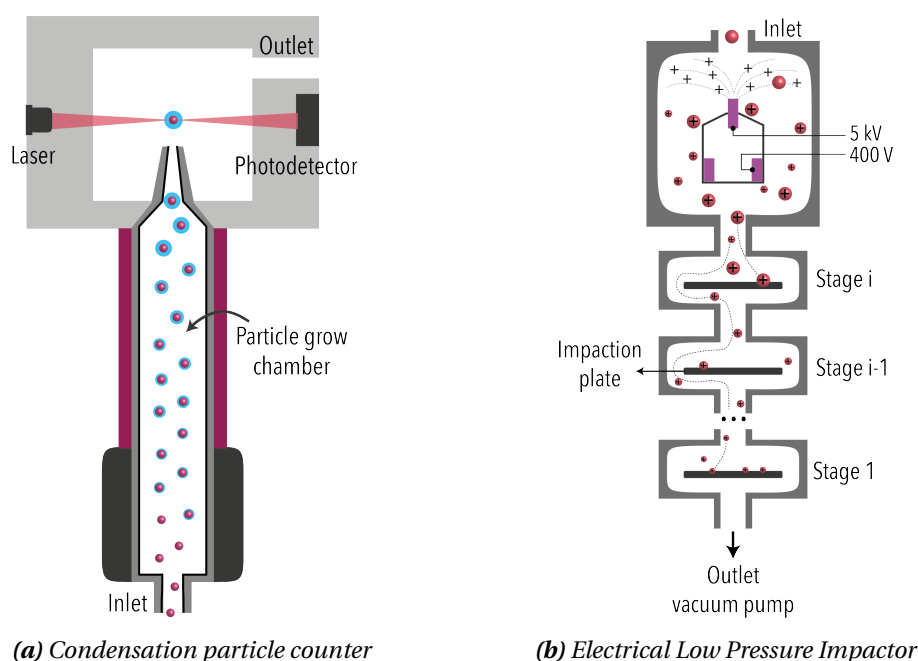


**Figure 1.23.** Real-time measuring devices.

Dust **shape and chemical nature** are studied by analysing airborne particles on a transmission electron microscope with X-ray fluorescence (TEM). The airborne particles are collected on 400 mesh copper TEM grids covered with a carbon film, which are placed on a mini particle sampler (MPS), see figure 1.24. Developed by The French National Institut of Industrial Environment and risks (INERIS) to make the particle collection simple, fast and versatile [159, 160]. This TEM grid holder works at low airflow rates, between 0.3 and 1 L/min, to protect the fragile TEM grids.

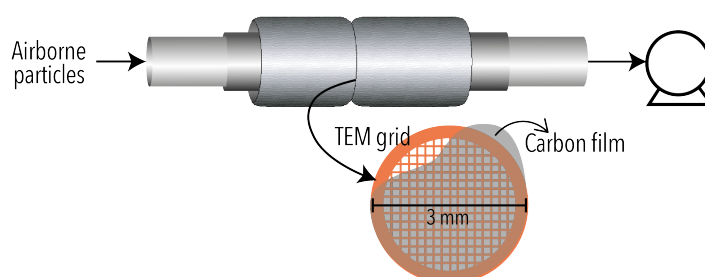


**Figure 1.24.** Mini particle sampler.

### 7.2.2.3. Vortex shaker - NF 17199-5

The vortex shaker (VS) device is composed of a stainless-steel cylindrical tube with an internal diameter of 31 mm and a volume of  $102 \text{ cm}^3$ . A sample volume of  $0.5 \text{ cm}^3$  is introduced, and the tube is mechanically agitated through orbital motions on the horizontal plane, with a displacement amplitude of 4 mm and a rotational speed of 1850

rpm. The airborne particles are transported to the sampling line using a filtered airflow of 4.2 L/min and pre-selected by a cyclone connected to a regulated pump to recover only the respirable fraction on the filter. The sampling line can be assembled in two configurations presented in figure 1.25. The first one (Fig.1.25a) consists of collecting the respirable mass fraction on a filter to determine  $w_R$  (Eq.1.20). In the second configuration (Fig.1.25b), the respirable fraction is divided using a flow splitter allowing the two real-time measurements - CPC and ELPI- and the collection of the third part of the aerosol on TEM grids - MPS [161].

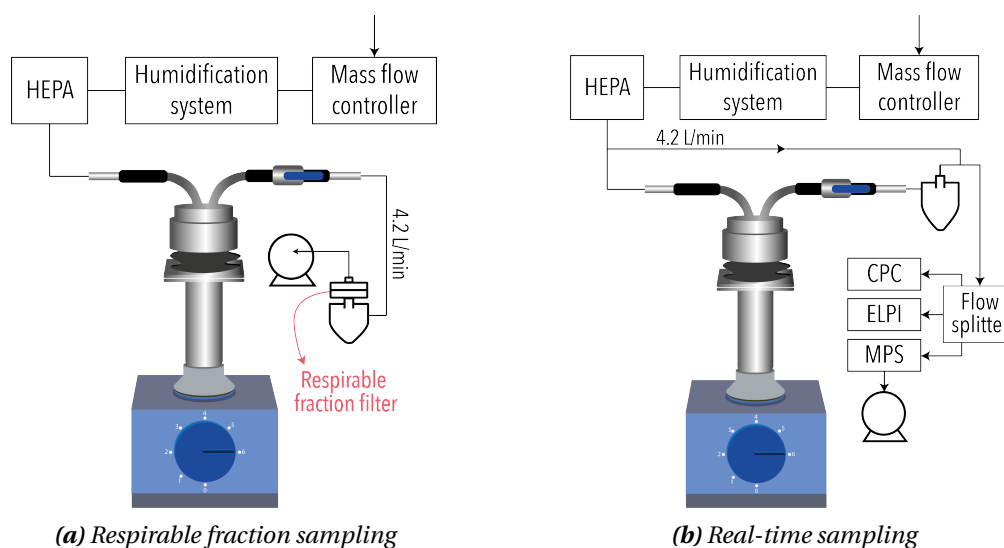


Figure 1.25. Vortex shaker method sampling configurations.

#### 7.2.2.4. Small rotating drum - NF 17199-4

As with the RD, dust generation in this method is produced by the multiple drops of the sample due to the small rotating drum (SRD) rotation [162]. The SRD is composed of a stainless-steel cylindrical drum with an internal diameter of 16.3 cm and a length of 23 cm. The drum has three longitudinal vanes that enable the sample recollection and drop. This method allows the characterisation of the aerosol emitted from 2 – 6 g of sample with the same sampling configurations as the VS (Fig.1.25), the respirable fraction and the real-time sampling.

The standards 17199-2 [163] and 17199-3 [164] describe the RD and CD methods for the characterisation of NOAA dust. These standards add the real-time measurement configurations shown in the VS and SRD versions adapted to the RD and CD, keeping the mass fractions measures specified on the standards 15051-2 [154] and 15051-3 [155].

The “dustiness” section highlights that the study of dust emission has been primarily focused on developing measuring methods and characterising raw materials since the 1920s. This state-of-the-art reveals a subject of study in the dust emission field, which is the effect of flow additives on the dust emission of powders, which is one of the aims of the present work.

## 8. Flowability and dustiness: what do we know?

Flowability and dustiness can be taken as the same property, in the sense that both represent the ability of a granular material to be in motion. Flowability describes the motion as a “liquid” and dustiness as a “gas”. Both end-use properties are not intrinsic properties of powders, being influenced by multiple parameters. Even if both are related to particle motion, their relationship is poorly studied. Cowherd et al. [144] relate the dustiness of 14 samples measured in an MRI tester with flowability using the AoR. Their results showed that powders with smaller AoR aerosolized more easily. Another similar study of the same year (1989) showed no correlation between the AoR and dustiness [165]. A more recent work characterised 27 powder samples using a CD tester and HR to evaluate flowability [145]. Their results showed that the relative particle emission increases with flowability, but the authors clarify that this does not necessarily mean that dustiness increases. From these studies, there is no clear relation between flowability and dustiness.

## 9. Conclusions

The first part of this chapter discusses the general background of granular matter terms and their motion behaviour. Powders can behave in the three states of matter because of the motion that experiences their particles. Their behaviour depends on the applied stress, the powder properties and the interparticle interactions. This part exhibits the complexity of powders and the study of their motion, as there is no universal law to predict their motion behaviour.

In the next part of the chapter, flowability and dustiness are defined, and the influence of intrinsic properties and environmental conditions are discussed, along with some of the most employed characterisation devices. These two terms describe the ability of the powder to move like a liquid or a gas. The particle and environmental characteristics influence flowability and dustiness, making their measurements complex. Consequently, over the years, a part of the research on the domain has been devoted to developing measuring techniques. The development of these techniques is done based on the stresses that are applied to powders through handling unit operations. No matter if flowability or dustiness is characterised, the different measuring devices generally provide different information, and their results are not easily comparable.

The chapter concludes with a small section presenting all the found research intended to relate the flowability and dustiness. It highlights the lack of information, as just three references were presented, two were in agreement at a certain level, and the third had no relevant results. From these results the relation between flowability and dustiness is not clear.

This state-of-the-art gives the bases for a better understanding of the research presented in this work. In addition, it highlights the interest in deepening the research in some almost unexplored areas of the domain that may contribute to the study of granular matter and their industry handling.



# 2

## Materials and methods

---

### 1. Introduction

In this chapter, we introduce the powders and flow additives used in our research and the formulation protocol based on the surface covered by the flow additives. As discussed in Chapter 1, the properties of powders, such as size and shape, have a significant impact on powder motion behaviour. Therefore the methods used to describe the physical properties of particles are also presented in this chapter. The selection of each characterisation method was based on the reasoning that aimed to extract conclusions that allow us to understand better the powders' motion behaviour. Moreover, a detailed description of the implemented protocols to assess the powders' flow behaviour and dust emission is provided. In particular, we have selected three flowability methods to describe powder flow behaviour in the quasi-static and dynamic regimes. For dustiness characterisation, we have chosen two standard methods to describe our sample's dust emission.

### 2. Powders

The granular matter is ubiquitous in daily life and present in various industries. The selection of the powders employed in this work sought to represent powders with different physical properties and different industries. This choice aims to facilitate the statement of broad conclusions without focusing on a single process or use. Four powders were chosen: microcrystalline cellulose, wheat flour, joint filler and glass beads. This chapter section describes each of the selected materials, highlighting their use and importance in their industry. We will refer to these powders as host powders/particles (HP).

#### 2.1. Microcrystalline cellulose

Microcrystalline cellulose (MCC) is an organic material used in multiple industries with a global market size of US\$ 1.2 billion in 2021 [166]. It is one of the most common

excipients in solid dosage forms used in the pharmaceutical industry, as it improves powders' compressibility, flowability and uniformity of ingredients content [167]. In the food industry, MCC is used as an anti-caking agent, bulking agent, and texturizer in various food products, including baked goods, processed meats, and dairy products [168]. In addition, MCC acts as a thickener, binder, and emulsion stabilizer in cosmetic products [169].

Considering the high use of MCC in multiple industries as well as its use in research, its inclusion in the present study was evident. In this work, we employed Avicel<sup>®</sup> PH102 (AP) from FMC Biopolymer<sup>®</sup>.

## 2.2. Wheat flour

Wheat flour (WF) is a widely used ingredient in the food industry, particularly in producing baked goods, pastries, pasta, and pet food. WF market size value reached US\$ 241 billion in 2022 [170]. We opted to work with an artisan-made Type 45 WF from the Poinignon flour mill (Fouigny, France). By choosing an artisanal WF, we ensured that no additives had been added to improve WF flow properties.

## 2.3. Joint filler

Joint fillers (JF) are used in the construction industry for filling gaps or joints between two surfaces. The market size of joint compounds in the construction industry reached US\$1.87 billion in 2021 [171]. In the present study, we work with a commercial JF from MAPEI<sup>®</sup> intended to grout tiles and finish walls.

## 2.4. Glass beads

Glass beads (GB) are used in various industries for different applications, such as shot peening, sandblasting, and reflective coatings. Besides, GB glass beads properties (spherical, smooth, hard particles) are used as "model materials" to study granular flows. Its market size depends on the use and is not specific to the material itself. The market size of GB varies according to their industrial applications. For example, GB is a type of retro-reflective material, which market size was valued at US\$5.6 billion in 2018. [172]. In the present thesis, we use Spheriglass<sup>®</sup> 3000-E from Potters<sup>®</sup> Industries LLC, which are intended to be used for highway safety marking.

## 2.5. Lactose

Lactose is a type of sugar found in milk and dairy products. It is an important ingredient in food as a bulking agent and a flavor enhancer. In the pharmaceutical industry, it works as a filler and binder to create tablets with evenly distributed active principles. The lactose market size was valued at US \$2 billion in 2022 [173]. The employed lactose was RetaLac<sup>®</sup>, a co-processed hypromellose/lactose-based excipient produced by MEGGLE, composed by equal parts of a K-type hypromellose polymer and  $\alpha$ -lactose monohydrate. RetaLac<sup>®</sup> is

designed as an excipient for direct compression and dry granulation of modified-release formulations. This powder was only used in the first experimental analysis (Chapter 3). It was not employed in the rest of the work since it was decided to work just with one pharmaceutical excipient, the microcrystalline cellulose.

### 3. Silica nanoparticles

Six S-NP, known as flow additives from Evonik<sup>®</sup>, were chosen based on the industrial expertise of the research team. In the first part of the work, the selection criterion was based on the behaviour towards water. Therefore, four references of precipitated silica SIPERNAT<sup>®</sup> were chosen, two hydrophilic, 500LS and 50S, and two hydrophobic, D10 and D17. In addition, to study the effect of the physical aspect (shape) of S-NP two references of AEROSIL<sup>®</sup>, fumed silica, were selected, R972 (hydrophobic) and A300 hydrophilic). SIPERNAT<sup>®</sup>s presents pop-corn-like structures and AEROSILs chain-like structures (Fig. 2.6).

Evonik preconises each of its references for specific uses. For instance, R972 and 500LS are recommended as flow aids in powders and thickeners in liquid systems, while D10 and A300 are suggested for liquid systems as a defoamer and for rheological control, respectively. 50S is normally for improving powder flowability, and D17 is used as an anticaking agent in fire-extinguishing powders. However, their use in industry and research varies from the Evonik's recommended use. For example, Müller et al. [77] employed various Evonik S-NP references, including D10 and 500LS, to study flow enhancement on pharmaceutical powders.

### 4. Powders mixtures and surface coverage

S-NP are generally added to product formulations using a standard mass fraction between 0.5% and 2% wt. This work evaluates the S-NP action based on the HP surface coverage (SC). Therefore, S-NP+HP mixtures are defined in two ways. The first is the traditional one, based on a mass fraction, and the second is according to the surface covered by the S-NP. The methodology of S-NP+HP mixtures based on the SC is explained below.

To evaluate how S-NP cover the HP, mixtures with a known mass fraction were prepared and mixed for 10 min at 67 rpm in a 3D shaker mixer (Turbula<sup>®</sup> T2E, WAB), using a single-use bottle to avoid cross-contamination. To estimate the surface coverage at 0.5% wt HP/S-NP Scanning Electron Microscopy (SEM) micrographs were analysed using ImageJ, as shown in figure 2.2. The SEM micrographs were first thresholded to highlight the S-NP over the HP (Fig.2.1b). Then, the freehand selection tool was used to manually select the analysis area to avoid producing misleading data due to HP topography, also highlighted by the threshold (Fig.2.1c). The selected area was the broadest possible, if

needed the HP rugosities (topography) were excluded from the analysis. The size and the surface coverage of S-NP of the selected area was determined using ImageJ analyse Particles tool. Four micrographs per sample were analysed to limit subjective image treatment choices.

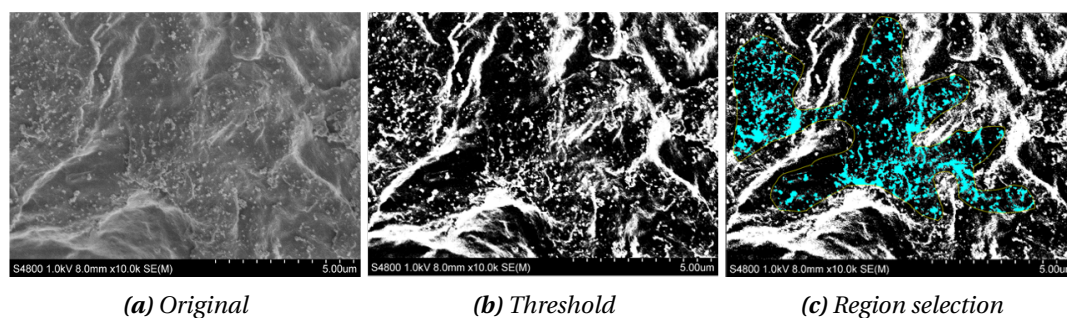


**Figure 2.1.** Surface coverage evaluation treatment.

From figure 2.2, it can be seen that HP appear to be better covered when mixed with hydrophobic S-NP (first and third rows) compared to hydrophilic S-NP. The image treatment allowed to quantify the SC (Table 2.1) and the a size characterisation of the S-NP covering the HP. The average size for the smallest aggregates observed was  $27 \pm 2$  nm; this category of aggregates accounts for less than 6% of the S-NP. This size range could indicate that a negligible part of S-NP are in their primary particle form. All S-NP median size ( $Dv50$ ) was between 35 and 60 nm. Discretization over this range was impossible due to software limitations.

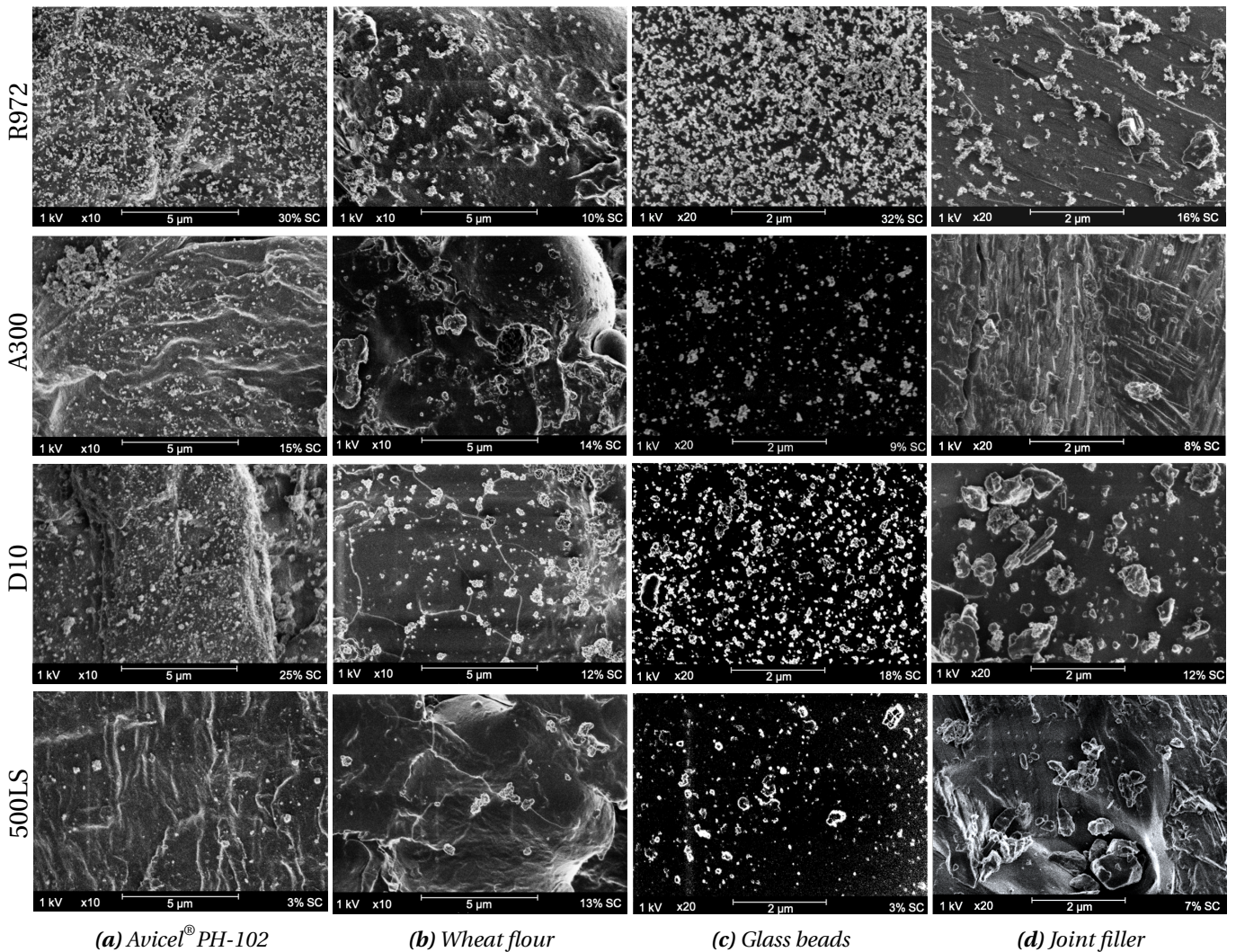


**Figure 2.2.** SEM micrographs of powders mixed with 0.5% wt of AEROSIL R972 (first row), AEROSIL 300 (second row), SIPERNAT<sup>®</sup> D10 (third row) and SIPERNAT<sup>®</sup> 500LS (fourth row)

**Table 2.1.** Surface coverage percentage of mixtures with 0.5% wt. of S-NP [%]

S-NP HP	R972	A300	D10	500LS
Avicel <sup>®</sup> PH-102	30	15	25	3
Wheat flour	10	14	12	13
Joint filler	16	8	12	7
Glass beads	32	9	18	3

The values presented in table 2.1 allowed to estimate the mass fraction required to achieve the SC of each NP/HP combination by proportionality. Figure 2.3 illustrates Avicel<sup>®</sup> PH-102 mixed with each S-NP to cover 40% of its surface. Mixtures of this HP with D10, R972 and A300 exhibited the expected SC with mass fractions ranging between 0.8 and 1.2% wt. In contrast, the AP+500LS mixture did not cover Avicel's surface but created

aggregates/agglomerates larger than  $1\ \mu\text{m}$  (Fig.2.3b).

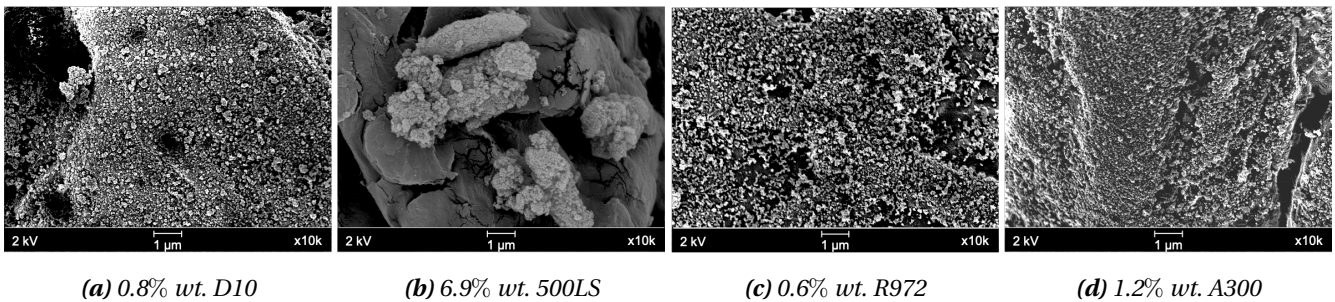


**Figure 2.3.** SEM micrographs of Avicel<sup>®</sup> PH-102 + S-NP mixtures for an estimated surface coverage of 40%.

Figure 2.4 shows coverages between 1 and 27% for different HP. The estimated SC, or calculated value, of these mixtures supports the proportional calculation. For instance, the coverage that was supposed to be at 14% was at ~13% (Fig.2.4a), for 1% was at ~2% (Fig.2.4b and 2.4c) and for 27% coverage was at ~24% (Fig.2.4d). The proportionality prediction using table 2.1 is thus quite good and validate the use of SC throughout this work.

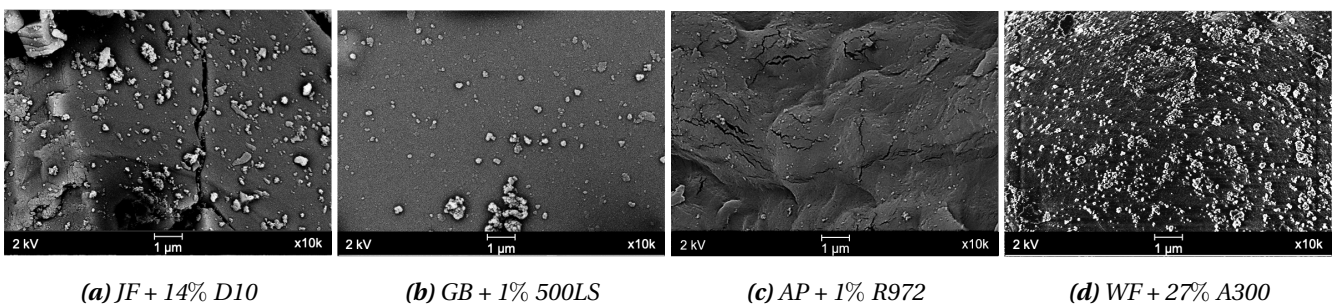


**Figure 2.4.** SEM micrographs of powder mixtures with different S-NP surface coverages

#### 4.1. Water activity and conditioning

All powders and mixtures were conditioned and maintained, at ambient temperature, inside sealed containers controlled by saturated salt/water solutions to control relative humidity at 30% (Lithium chloride - *LiCl*) and 60% (Sodium Chloride - *NaCl*). Samples were allowed to equilibrate for 7 days to this environment conditions. It is important the JF and GB do not achieve at the RH in which they are conditioned, which agrees with water sorption results (Fig.2.9). The water activity,  $a_w$ , was measured using an Aqualab 4TE from METER<sup>®</sup> before and after each test to follow the possible change in the sample humidity.

## 5. Materials physical characterisation

The aims of this section are to outline the selected characterisation techniques and to provide the insightful information that can be extracted from each test, highlighting their significance to the present work.

### 5.1. Particles shape

The physical shape of powder particles was determined using the Gemini 3 Scanning Electron Microscope (SEM) from Zeiss equipped with a field-emission gun operating at 2 kV. The samples were mounted on double-sided tape and coated with a uniform layer of gold-palladium using a Desk V – TSC from Denton Vacuum, under air purge, for a period of 1 minute. Figure 2.5 presents the micrographs of each material, showing that there are wide differences from one another in terms of shape and rugosity. The AP particles have an isometric rod shape with a rough surface, while WF is composed of a major irregular structure (gluten) surrounded by globule-like structures (starch). The JF particles are an uneven shape with flat surfaces, and GB are mostly spherical, with irregularities on the surface of some particles. SEM images at various magnification of each powder are presented in figures 3.5, 3.6, 4.4, 4.5, 5.5 and 5.6 (Chapters 3, 4 and 5).

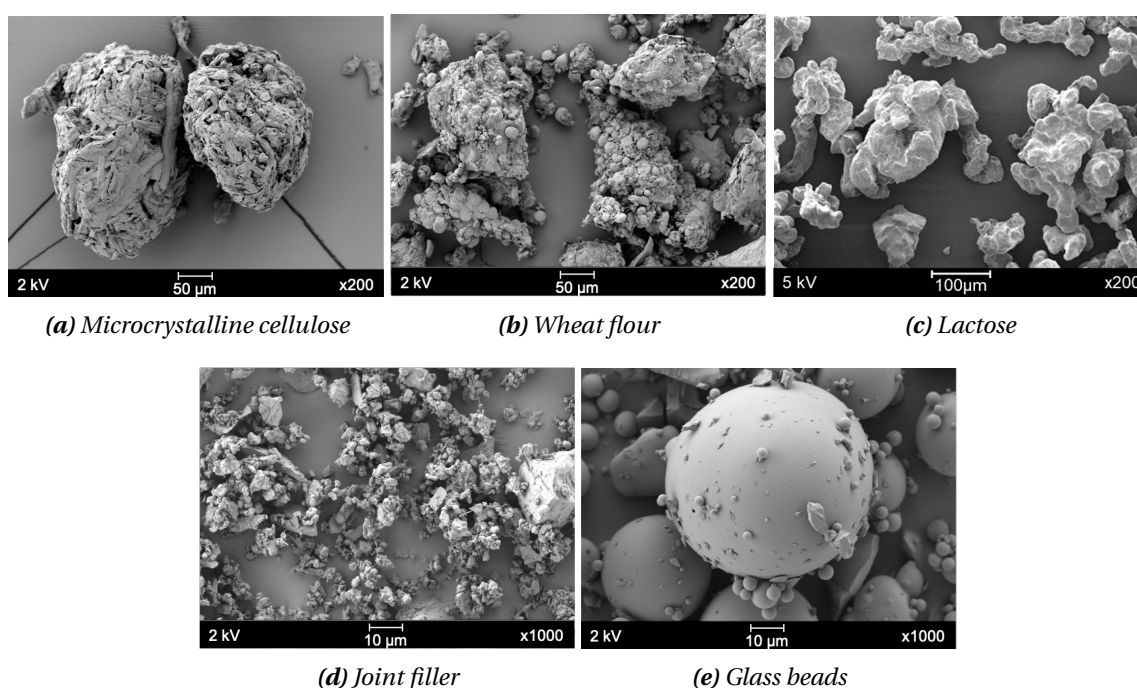


**Figure 2.5.** SEM micrographs of powders

S-NP shape was assessed using a 2100-F transmission electron microscope (TEM) from Jeol with a high tension of 200 kV. The TEM micrographs of each reference can be observed in figure 2.6, where a distinct shape pattern can be associated according to their synthesis process. The SIPERNAT<sup>®</sup>s showed sponge-like structures with circular-like

primary particles, while the AEROSILs exhibited chain-like structures with elongated primary particles.

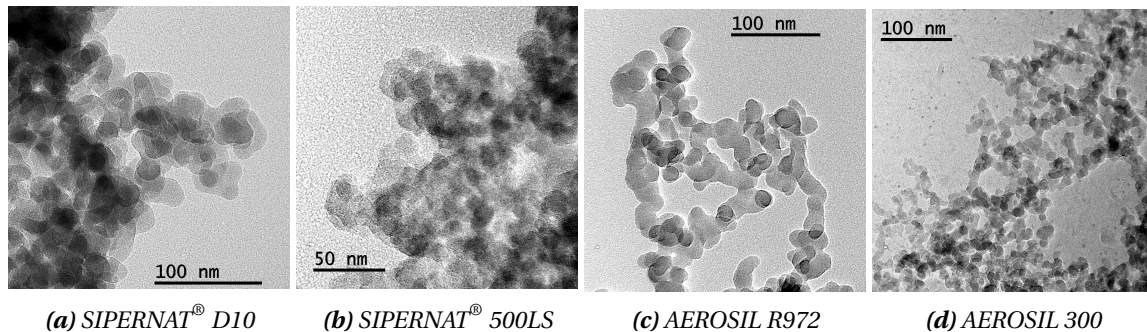


**Figure 2.6.** TEM micrographs of silica nanoparticles

## 5.2. Particle size distribution

To characterise particle size distribution (PSD) the laser diffraction technique was employed using a Mastersizer 3000 from Malvern Instruments. Ethanol was used as a dispersant to avoid dissolution, and triplicate measurements were performed. The particle size distribution of the powders is presented in figure 2.7, with their corresponding representative diameters (tables 3.2 and 4.1) and 5.3. From the figure, it is depicted that all powders are polydisperse. The wider dispersion is observed for WF, JF, and GB with particles going from 1  $\mu\text{m}$  to 300  $\mu\text{m}$ . The powders with the bigger particles are AP and Retalac.

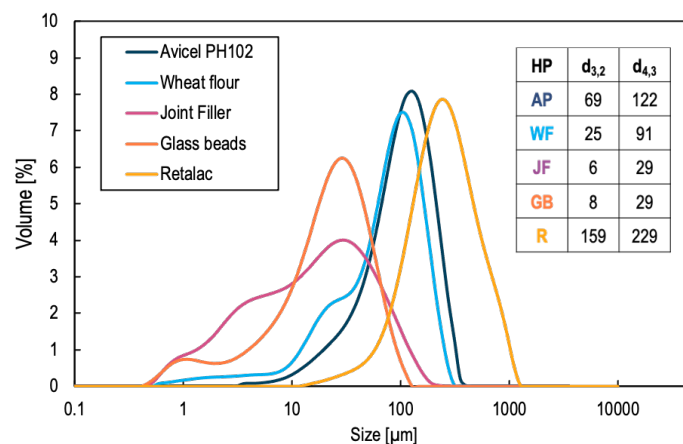


**Figure 2.7.** Powders particle size distribution.

The S-NP primary particle size determination was assessed by randomly selecting an average of 100 particles from TEM micrographs and measuring them with the ImageJ software free-hand tool. The identification of 500LS primary particles was unfeasible because the nanoparticles seems to aggregate stacked atop one another, as depicted in figure 2.6b. D10 and R972 presented comparable sizes of  $24 \pm 5$  nm (Fig.2.6a) and

$25 \pm 5$  nm (Fig.2.6c), respectively, while A300 were the smallest S-NP with a mean size of  $15 \pm 5$  nm (Fig.2.6d). Notably, hydrophobic S-NP were observed to generate larger primary particle sizes, due to the treatment applied for imparting hydrophobicity. This chemical treatment involves reacting the silanol groups (Si-OH) with organic groups located at the surface of the silica particles, consequently rendering them water-repellent increasing their size [174].

### 5.3. Specific surface

The available surface of the interaction of granular materials with the environment (gas or liquid) is called the specific surface ( $a_{BET}$ ). It is determined based on the physical adsorption of a gas molecules monolayer onto the surface of the powder (Eq.2.1). The most commonly used gas is nitrogen ( $N_2$ ).

$$a_{BET} = \frac{V_m N_a A_{N_2}}{V_{N_2} m} \quad (2.1)$$

where  $N_a$  is Avogadro's number,  $A_{N_2}$  is the cross-sectional area of  $N_2$  ( $A_{N_2}=0.162$  nm<sup>2</sup>),  $V_{N_2}$  is the molar volume of  $N_2$ , and  $m$  is the sample mass.

To estimate the amount of  $N_2$  molecules on the monolayer the Brunauer-Emmett-Teller (BET) [175] method is the most widely used. It is based on the  $N_2$  adsorption isotherm and is represented by the following equation:

$$\frac{P}{V(P_0 - p)} = \frac{1}{V_m C} + \frac{C - 1}{V_m C} \frac{P}{P_0} \quad (2.2)$$

where  $P$  and  $P_0$  are the equilibrium and saturation pressure of the  $N_2$  at a given temperature.  $V$  is the adsorbed quantity,  $V_m$  is the monolayer adsorbed gas quantity, and  $C$  is the BET constant based on adsorption energy. In figure 2.8, the BET plot of Avicel<sup>®</sup> PH-102 is depicted from the slope, and the intercept  $V_m$  is estimated.

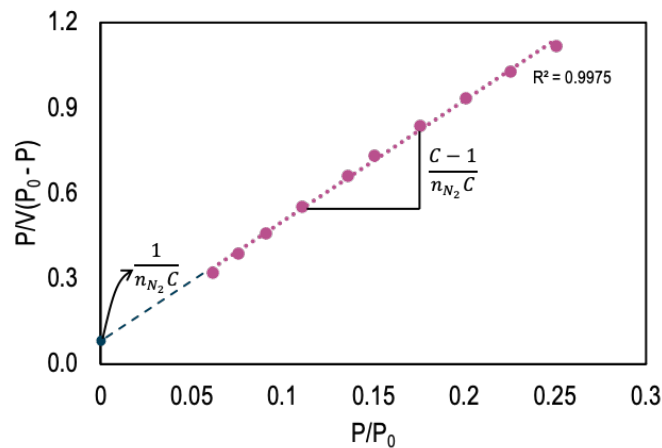


Figure 2.8. Specific surface BET calculation method, values obtained from Avicel<sup>®</sup> PH-102.

The BET theory allows to determine the number of molecules required to form a monolayer without being entirely covered. To do so, the following hypothesis should be fulfilled [175]:

- The molecules on the last adsorb layer must be at equilibrium with the environment vapour.
- There is no interaction between the lateral adsorbed molecules.
- The adsorption energy of the first layer is constant and greater than the others.
- The adsorption energies of the layers above the first one are the same and equal to enthalpy of liquefaction.

The specific surface area of powders was measured using a TriStar II Plus instrument from micromeritics. Prior to the analysis samples were vacuum dried during 12 hours at 20° C. Table 2.2 displays the  $a_{BET}$  values for each powder and S-NP. It is observed that most powders exhibit a low  $a_{BET}$  ranging from 0.3 to 1.1  $m^2/g$ , while S-NP has a significantly higher  $a_{BET}$ , with values ranging from 90 to 500  $m^2/g$ .

#### 5.4. Pycnometric density

Pycnometric or true powder density was determined in a Helium pycnometer (AccuPyc 1330, Micromeritics). All data presented correspond to the average of ten measurements obtained from one powder sample.

The results of the pycnometric density and  $a_{BET}$  (Table 2.2) allows to classify powders as NM using the specific surface area by volume (VSSA) according to the European commission [32]. This characteristic is the product of the powder true density and the specific surface area. According to the VSSA results, all flow additives were classified as NM, with a VSSA above 60  $m^2/cm^3$ . On the contrary, the powders' VSSA values were below 6  $m^2/cm^3$ , being not considered as NM. GB  $a_{BET}$  is not specified, since is so small that it was not possible to measure it.

**Table 2.2.** Samples nanomaterial classification according to VSSA.

Sample	Pycnometric density [ $g/cm^3$ ]	$a_{BET}$ [ $m^2/g$ ]	VSSA [ $m^2/cm^3$ ]
Avicel <sup>®</sup> PH-102	1.6	1.0	1.6
Wheat flour	1.5	0.3	0.4
Joint filler	2.8	1.1	3.1
Glass beads	2.7	-	1.3
SIPERNAT <sup>®</sup> D10	2.0	90*	180
SIPERNAT <sup>®</sup> 500LS	2.2	450*	990
AEROSIL R972	2.3	110*	253
AEROSIL 300	2.7	300*	810
SIPERNAT <sup>®</sup> 50S	2.0	90*	180
SIPERNAT <sup>®</sup> D17	2.1	500*	1050

\*Product data sheet

### 5.5. Behaviour towards water

As explained in sections 6. and 7., humidity can significantly influence powders' motion behaviour. The aim of performing this characterisation in our study is to assess the effect of S-NP on powders' behaviour towards water and, by extension, determine if their mechanism of action could be related to the mitigation of capillary forces (see section 3.3. and Fig.5.8).

Water sorption isotherms were obtained at 25°C in a dynamic vapour sorption (DVS-2) from Surface Measurement Systems (SMS), using a Cahn microbalance with a resolution of 5 mg. Before scanning, samples were vacuum dried for 60 minutes. Water sorption isotherms follow the same principle as the BET analysis, varying the gas water vapour at different relative pressures and measuring the sample mass to evaluate the sorption.

Figure 2.9 illustrates the water sorption isotherms of the powders. The cycles, adsorption-desorption shows that AP, WF and Retalac have a hydrophilic behaviour and absorb water from low relative humidity. In contrast, JF absorbs/adsorbs almost anything with a maximum change of mass of 0.15%.

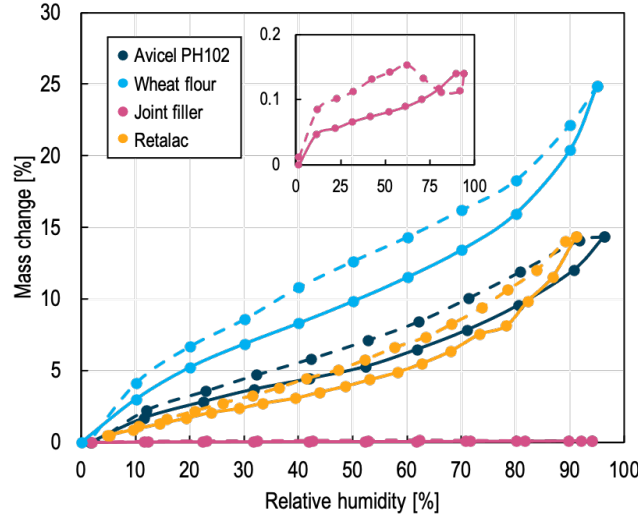


**Figure 2.9.** Water sorption isotherms of host powders at 25°C. The sorption curves are represented with a solid line, and desorption curves with a dashed line.

## 5.6. Surface energy

The inverse gas chromatography (IGC) allows the characterisation of the surface properties of divided solids, more specifically the dispersive surface energy ( $\gamma_s^d$ ). According to Cares-Pacheco et al. [176], surface energy is sensitive to the sample surface roughness and porosity. In this study we are interested in evaluating the surface modification of the HP by the addition of S-NP to deepen the understanding of their mechanism of action.

IGC in the infinity dilution region IGC-ID is based on the physical adsorption of gas molecules on a solid surface. Unlike analytical gas chromatography, in IGC-ID, the studied solid is the stationary phase, and well-identified vapour molecules, called probes, are used to determine the interaction capacities of the material packed into the column (Fig.2.10). The retention time  $t_N$  results from the interaction between the solid's surface and the probe molecule's. If the probe molecules are n-alkanes and the adsorption takes place on a non-polar solid, the interaction forces are dominated by dispersive interactions (London type). Based on the Dorris-Gray [177] model, by injecting a series of n-alkanes as probe molecules, their retention volume allows for determining the dispersive surface energy,  $\gamma_s^d$  [mJ/m<sup>2</sup>] from the following equation [176]:

$$\gamma_s^d = \frac{1}{\gamma_{CH_2}^d} \left[ -\frac{RT}{2N_a a_{CH_2}} \ln \frac{V_{N+1}}{V_N} \right]^2 \quad (2.3)$$

where  $V_N$  is the specific retention volume calculated from  $t_N$  by considering the pressure drop along the column during elution;  $N_a$  is the Avogadro number,  $a_{CH_2}$  is the surface area of  $CH_2$  molecule ( $6 \cdot 10^{-18} m^2$ ),  $\gamma_{CH_2}^d = 35.6 - 0.058(T - 20)$  is the surface energy of a methylene group,  $R$  is the perfect gas law constant and  $T$  is the column temperature.

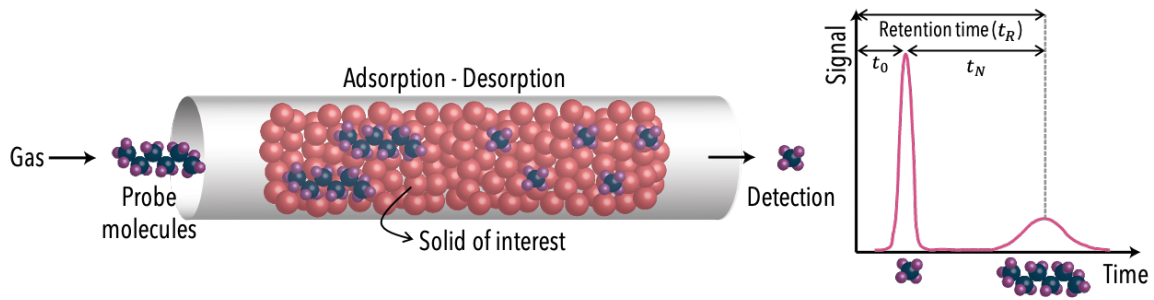


**Figure 2.10.** Inverse gas chromatography principle (adapted from [176]). The net retention time is given by  $t_N = t_R - t_0$  where  $t_R$  is the time spent for a probe molecule to pass through the powder column, and  $t_0$  corresponds to the time for a non-adsorbed molecule—methane—to do it.

The  $\gamma_s^d$  of the samples were measured by the NeuronIC IGC from Adscientis, France. Samples were placed into a stainless-steel column with a 100 mm length and 4 mm internal diameter. Before the analysis, each powder column was conditioned in-situ in the NeuronIC for 16 hours at a temperature of 25°C. Helium was used as carrier gas at a 10 mL/min flow rate. The retention times of methane and probe molecules were determined using a flame ionization detector (FID). The software Nucleus 3.2.4 was used to inject a homologous series of vapour n-alkanes (hexane, heptane, octane and nonane). The Solid 3.3.0 software, also from Adscientis, was used for the calculations. The  $\gamma_s^d$  of the HP and the S-NP D10 is presented in table 2.3.

**Table 2.3.** Surface energy of host powders and SD10.

Sample	Sample mass [mg]	Surface energy [ $mJ/m^2$ ]
Avicel® PH-102	785.1	$57.8 \pm 0.7$
Wheat flour	1190.3	$42.8 \pm 0.2$
Joint filler	2116.7	$39.9 \pm 0.3$
Glass beads	2573.3	$47.2 \pm 0.4$
SIPERNAT® D10	103.5	$29.3 \pm 0.1$

## 6. Motion characterisation techniques

This section presents the selected characterisation techniques to describe powders flow behaviour and dustiness emission.

### 6.1. Flowability

#### 6.1.1. Densification

Granular material transport is a fundamental handling operation that all powders undergo at some stage during the production chain and storage. In the course of this process, powders tend to compact or consolidate as a result of vibrations or shocks

generated by their movement [111]. Therefore, characterising the flow behaviour of powders in similar conditions is of great interest. Consequently, the first chosen method to characterise flowability was through the densification of powders (see section 6.2.). To do so, three instruments were employed, the Densitap<sup>®</sup> from Granuloshop<sup>®</sup>, the FT4 powder rheometer from Freeman Technology<sup>®</sup>, and an Instron<sup>®</sup> press.

The Densitap, studies densification under vibrations transmitted by tapping. This device is one of the most used in the pharmaceutical and food industry due to its easy and fast operation, as previously described in section 6.2.2.1. [50, 104–106].

The protocol used to evaluate powder densification, through tapping, consisted in measuring the change in bulk volume, after each tap for the first 10 taps, followed by measurements every 10 taps up to 100, every 100 taps up to 1000, and every 1000 taps thereafter until the sample volume no longer changed after 4000 taps.

The other two devices, the FT4 compression cell and the Instron press, evaluates densification by uniaxial compression. The FT4 and the press are not commonly used to describe powders' flow behaviour. However, Uniaxial Compression Testers (UCT) control the force/energy supplied to the bulk compared to traditional tapping devices, such as Densitap. Thus, these devices allow the comparison of the compaction of the powders at the same level of force provided, which is not the case with tapping devices. To distinguish from traditional testers, the *HR* is denoted as  $HR_c$ .

The FT4 cell and the developed cell press geometry are illustrated in figure 2.11. Both devices are equipped with a cell of 25 mm in diameter, 20 mm in height and a 24 mm in diameter piston. The protocol of the FT4 differs from the press because it has a mechanical conditioning step (Fig.2.11a). According to the supplier, this step intends to provide the same mechanical history for each sample. The effect of this step was evaluated, and it is discussed in section 3.3.. The UCT procedure consists of pouring an excess of powder into the cell, which is then removed using the cell pivotal upper part, for the FT4, or with an anti-static plastic ruler, for the press, to ensure a final volume of 10 mL. The sample is then compressed with a rate of 0.4 N/s and different compression protocols were performed.

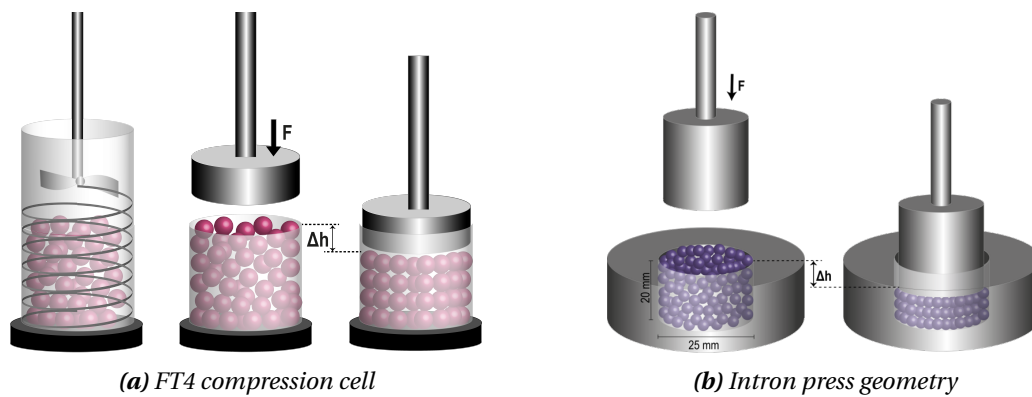


Figure 2.11. Uniaxial compression densification testers.

The force applied and piston/powder height were measured throughout the tests. In the FT4, four compression protocols were performed: 2 N steps, 4 N steps and 10 N steps until 40 N. The fourth consisted of a "random" steps protocol (2, 5, 6, 13, 15, 26, 30, 32 and 40 N). In the press, just a force ramp of 10 N steps until 50 N is employed. At each step, the pressure was maintained for 60 s to ensure the steady state was reached. The force applied was selected according to previous vibration studies [50], showing that the powder samples used in this work achieved their maximal compaction state under free surface conditions below 50 N. It is preconized that under these conditions, particles cannot be broken or deformed to any significant extent [51, 178].

### 6.1.2. Shear test - plastic failure

Shear tests describe powder flow behaviour through the flow factor on the quasi-static regime. Nevertheless, this test was first conceived by Jenike for silos design. Even if, in the present work, we are only going to use the flowability indicators characterisation, this technique has been linked to industrial powder handling since its development.

Shear tests were conducted using the FT4 shear cell, which is a rotational uniaxial cell (Fig.1.14), described in section 6.2.2.2.. This experimental procedure allows the classification of powder flow through the  $ff$  (Fig.1.13). In conjunction with the densification method, these methodologies assess the flow behaviour under a consolidated quasi-static regime. In addition to the  $ff$ , the measurement of cohesion and friction can provide a more comprehensive understanding of the influence of NP on flowability.

The test protocol is described in the norm ASTM D7891-15 [179] and consists of four steps (see Fig. 2.12):

1. Mechanical conditioning: the powder bed is mechanically conditioned - aerated state - by a propeller, as in the compression test.

2. Compression: the vented piston applies a normal stress to the powder bed, and then the vessel is split, creating a powder bed of 10mL.
3. Pre-consolidation/Pre-shearing: the shear piston subjects the powder to a specified normal load,  $\sigma_c$ , followed by a pre-shear at the same normal stress until the steady-state shear stress is reached. Then, the piston stops and rotates in the opposite direction and establishes a zero torque level.
4. Shearing: the powder bed is sheared at a normal shear stress  $\sigma_i$  ( $\sigma_i < \sigma_c$ ) progressively until the yield point is achieved. This process is repeated 5 times with different normal shear stresses. Each yield point is recorded and used to build the yield locus which provides the samples' cohesion, flow function and other flow parameters.

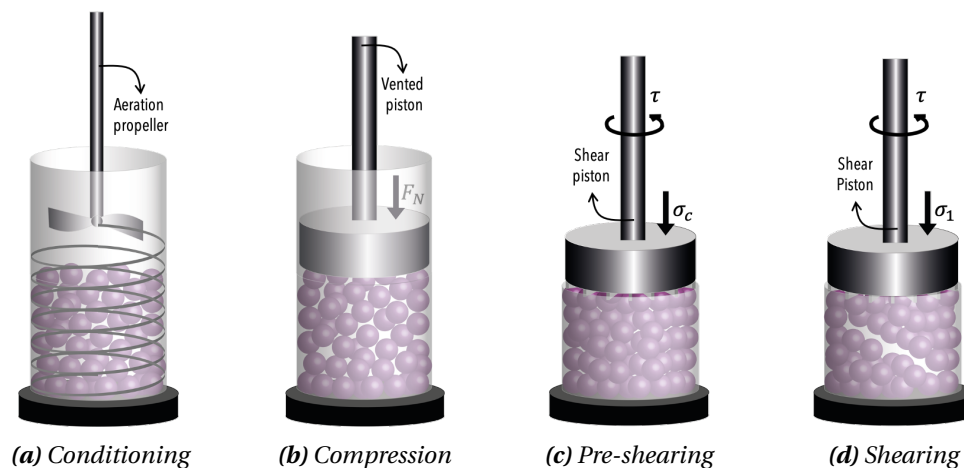


**Figure 2.12.** FT4 shear test steps described in the standard ASTM D7891-15 [179].

In this thesis, we worked with two pre-consolidation/shear stress programs. The first was the standard program with 6kPa of pre-consolidation stress and normal shear stresses of 4, 3.5, 3, 2.5, and 2 kPa. The second program was created to evaluate the behaviour of the consolidated powder with a higher strength to directly compare  $HR_c$  and  $ff$  at a similar consolidation. In this case, pre-consolidation stress was set to 66 kPa, and normal shear stresses to 50 - 40 - 25 - 17 - 7 kPa.

### 6.1.3. Flow through an orifice

Granular materials flow through orifices during handling in multiple industrial operations at different scales. For example, powders are frequently stored in silos to be eventually discharged, most products must be precisely dosed into their packaging. At smaller scales, the dosage of powder medicines is used to manufacture compressed tablets. Given the significance of this unit operations in industry and its associated challenges, examining the flow of our samples through an orifice could provide valuable insights into their flowability evaluation. This dynamic measurement allow us to describe powder flow behaviour on the "liquid" regime and compare it to the previously described techniques

based on the quasi-static regime.

We use a homemade flow meter, illustrated in figure 2.13. This device comprises a 500 mL sample cylinder with a 54 mm inner diameter and a moving platform where the orifice geometries are placed. The orifice geometries' diameters go from 35 to 1 mm in diameter. The flowing sample is recovered in a plastic beaker at the collecting plate, which is connected to a compression charge cell weight, from RS PRO. The device is grounded to avoid the electrostatic charging of powders.

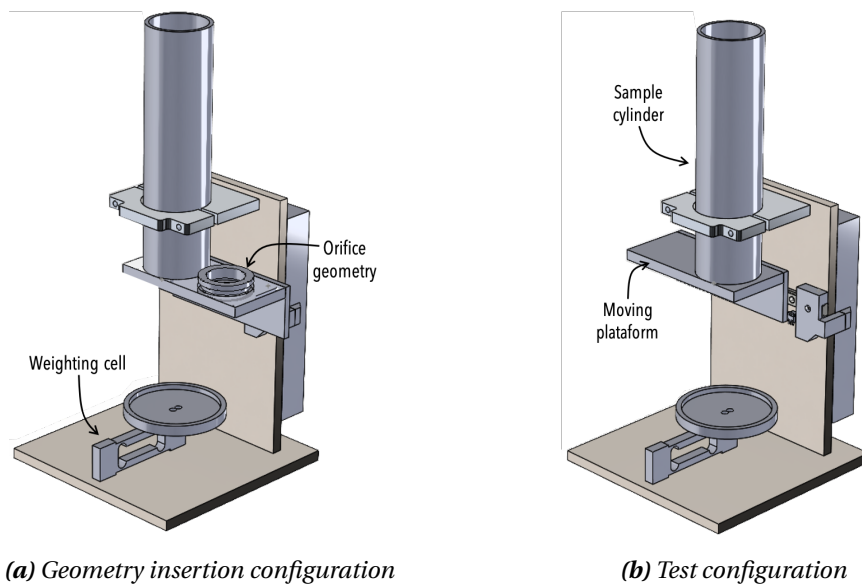


**Figure 2.13.** Home-made flow tester.

The testing protocol comprises the following steps: first, 150 g of the sample is added to the cylinder, and the largest orifice geometry is positioned. Next, the moving platform is shifted to the left side, allowing the powder to flow through the orifice. The weighing cell is connected to a computer that registers the mass evolution over time. After this, the orifice geometry is replaced with the next smallest diameter, and the protocol is repeated similarly. This sequence of events is iterated until each orifice geometry has been tested. Regarding the data treatment, it was established that only the runs in which a minimum of 5% of the mass had been collected would indicate powder flow.

## 6.2. Dustiness

The samples' dustiness was evaluated using the RD and the VS, considering the available resources and the information that could be collected from each device. The RD (refer to section 7.2.2.1.) was selected because it is the only dustiness device that allows the three fraction collections (inhalable, thoracic, and respirable), and it has been related to low-energy powder handling processes, such as, granulation and transfer operations. In contrast, the VS (refer to section 7.2.2.3.) represents highly energetic processes, such as, mixing and powder transport.

In the VS, three dustiness measurements are evaluated:

1. The respirable fraction: collected on a filter placed on a GK2.69 cyclone [157] connected to a regulated pump (Gillian 5000, GilAir).
2. The size distribution: measured with an electrical low-pressure impactor (ELPI<sup>®</sup> + from Dekati [158]).
3. The number concentration: evaluated using a condensation particle counter (CPC) Model 3007 from TSI<sup>®</sup> [153].

In addition, the dust emitted particles are collected on 400 Mesh TEM grids covered with a holey carbon film using a mini particle sampler (MPS from Ecomesure) [160] to evaluate their physical aspect.

The RD and the VS follow the specifications of the standards NF 15051-2 [154] and NF 17199-5 [161]. The tests were performed at two different airflow humidity conditions 30% RH and 50% RH. In addition, samples were conditioned in sealed chambers at 30% RH and 50% RH. These humidity conditions for the tests airflow and the samples were used to assess the influence of humidity on dustiness. The first condition evaluated, referred to as 50-50, followed the standard recommended conditions, with both the test and sample being conducted at 50% RH. The next condition, 50-30, involved testing the standard airflow at 50% RH while varying the sample RH to 30% RH. Lastly, Both conditions were evaluated at 30% RH in the 30-30 configuration.

## 7. Conclusion

Powder research studies tend to develop the investigation focusing on an application, such as pharmaceuticals, cosmetics or food. It is uncommon for powders used in multiple sectors to be studied together. Therefore, the powders selected for this study were chosen to represent different industries and to be very distinct from one another. Their marked differences were exhibited through microscopy characterisations and size distributions. In addition, six different silica nanoparticles were chosen to evaluate their action on flowability enhancement, considering their synthesis, behaviour towards water, and shape.

In general, adding flow additives for improving powders' flowability is done by a "standard" amount based on a mass fraction. Notwithstanding, our research intends to associate silica nanoparticles' effect with surface coverage. Therefore, a protocol was developed and validated to characterise and evaluate the host powder's surface coverage. From the protocol development, we could already conclude that hydrophobic S-NP tends to cover better the surface of the HP. Besides, it was highlighted that each S-NP/HP

combination presented a specific SC coverage suggesting that a "standard" mass fraction does not result in a similar SC on different samples.

Since we are interested in evaluating the effect of S-NP through SC, the physical characterisations of the materials included techniques to evaluate the surface state of the samples by the dispersive surface energy and the specific surface. These characterisations might be useful in understanding the S-NP effect on the surface state of powders and, by extension, their influence on motion behaviour.

In the final part of the chapter, the choice of flow behaviour and dust emission techniques were explained, along with their corresponding protocols. The selection of devices was based on their ability to provide multiple results per end-use property, which allows describing powders' flowability and dust emission using multiple indicators that may provide enough information to relate them.

The following three chapters contain the results of the present work, along with Chapter 6. Each chapter presents a synthesis of the publication's findings and additional results that were not included in the original publication.



# 3

## Flow behavior and densification

This chapter evaluates powder densification through two methods: vibration using the traditional Densitap and uniaxial compaction (UCT) employing the FT4 and Instron press. Firstly, the densification dynamics of two pharmaceutical excipients, Avicel PH102 and Retalac, are studied and correlated to the Chicago (Eq. 3.1) and KWW (Eq. 3.2) models under different RH conditions, 30% and 60% RH.

The interest in evaluating powder densification under vibration and uniaxial compaction was to evaluate the possibility of comparing the results from each test. Therefore, the energy supplied by each test was quantified and estimated from the applied force. For the Densitap, a force sensor placed on the base of the graduated cylinder was employed to measure the force signal (Fig.3.1). The energy applied to the samples from each tap was between 200 and 215 N peak-to-peak. In the UCT, the force applied is specified in the protocol. The comparison between these two densification methods according to the applied energy to the powder bed is shown in Figure 3.14.

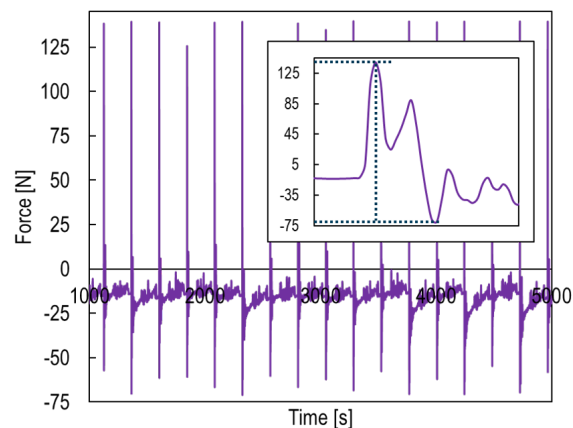


**Figure 3.1.** Force sensor signal measurement of the tapping vibrations of a Densitap.

We further examine the effect of adding flow additives to AP and R, focusing on their impact under different RH conditions (30% and 60%), two flow additive mass fractions (0.5% and 2% wt.), and the hydrophobic and hydrophilic behaviour of the flow additives towards water. These results are shown in figures 3.16 and 3.17.

The last section aims to present the densification characterisation of the HP that was not included in the publication.

Main conclusions of this result chapter:

- The dynamic compaction evaluated with Densitap of Avicel Ph102 and Retalac fitted well the two tested models, allowing the correct prediction of the maximal compaction but without a good prediction of the required taps to achieve it.
- The uniaxial compaction test was shown to be more sensitive to the influence of humidity on the flow behaviour than the Densitap.
- Flowability improvement by S-NP seems to be related to the HP surface coverage rather than the mass fraction.
- Hydrophobic S-NP covered the HP better than the hydrophilic references, increasing the flow behaviour.

## Effects of humidity and glidants on the flowability of pharmaceutical excipients. An experimental energetical approach during granular compaction

Maria Graciela Cares Pacheco<sup>a</sup>, Maria Camila Jiménez Garavito<sup>a,b</sup>, Anaïs Ober<sup>a</sup>, Fabien Gerardin<sup>b</sup>, Eric Silvente<sup>b</sup> and Véronique Falk<sup>a</sup>

<sup>a</sup> *Université de Lorraine, CNRS, LRGP, F-54000 Nancy, France*

<sup>b</sup> *Department of Process Engineering, Institut National de Recherche et de Sécurité, 54519 Vandœuvre, France*

Article published in the International Journal of Pharmaceutics

DOI: [10.1016/j.ijpharm.2021.120747](https://doi.org/10.1016/j.ijpharm.2021.120747)

### Abstract

Granular materials are part of the design, production and final products of different industrial sectors. Powder flowability is a major topic in manufacturing and transport as it is closely related to process feasibility. Nonetheless, the flows of granular materials are not easy to describe or quantify, even in the simple case of dry monodisperse cohesionless particles. Flowability assessment is not a standard or normalized issue; still, no test predicts powder flow behaviour in all the different mechanical situations encountered during processing.

This study aims (1) to evaluate flowability, as device-related, through the energy supplied to the powder bed and (2) to study the effect of glidants and moisture content on flowability. To illustrate these proposes, the flowability of two well-known pharmaceutical excipients, Avicel<sup>®</sup> PH-102 and Retalac<sup>®</sup>, mixed with four different types of precipitated nano-silica (SIPERNAT<sup>®</sup> D10, D17, 50S and 500LS), was assessed using two granular compaction devices: Densitap<sup>®</sup> and FT4<sup>®</sup> compaction cell. Our results show that the hydrophilicity of colloidal silica affects surface coverage, ranging from 6% to over 80%. Binary mixtures with hydrophobic additives, D10 and D17, generated smaller silica aggregates with a wider spread on the surface of host particles. For Retalac<sup>®</sup> conditioned at 30% RH, HR values changed from 1.30 (acceptable flow) to 1.17 (good flow). For Avicel<sup>®</sup> PH-102, conditioned at 60% RH, HR values changed from 1.22 (fair flow) to less than 1.10 (excellent flow).

**Keywords:** *Glidants, Flowability, Granular compaction, Air humidity, Force/energy approach*

## 1. Introduction

Those who work with granular materials, fine or coarse, such as powders, know that the same powder may flow well in one container but poorly in another. Despite all the available studies describing flow characteristics, it is often difficult to extract common features and general trends for granular materials that are not glass beads. Granular flow complexity is related to its multidimensional character as it links the local particle interactions and their global mechanical behaviour, including bulk properties, equipment design, processing conditions, and environmental conditions. The difficulties and limitations of flow behaviour assessment have been well-reviewed [14, 47, 50, 96]. To

better understand granular-flow behaviour, it seems fundamental *to differentiate powder flow, as an observation, from powder flow quantification* related to the assessment method, also known as *flowability*. Flowability is device-dependent, and describes the ability to flow in a desired manner in a specific piece of equipment [14, 50]. Different parameters or indexes can be obtained from the multiple flow testers available on the market. Each one of these devices "estimates/quantifies" flowability under specific mechanical conditions. Still, no one test will predict powder flow behaviour in all the different mechanical situations encountered during processing and transport. In practice, whether in the laboratory or during the manufacturing process, from know-how or through measurements, the type of test method that describes the best flowability in a given application is chosen.

Densification, or compressibility, or compactness, is a flow property arising from the collective forces acting on the media. When energy is transferred into a granular material, the grains begin to reorganize themselves in a denser structure. This energy can be transmitted to the powder bed using uniaxial compression or vibration. Generally, during uniaxial compression, particles undergo elastic, plastic, or visco-elastic/visco-plastic deformation. Softer solicitations, such as vibrations, give rise to the geometric rearrangement of particles. Compaction by vibration can be divided by subjecting the granular system to harmonically driven motions [50] or to free-falls performances, commonly denoted as tapping [180].

Several studies focus on the densification of granular media because it covers many fields from pharmaceuticals to Geotech industries [181]. As there is no universal mathematical model to predict flow behaviour in every situation, the dynamics of compaction under vibration have been described by several empirical or heuristic models, mostly using glass beads [180, 182–184]. In this work, we will simply validate whether two of the most used models fit the dynamic behaviour of two excipients, widely used in the pharmaceutical industry.

The first and the most famous model is the one proposed by Knigh et al. (1995) from the James Frank Institute at the University of Chicago [182]:

$$\rho(N) = \rho_f - \frac{\Delta\rho}{1 + B \ln(1 + \frac{N}{\tau})} \quad (3.1)$$

where  $N$  is the number of taps,  $\rho_f$  is the final compactness,  $\Delta\rho$  is the difference compared to the initial compactness of the bed, while the  $B$  and  $\tau$  parameters are defined as a function of the acceleration, the control parameter.

The first term shows the rapid arrangement of the particles, while the second expresses that the steady state is reached asymptotically, logarithmic slow [184]. This also indicates

that grains behave in a manner similar to glass [183].

The densification of dry granular materials under tapping is often better fitted by an empirical law developed by Kohlrausch-Williams-Watts (KWW model), [180]:

$$\rho(N) = \rho_{\infty} - \Delta\rho \cdot \exp\left(-\left(\frac{N}{\tau}\right)^{\beta}\right) \quad (3.2)$$

where  $\rho_{\infty}$  is the compactness at the steady-state,  $\tau$  is the characteristic relaxation time describing the arrangement of grains until the steady-state is reached and  $\beta$  is the stretching exponent.

From a technological point of view, powder flow is essential to processing efficiency. The aim is to facilitate manufacturing, including flow through hoppers, sieving, pouring, blending, transport, filling, compaction and tableting, even if this rarely brings an added value to the end-use product.

The flowability of cohesive powders can be remarkably improved by the use of flow additives or glidants [185]. For several years, flow regulators have been systematically added to a significant number of formulated products, without any studies validating its function besides process feasibility. In the pharmaceutical industry, the use of glidants is mostly based on historical know-how or trial error methods, without any measurements of the effect on end-use properties [83].

Amorphous silica powders (NP-SC) were introduced quite easily under the hypothesis that only crystalline silica is considered a toxic form at a micrometric scale. Nonetheless, some recent risk assessment studies carried out at the National Institute of Scientific Research in France (INRS) demonstrated the in-vitro cytotoxicity of amorphous silica, which is also highly incremented by reducing the size of the particles [186]. Therefore, it is crucial to focus on the role of silica nanoparticles on the end-use properties of powders, especially on their flowability, to optimize the choice of additives, minimize their quantity, or to replace them. Nevertheless, to do so, it is essential to better understand how they interact within the formulations/media into which they are added.

Different flow regulator action mechanisms have been proposed in the literature. The first is related to a purely mechanical effect, and the second is related to interparticle forces. A mechanical effect will occur when surface additives allow particles to easily roll over one another, thus reducing friction [26]. The physical mechanism by which interparticle adhesive forces are reduced is less exact, or at least not universal. When referring to interparticle forces, two mechanisms have been proposed. The first is related to surface chemistry changes, and the second concerns spacers among host particles [81, 187, 188].

The aims of this work are (1) to obtain a deeper understanding of how granular compaction is related to flow behaviour by confronting different compaction tests, thus pointing out a standard physical parameter: the specific energy supplied to the powder bed; (2) to study the effect of glidants and environmental moisture conditions on flowability.

To illustrate these aims, granular compaction was performed using two compaction devices: the well-known DensiTap<sup>®</sup> and the FT4 compression module. Measurements were carried out in the elastic domain, using two pharmaceutical excipients, lactose and microcrystalline cellulose. Several different types of precipitated nano-silica were used as surface additives, differentiated by their hydrophilicity and size distribution. Powder flowability was determined, or classified, according to the Hausner ratio (HR), a widely used index in the industry [50].

## 2. Materials and methods

### 2.1. Powder Materials

#### Excipients as host powders

For this study, two well-known pharmaceutical ingredients having excellent compactibility were chosen: Avicel<sup>®</sup>PH-102 and RetaLac<sup>®</sup>. Avicel<sup>®</sup>PH-102 is a high purity microcrystalline cellulose produced by FMC Biopolymer<sup>®</sup> generally used in the pharmaceutical industry for direct compression tableting. RetaLac<sup>®</sup> is a co-processed hypromellose/lactose-based excipient produced by MEGGLE, composed by equal parts of a K-type hypromellose polymer and  $\alpha$ -lactose monohydrate. RetaLac<sup>®</sup> excipient is specifically designed for direct compression and dry granulation of modified release formulations.

#### Nanoparticles as flow regulators

The SIPERNAT<sup>®</sup> brand from Evonik was chosen for flow regulation in bulk powders. SIPERNAT<sup>®</sup>s are highly porous colloidal silicon dioxide powders produced by precipitation from an aqueous solution. From the large pannel of SIPERNAT<sup>®</sup> NPs, two with hydrophobic properties, the D10 and D17, and two hydrophilics, the 50S and the 500LS, were chosen. Both, D10 and D17 are rendered hydrophobic by chemical surface treatment. D10 is used in a great variety of defoamer while D17 primary application is as an anticaking agent in fire extinguishing powders. 50S and 500LS products are high absorption capacity carriers able to absorb liquids up to three times of their own mass. The 50S is normally used in plant formulations as wettable powder and water-dispersible granule. The 500LS is recommended as a viscosity modifier in liquid systems and flow aid and anti-caking agent for fine powders.

## Samples conditioning

All samples were conditioned and maintained, at ambient temperature, inside sealed containers controlled by saturated salt/water solutions to control relative humidity at 30% (Magnesium chloride -  $MgCl_2$ ) and 60% (Sodium Chloride -  $NaCl$ ). Samples were allowed to equilibrate until they reached the environment conditions, validated by daily water activity,  $a_w$ , measurements using an Aqualab 4TE from METER®.

To study surface additives influence on flowability, bulk powders were weighted with 0.5 and 2% w/w of each flow regulator and blended in a 3D shaker mixer Turbula® T2F from WAB group for 20 minutes. It should be noted that no differences in flowability assessment were obtained when the mixing time increased from 10 to 60 minutes. Once the mixtures were made, samples were conditioned and maintained, at ambient temperature, inside sealed containers controlled by saturated salt/water solutions as described above.

## 2.2. Powders physical characterisation techniques

Particle size distributions were measured by laser diffraction in liquid media with a Mastersizer 2000 from Malvern Instruments. Ethanol was used in order to improve particles dispersion and to avoid dissolution. All samples were analysed in triplicate to ensure reproducibility, with an instrument uncertainty of 1 [ $\mu m$ ].

Particles morphology analyses were assessed with a JSM T330A Scanning Electron Microscopy (SEM) from JEOL, and a field emission gun operating at 5 kV. Before analysis, samples were placed onto doubled-sided adhesive and coated with Gold-Palladium mixtures during 6 min using an Ion SPUTTER JFC-1100 under air purge. Particles/glidants mixtures were analysed with a Field Emission SEM from ZEISS, Merlin Compact with the proven GEMINI I electron column. Samples were placed onto carbon conductive tape and coated about 20 nm with carbon. EDS analysis were performed with a QUANTAX-XFlash6 detector with a peak resolution of 129eV, from Bruker. EDS was performed to confirm the presence of colloidal silicas on the surface of host powders.

Water sorption isotherms were performed at 20°C in 3 Flex from Micromeritics. Before scanning, samples were vacuum dried during ten hours at 15° C. The true density analysis of powder was performed in an AccuPyc 1330 Helium pycnometer from Micromeritics. All data measurements are the average of ten measurements obtained from one powder sample.

## 2.3. Granular compaction devices

### Vibration, free surface conditions

To determine flowability from tapped density measurements, different methods and devices can be used. The most used, described on the United States Pharmacopoeia,

suggests freely pouring a test sample weight of 100 g in a 250 mL volumetric cylinder as shown in Fig. 3.2. The protocol consists of measuring the unsettled apparent volume,  $V_0$ , and carrying out 10, 500, and 1250 taps on the same powder sample and reading the corresponding volumes to the nearest graduated unit. If the difference between  $V_{500}$  and  $V_{1250}$  is less than or equal to 2 mL,  $V_{1250}$  is the tapped volume. If the difference between  $V_{500}$  and  $V_{1250}$  exceeds 2 mL, repeat in increments of  $V_{1250}$ , until the difference between succeeding measurements is less than or equal to 2 mL [107].

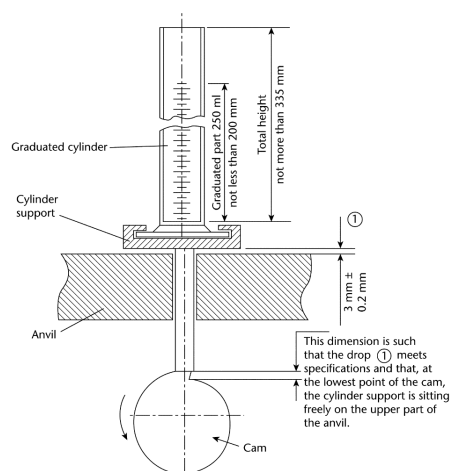


Figure 3.2. Apparatus description from [107].

In this study, DensiTap<sup>®</sup> from Granuloshop<sup>®</sup> was used for measuring bulk density with a graduated glass cylinder of 250 mL. In this device, the tapping action is provided, under zero shear conditions, by a rotating cam that raises the cylinder platform through a fixed distance of 3 mm at a nominal rate of 250 drops per minute. About 150 mL of powder was freely poured using a funnel into the vessel allowing the aerated density to be determined. It should be noted that it is impossible to fit 100 g of Avicel<sup>®</sup> PH-102 or RetaLac<sup>®</sup> in a 250 mL container; this is similar for a wide range of pharmaceutical excipients.

Several authors suggest that flow behaviour analysis using tapped density data is strongly affected by the highly irreproducible initial pouring of the powder. As described in previous works, [50], we found a highly reproducible initial state when controlling powder moisture conditioning. Thus, the data error was determined by considering systematic and random errors, and to do so, each experiment was repeated 3 times.

### Uniaxial compaction, packed bed conditions

Compressibility studies in packed bed conditions were performed using an FT4 powder rheometer from Freeman Technology<sup>®</sup>. The samples were poured into a borosilicate split vessel. The test started with a mechanical conditioning step by establishing uniform stress in the powder bed (Fig. 3.3, left). When the conditioning cycle is over, the vessel splits allowing a precise volume of 10 mL to be attained. The analysis was achieved by applying

increasing levels of force directly onto the granular media with a vented piston, allowing the trapped air within the powder to escape, and by measuring volume changes depending on the applied load (Fig. 3.3, right).

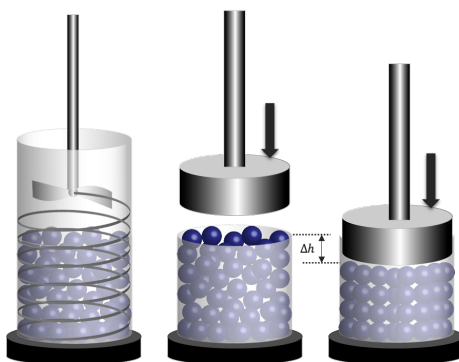


**Figure 3.3.** FT4 rheometer compressibility test, from conditioning to compaction.

During the test, the changes in volume for a given applied normal stress were collected. In order to determine the specific energy supplied to the granular media an external data treatment must be carried out. In fact, FT4 software determines the energy supplied to the powder by using a trapezoidal numerical integration. Nevertheless, this data treatment lacks of physical meaning as it integrates all height changes, even the non-decreasing ones. As the height sensor is extremely sensitive, the energy provided to the system is calculated as time-dependent and so, aberrant values can be obtained. In order to give a mechanical sense to the experimental data, the specific energy supplied to the system was determined with Matlab<sup>®</sup> by discretizing the normal stress values as function of the packed bed height evolution. To do so, it is necessary to identify the areas where the normal stress is kept constant by the derivative of force with respect to time (Fig. 3.4.a in red). Then, to determine an average force, and to be able to relate it to displacement values, we selected around 20 data values in the red zone, where non-evolution was found. Finally, each setpoint gave rise to a specific energy value which is related to HR as shown in Fig. 3.4b.

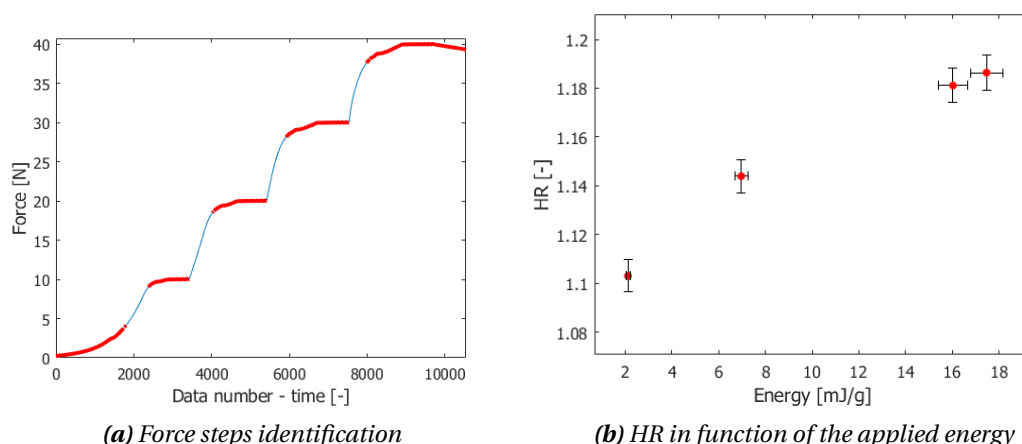


**Figure 3.4.** Example of FT4 compaction test data treatment. Applied normal stress increments of 10 N until 40 N.

To allow a better comparison between the devices, their characteristics and operating conditions are summarized in Table 3.1. It should be noted that powder humidity conditioning and control allowed us to obtain a highly reproducible initial state, regardless of the device. This argument allowed us to validate the use of HR as a flow behaviour index, others could be used (Carr, Void ratio).

**Table 3.1.** Devices characteristics

Characteristics/Device	Densitap	FT4
Compaction by	vibration: Free falls	Normal stress
Particles reorganisation	Free surface	Packed bed
Scanning	Number of taps	Force [N]
Quantity of powder [mL]	150	10
Vessel material	borosilicate glass	borosilicate glass
Applied Force [N]	215	0 - 40
Vessel dimensions [mm] (diameter/height)	26/300	25/30

## 3. Results & Discussions

### 3.1. Physical characterisation

The particle size distribution analysis, summarized in Table 3.2, shows that Avicel PH-102 particles are bigger than Retalac. From the SEM images, scale bar of 100  $\mu\text{m}$  and 500  $\mu\text{m}$ , Avicel<sup>®</sup>PH-102 particles exhibit an isometric rod shape with a rough surface (Fig. 3.5), while Retalac<sup>®</sup> seems to be composed of agglomerates of amorphous-like particles (Fig. 3.6). Absorption/Desorption isotherms showed that both excipients are hydrophilic and absorb water at low moisture content (Fig. 3.7). Samples' sorption behaviour analyses determined our moisture conditioning choice, 30 and 60% RH.

Table 3.2. Excipients as host particles

Powder	Particle size distribution $\approx 1$ [ $\mu\text{m}$ ]					behaviour towards water **
	$d_{10}$	$d_{50}$	$d_{90}$	$d_{32}$	$d_{43}$	
Avicel® PH-102	29	104	248	40	126	Hydrophilic
RetaLac	89	203	408	159	229	Hydrophilic

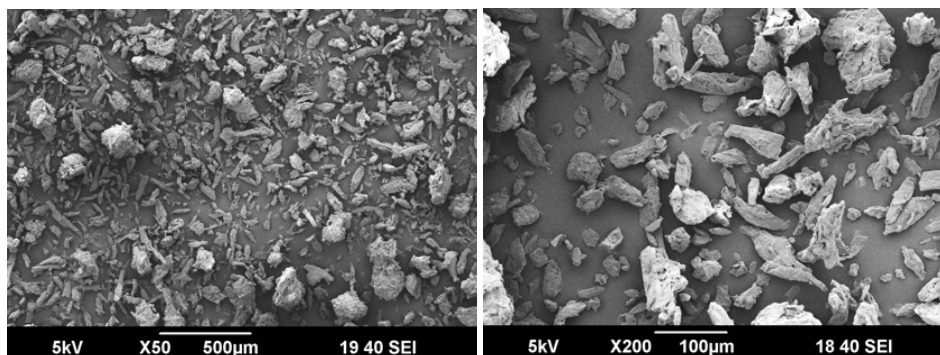


Figure 3.5. SEM micrographs of Avicel® PH-102, at different magnifications.

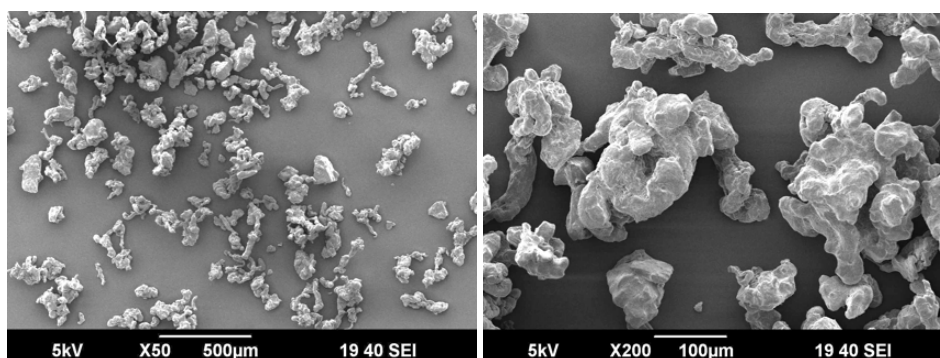


Figure 3.6. SEM micrographs of RetaLac®, at different magnifications.

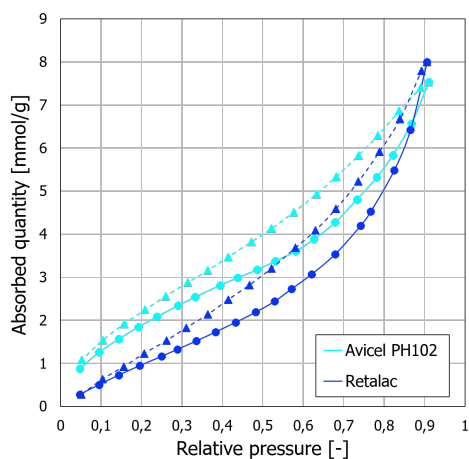


Figure 3.7. Water sorption isotherms of Avicel® PH-102 (cyan) and RetaLac® (blue), at 20°C. Sorption curves are represented with a solid line, and desorption curves with a dashed line.

Some of the physical characteristics of the silica nanoparticles are shown in Table 3.3. Supplier size specifications describe micro-size particles/aggregates using laser diffraction. The European Commission proposes that materials can be classified as nanomaterials (NM) if their volume-specific surface area, VSSA, is larger than  $60 \text{ m}^2/\text{cm}^3$  [33]. Thus, according to the VSSA estimations, SIPERNAT<sup>®</sup>s D10, D17, 50S and 500LS can be considered as NMs.

**Table 3.3.** Physical characteristics of silica nanoparticles

SIPERNAT <sup>®</sup>	Particle size distribution			BET ** [ $\text{m}^2/\text{g}$ ]	VSSA* [ $\text{m}^2/\text{cm}^3$ ]	behaviour towards water **
	$d_{50}$ **	$d_{50}$ *	$d_{32}$ *			
D10	6.5	7	7	90	178	Hydrophobic
D17	10	8	6	100	201	Hydrophobic
50S	18	16	14	500	1060	Hydrophilic
500LS	10.5	14	12	450	968	Hydrophilic

\*\* Evonik data, \* our data, both in [ $\mu\text{m}$ ]

### 3.2. Dynamics of compaction under free surface conditions

The evolution of powders compactness during vibration according to the number of taps is presented in figure 3.8. As expected, poorly flowing powders, such as Avicel<sup>®</sup> PH-102, are more compressible. Also, the repeatability from 3 experiments showed a larger random error using Retalac<sup>®</sup>, despite the conditioning (Fig. 3.8).

It is common use in scientific literature to determine tapped density systematically after 500 taps, as the number of taps suitable to reach the steady state [189]. For Avicel<sup>®</sup> PH-102 at 500 taps, the powder bed had not reached its maximal compaction state and so, the HR value obtained at this state (or time) is significantly different from the one obtained after 10 000 taps (Fig. 3.8.a). Using  $\text{HR}_{500}$  Avicel<sup>®</sup> PH-102 flowability is classified as "Acceptable", while at 10 000 taps is classified as "Cohesive", which is consistent with its flow behaviour observed with the naked eye. In difference, for RetaLac<sup>®</sup> samples, there is not a significative evolution of the powder compactness after 500 taps (Fig. 3.8.b).

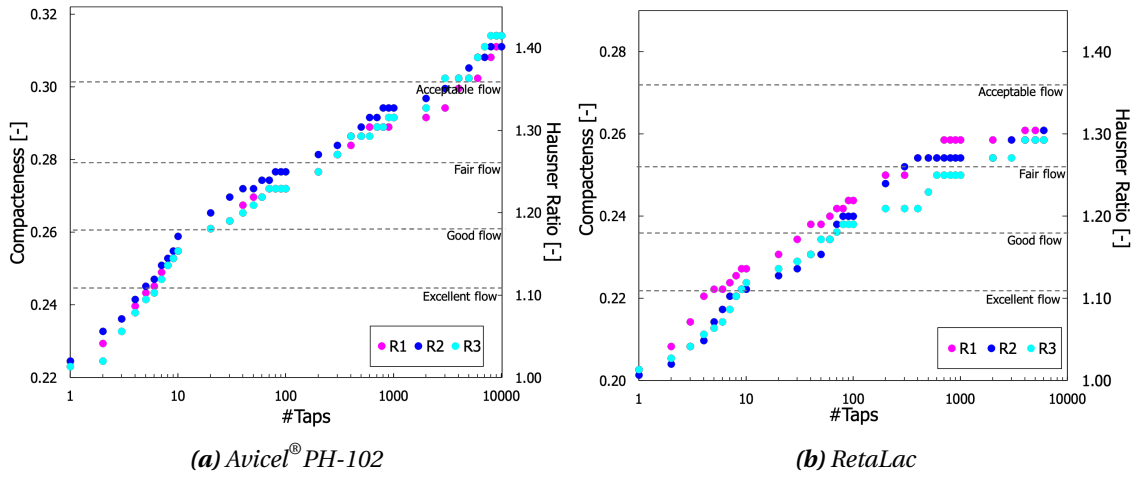


Figure 3.8. Study of the dynamic of compaction in Densitap<sup>®</sup> samples conditioned at 30% RH.

It should be noted that both samples exhibit an easily reproducible initial state regardless the moisture content. Moreover, the moisture content at 30% or 60% RH has no influence on samples compaction when using Densitap as a flow tester (Fig. 3.9).

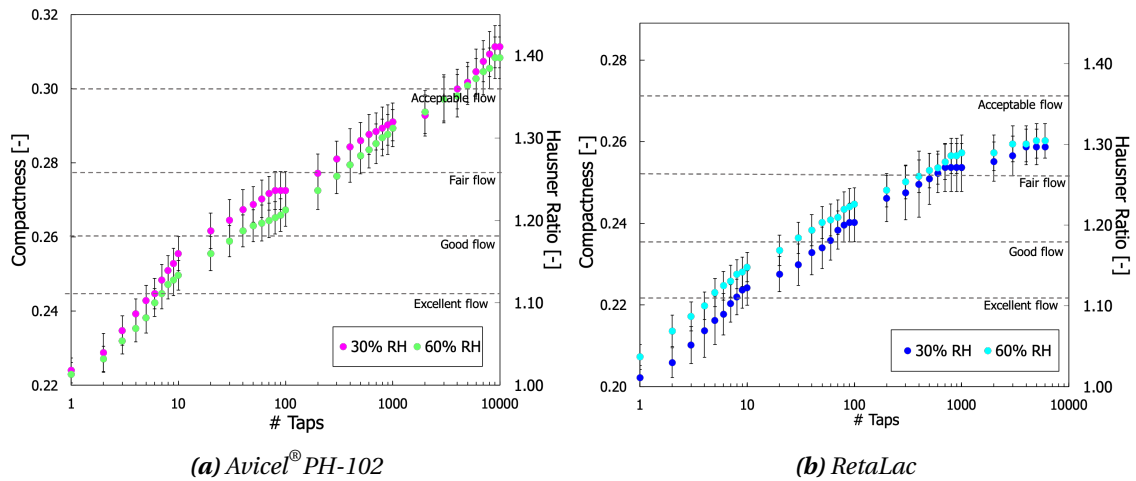
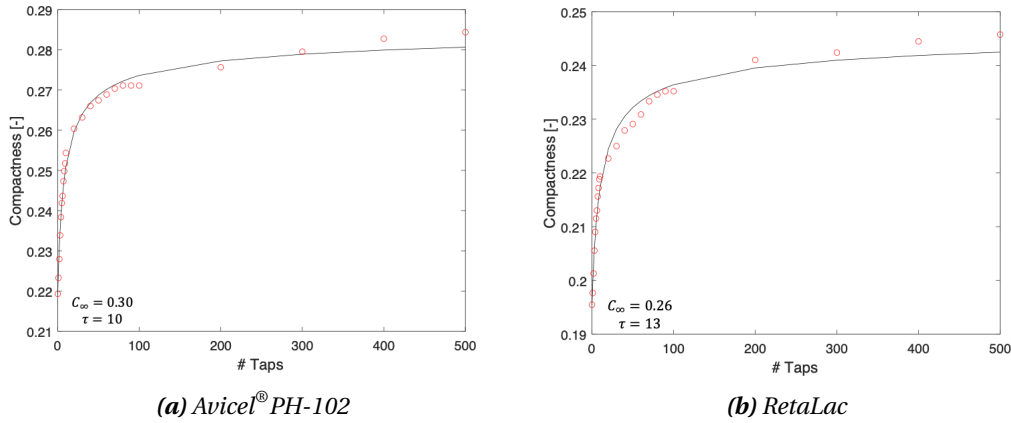


Figure 3.9. Dynamic of compaction as function of the powder moisture content using Densitap<sup>®</sup>.

### Modeling

The mathematical model describing the dynamic of compaction showed a similar fit for the Chicago and the KWW model with, in both cases, at least a 97% prediction interval (Figs. 3.10 and 3.11). The limitation of the Chicago model lies in the fact that it does not fit the experimental data when approaching the stationary state (Fig. 3.10). Thus, it fails to predict the number of taps needed to reach the steady state,  $\tau$ . For example, for Avicel<sup>®</sup> PH-102 the predicted number of taps needed to reach the steady state was around 100 000 taps while experimentally, only 8 000 taps are required. Nevertheless, the  $\rho_\infty$  parameter obtained from the model is predicted fairly accurately. For example for Avicel<sup>®</sup> PH-102  $\rho_\infty = 0.29 \pm 0.01$ , while experimental data showed a  $\rho_\infty = 0.31 \pm 0.01$ .



**Figure 3.10.** Chicago Model obtained from iterative minimization using Densitap data (500 taps). Samples conditioned at 30% RH.

In the KWW model,  $\rho_f$  is used as a minimization parameter better fitting the experimental data when reaching the steady state. In this case, the value of  $\tau$ -parameter, seems to be more representative of the progressive arrangement of grains. Nonetheless, a slight deviation from the model is detected for the first 40 taps (Fig. 3.11). Similar results were obtained for the samples conditioned at 60% RH.

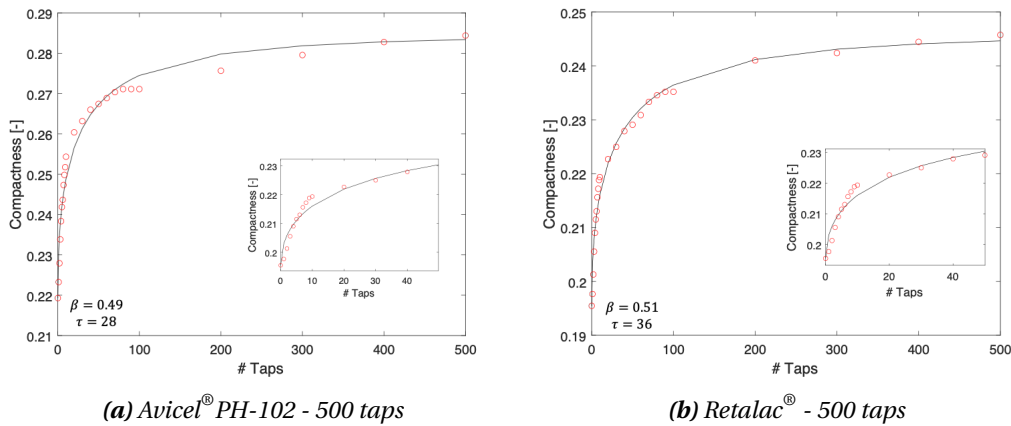


**Figure 3.11.** KWW model obtained from iterative minimization using DensiTap data (500 taps). Samples conditioned at 30% RH.

The mathematical model describing the dynamic of compaction showed a similar fit for the Chicago and the KWW model with, in both cases, at least a 97% prediction interval (Figs. 3.10 and 3.11). Rondet et al. [181] compared different densification models highlighting that the KWW equation ensures the best mathematical fitting of the experimental data using  $R^2$  as a fit parameter. This statement is accurate for powders such as Kaolin and Calcium phosphate. Nonetheless, when they analysed unsaturated microcrystalline cellulose, the authors found a better agreement between the KWW and Chicago model, which agrees with our results. Differences can also arise from the use of  $R^2$ , as an inadequate parameter to determine the goodness of fit for nonlinear models.

### 3.3. From compressibility to flowability, an energetic approach

In this section, we study flowability from compressibility as a function of the consolidation strength. To do so, each applied load gives rise to a steady compaction state that can be related to the HR value. In order to study the energy impact, we tested four different ramps of force from 2 to 40N. Some of the results are shown in figure 3.12.a using Avicel® PH-102 conditioned at 60% RH. As shown in the figure, powder compactness and flowability evolve exponentially with the specific energy supplied to the powder bed.

Compressibility is surprisingly independent of the force ramp step, meaning that the powder's previous mechanical history does not influence its compaction behaviour. We always obtained the same compaction state for a given energy, indifferent to previous loads. To deepen such a statement, we decided to study the influence of the conditioning step, which intends to provide a reproducible initial state by subjecting the samples to the same mechanical treatment, acting as an aeration phase. Two force ramps were tested with and without the conditioning step. Results in figure 3.12.b showed no significant difference between the samples subjected to mechanical conditioning and the simple act of freely pouring the powder. In this case, compressibility, and so flowability, seemed to only be affected by the maximal load supplied to the granular media.

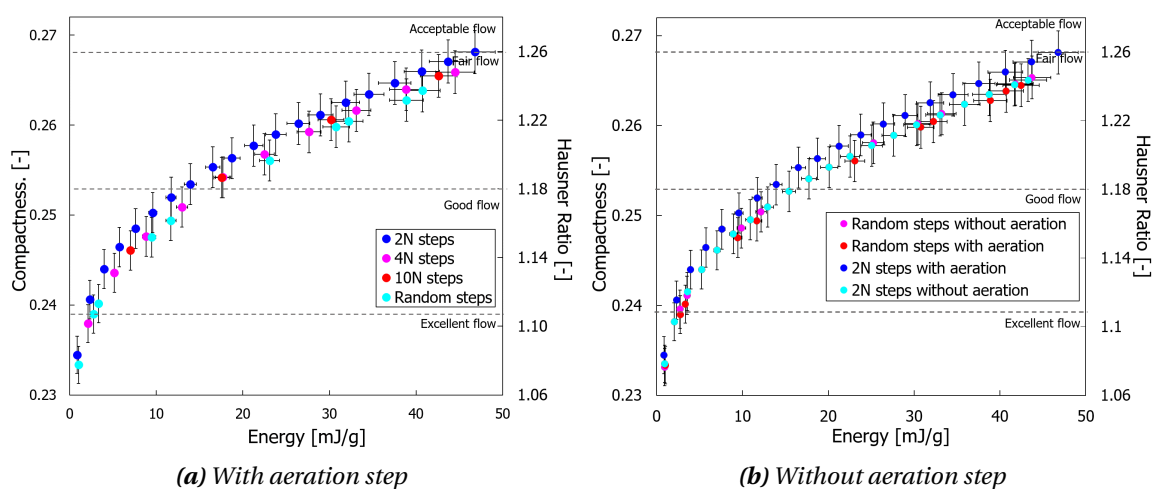


**Figure 3.12.** FT4 compaction test at different force ramps with Avicel® PH-102 at 60% RH.

The effect of moisture content on compactness, and so on flowability, is presented in Figure 3.13. For Avicel® PH-102, the sample conditioned at 30% RH had a better flowability than the one conditioned at 60% RH, despite the specific energy supplied to the media (3.13.a). It is well-known that the moisture content in granular media favors the formation of liquid bridges, thus increasing particle cohesion and decreasing flowability. Notwithstanding, for Retalac, moisture content seems to not have any influence on its flowability.

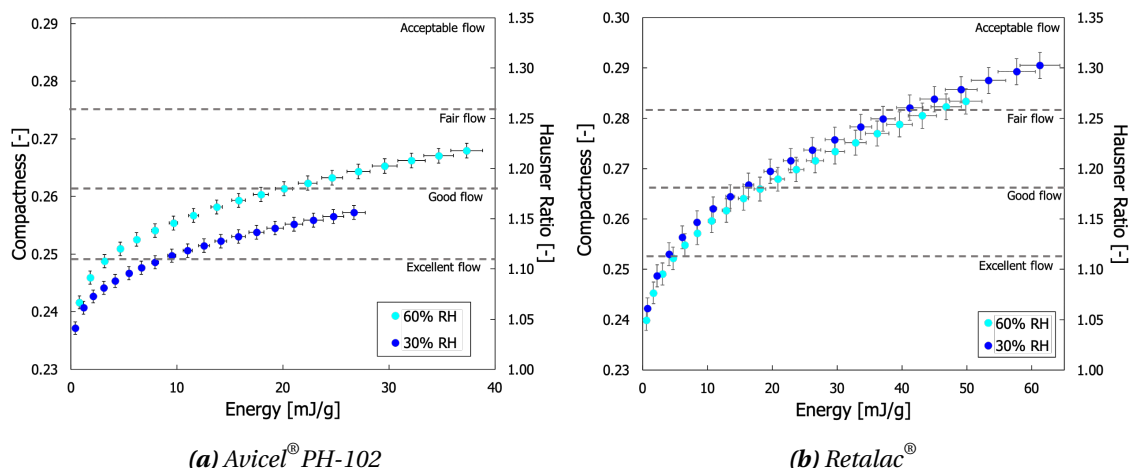


**Figure 3.13.** Compactness and flowability assessment as a function of the specific energy supplied to the system. Samples conditioned at 30% and 60% RH.

Avicel<sup>®</sup>PH-102 results are in contradiction with those obtained with Densitap<sup>®</sup> (Fig. 3.9.a). Unlike Densitap, the compression test allows a good differentiation of the two environmental conditionings. The strength of the applied load could explain this. Densitap<sup>®</sup> transfer a force of about 215 N to the granular media, while in FT4 experiments the maximal load is about 40 N. At low applied forces, like those provided by the FT4 compaction cell, some granular materials, more precisely cohesive powders, such as Avicel<sup>®</sup>PH-102, will not reach a high compaction state (Fig. 3.14). For example, in this case, using FT4 and Densitap, the flowability could be described as *Good* to *Fair*, with *Fair* being more appropriate for the real flow behaviour of the powder. On the contrary, Retalac<sup>®</sup> samples can be classified as having an *Acceptable flow*, regardless of the device. In summary, FT4 results describe flowability during uniaxial compression at low consolidation strength, and so, powder flow properties could differ for higher consolidation stress as shown in figure 3.14. The energetic approach allows us to understand the differences, or similarities, in flowability assessment when comparing devices.

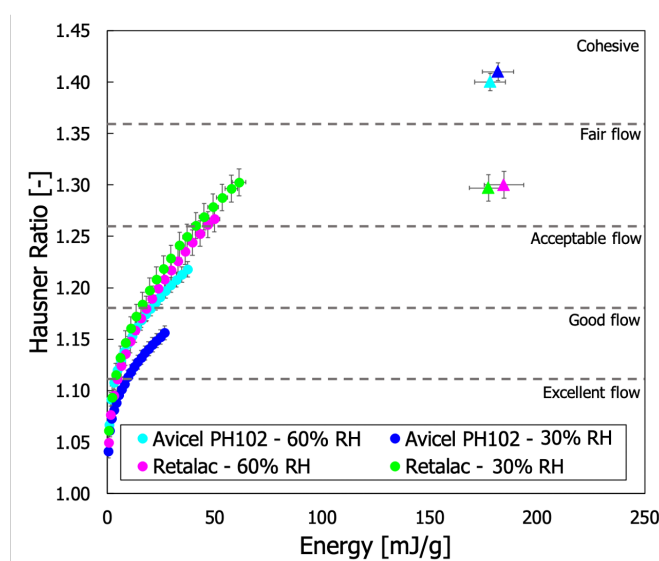


**Figure 3.14.** Flowability assessment as function of the specific energy supplied to the granular media using FT4 (circles) and Densitap (triangles) devices.

### Colloidal silicas as glidants

Both host powders were weighed with 0.5 and 2% w/w of SIPERNAT<sup>®</sup> 50S, 500LS, D10 and D17 (Figs.3.15 and 3.16). For binary Retalac<sup>®</sup> mixtures conditioned at 30% RH, all the configurations studied, in terms of the type of glidant and concentration, significantly improved powder flowability (Fig.3.15.a). In contrast, no statistically significant differences were obtained between flow regulators. The increase in moisture content of binary mixtures at 60% RH showed similar results (Fig.3.15.b). In the case of Avicel<sup>®</sup> PH-102, the four NPs used in our study, D10, D17, 50S and 500LS, significantly improved the flowability of the host particles regardless of the moisture content (Figs.3.16 and 3.17). Firstly, no statistically significant differences between NPs with the same behaviour towards water were found (Fig.3.16.a). Secondly, no differences were obtained when increasing the amount of NPs added to the host particles, independent of its hydrophilic nature (Fig.3.16.b).

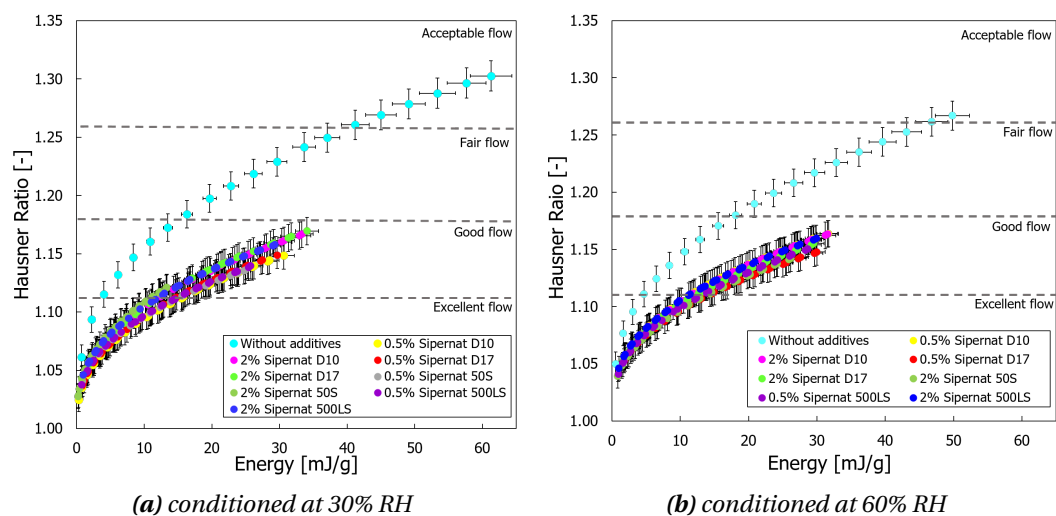


**Figure 3.15.** Flow influence of NPs for RetaLac using FT4. Force ramp from 0 to 40 N using a 2 N step.

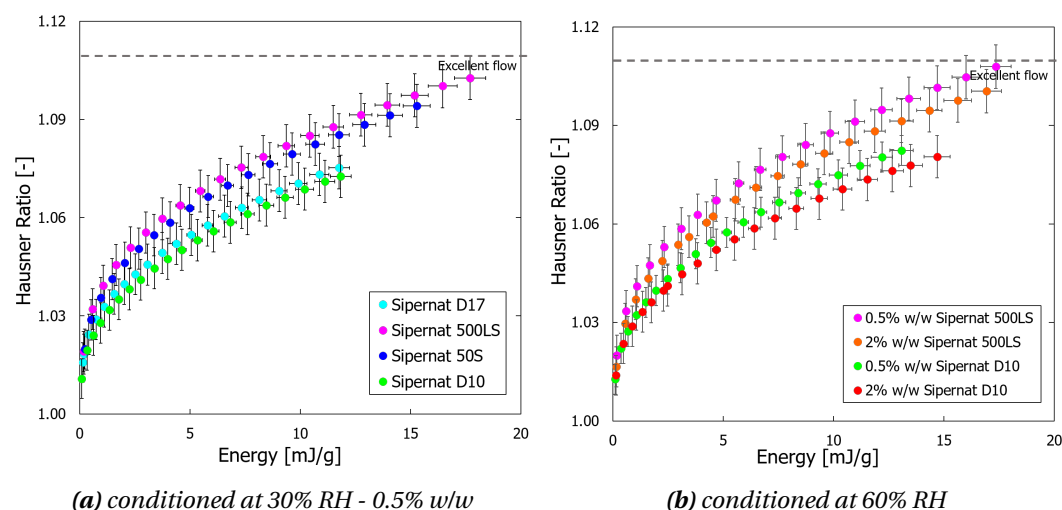


**Figure 3.16.** Flowability influence of NPs for Avicel<sup>®</sup> PH-102 using FT4. Force ramp from 0 to 40N using a 2N step.

In summary, the effect of adding 0.5% w/w of SIPERNAT<sup>®</sup> D10 or 500 LS, on Avicel<sup>®</sup> PH-102 flowability at different moisture conditions is presented in figure 3.17. In this case, despite the moisture content, both glidants, D10 and 500LS, improved significantly the flowability of the excipient, with a better performance of the hydrophobic one, D10. Similar results were obtained by Müller et al. [77]. In their work, the authors observed, using binary mixtures of corn starch, that hydrophobic flow regulators reduce cohesive forces to a greater extent than hydrophilic ones. Ruzaidi et al.[81] also showed that hydrophobic nano-silica improved ibuprofen's flowability slightly more than the hydrophilic one. In comparison, Zimmermann et al. [190] did not find any direct correlation between the hydrophilicity of the nanomaterials (fumed nano-silica, Aerosils<sup>®</sup> and their ability to reduce the tensile strength of powder mixtures with corn starch.

Several hypotheses could explain this behaviour. The first one is related to surface chemistry changes. As Avicel® PH-102 is highly hydrophilic, its surface modification may reduce the liquid bridge formation during moisture conditioning. The second one is related to the size of the additives. Kojima et al. [191], using binary mixtures of polymer powder with Aerosils®, showed that the smaller the size of the colloidal silica and their aggregates, the more effectively they worked as lubricants, thus reducing internal friction. Similar results were obtained by Müller et al. [77], who worked with binary mixtures at 0.2% w/w. Nonetheless, in our case, when comparing SIPERNAT® 50LS to 500LS or SIPERNAT® D17 to D10, which are only differentiated by a grinding step, no improvements on flowability were observed.

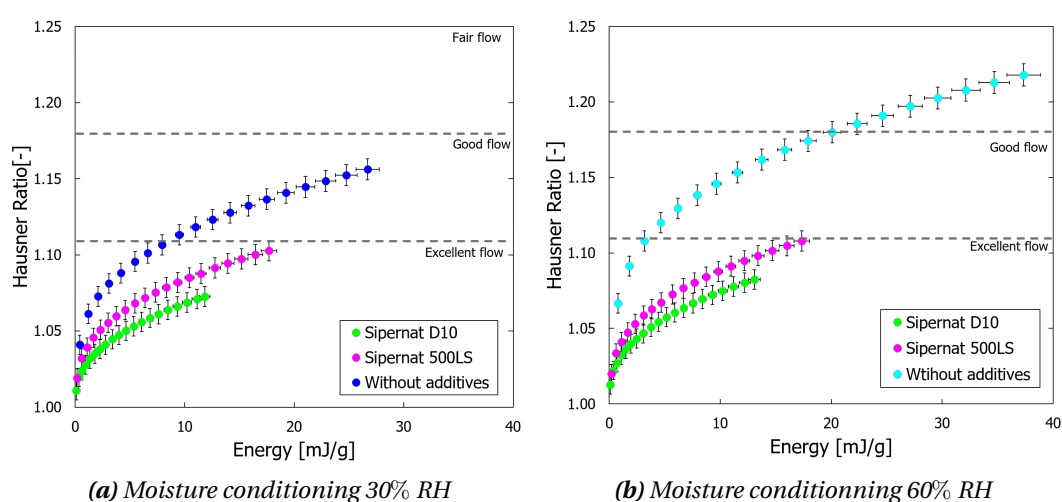


**Figure 3.17.** Influence of Sipernats D10 and 500LS in the flowability of Avicel® PH-102. Mixtures prepared with 0.5% w/w of S-NPs and conditioned in different moisture environments.

To get a better look at these results, the SEM analysis of Avicel® PH-102 when adding 0.5% w/w of NPs is shown in figures 3.18, 3.19, 3.20 and 3.21. From SEM micrographs, it is possible to note that the VSSA values are not representative of the NM's size. Hydrophobic NPs (Figs. 3.20 and 3.21), with a smaller VSSA value, gave rise to smaller aggregates than the hydrophilic ones (Figs. 3.18 and 3.19). Bulk powder mixture with hydrophilic additives showed large aggregates/agglomerates (200 nm) adsorbed on the surface of the Avicel® PH-102 particles. In difference, Zimmerman et al. [190] never found large agglomerates of fumed nano-silica adsorbed on the surface of the corn starch particles.

It should be expected that the particle/glidant bond strength influences the flow regulating potency of the NPs. The chemical treatment undergone to produce hydrophobic NPs decreases the number of hydrogen bonds. The lack of additional hydrogen bonds generates aggregates/agglomerates with an inferior bond strength, and so deagglomerate easily, thus giving rise to smaller aggregates. This statement was validated in our study comparing figures 3.19 and 3.20. The smaller the NP aggregates the better the surface coverage.

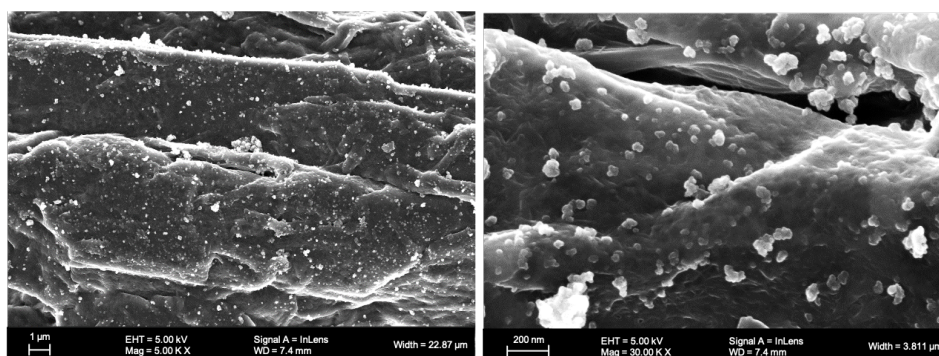


Figure 3.18. SEM micrographs of Avicel<sup>®</sup> PH-102 with 0.5% w/w of 50S, conditioned at 30% RH.

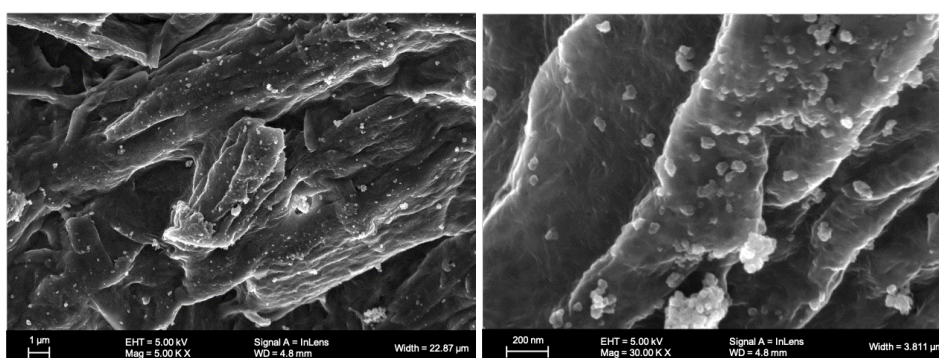


Figure 3.19. SEM micrographs of Avicel<sup>®</sup> PH-102 with 0.5% w/w of 500LS, conditioned at 30% RH.

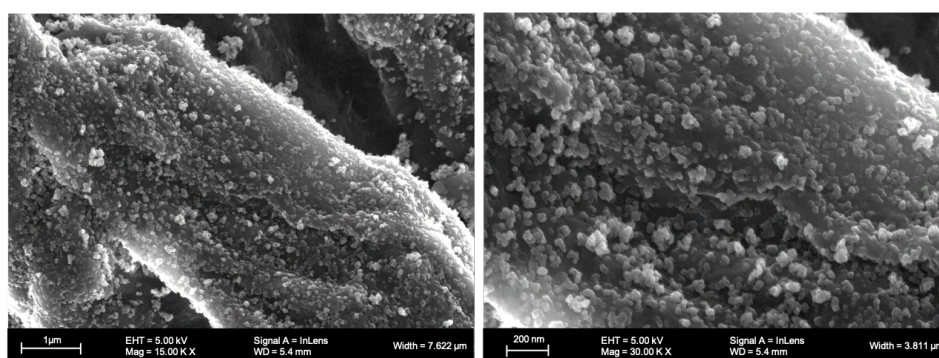
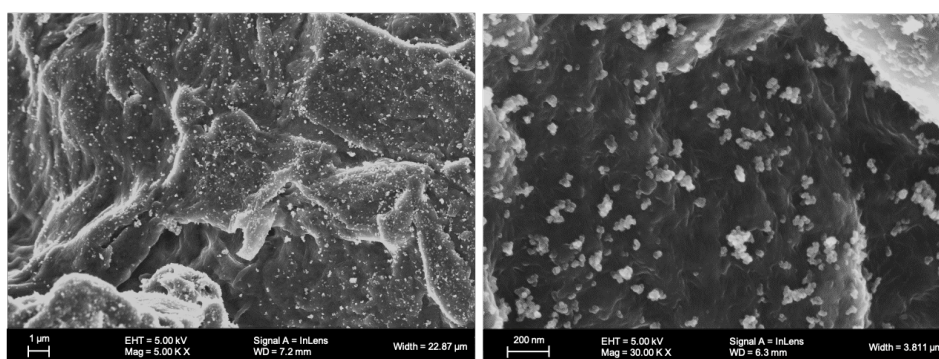


Figure 3.20. SEM micrographs of Avicel<sup>®</sup> PH-102 with 0.5% w/w of D10, conditioned at 30% RH.



**Figure 3.21.** SEM micrographs of Avicel<sup>®</sup> PH-102 with 0.5% w/w of D17, conditioned at 30% RH.

The flow regulating potency of the nano-additives also depends on the interparticle contacts: particle-to-particle, particle-to-silica, or silica-to-silica. This statement is related to the amount of NPs added to the mixtures using a relatively simple mathematical analysis (spherical monodisperse nanoparticles with random packing) like the one described by Valverde et al. [185]. In our case, we estimated that when adding 0.5 or 2% w/w of colloidal silica, the interaction between the grains is governed by silica-to-silica interactions. This rather rough estimation supports our results and could explain why no differences were found when increasing the amount of NPs added to the mixtures, independently of their hydrophilicity (Figs. 3.16 and 3.17). All this somewhat rejects the assumption that the silica adsorbates lead to a flatter surface. Moreover, the change in the mixtures' surface chemistry, related to the glidants' hydrophilicity, improved flowability similarly, regardless of the moisture conditioning environment of the samples (Figs. 3.16 and 3.17). The mathematical approach also suggests that to cover the surface with 0.5% w/w, the adsorbates should measure 300 nm. Nonetheless, Fig. 3.20 shows that binary mixtures with SIPERNAT<sup>®</sup> D10 generated a high coverage of particles with monodisperse fine adsorbates of around 50 nm.

When possible, surface coverage was also estimated using SEM micrographs using ImageJ software (Table 3.4). The number of adsorbates was determined in different regions of Avicel's surface of binary mixtures. For hydrophobic adsorbates, we obtained about 17% coverage for SIPERNAT<sup>®</sup> D17 and, at least, 80% for SIPERNAT<sup>®</sup> D10. For hydrophilic silica additives, a smaller surface area of the host particle was covered, from 6 to 16% for SIPERNAT<sup>®</sup> 500 LS and 50S, respectively. Even if this image analysis lacks statistical significance, it shows, and corroborates, that smaller adsorbates give rise to a better surface coverage, despite its hydrophilicity. It also highlights similar surface coverages with SIPERNAT<sup>®</sup> 50S and D17 binary mixtures, with a few bigger aggregates for 50S. Interestingly, although SIPERNAT<sup>®</sup> D10 produced a higher surface coverage, almost total (Fig. 3.20), flowability enhancement was obtained at lower surface coverages, similarly to when using SIPERNAT<sup>®</sup> D17.

In the literature, different surface coverage mass ratios, w/w, are proposed to improve

flowability. Fulchini et al. [188] found an optimum surface area coverage of around 30% w/w for mixtures of glass beads made cohesive by silanization. In their case, higher surface area coverages decreased flowability. According to Ruzaidi et al. [81], for host particles with a mean diameter of 60  $\mu\text{m}$ , the required amount of NPs to improve the powders' flowability is between 0.5 and 1% w/w. From our results, we can conclude that powder flowability improvement by glidants seems to be related to both of the following: nano-silica aggregate size distribution (obtained after mixing) and surface area coverage. We propose to define the amount of NPs to add to powder formulations in terms of surface coverage and not through mass ratios (w/w). A good example is proposed by Zhu et al. [192]. The authors determined by modeling the optimal size of nano additives and the minimal surface area coverage for binary mixtures of zeolite fine powder and nano-silica. It was suggested that, in order to reduce cohesiveness and to improve flowability, zeolite particles (0.5 - 50  $\mu\text{m}$ ) should be covered with about 1% of 10 nm-additives.

**Table 3.4.** ImageJ software Analysis of SEM micrographs of Avicel<sup>®</sup> PH-102 surface in binary mixtures of 0.5% (w/w).

SIPERNAT <sup>®</sup>	Surface [ $\mu\text{m}^2$ ]	Adsorbates' number [-]	Adsorbates' size [nm]	Coverage [%]
50S	11	256	18 to 532	16
500LS*	3.8	57	27 - 236	6
D17	9	214	17 to 316	17
D10 **			$\leq 100$	$\geq 80$

\* low contrast      \*\* naked eye

## 4. Conclusions

We have developed an experimental approach based on the energy supplied to powders during compaction under zero shear conditions. In these studies, we measured granular densification (bed height changes) as a function of the force applied to the system. Compaction is achieved during vertical tapping using Densitap and by subjecting the samples to low levels of stress during uniaxial compression using FT4. The compressibility of the powder bed was determined by the amount of energy supplied to the system during the test, but it could also be affected by the sample pre-consolidation state. We obtained a highly reproducible state by only conditioning the powder in a controlled moisture environment, thus validating the index choice.

Measurements were carried out to determine the moisture content's effect and the use of nanoparticles on the bulk flow properties of two well-known pharmaceutical excipients, Avicel<sup>®</sup> PH-102 and Retalac<sup>®</sup>. The influence of the moisture content influence was evaluated by conditioning the samples at 30 and 60% RH, while the impact of flow regulators impact was assessed by adding 0.5 and 2% w/w of precipitated silica nano-additives. From these measurements, we found an increase in flowability regardless

of the glidant amount. Adding more silica from 0.5 to 2% w/w did not seem to reduce internal friction.

We also noted that all SIPERNAT<sup>®</sup> grades showed different levels of disaggregation. Surface coverage analysis showed that adding NPs reduced the size of the contact zone, thus decreasing particle-to-particle interactions, and so, cohesion. The hydrophilicity of the colloidal silica affected surface coverage. Binary mixtures with hydrophobic additives generated smaller silica aggregates that were better spread over the surface of the host particles, explaining its better performance. In conclusion, the improvement of powder flowability by flow additives seemed to be strongly related to both the surface area coverage, and the nano-silica aggregate size. We suggest choosing the type and the amount of nanomaterials to add to formulations by considering both the surface area coverage and the size of the flow regulators after mixing. These parameters somehow describe/determine the type of interactions or their transition: particle-to-particle, particle-to-silica, or silica-to-silica.

Finally, the dynamic of compaction of Avicel<sup>®</sup> PH-102 and Retalac<sup>®</sup> were fit by the Chicago and the KWW model. Nonetheless, only the  $\rho$ -parameter (final compactness) from the Chicago equation was correctly related to the steady state.

In conclusion, as a general trend, we suggest studying flowability from granular compaction measurements by means of densification strength, related to the force or the energy supplied to the media. An energetic approach shows and explains the differences in flowability assessment between flow-testers. We have observed that device-related flowability agrees with the granular media flow, as an observation, when determined at the densest compaction state.

## 5. Host powders densification characterisation

In addition to the publication findings, in this section, the densification characterisation of the host powders, Avicel PH102 (AP), wheat flour (WF), joint filler (JF) and glass beads (GB), not included in the publication is presented. In figure 3.22, the  $HR_c$  is presented for all powders according to the number of taps. Similar to the AP behaviour, the JF requires at least 7000 taps to achieve its maximal compaction state according to the applied energy/force. In contrast, the other powders seem to be well described with only 500 taps, the commonly used protocol in the industry.

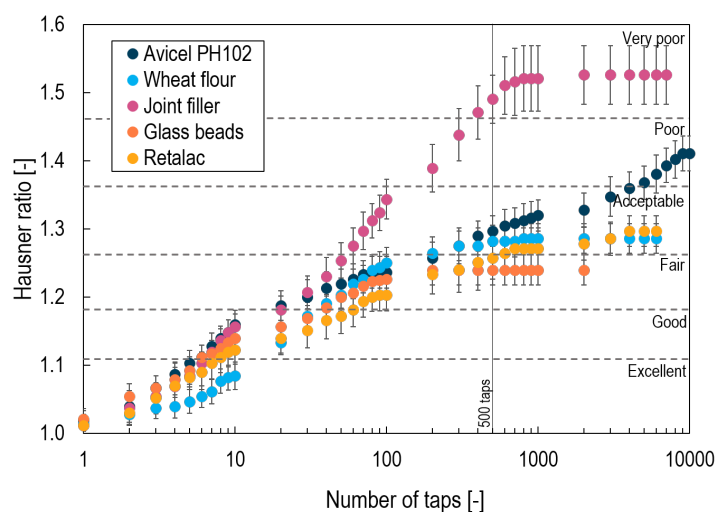


**Figure 3.22.** Granular densification expressed by HR of Avicel<sup>®</sup> PH-102, wheat flour, joint filler, glass beads and Retalac<sup>®</sup> assessed with a Densitap.

Furthermore, the influence of relative humidity (30% and 60%) was evaluated for all the HP. In the Densitap, no differences between the two tested conditions were presented in all of the HP. In contrast, the FT4 results showed that for AP and JF, the  $HR_c$  was smaller at RH influence on flowability for the AP and the JF. This result suggests that at 30% RH compared to 60% RH, suggesting less capillary forces in the former conditions. The other powders did not show any effect of the humidity at the tested conditions. The differences between the results on Densitap and the FT4 may indicate that the energy supplied by Densitap seems to overcome interparticle interactions due to capillary forces provided by 60% RH. Therefore, the uniaxial compression test was preferred for the following work to characterise powder densification since it is more sensitive than the Densitap. In addition, it is easily adaptable to the industry since it only needs a cylinder-piston system with force and displacement sensors. At low forces, it allows analysing of effects on the powders' flowability, such as the action of humidity. It also allows us to provide the system with a specific force to make comparing samples more accurate.

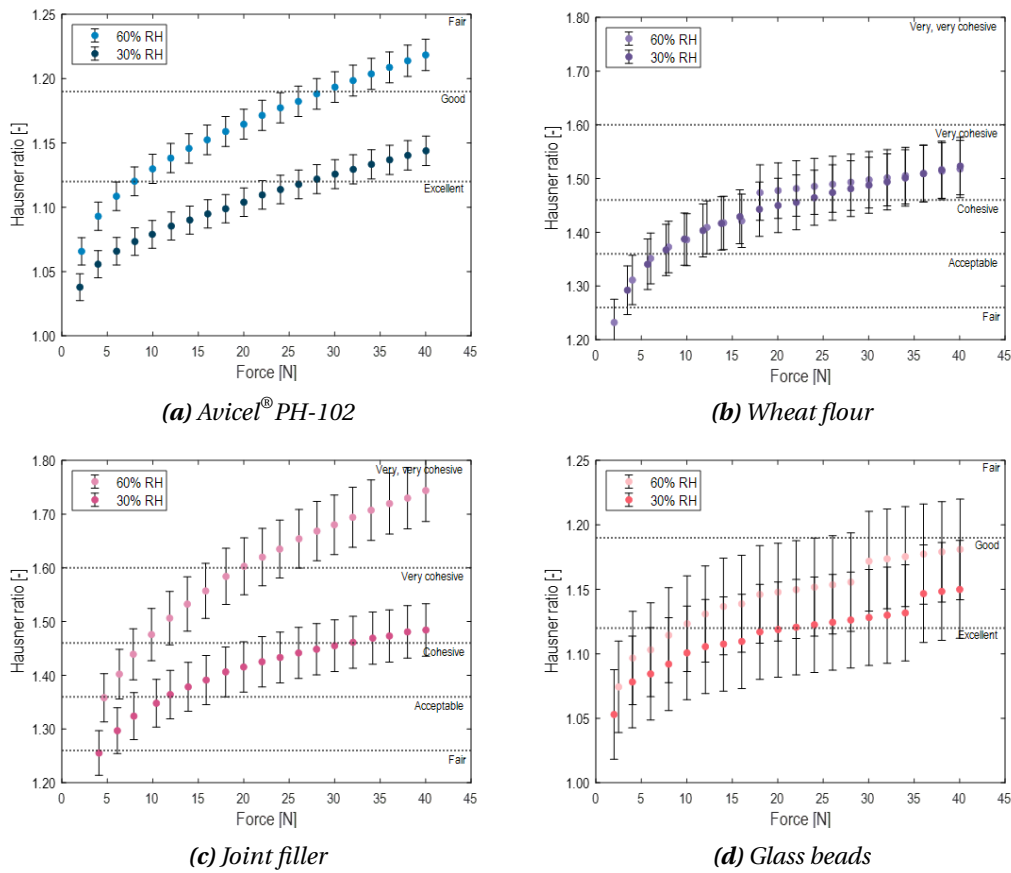


Figure 3.23. Powders flowability behaviour at 30% and 60% RH measured by FT4 compression test,  $HR_c$ .

On the other hand, if the force/pressure to which the powder is subjected in certain industrial processes is known, it is possible to simulate the densification of the powder and possibly evaluate its flowability under specific conditions. It is clear that it needs further development and testing for correlation with industrial processes, but it can be a quick and easy tool that does not require a specific piece of equipment. In this work, we validated this technique using an Instron press, and the results were the same as with the FT4 if the compression rate was kept the same.



# 4

## Surface coverage and flowability

---

The previous results suggested that flow enhancement with glidants might be associated with surface coverage (SC). Consequently, our interest was in evaluating how S-NP cover HPs and whether the coverage is consistent across particles. Then, the main focus is identifying the factors influencing flowability, particularly when adding glidants. Three action mechanisms of S-NP in flow behaviour were considered: (1) mechanical effect where the S-NP act by reducing friction, allowing host particles (HP) to roll without slipping [26] (Fig.4.1.a). The second proposes that glidants (2) act as spacers, increasing the distance between HPs, and thus reducing van der Waals forces,  $F_{vdW}$ , and liquid bridge creation (Fig.4.1.b) [81, 188]. The third mechanism alludes to (3) surface energy, rugosity, and chemistry modifications (Fig.4.1.c). In this hypothesis, S-NP acts similarly to physicochemical changes in a material affecting its surface energy.

To evaluate these three mechanisms of action and other influential factors on flowability, a D-Optimal experimental design consisted of 51 experiments evaluating five factors and four responses (Fig.4.2).

The last section, not included in the publication, aims to deep into the relationship between interparticle forces and flowability.

Main conclusions of this results chapter:

- *Powder's nature is the most influential factor in flowability.*  
This exposes the difficulty in drawing broad conclusions without referring to the sample, highlighting the complexity and challenges of providing global conclusions in powder technologies.
- *Bulk friction is not significant when interparticle forces govern or influence flow behaviour.*
- *Surface coverage strongly depends on S-NP/HP interaction strength.*

- *Hydrophobic S-NP improved flow behaviour, whereas the hydrophilic ones did not always act as actual glidants.*

This raises questions regarding the role of S-NP as spacers. If the S-NP action mechanism were solely related to spacing HP, it is expected to have a similar effect regardless of the S-NP's behaviour towards water.

- *Dispersive surface energy measurements showed that S-NP addition modified the surface energy of the samples HP.*
- *A surface coverage of 40% seems enough to enhance the flowability of cohesive powders.*

A protocol is proposed for determining the optimal quantity of S-NP based on the SC. Notably, the SC of all HP analysed in this study was less than 2% wt. By implementing this protocol, it may be possible to minimise S-NP use, thereby reducing the risk of occupational exposure associated with these materials.

## Silica nanoparticles as glidants for industrial processing: a statistical approach

Maria Camila Jiménez Garavito<sup>a,b</sup>, Maria Graciela Cares Pacheco<sup>a</sup>, Fabien Gerardin<sup>b</sup> and Véronique Falk<sup>a</sup>

<sup>a</sup> *Université de Lorraine, CNRS, LRGF, F-54000 Nancy, France*

<sup>b</sup> *Department of Process Engineering, Institut National de Recherche et de Sécurité, 54519 Vandœuvre, France*

Article published in the Industrial & Engineering Chemistry Research Journal

DOI: [10.1021/acs.iecr.2c02455](https://doi.org/10.1021/acs.iecr.2c02455)

### Abstract

Granular flows have been the Achilles heel of industrial development. In the past years, the glidant (flow-aids) addition, mostly amorphous silica nanoparticles (S-NP), has become a step in formulation to ensure process feasibility. Human and environmental exposure to S-NP has not been thoroughly evaluated, raising concerns about their toxicity. The action mechanism of glidants on flowability has been mainly attributed to a reduction of van der Waals forces, acting as spacers among particles. Notwithstanding, other action mechanisms could alter the flow, such as friction or surface energy modifications. This work aims to evaluate these action mechanisms through a D-Optimal experimental design. Results indicate that friction plays no role in complex granular flows when interparticle forces act on the rheology. Flow enhancement is surface-related, mainly related to microscopic grain-level properties. The size of the S-NP depends on grain-to-glidant interactions, which define surface coverage and flowability. Finally, a formulation strategy focusing on surface coverage is presented to mitigate the risk.

**Keywords:** *Granular matter, industrial powders, silica nanoparticles, glidants, flowability, surface coverage, D-Optimal design*

## 1. Introduction

Granular matter is ubiquitous in daily life and industry; after water, it is the second most frequently manipulated material form. Nevertheless, even today handling grains entails some sloppy and/or dangerous operations [3, 47, 193, 194]. Why? because unlike elastic solids or fluids, many crucial questions relating to the flow of granular materials remain unanswered. Indeed, we lack a well-understood theory. Since Coulomb, in the eighteenth century, many continuum models for dense granular flow have been proposed, from a soil mechanics perspective [4, 47] to fluid dynamical approaches [195–197]. However, none of them accurately describes ALL granular flows. Indeed, even if the flow dynamics of monodisperse, rigid, cohesionless grains, such as glass beads, can now be better assessed [196], the behaviour of industrial granular materials such as geophysical matter, raw materials, food, pharmaceuticals, cosmetics, is considerably less well understood.

Granular flow is critical to process feasibility because it affects several operational steps including formulation, filtration, sieving, micronization, storage, and transport [50, 51, 93]. As consequence, dangerous situations are often solved by operators such as manual intervention inside of the equipment, generating direct contact with products; the use of tools, like hammers, to deblock feeders and silos by hitting them, which degrades installations simultaneously [47, 110]. The dust generation during these operations increases the risk of dust inhalation, explosion and fire. Granular flow problems have been managed by (1) modifying facilities [198], which is seldom a universal solution; (2) adding a fluidization operation [199], which also requires a separation operation and thus increases process complexity; (3) adding glidants to formulations, which is considered the most effective option with the best benefit-cost ratio [50, 51, 77–80, 83]. Among glidants, nanomaterials (NM) have become an essential part of product formulation in many industrial sectors, including pharmaceutical, cosmetics, food, and aerospace industries [200–202]. According to the European Commission [203], a NM is “a natural, incidental or manufactured material containing free particles, in aggregate or agglomerate form, of which at least 50% of the particles, in numerical size distribution, have one or more external dimensions between 1 nm and 100 nm”. In 2012, global NM production was estimated at about 11 million tons per year, representing a market value of 20 billion euros [204]. One of the most frequently encountered NM, in terms of both production and use, is amorphous silica. Amorphous silica is the second most abundant element in the earth’s crust after oxygen. Silica nanoparticles (S-NP) are widely used in the food and pharmaceutical industries as a thickener/stabilizer in emulsions, to favor particle suspension in aerosols, or to enhance flow for dry powders [76, 205].

Based on data gathered by our group, manufacturer feedback indicates that S-NP are regularly used as flow enhancers in formulation over an empirical range of 0.5-2% wt [206]. Several studies report hydrophobic S-NP to outperform hydrophilic S-NP in terms of flowability [51, 77–79]. Ideal concentrations are in the 0.1-2% wt range, with better performance near the upper limit [80–84]. However, some other authors indicate that adding higher amounts of S-NP does not always increase powder flow, and in some cases it could even worsen it [50, 83, 87, 88].

The recommended proportion of S-NP, varying from 0.1% to 10% wt, depends on their function. The U.S. Food and drug administration (FDA) approves the use of S-NP as a pharmaceutical excipient and food additive, limiting their concentration depending on the product. For example, in foods, the authorized limit is less than 2% wt [207]. In 2018, the European food safety authority (EFSA) re-evaluated S-NP use, authorizing 0.2% to 3% wt, and establishing a “not specified” recommended daily intake due to an insufficient capacity to adequately characterise the additive in food applications [208].

The toxicity of S-NP has been a recurring concern over the years [209–214]. Murugadoss

et al. [23] reviewed studies performed from 2010 to 2016, and found that S-NP, in general, produces acute toxic effects in both *in vitro* and *in vivo* studies. Furthermore, the authors' conclusions indicate that the use of smaller particles induced more pro-inflammatory effects than micrometric particles. Most studies in the scientific literature focus on *in vitro* and *in vivo* experiments, making no attempt to extrapolate the results to real human exposure and its potential health effects. These limitations can be explained by the complexity of representing a realistic exposure scenario, or by a lack of available epidemiological data [23]. One exposure study conducted in Swedish foundries found that workers exposed to respirable silica presented higher morbidity following stroke compared to the general population [215]. S-NP has also been shown to induce cytotoxicity in human cells and alter the immune response *in vitro* and *in vivo* [216]. Despite these observations, S-NP are still considered non-toxic and non-irritant by the regulatory authorities. A survey of commercial food products revealed that in 14 samples, 10 contained from 2 to 200 mg of S-NP per serving [208], and the individual daily intake of S-NP is estimated to be about 20–50 mg [217]. In addition, studies have shown that S-NP are one of the most released NM into the environment [218]. Ale et al. [219] reviewed the ecotoxicity of S-NP on aquatic organisms showing that the release of these particles into the water may cause a wide variety of toxic mechanisms in the ecosystem, from species growth inhibition to cytotoxicity.

The effects of S-NP on individuals and the environment have not yet been adequately investigated, future investigations will require international scientific and legislative efforts. In consequence, it appears that one of the first priorities should be to limit the use of S-NP as flow enhancers, or to substitute them. To accomplish this, it is vital to understand how they interact with the material to which they are added, to determine the mechanisms involved in enhancing granular flow. This understanding may lead to the development of viable solutions presenting fewer risks. The study presented here was developed from these ideas.

How do glidants act? Two mechanisms of action are found in the literature. The first suggests a (1) mechanical effect where the S-NP act by reducing friction, allowing host particles (HP) to roll without slipping [26] (Fig.4.1.a). The second proposes that glidants (2) act as spacers, increasing the distance between HPs, and thus reducing van der Waals forces,  $F_{vdW}$ , and liquid bridge creation (Fig.4.1.b) [81, 188]. In this work, it is proposed a third mechanism alluding to (3) surface energy, rugosity, and/or chemistry modifications (Fig.4.1.c). In this hypothesis S-NP act similarly to physicochemical changes in a material affecting its surface energy [220–222].

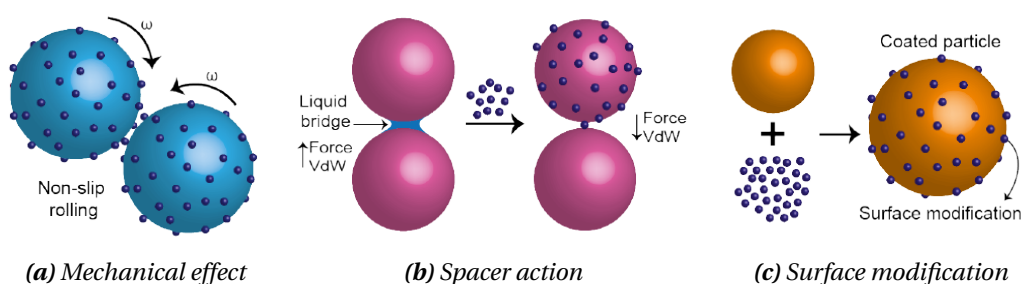


**Figure 4.1.** Mechanisms of action of flow agents.

This work aimed to address three questions:

- Why add S-NP? Do they always act as flow regulators?
- How do S-NP act: which is their action mechanism over flowability?
- How much should be added to enhance flow behaviour and mitigate the risk of exposure?

To do so, a D-Optimal design was chosen. The question "why" was addressed through the ability of S-NP to enhance flow behaviour, evaluated using two flow indexes: the flow factor,  $ff$  [4, 47], and the Hausner ratio,  $HR$  [50, 51]. The question "how" was assessed by evaluating the validity of the three mechanisms of action by associating them to: (1) bulk friction,  $\mu$  (fig. 4.1.a), (2) bulk adhesive interactions,  $c$ , both obtained using a shear tester and (3) dispersive surface energy employing an inverse gas chromatograph (fig. 4.1.b). Finally, the question "how much" was addressed by relating the amount of S-NP to the mixture flow behaviour.

## 2. Experimental Design: Materials and methods

The responses, factors and levels chosen to study how S-NP affect granular flows are presented in figure 4.2. Responses are expressed as bulk friction [-], bulk adhesive interactions [kPa] and two dimensionless flow parameters:  $HR$  and  $ff$ . As the experimental design involved a number of factors with mixed levels, a D-Optimal design was chosen. Three categorical factors were defined as follows: host particles, S-NP as glidants, and the mixing protocol. The following numerical factors were added: surface coverage [%] and the moisture conditioning [RH %]. The experimental design is shown in the supporting information file (see section 5., table 4.4). A total of 51 experiments were performed, with five replication points. The optimal criteria was a D-Optimal, which is the best finding the effects, that operates by maximizing the determinant of the information matrix ( $|X'X|$ ). Statistical analyses were performed using Design Expert<sup>®</sup> 13 (Stat-Ease).

Responses	Friction coefficient [-]	Adhesion force [kPa]	Flow factor [-]	Hausner ratio [-]	
Factors	Powders	Glidants	Moisture conditioning [%]	Surface coverage [%]	Protocol
Levels	Avicel PH102	Aerosil R972	30	1	A
	Wheat flour	Aerosil 300		14	
	Joint filler	Sipernat D10	60	27	B
	Glass beads	Sipernat 500LS		40	

Figure 4.2. Design of experiments: responses, factors and levels.

## 2.1. Factors

### Host powders

Four granular materials commonly used in industry, differing in size, shape, elasticity, rugosity, and flow behaviour, were selected as HP: wheat flour (WF), microcrystalline cellulose (MCC), joint filler (JF), and glass beads (GB). The purpose of using such different powders is to bring to the fore their heterogeneities (size, shape and rugosity) to seek broader conclusions about the granular matter. WF is widely used in the food industry. To be certain that our samples had not been treated with glidants, an artisanal T45 flour (Type 00, Euro 450 flour or American Cake flour) was obtained from the Poinsignon flour mill (Fouigny, France). MCC (Avicel<sup>®</sup> PH-102 (AP) from FMC Biopolymer<sup>®</sup>), is frequently added as the main excipient to cosmetics and pharmaceutical products for its capacity to form compacts. JF (MAPEI<sup>®</sup>), is used in the construction industry to grout tiles and finish walls. Finally, GB have been extensively used to describe the physics of granular flows. The GB, Spheriglass<sup>®</sup> 3000-E (Potters<sup>®</sup> Industries LLC), are used for highway safety marking.

### S-NP as flow regulators

Silica flow regulators were chosen from the extensive range of AEROSIL<sup>®</sup> and SIPERNAT<sup>®</sup> references (Evonik). AEROSILs correspond to fumed silicas with chain-like structures; they are produced by flame hydrolysis. In contrast, SIPERNAT<sup>®</sup>s are produced by precipitation giving rise to porous sponge-like structures. To study how S-NP affinity for water affects HP flow, two hydrophobic S-NP, SIPERNAT<sup>®</sup> D10 and AEROSIL<sup>®</sup> R972, and two hydrophilic S-NP, SIPERNAT<sup>®</sup> 500LS and AEROSIL<sup>®</sup> 300 were selected. In the following, S-NP it is also used as S-NP as they are mostly in an aggregate state.

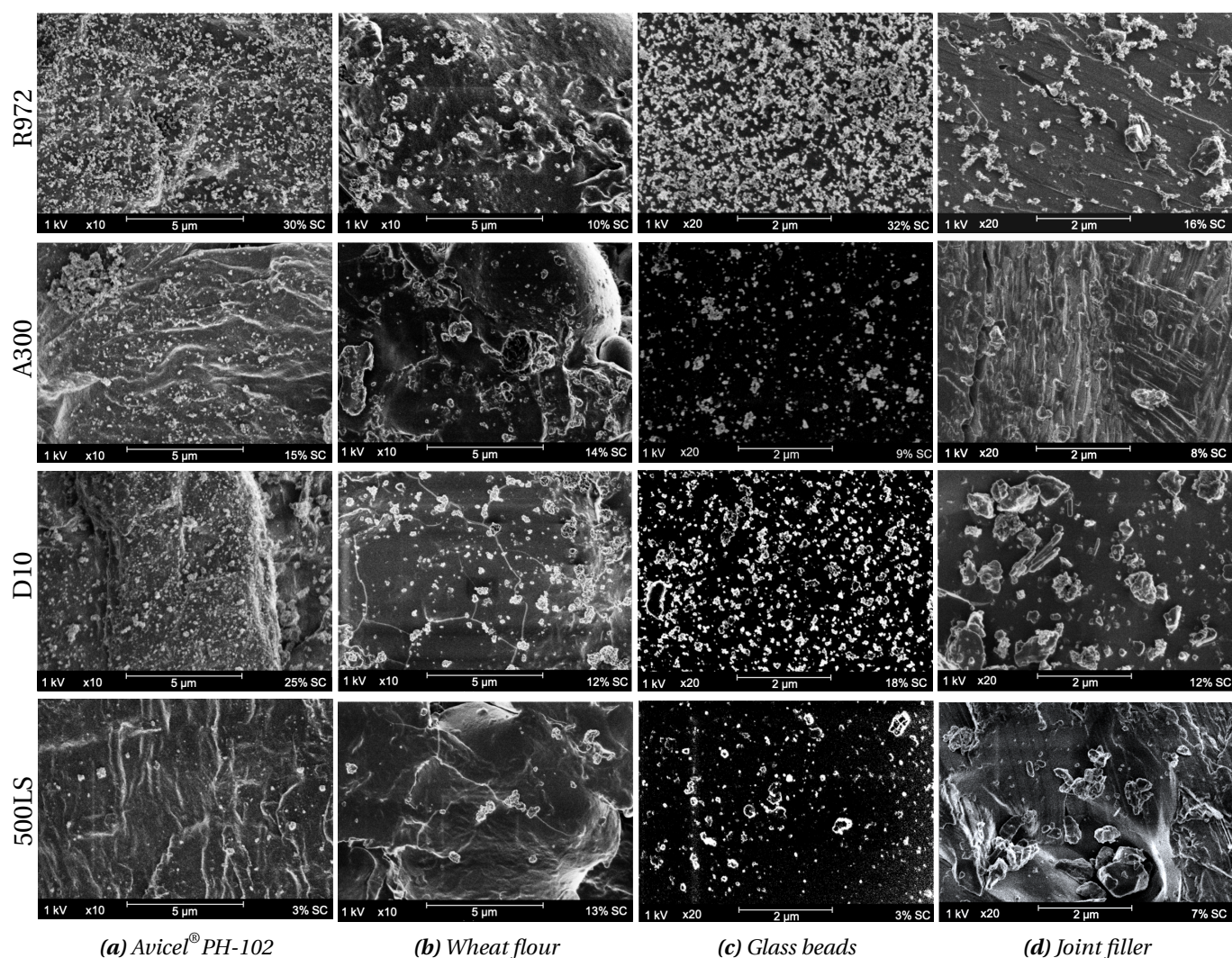
### Surface coverage

To study HP coverage, 0.5% wt mixtures of HP/S-NP were prepared and mixed for 10 min at 67 rpm in a 3D shaker mixer (Turbula<sup>®</sup> T2E, WAB), using a single-use bottle to avoid cross-contamination. To estimate the surface coverage at 0.5% wt HP/S-NP Scanning Electron Microscopy (SEM) micrographs (Fig.4.3) were analysed using ImageJ.

The micrographs were first thresholded to highlight S-NP over HP. Then, the size and the surface coverage of S-NP were determined using the analyse Particles tool. The freehand selection tool was used to manually select the area of analysis to avoid producing misleading data due to HP topography. Four micrographs per sample were analysed to limit subjective image treatment choices. The selected area was the broadest possible; when needed, the rugosities of the HP were excluded from the analysis.

The SEM micrographs (Fig.4.3) allow comparison of the surface coverage of powders mixed with the same S-NP mass fraction (0.5% wt). HP appear to be better covered when mixed with hydrophobic S-NP, the first and third rows. Also, hydrophobic S-NP cover the surface with larger aggregates (observable to the naked eye) than hydrophilic NPs. The S-NP providing least coverage of the host particles' surface, 500LS, also formed the largest aggregates. The average size for the smallest aggregates observed were  $27\pm 2$  nm, this category of aggregates accounts for less than 6% of the S-NP. This size range could indicate that a negligible part of S-NP are in their primary particle form. The median size ( $D_{v50}$ ) of all samples was between 35 and 60 nm. Discretization over this range was impossible due to software limitations. Nevertheless, this result shows that no matter which S-NP reference is used, nanometric aggregates are always present. Castellanos [28] have shown that NPs aggregates size is independent of the HP size, with sizes around 40 – 60 nm. This behaviour is explained due to the aggregates fractal dimension of 2.5, which is the value presented by Witten and Sander's diffusion-limited aggregation (DLA) model [223]. DLA model suggests a controlled growth, which results in similar size aggregates. The surface coverage percentage (SCP) of the powder mixtures measured is shown in figure 4.3. Except with wheat flour, <sup>®</sup>R972 consistently provided the best coverage, followed by SIPERNAT<sup>®</sup> D10.

The influence of the mixing process on S-NP-HP mixtures has been studied by several authors [216]. Severe mixing conditions are reported to produce no improvement in powder flow behaviour [79]. Indeed, some authors report that hydrophobic S-NP require a shorter mixing time to achieve the same coverage as hydrophilic S-NP. Thus, efficiency may depend on the strength of the aggregates, which is expected to be lower in hydrophobic NPs due to their lack of hydrogen bonds [77, 79, 224]. The surface coverage results presented in figure 4.3 corroborate these previous reports. However, the differences in coverage between hydrophobic and hydrophilic NPs may not be solely due to the mixing conditions. In effect, the interaction between HP and S-NP seems to play a significant role. This role can be acknowledged in how S-NP coverage varies between distinct powders. The differences in coverage are indicated in the bottom right corner of each image in figure 4.3. These percentages were used to calculate the proportion of NPs required to reach a specific surface coverage (DoE Table 4.2) for each HP – S-NP combination.

(a) Avicel<sup>®</sup> PH-102

(b) Wheat flour

(c) Glass beads

(d) Joint filler

**Figure 4.3.** SEM micrographs of powders mixed with 0.5% wt of <sup>®</sup>R972 (first row), <sup>®</sup>300 (second row), SIPERNAT<sup>®</sup> D10 (third row) and SIPERNAT<sup>®</sup> 500LS (fourth row)

### Samples conditioning and mixing protocol

To study affinity for water, both HP and S-NP, were conditioned according to the protocol described previously [51]. Although mixing was always performed in a 3D shaker mixer (Turbula<sup>®</sup> T2F, WAB) for 10 min, the “mixing protocol” factor was studied at two levels. Protocol A consists of mixing the HP with S-NP after conditioning and then immediately performing the tests. Protocol B consists of mixing HP and S-NP without any prior conditioning, then placing the mixture at the required RH for at least 7 days before performing tests.

## 2.2. Responses: flow characterisation in the quasi-static regime

### Friction, Adhesive interactions and the Flow factor - Torsional shear test

The shear test seeks to measure the bulk forces governing a powder's behaviour through plastic failure measurements. This rigid-plastic failure is described by the Coulomb yield criterion [4]:

$$\tau = \mu\sigma + c \quad (4.1)$$

where  $\mu$  is a friction coefficient, and  $c$  represents adhesive interactions between grains. Both parameters depend on the material's nature. The physical origins of the frictional properties of grains remain unclear.

The cohesion parameter emerges from the famous Mohr-Coulomb mathematical calculations. Herein, the  $c$  and  $\mu$  coefficients are related to the flow of the mixture and to the mechanisms of action of S-NP. More specifically,  $c$  is related to surface energy modifications with S-NP working as a spacer, whereas  $\mu$  correlates with the mechanical effect as it is the bulk coefficient of friction. Jenike [110] flow rule allows to relate plastic failure to a dimensionless flow-parameter,  $ff$ ; if its value is greater than 10, the granular material is considered free-flowing [47].

Shear-to-failure tests were performed in an FT4 powder rheometer shear cell to measure  $c$ ,  $ff$  and the  $\mu$  for samples based on a packed-bed shear test. The protocol is described in standard ASTM D7891-15 [179]. The pre-consolidation stress was set to 66 kPa, and normal shear stresses to 50 - 40 - 25 - 17 - 7 kPa.

### Hausner ratio - uniaxial compression, $HR_c$

Powder flow was also assessed from consolidation measurements based on the HR, as measured by uniaxial compression in an Instron press with adapted geometry. This technique was selected to characterise powder flow behaviour due to the relation between powder compaction and flowability. A free-flowing powder does not have good compaction. This property is the base of the  $HR$  classification, which is generally applied to free surface systems, where the  $HR$  corresponds to the ratio of the aerated density and the compacted density at each force applied. This work used the uniaxial compression density instead of the compacted density obtained under free surface conditions. Compared to traditional tapping devices, uniaxial compression testers (UCT) control the force/energy supplied to the bulk [51]. Indeed, these authors believe that HR is correctly related to flowability when obtained at the densest compaction state, which cannot always be reached in conventional tapping devices [50]. The main differences between both procedures are the degrees of freedom and the energy dissipation within the bulk, which is much greater under vibration. To distinguish from traditional testers,

the  $HR$  was denoted as  $HR_c$ . The closer the  $HR_c$  is to 1, the greater the powder's flowability.

The first step of this test involved pouring the powder into a 10 mL stainless steel cell; excess was removed using an antistatic plastic ruler to ensure a final volume of 10 mL. The sample was then compressed in 10 N steps until 50 N at a rate of 0.4 N/s. The force applied and piston/powder height were measured throughout the test. At each step, the pressure was maintained for 60 s to ensure that the steady-state had been reached. The details of this technique and the data treatment has been described in previous work [51]. The force applied was selected according to previous vibration studies [50], showing that the powder samples used in this work achieved, under free surface conditions, their maximal compaction state below 50N. We preconize that under these conditions particles cannot be broken or deformed to any significant extent [51, 178].

### 2.3. Physical powder characterisation techniques

Particle size distribution was measured in triplicate by laser diffraction in liquid media using a Mastersize 3000 (Malvern Instruments), ethanol was used as a dispersant to avoid dissolution. Particle morphology images were determined by SEM (Gemini 3, Zeiss) with a field-emission gun operating at 2 kV. Samples were placed on double-sided tape and then coated for 1 min with a gold-palladium layer using a Desk V - TSC (Denton Vacuum) under air purge. Nanoparticles were characterised using a 2100-F transmission electron microscope (TEM) from Jeol with a high tension of 200 kV. Images were recorded with a Gatan Orius SC 200 D camera. An average of 100 primary particles were randomly selected, measurements were determined using ImageJ. True powder density was determined in a Helium pycnometer (AccuPyc 1330, Micromeritics). All data presented correspond to the average of ten measurements obtained from one powder sample.

Surface energy analyses were carried out using the NeuronIC inverse gas chromatography (IGC-ID) from Adscientis. The samples were packed into a stainless-steel column of 100 mm length and 4 mm internal diameter. Prior to analysis, each column was conditioned at 25°C for 16 hours. Helium was used as a carrier gas at 10 mL/min. The retention times of probe molecules and methane were determined using a flame ionization detector (FID). Dispersive surface energy,  $\gamma_s^d$ , was determined by injecting a homologous series of vapor n-alkanes (hexane, heptane and octane) using the software Nucleus 3.2.4 and calculated using Solid 3.3.0 from Adscientis following Dorris–Gray and Schultz approach.

## 3. Results & Discussions

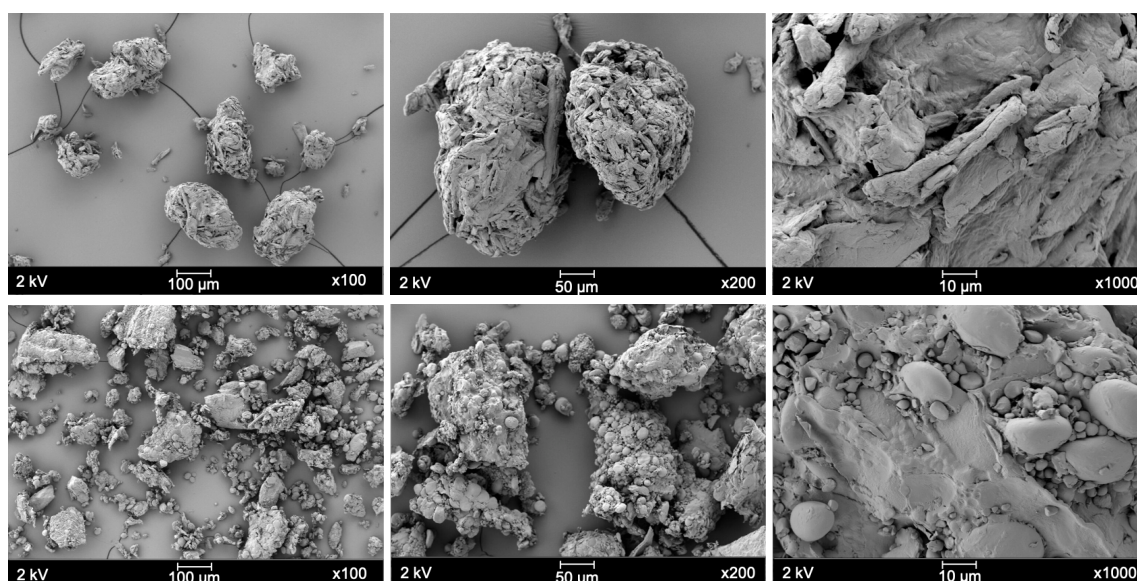
### 3.1. Physical characterisation

Table 4.1 presents the particle distribution for all the powders tested. All samples showed a polydisperse distribution, as seen in the SEM micrographs in figure 4.4 (Avicel® PH-102

and wheat flour) and figure 4.5 (joint filler and glass beads). Particle size was larger for Avicel® PH-102 and wheat flour compared to the joint filler and the glass beads. From these observations, wheat flour can be seen to be composed of a major irregular structure surrounded by globule-like structures (starch), whereas Avicel® PH-102 particles have an isometric rod shape with a rough surface. The images of the joint filler reveal an uneven shape with flat surfaces, whereas the glass beads were mostly spherical, with irregularities on the surface of some particles.

**Table 4.1.** Powder characteristics.

Powder	Particle size distribution $\approx 1$ [ $\mu\text{m}$ ]					Pycnometric density [ $\text{g}/\text{cm}^3$ ]	Surface energy $\gamma_s^d$ [ $\text{mJ}/\text{m}^2$ ]
	$d_{10}$	$d_{50}$	$d_{90}$	$d_{32}$	$d_{43}$		
Avicel® PH-102	35	111	225	69	122	1.55	57.8±0.7
Wheat flour	17	83	177	25	91	1.46	42.8±0.2
Joint filler	2	18	72	6	29	2.81	39.9±0.3
Glass beads	4	24	60	8	29	2.66	39.6 [225]



**Figure 4.4.** SEM micrographs of Avicel® PH-102 (first row) and Wheat flour (second row) at various magnifications (x100, x200 and x1000).

The physical characteristics of silica glidants are summarized in Table 4.2. Their volume-specific surface area, VSSA, was used to class them as NM according to the European Commission definition [226]. Figure 4.6 shows TEM micrographs of the four glidants. SIPERNAT® S-NP have a cloud-like shape, whereas AEROSILs form chain-like aggregates. In these images, the difference in size of hydrophilic and hydrophobic S-NP can be clearly observed. However, since 500LS aggregates are stacked one on top of the other, it was impossible to measure the mean primary particle diameter. The mean diameter of primary particles determined for the other particles shows that hydrophobic

S-NP are larger than hydrophilic S-NP. This size relation was expected as a result of the surface treatment applied to naturally hydrophilic S-NP to make them hydrophobic. The treatment consists of reacting the silanol groups (Si-OH) at the surface of the hydrophilic particles with organic groups to make the particles water-repellent, increasing their size [174].

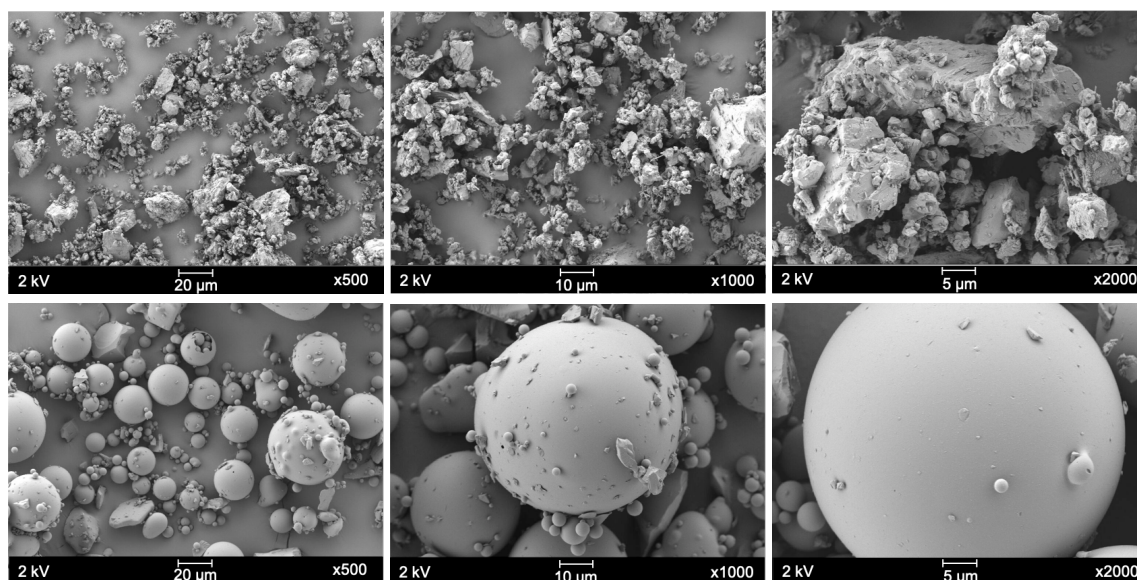


**Figure 4.5.** SEM micrographs of Joint filler (first row) and glass beads (second row) at various magnifications (x500, x1000 and x2000)

**Table 4.2.** Nanoparticles characteristics

Reference	Pycnometric density [ $g/cm^3$ ]	VSSA [ $m^2/cm^3$ ]	Primary particle mean diameter [nm]	Affinity towards water
SIPERNAT <sup>®</sup> D10	2.0	180	$24 \pm 5$	Hydrophobic
SIPERNAT <sup>®</sup> 500LS	2.2	990	-	Hydrophilic
SIPERNAT <sup>®</sup> R972	2.3	253	$23 \pm 5$	Hydrophobic
SIPERNAT <sup>®</sup> 300	2.7	810	$15 \pm 5$	Hydrophilic

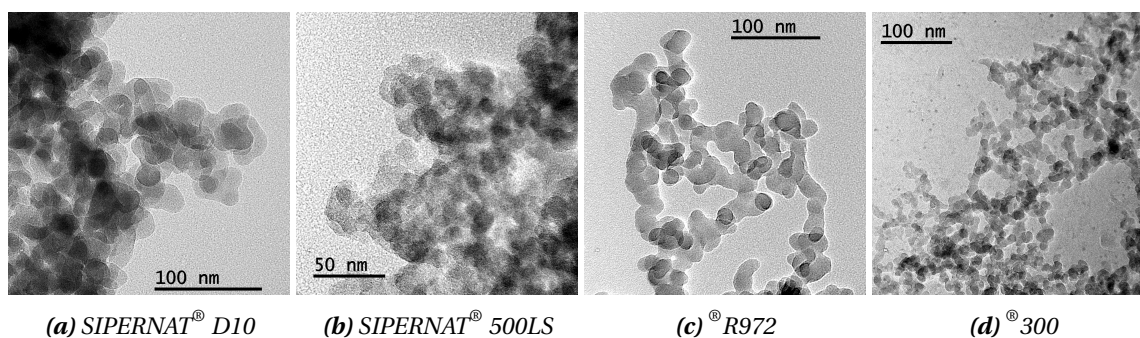


**Figure 4.6.** TEM micrographs of silica nanoparticles

### 3.2. Experimental Design

#### Host powder flow behaviour

Powder flow characteristics for the four HP tested in their pure forms are listed in table 4.3.  $HR_c$  measurements indicate that Avicel<sup>®</sup>PH-102 and glass beads present “good” flow behaviour, whereas wheat flour and joint filler are considered “very cohesive”, despite RH conditioning. These results concur with the visual analysis of powder flow (Fig.4.10). Based on the flow factor, the Avicel<sup>®</sup>PH-102 at 30% RH, the glass beads, and the wheat flour can all be considered free-flowing powders. The differences between  $HR_c$  and  $ff$  for wheat flour may be due to powder properties that could influence packed-bed conditions such as adhesive interactions, elasticity (Young’s modulus) and hardness[90]. RH influenced the cohesive behaviour of Avicel<sup>®</sup>PH-102 and wheat flour. Thus, Avicel<sup>®</sup>PH-102 increased its cohesion as RH increased, possibly due to increasing capillary forces. Conversely, both cohesion and friction were reduced for wheat flour at higher RH. This behaviour could be due to a lubricating effect of moisture on the flour particles.

**Table 4.3.** Flow behaviour parameters of host powders

Powder	RH [%]	$HR_c$ [-]	$c$ [kPa]	$ff$ [-]	$\mu$ [-]
Avicel <sup>®</sup> PH-102	30	1.12 ± 0.01	2.4 ± 0.6	13.9 ± 3.7	0.6 ± 0.0
	60	1.21 ± 0.01	4.2 ± 0.4	7.7 ± 0.6	0.6 ± 0.0
Wheat flour	30	1.57 ± 0.05	2.8 ± 0.3	11.0 ± 1.4	0.2 ± 0.0
	60	1.59 ± 0.06	1.7 ± 0.2	18.5 ± 2.1	0.1 ± 0.0
Joint filler	30	1.44 ± 0.05	3.7 ± 0.1	7.7 ± 0.3	0.6 ± 0.0
	60	1.77 ± 0.06	4.1 ± 0.6	7.3 ± 1.0	0.7 ± 0.0
Glass beads	30	1.16 ± 0.01	1.3 ± 0.5	23.3 ± 1.8	0.6 ± 0.0
	60	1.20 ± 0.01	1.0 ± 0.1	30.4 ± 3.8	0.5 ± 0.0

#### Surface coverage

Our method to determine surface coverage was validated using Avicel<sup>®</sup>PH-102 at 40% theoretical coverage (Fig.4.7). Mixtures of this HP with D10, R972 and A300 exhibited the expected surface coverage, at mass fractions ranging between 0.8 and 1.2% wt. Most S-NP measured less than 100 nm (Fig.4.8). In contrast, the AP+500LS mixture produced about 2% of aggregates/agglomerates larger than 1  $\mu$ m (Figs. 4.7 -4.8), and laser diffraction analysis revealed a bimodal size distribution, with a first peak at 10  $\mu$ m. This result confirms that SIPERNAT<sup>®</sup> 500LS forms clumps and does not cover the host particles as the others S-NP.

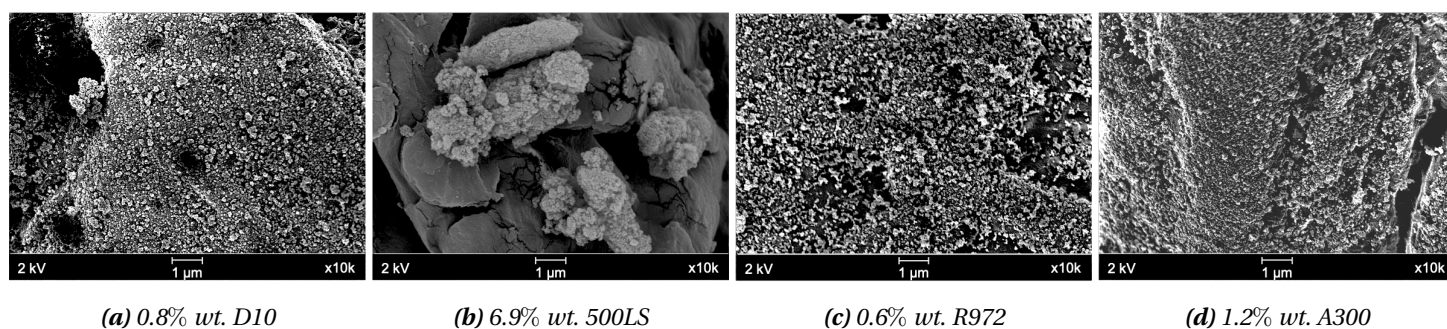


Figure 4.7. SEM micrographs of Avicel® PH-102 + S-NP mixtures for a theoretical surface coverage of 40%.

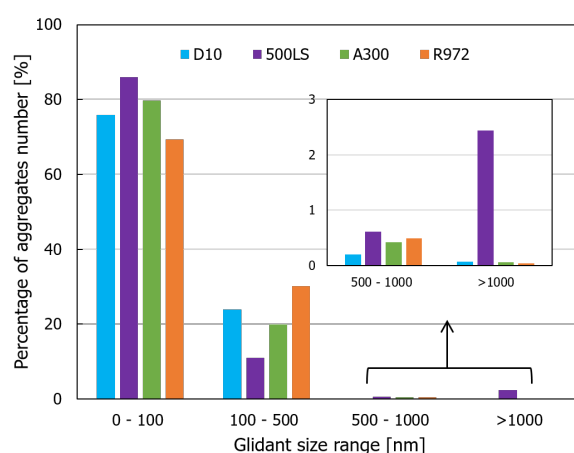


Figure 4.8. S-NP number distribution for Avicel® PH-102 at 40% of surface coverage.

In figure 4.9 SCP for other mixtures are shown. The estimated SCP in these mixtures generally support the proportional calculation described in section 2.1.. Thus, the powder coverage that was theoretically 14% (Fig.4.9a) was really at ~13%, for an expected coverage of 1% (Fig.4.9b and 4.9c) mixtures were at ~2% and for the theoretical 27% coverage (Fig.4.9d) a real coverage of ~24% was measured. The prediction is thus quite good.

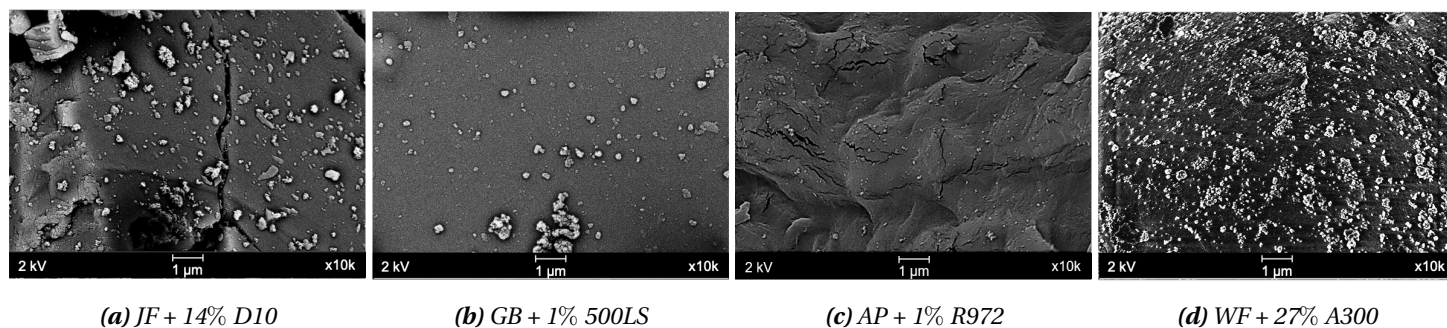


Figure 4.9. SEM micrographs of powder mixtures with different theoretical S-NP surface coverages

### D-Optimal experimental analysis

The D-Optimal experimental design matrix with the experimental results is presented in the supporting information file (see section 5., table 4.4). All 51 HP+S-NP mixtures, categorized by experimental run, were photographed after simple pouring (see supporting information file, section 5., figure 4.15). As shown in figure 4.10 bulk physical appearance clearly changed when S-NP were added. When granular flow was enhanced, the bulk blended well and had a regular form (Fig.4.10, columns 4 and 5). In contrast, when flow was not improved, the bulk appeared uneven and tended to form agglomerates (Fig.4.10, columns 2 and 3).



**Figure 4.10.** Visual assessment of sample images to determine flow. The first column presents pure host particles. Columns 2 and 3 correspond to runs where flow behaviour was not improved. Columns 4 and 5 show runs where flow was enhanced for the mixtures. The numbers in the images indicate the number of the run on the DoE matrix (see supporting information file in section 5., table 4.4)

As we work with a D-Optimal design, the mathematical modelling was chosen for each response in the after treatment by setting a p-value of 0.05 for statistical significance. For the  $HR_c$ , the  $ff$  and the  $c$  responses, the best fit was achieved with a 2FI model, which is a sequential sum of squares for the two-factor interaction terms. Bulk friction  $\mu$ , in contrast, was analysed using a linear model without interactions.

The factors identified as significant for each response are shown in figures 4.11 and 4.12. The statistical analysis of the DoE was challenging because the granular media, host particles, was the most significant factor for all responses (p-value < 0.0006). It was thus

difficult to draw broad conclusions on S-NP action mechanisms without reference to the granular material. This result demonstrates that granular flows are extremely sensitive to grain properties. From a statistical perspective, several warnings arise, as some very significant effects for one granular sample had no statistical significance in another. For example, as previously stated [51], analysis of raw data indicated that hydrophobic S-NP boosted flowability better than hydrophilic S-NP. In contrast, herein, the affinity for water of the S-NP was not found to have a significant effect on granular flows.

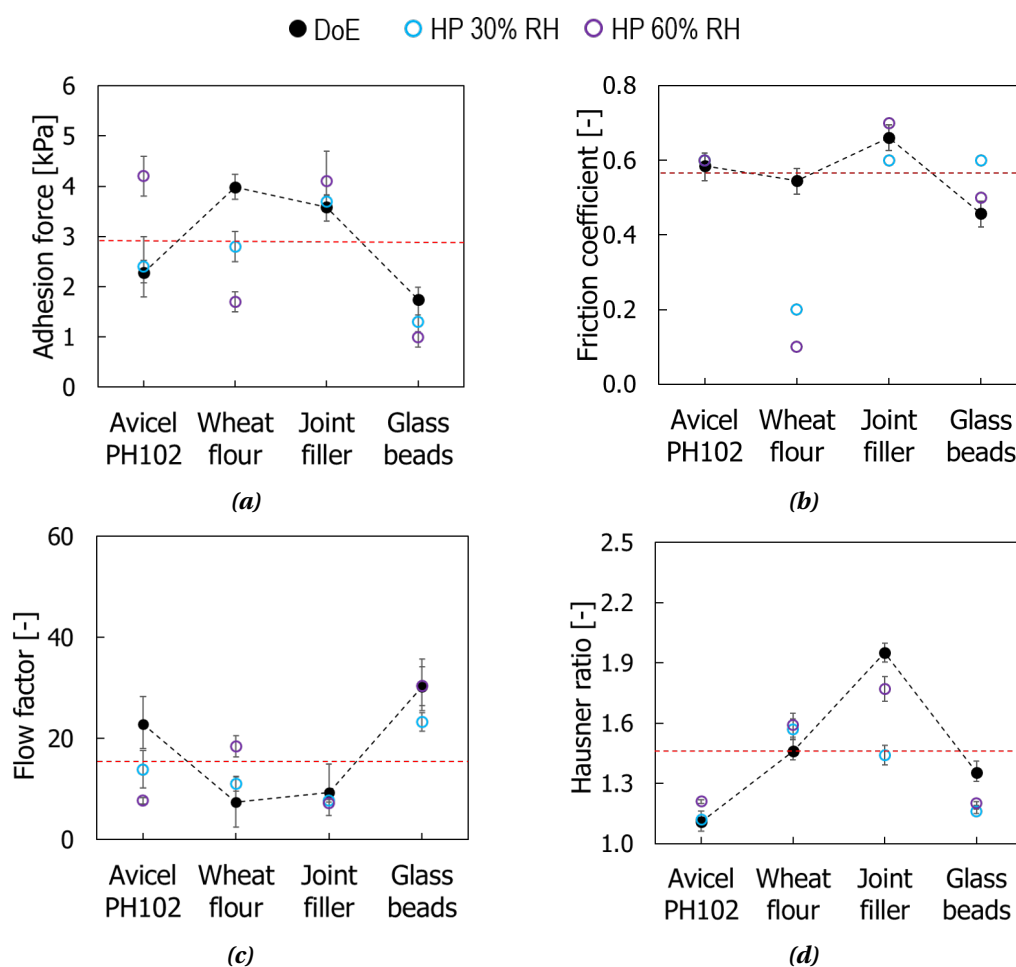


**Figure 4.11.** Influence of the nature of the granular media studied on responses measured in the DoE: a) adhesion force, b) friction coefficient, c) flow factor, and d) Hausner ratio

The second, and final, general conclusion is that reducing bulk friction does not seem to affect flow enhancement. In fact, regardless of whether S-NP is modified or not, the internal bulk friction,  $\mu$ , had no repercussions on  $HR_c$  and  $ff$ , the parameters used as indicators of flow in the quasi-static regime. No other general conclusions on modifications of bulk adhesive interactions and these flow parameters could be drawn.

The moisture conditioning factor was only significant for bulk adhesive interactions,  $c$ , which increased for 60% RH compared to 30% RH (Fig.4.12a). The mixing protocol factor

was significant only for the flow factor  $ff$ , indicating that protocol A (powders conditioned before the mixing process) provided better flow behaviour than protocol B (Fig.4.12.b). For instance, S-NP might be better able to regulate moisture in a preconditioned powder compared to when pre-covered particles are exposed to moisture (protocol B). Finally, glidants were found to play a significant role in  $HR_c$  response, with the 500LS aggregates having the least impact on flow enhancement (Fig.4.12.c).

Some other interesting results were that moisture conditioning of pure samples had a very significant influence on flow behaviour. However, when S-NP were added to powders, moisture had a less significant influence on flow, regardless of the water-affinity of the S-NP. This difference in behaviour suggests that the addition of S-NP changes the HP's surface energy.

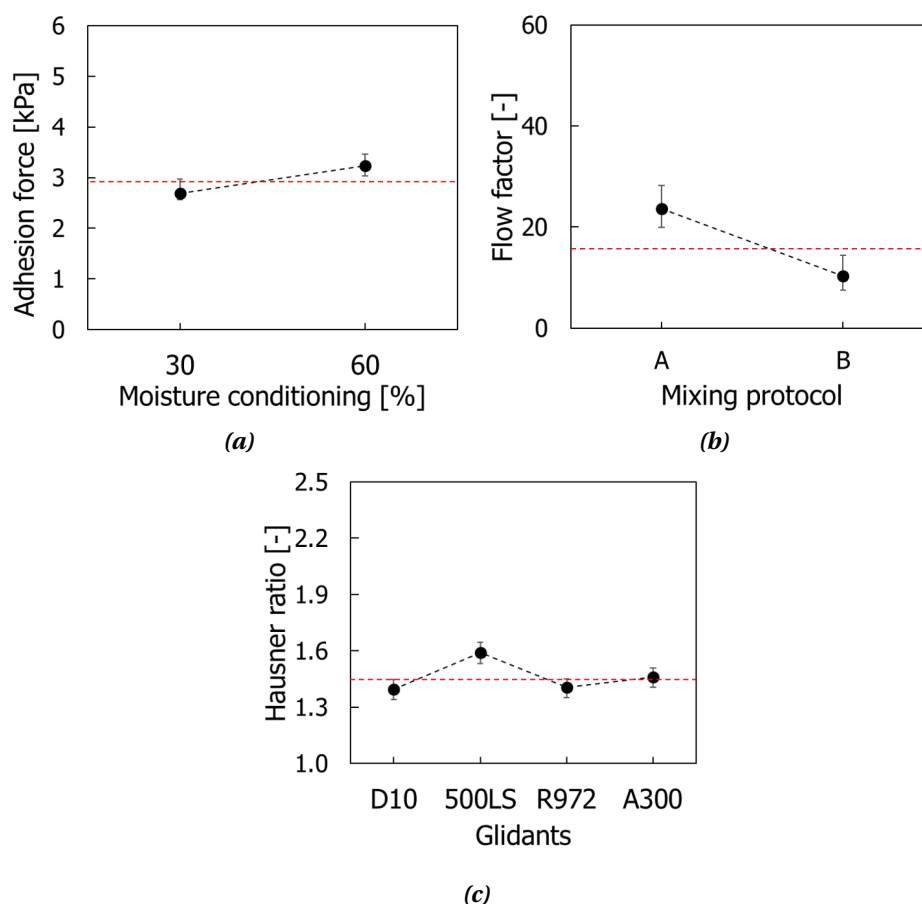


**Figure 4.12.** Moisture conditioning, mixing protocol, and glidant added significantly affect DoE Responses: a) adhesion force, b) flow factor, and c) Hausner ratio

### 3.3. Why, how and how much?

**Why?** Because, our experimental results show, with statistical significance, that adding S-NP to wheat flour, microcrystalline cellulose, joint filler, and glass beads improves their

flowability when evaluated using  $HR_c$  and  $ff$ . S-NP addition has such an effect on the HP that flowability enhancement is observable to the naked eye through the physical appearance changes of the bulk, becoming smother and regular without agglomerates, as shown in figure 4.10. The experimental design showed that flow enhancement relates to the HP intrinsic properties and surface coverage. Thus, these results show that for a quite dissimilar variety of powder samples (different degrees of cohesion, size, hardness, elastic moduli, behaviour towards water, chemical nature, surface energy ...) the addition of S-NP can easily improve their flow behaviour. And are a cost-effective alternative to other solutions such as modifying facilities [198], adding fluidization and/or vibration operations [199].

**How?** Our results corroborate, as previously suggested [28, 187, 227], that the mechanism of action of glidants in granular flows is surface-related and operates at the interface level. S-NP then acts on powders by reducing interparticle forces. Indeed, the mechanical effect (Fig.4.1.a) is the only one of the three action mechanisms proposed in the literature that does not act at the surface, or interface, level. The bulk friction, determined by analysing plastic failure in the quasi-static regime, changed randomly between runs and shared no meaningful link with flow behaviour. Still, friction is the main parameter in granular physics to describe the rheology of simple granular materials such as sand and glass beads [96, 197, 228]. Our results suggest that when interparticle forces play a role in the rheology, even for low cohesive particles such as Avicel<sup>®</sup> PH-102, the friction influence is less significative and no longer describes flowability.

Several models have been proposed to describe adhesive interactions  $F_{vdW}$  [56, 229], among them Rumpf's model [77, 84], which considers two smooth spherical HP separated by a single spherical NP:

$$F_{vdW} = -\frac{A}{6} \left[ \frac{R_1 r}{H^2 (R_1 + r)} + \frac{R_1 R_2}{(2H + 2r)^2 (R_1 + R_2)} \right] \quad (4.2)$$

where  $A$  is the Hamaker constant,  $r$  is the glidant radius,  $R_1$  and  $R_2$  are the HP radius.

As shown in figure 4.13, Eq.4.2 can be used to estimate the theoretical optimum flow based on the additive radius that reduces  $F_{vdW}$  to the greatest extent. For HP with diameters between 5 and 120  $\mu\text{m}$ , the minimal adhesive force between HP particles is obtained for glidants with diameters from 6 to 17 nm. Based on this estimation, it is clear that S-NP size influence the  $F_{vdW}$  reduction, either as primary particles or as aggregates. For our glass bead sample, the only "smooth spherical particles" in the group tested (Fig.4.13 cyan line), to reduce van der Waals forces between particles, the primary S-NP form should measure about 6 nm. This conclusion explains why 500LS has no, or only a minor, effect on granular flow as it forms S-NP bigger than 1  $\mu\text{m}$  in the mixtures (Fig.4.10). In addition, we can conclude that increasing the polydispersity of formulations by adding

fine particles may not enhance flow because this approach acts at the macroscopic level.

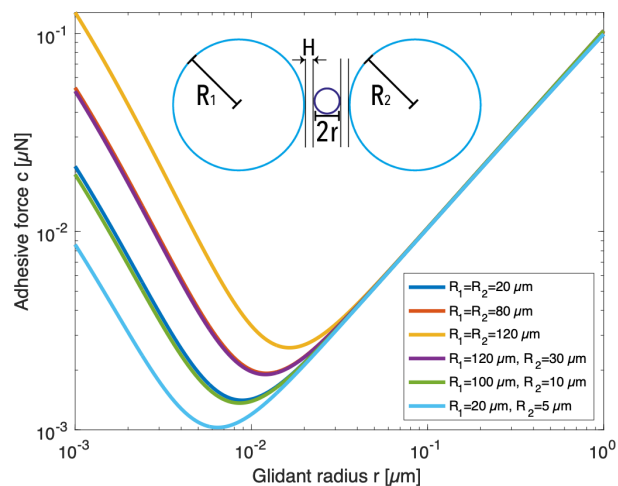


**Figure 4.13.** Adhesive force as a function of glidant radius.  $A$  and  $H$  were taken as  $10^{-19}$  J and 0.4 nm, respectively.

Although neither SIPERNAT<sup>®</sup> D10 nor AEROSILs A300 or R972 was observed as isolated NPs, all four references exhibited polydisperse sizes and shapes, with most aggregates ranging from 35 to 60 nm in size (see section 3.2.). Despite this characteristic, only the two hydrophobic S-NP aggregates (SIPERNAT<sup>®</sup> D10 and AEROSIL R972) increased flow in all the configurations studied. For example, Avicel<sup>®</sup> PH-102, and joint filler improved their flow behaviour with 40% SC for the hydrophobic S-NP (SIPERNAT<sup>®</sup> D10 and <sup>®</sup>R972) but not for hydrophilic S-NP (SIPERNAT<sup>®</sup> 500LS and <sup>®</sup>300). If S-NP acts only as spacers, no matter the type of S-NP, at the same SC (see Fig.4.14), similar flow enhancement should be obtained. These results lead us to the hypothesis of surface energy modifications. To validate this statement, mixtures of Avicel<sup>®</sup> PH-102, wheat flour, and joint filler with 40% SC of SIPERNAT<sup>®</sup> D10 were characterised using IGC-ID. The results were  $56.4 \pm 1.6$ ,  $39.6 \pm 0.3$ , and  $32.8 \pm 0.2$  for Avicel<sup>®</sup> PH-102, wheat flour and joint filler mixtures, respectively. The mixtures' surface energy decreased compared to the HP (Table 4.1), showing that surface energy changes could be the main mechanism responsible for flow enhancement. For Avicel<sup>®</sup> PH-102, the diminution is not statistically significant due to high surface energy differences with D10 ( $\gamma_s^d = 29.3 \text{ mJ/m}^2$ ). In this case, the probe molecules "sense" these differences, and  $\gamma_s^d$  value is mainly influenced by the higher energy sites. Using IGC at Finite Concentration (IGC-FC) as a characterisation technique will probably be better. IGC-FC gives access to surface heterogeneity in the form of an "adsorption energy distribution". It allows representing the various sites more suitable for heterogeneous samples (geometrical, energetic, or chemical).

Interestingly, water sorption isotherms were not sensitive to the water affinity of S-NP. It appears that the gap between microscopic properties and macroscopic behaviour has

been attempted.

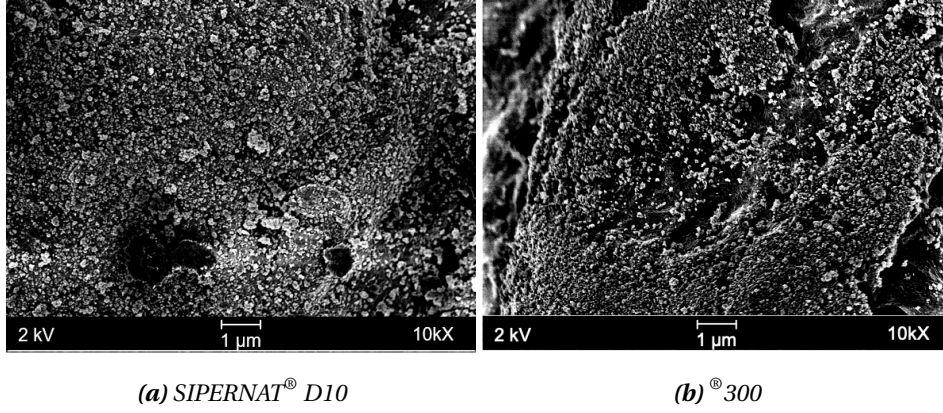


**Figure 4.14.** Avicel® PH-102 covered with 40% SC

The granular bond number,  $Bo_g = F_{adhesive}/W_g$ , defined as the ratio of adhesive interparticle forces to gravity force, can be used to relate interparticle forces to the flow factor using the Capece et al [54] experimental approach:

$$ff = 15.7 \dot{B}o_g^{0.27} \quad (4.3)$$

From this empirical model, we have also validated that interparticle adhesive forces decrease when adding S-NP.

**How much?** Our results demonstrate that there is no standard amount of glidant required to enhance flow behaviour, the amount required depends on the host material. Indeed, poorer flowing samples need more coverage than those presenting better flow behaviour (Fig.4.10).

Valverde et al. [227] proposed that the amount of S-NP required could be estimated based on the expected types of interparticle contact (HP-HP, HP-NP, NP-NP). When HP-HP contacts predominate, the average distance between NP,  $s$ , should be  $s = \sqrt{2d_p d_a}$ , where  $d_p$  is the HP diameter and  $d_a$  is the diameter of NP aggregates.

$$\%X_{HP-HP} = 100 \cdot 0.64 \cdot \frac{\pi}{8} \cdot \frac{d_a^2}{d_p^2} \quad (4.4)$$

When the distance between NP is less than  $s = 2d_a$  the contact configuration changes from HP-NP to NP-NP, and in this case, the required quantity can be calculated using Eq.4.5. The values for the distance and the mass fraction in the HP-NP contact are between the values of the HP-HP and NP-NP contacts.

$$\%X_{NP-NP} = 100 \cdot 0.64 \cdot \frac{\pi}{4} \cdot \frac{d_a}{d_p} \quad (4.5)$$

If we apply eqs. 4.4 and 4.5 the mass fractions required to create NP-NP or HP-HP contacts with  $d_p = 120$  to  $20 \mu\text{m}$  and  $d_a = 1, 0.5, 0.1$  and  $0.05 \mu\text{m}$  range from 0.02 to 2.5% wt for the

NP-NP contacts and from  $4 \cdot 10^{-6}$  to  $6 \cdot 10^{-2}$  % wt for the HP-HP contact. Our results show that surface coverage from 1 to 40% are produced by mass fractions ranging from 0.02 to 2.38% wt (excluding 500LS as it does not cover the HP surface). Still, flow behaviour was only enhanced over the range 0.02 to 1.84% wt based on  $HR_c$ ,  $ff$  and visual observation (see Fig.4.10). For instance, Fulchini et al. [188] have found an optimal surface coverage of 20% (0.94% wt) for glass beads covered with zeolite. Huang et al. [230] concluded that for achieving a flow enhancement, the SC should be between 10% and 30% for several pharmaceutical powders covered with two types of precipitated S-NP. Both studies agree with our results regarding mass fraction and SC showing that each HP/S-NP interaction gives rise to different optimal SC.

The differences between the theoretical approach assuming spherical particles (Eqs.4.4 and 4.5) and our results highlight the necessity for a surface coverage-based experimental approach. From SEM micrographs we have observed that up to 14% SC the contacts between grains seems to be S-NP-S-NP (Fig.4.9a) whereas above 27% SC (Figs. 4.9d, 4.7a, 4.7c and 4.7d) the HP surface changes as it becomes covered by the S-NP.

From a technological point of view, a process of trial and error to adjust mass fractions to ensure process feasibility has merit as a relatively effective, rapid empirical solution. To take safety concerns into account, with the aim of mitigating the risk of exposure to S-NP, we propose that the amount of glidant required to increase flow behaviour be determined by studying how the S-NP covers the HP, without exceeding 40% SC, which is similar to the range proposed by Huang et al [230].

The procedure could be as follows. First, characterise the HP-NP mixture at a given fraction of NPs (0.5% wt for example) by surface imaging. Then, produce three mixtures creating different surface coverage (from 14 to 40) to study their flow behaviour using the flow-tester that best reproduces the industrial process or unit operation to be applied. For example, for a silo use shear testers (plastic failure), for conveying use inclined planes or a funnel flow meter.

## 4. Conclusions

There is considerable interest in understanding and improving how granular matter is handled in industrial processing, mainly in terms of its flow behaviour. In this paper, we extend knowledge of this subject by determining how glidants work on a variety of industrial powders. The three mechanisms of action presented in figure 4.1 were assessed based on  $\gamma_s^d$ ,  $\mu$  and  $c$  coefficients and two flow parameters obtained from shear-to-failure and compression measurements,  $ff$  and  $HR_c$ . A 51-experiment D-Optimal design was used to study five factors (powder, glidants, relative humidity, surface coverage, and mixing protocol). Statistical analysis indicated that flow behaviour of powders mixed

with glidants closely depends on the powder's nature – grain properties, which are a key parameter, complexifying general conclusions. Despite this complexity, a remarkable and obvious conclusion was that bulk friction has no influence on granular flows in the quasi-static regime, and thus granular flow varied randomly between DoE runs. In addition, from the  $\gamma_s^d$ ,  $c$  and  $ff$  results, it could be concluded that flow enhancement might be governed by surface modification of the HP and/or by the glidant acting as a spacer. The glidants' mechanisms of action are surface-related and operate at a microscopic level.

Glidant addition should therefore be more focused on surface energy modifications. Thus it is proposed to mainly use hydrophobic S-NP. The surface coverage and size of the S-NP depends on the adhesive interactions between HP and S-NP. Consequently, calculations based on mass fractions may lead to addition of suboptimal amounts of glidants to formulations. For highly cohesive samples, we observed that HP/S-NP type interactions increased flowability. In these cases, SEM images showed that 40% SC might be enough to increase powder flow. For less cohesive samples, like glass beads, lower amounts of S-NP may be sufficient (14% SC). Based on these conclusions, we proposed a protocol to determine how S-NP covers a HP, based on SEM image characterisation to establish the coverage for a known mass fraction. This coverage should then be extrapolated to achieve the desired coverage. Flow quantification is required to assess the effect of the S-NP on flow enhancement. The application of this methodology should reduce the risk of worker exposure during powder handling.

In this article, we only studied flow in the quasi-static regime. The influence of S-NP on the loose gas-like regime, where the flow is rapid and dilute, and grains interact via collisions, will be the subject of a separate paper currently in preparation.

## 5. Annex

**Table 4.4.** D-Optimal experimental design matrix and experiments results,  $p$ -value=0.05.

DoE	Surface coverage [%]	Mass fraction [%]	RH [%]	Protocol	Powder	S-NP	HRc [-]	$c$ [kPa]	$ff$ [-]	$\mu$ [-]
1	40	1.60	30	B	Joint filler	D10	1.87	2.97	9.60	0.66
2	1	0.03	60	A	Joint filler	R972	1.82	3.26	8.86	0.65
3	1	0.07	60	A	Joint filler	500LS	1.79	3.53	8.27	0.66
4	40	1.06	60	A	Glass beads	D10	1.23	3.53	8.27	0.66
5	1	0.06	60	B	Joint filler	A300	1.85	3.26	8.86	0.66
6	1	0.02	60	B	Avicel®PH-102	R972	1.14	3.78	8.22	0.56
7	27	0.90	60	A	Wheat flour	A300	1.24	4.17	7.07	0.64
8	40	5.74	30	A	Glass beads	500LS	1.73	2.91	10.52	0.49
9	1	0.04	30	B	Wheat flour	500LS	1.60	4.05	7.29	0.53
10	27	0.85	30	B	Avicel®PH-102	A300	1.07	1.86	16.64	0.54
11	1	0.04	60	B	Wheat flour	500LS	1.56	4.79	5.46	0.36
12	14	0.27	60	B	Avicel®PH-102	D10	1.05	3.36	9.62	0.54
13	40	2.38	60	B	Joint filler	A300	2.18	5.14	5.66	0.67
14	40	1.34	30	A	Wheat flour	A300	1.38	3.54	8.43	0.65
15	40	2.20	30	A	Glass beads	A300	1.38	3.59	8.30	0.50
16	1	0.14	60	A	Glass beads	500LS	1.25	0.88	34.23	0.39
17	40	2.38	30	A	Joint filler	A300	2.02	5.42	5.42	0.68
18	14	0.52	60	A	Wheat flour	500LS	1.33	4.59	6.48	0.62
19	1	0.14	60	B	Glass beads	500LS	1.27	1.01	29.83	0.39
20	40	0.77	30	B	Avicel®PH-102	D10	1.04	0.40	76.82	0.50
21	1	0.02	30	B	Avicel®PH-102	R972	1.08	2.64	11.96	0.62
22	40	5.74	30	B	Glass beads	500LS	2.05	2.51	12.25	0.49
23	1	0.03	60	B	Wheat flour	A300	1.63	6.27	4.31	0.42
24	40	1.55	60	A	Wheat flour	D10	1.18	3.05	9.68	0.64
25	1	0.04	30	A	Wheat flour	D10	1.70	3.94	7.43	0.36
26	40	2.61	30	A	Joint filler	500LS	2.48	4.19	7.07	0.64
27	1	0.05	30	B	Wheat flour	R972	1.62	4.42	6.54	0.35
28	1	0.03	30	A	Avicel®PH-102	A300	1.12	0.93	28.54	0.84
29	1	0.06	30	B	Joint filler	A300	1.70	3.73	7.84	0.65
30	40	1.22	30	B	Joint filler	R972	2.20	3.28	8.72	0.67
31	40	6.86	30	B	Avicel®PH-102	500LS	1.23	2.17	14.18	0.59
32	14	0.77	60	A	Glass beads	A300	1.46	2.02	14.96	0.41
33	40	1.84	60	A	Wheat flour	R972	1.26	3.20	9.24	0.65
34	1	0.04	60	B	Joint filler	D10	1.86	3.24	8.89	0.66
35	40	1.26	60	A	Avicel®PH-102	A300	1.11	2.49	12.43	0.58
36	27	0.40	30	A	Glass beads	R972	1.26	1.36	22.25	0.40
37	40	1.55	60	A	Wheat flour	D10	1.19	3.16	9.46	0.61
38	40	1.22	60	A	Joint filler	R972	1.84	3.08	9.29	0.67
39	40	0.64	60	B	Avicel®PH-102	R972	1.04	1.74	17.79	0.56
40	14	0.56	30	B	Joint filler	D10	1.79	3.13	9.30	0.66
41	40	1.49	60	A	Wheat flour	500LS	1.29	3.96	7.60	0.58
42	40	0.64	60	B	Avicel®PH-102	R972	1.04	1.12	24.04	0.84
43	1	0.01	30	B	Glass beads	R972	1.29	0.97	31.96	0.41
44	40	0.64	30	B	Avicel®PH-102	R972	1.03	1.52	19.89	0.43
45	40	0.60	60	B	Glass beads	R972	1.19	0.23	131.19	0.51
46	1	0.04	30	A	Wheat flour	D10	1.64	4.79	6.34	0.56
47	1	0.03	60	A	Avicel®PH-102	A300	1.11	3.78	8.29	0.56
48	1	0.03	30	B	Joint filler	R972	1.71	3.79	7.75	0.65
49	14	2.40	60	B	Avicel®PH-102	500LS	1.18	2.91	10.69	0.56
50	14	0.37	30	B	Glass beads	D10	1.15	0.8	37.22	0.39
51	14	0.64	30	B	Wheat flour	R972	1.30	3.59	8.44	0.65

The following image presents the physical aspect of all 51 runs of the DoE. This allows visual comparison of the flow behaviour.



Figure 4.15. Physical aspect of powder mixtures of the experimental design runs.

## 6. Flow factor and interparticle forces: An attempt to go further in the reflexion

In addition to the main publication findings, in this section, we will present some attempts to relate the macroscopic powder flow behaviour with the interparticle adhesive forces using different models proposed in the scientific literature [54, 55, 58, 111]. As previously described (Eq.4.3) the first model was proposed by Capece et al., [54] and relates the  $ff$  to the granular Bond number ( $Bo_g$ ) using two fitting parameters  $\alpha$  and  $\beta$  (Eq.4.6):

$$ff_P = \alpha(Bo_g)^{-\beta} \quad (4.6)$$

From the empirical model,  $ff$  was determined using the Schulze ring shear test at 1 kPa pre-consolidation,  $ff_P$ . The samples were pure pharmaceutical excipients and four mixtures of pure powders with flow additives.

A  $Bo_g$  value greater than 1 indicates that the cohesive forces govern the flow behaviour, whereas a  $Bo_g$  value less than 1 implies that gravitation controls flowability.

Different models can be used to estimate  $F_{vdW}$  theoretically. The first model used to estimate the cohesion between pure powders was the Rumpf multiasperity model.

$$F_{vdW} = -\frac{A}{12z_0^2} \left[ \frac{d_p}{2(H_0/z_0)^2} + \frac{3d_{asp}d_p}{d_{asp} + d_p} \right] \quad (4.7)$$

where  $A$  is the Hamaker constant,  $z_0$  is the equilibrium separation distance (assumed 0.4 nm),  $d_p$  is the HP diameter,  $d_{asp}$  is the asperity diameter, which is assumed to be 200 nm describing the particles "natural roughness" [229] and  $H_0$  is the separation distance ( $H_0 = z_0 + d_{asp}/2$ ).

Adhesive forces, for powders containing flow additives, were evaluated using the equation proposed by Hamaker in 1967 (Eq.4.8). Capece et al. [54] assumed the diameter of the flow additive ( $d_{asp-NP}$ ) to be 16 nm because this value corresponds to the primary size particles of their flow additive. However, as presented in section 4. and in the following the size of S-NP agglomerates, regardless of the primary size of the flow additives, ranged from 40 to 60 nm, consistent with previous observations made by Castellanos [28]. Therefore, a value of  $d_{asp-NP} = 50$  nm was used.

$$F_{vdW} = \frac{Ad_{asp-NP}}{24z_0^2} \quad (4.8)$$

The Hamaker constant,  $A$  was calculated using Frenkel's equation:

$$A = 24\pi D_0^2 \gamma_s^d \quad (4.9)$$

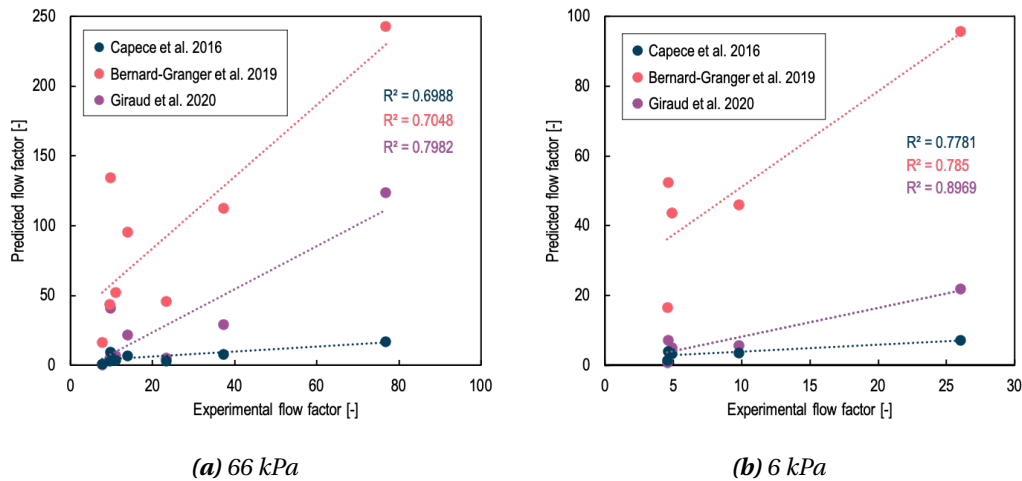
where  $D_0$  is the cut-off distance, assumed 0.165 nm and  $\gamma_s^d$  [ $mJ/m^2$ ] the dispersive surface energy.

Table 4.5 presents the  $B_{o_g}$  estimated from Eqs. 4.8-4.9 and the  $ff$  values obtained experimentally at 6 and 66 kPa for the HP and HP+SD10 with 40% SC. Figure 4.16 shows the relationship between the experimental values  $ff$  and those obtained from the literature models  $ff_P$  using three different sets of fitting parameters ( $\alpha$  and  $\beta$ ):  $\alpha = 14.8$  and  $\beta = 0.28$  evaluating pharmaceutical powders using the Schulze ring shear test at 1 kPa [55],  $\alpha = 204$  and  $\beta = 0.29$  obtained from alumina powders [71] and  $\alpha = 89.5$  and  $\beta = 0.54$  studying oxide powders [58]. The last two results were obtained using the FT4 at 9 kPa.

**Table 4.5.** HP and HP+40%SC SD10 sauter diameter,  $d_{3,2}$ , pycnometric density,  $\rho$  and the dispersive surface energy,  $\gamma_s^d$  used to estimate the Hamaker constant,  $A$ , the Bond number,  $B_{o_g}$ , the cohesion/adhesion force,  $F_{vdW}$ . The experimental values of  $ff$  measured at 66 kPa,  $ff_{66kPa}$ , and at 6 kPa,  $ff_{6kPa}$ .

Formulation	$d_{3,2}$ [ $\mu\text{m}$ ]	$\rho$ [ $\text{kg}/\text{m}^3$ ]	$\gamma_s^d$ [ $\text{J}/\text{m}^2$ ]	$W_g$ [ $\text{kg}$ ]	$A$ [ $\text{J}$ ]	$F_{vdW}$ [ $\text{N}$ ]	$B_{o_g}$ [-]	$ff_{66kPa}$ [-]	$ff_{6kPa}$ [-]
AP	70	1550	0.06	2.7E-09	1.2E-19	3.7E-08	1.4E+01	13.9	26.0
WF	32	1460	0.04	2.5E-10	8.8E-20	2.7E-08	1.1E+02	11.0	4.6
JF	7	2810	0.04	4.4E-12	8.2E-20	2.5E-08	5.7E+03	7.7	4.5
GB	23	2666	0.05	1.8E-10	9.7E-20	3.0E-08	1.7E+02	23.3	9.8
AP+SD10	70	1565	0.06	2.8E-09	1.2E-19	1.5E-09	5.5E-01	76.8	-
WF+SD10	32	1482	0.04	2.5E-10	8.1E-20	1.1E-09	4.2E+00	9.7	-
JF+SD10	7	2787	0.03	4.3E-12	6.7E-20	8.8E-10	2.0E+02	9.6	4.9
GB+SD10	23	2623	0.05	1.7E-10	1.0E-19	1.3E-09	7.7E+00	37.2	-

The results obtained from the models in figure 4.16 showed a poor correlation to the experimental  $ff$  values, either at 6 kPa or 66 kPa. While a slight increase in  $R^2$  was observed at 6 kPa, the model's predicted values remain inaccurate.



**Figure 4.16.** Model fitting between the experimental flow factor, at high and low consolidations, and the predicted flow factor (Eq.4.6) using the fitting parameters:  $\bullet$   $\alpha = 14.8$  and  $\beta = 0.28$  [55],  $\bullet$   $\alpha = 204$  and  $\beta = 0.29$  [71],  $\bullet$   $\alpha = 89.5$  and  $\beta = 0.54$  [58].

Cares-Pacheco and Falk [111] conducted an original analysis from over 150 industrial powder samples of the yield locus variables showing that the flow factor can be related to bulk adhesive interactions  $c$ , independently of the sample and the shear device:

$$ff = 0.58C^{-0.94} \quad (4.10)$$

with  $C$  a dimensionless number, called the adhesive number, given by the ratio  $C = c/\sigma_p$ , with  $\sigma_p$  the confining normal stress applied during the test (in this case, 6 and 66 kPa).

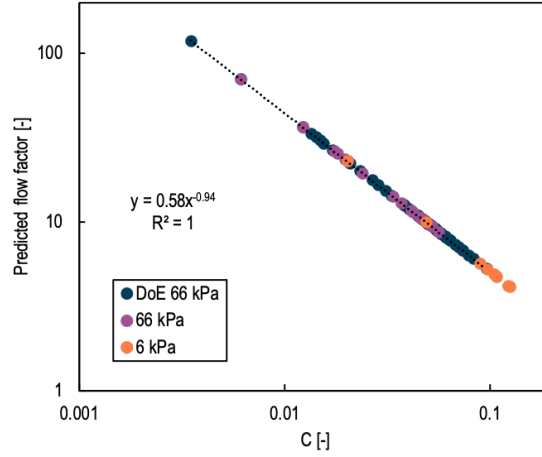


**Figure 4.17.** Cares-Pacheco and Falk model (Eq.4.10) evaluated with the 51 DoE points at 66 kPa, the four HP and the HP+SD10 formulation at 40% SC measured at 6 kPa and 66 kPa.

Figure 4.17 shows the strong fit of the model (Eq.4.10) with our 51 DoE formulations at 66 kPa and the set of 8 formulations evaluated at 6 and 66 kPa. This model allows the prediction of the  $ff$  from  $C$ . To relate  $ff$  to interparticle forces, we employed the Rumpfs description, which assumes an isotropic granular material, an isotropic contact network and that all contacts break at the shear threshold in two dimensions:

$$\sigma_c \approx \frac{\mu\phi Z N_c}{\pi d^2} \quad (4.11)$$

where  $N_c$  is the number of contacts,  $\phi$  is the compactness, and  $Z$  is the coordination number assuming there is an isotropic granular material, an isotropic contact network and that all contacts break at the shear threshold in two dimensions.

Considering that bulk adhesive interaction from the Coulomb criterion represents the yield stress at zero confining stress, it is reasonable to assume that  $\sigma_c \approx c$ . Consequently:

$$c \approx \frac{\mu\phi Z W_g B o_g}{\pi d^2} = \frac{\rho g \mu \phi Z d B o_g}{6} \quad (4.12)$$

By replacing the  $c$  on the equation 4.10, we obtain:

$$ff = 0.58 \left( \frac{\rho g \mu \phi Z d B o_g}{6 \sigma_p} \right)^{-0.94} \quad (4.13)$$

Figure 4.18 presents the results of the predicted  $ff$  from equation Cares and Falk model and Rumpf theory. The predictability of Eq. 4.13 is quite low and does not allow us

to relate the flow factor to interparticle interactions properly. This result might be explained by the several hypotheses that describe either  $Bog$ , or interparticle forces: spherical and monodisperse particles, isotropic contact... one interaction site... All these efforts highlight the complexity of describing powder flow behaviour and the need for further research on the domain to improve the description of interparticle interactions. To finally achieve the breakthrough needed in granular flow understanding, contact mechanics theories and their experimental assessment must be improved to establish the relationship between interparticle forces and bulk behaviour.

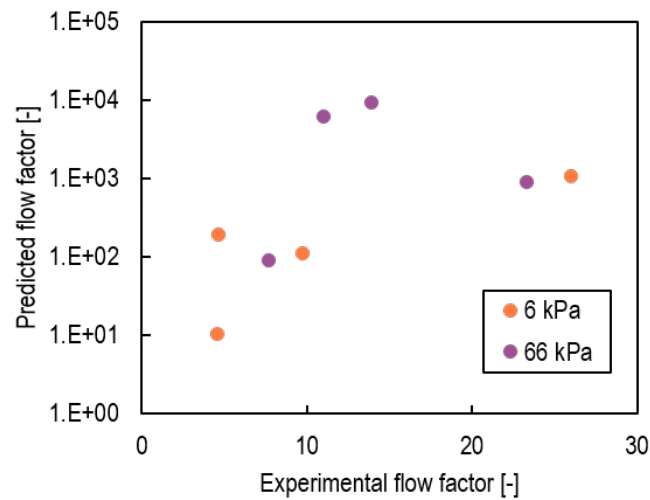


**Figure 4.18.** Flow factor prediction according to eq.4.13 for HP measured at 6 and 66 kPa.



# 5

## Dustiness and glidants

---

In this chapter, after studying the mechanisms of action and the effect of NP on powder flowability, the study shifted towards the dust emission impact. The main focus was to study the effect of adding silica nanoparticles on the dustiness of powders. The previous chapter's findings allowed us to select SIPERNAT D10 (SD10) for its ability to improve flowability independently of the nature of the powder. In addition, all of the SD10+HP mixtures were prepared to cover 40% of the HP surface since this surface coverage produced the most significant improvement in flowability.

The last section, not included in the publication, aims to deep into HP and SD10 interaction and their relation with dustiness.

Main conclusions of this results chapter:

- *S-NP addition increased the thoracic and inhalable fractions in all studied samples measured in the rotating drum.*
- *The relative humidity effect on dustiness is powder related.*
- *S-NP tend to be detached from the HP surface by the action of a mechanical solicitation emitting nano-dust.*  
The ease with which S-NP detaches from the HP relates to the HP/S-NP adhesion interactions. The stronger the adhesion interactions, the less dust is emitted.
- *Dispersive surface energy allows quantifying the HP/S-NP adhesive interactions by correlating them with the dustiness results.*
- *The addition of S-NP disperses the primary particles of the HP, which allow the HP to reach farther in the respiratory system, according to TEM micrographs.*
- *From an occupational safety perspective, adding S-NP increases the risk of inhalation of HP and S-NP and, by extension, the risk of fire and explosions.*

## The effect of silica nanoparticles on the dustiness of industrial powders

Maria Camila Jiménez Garavito<sup>a,b</sup>, Maria Graciela Cares Pacheco<sup>a</sup>, Olivier Witschger<sup>b</sup>, Sébastien Bau<sup>b</sup>, Fabien Gerardin<sup>b</sup> and Véronique Falk<sup>a</sup>

<sup>a</sup> *Université de Lorraine, CNRS, LRGP, F-54000 Nancy, France*

<sup>b</sup> *Department of Process Engineering, Institut National de Recherche et de Sécurité, 54519 Vandœuvre, France*

Article published in the Advanced Powder Technology Journal special issue WCPT9

DOI: [10.1016/j.appt.2023.104105](https://doi.org/10.1016/j.appt.2023.104105)

### Abstract

Industrial powders are prompt to be airborne during processing. High dustiness levels may cause process complications like cross-contamination, product loss and filter clogging while increasing the risk of inhalation, dust explosion and fire. Thus, dustiness is often associated with occupational exposure. Despite this, powder products are usually composed of multiple ingredients with silica nanoparticles (S-NP) systematically added to ease their handling. Surprisingly, the relationship between dustiness and product formulation has not been commonly studied. This work investigates the influence of S-NP, SIPERNAT D10 (SD10), on the dustiness of four industrial powders—Avicel<sup>®</sup> PH-102, wheat flour, joint filler, and glass beads—using two standard methods: the rotating drum (EN 15051-2) and the vortex shaker (EN 17199-5). Our results show that the dustiness of mixtures powder+SD10 are statistically higher than those of the powder alone and can reach the levels of SD10. TEM micrographs from airborne particles collected in the vortex shaker showed that SD10 detached from the surface of the powder during aerosolisation, emitting nanometric dust; adding SD10 increases the potential for inhalation exposure during industrial processing and handling. Surface energy analysis by inverse gas chromatography (IGC) leads us to conclude that stronger powder-to-SD10 interactions result in less dust emission.

**Keywords:** *Dustiness, Rotating drum, Vortex shaker, Powders, Silica nanoparticles, Inverse gas chromatography*

### 1. Introduction

Dustiness is defined as the ability of a powder to be dispersed in air due to a mechanical solicitation [231], generating airborne particles—aerosol [232]—whose size is below 100  $\mu\text{m}$  [119]. Industrial powders often become airborne during processing. Indeed, dust emission is a common phenomenon in unit operations that involve the manual transfer of powders, or handling, like pouring and weighting and mechanical actions like sieving, conveying, calibration, crushing and granulation [25]. The mechanical solicitation applied to the samples during these activities is not easy to quantify, which is probably why dustiness studies have focused on developing measuring techniques over the years [233–235].

From a technological point of view, dustiness can also be seen as an end-use property. High dustiness levels may cause process complications such as cross-contamination, product loss and filter clogging while also increasing the risk of inhalation, dust explosion and fire [236]. Thus, dustiness is often associated with occupational exposure because most classifications—or indices—are based on the extent to which particles reach the respiratory system (Fig.5.1), which depends on the size of the airborne particles. The largest particles reach the extrathoracic region and are eliminated in a few hours, while the tiniest particles reach the alveoli and take 12 to 100 days to be evacuated [130].

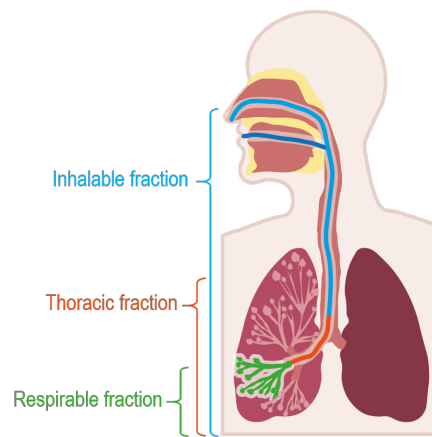


**Figure 5.1.** Schematic of health-related aerosol fractions.

The inhalation of airborne particles can cause undesirable consequences for employees' health [124]. For example, Baker's asthma caused by the inhalation of wheat flour is the most common type of occupational asthma in France and is among the first types in most European countries [125]. This well-known disease affects 44.5% of bakers, according to a study of bakeries in Poland [126]. A similar occupational disease caused by inhalation of crystalline silica is silicosis which causes chronic inflammation and pulmonary fibrosis [127]. Other studies on occupational inhalation of industrial dust have shown that workers exposed to cement aerosols lower their lung function parameters [128]. A review that focused on reactions to food powder dust highlighted that workers inhaling fish, seafood, soybeans, eggs, grains, and chicken, and other powdered foods, had respiratory manifestations ranging from rhinitis to asthma [129]. Studies have found that dust exposure can generate serious health consequences depending on the nature and size of the powder [25, 128–130]. Because to the health consequences, some dust exposures are regulated or the subject of strict recommendations. In France, from 2023, the occupational exposure limit (OEL) of the average concentrations of inhalable and respirable dust must not exceed 4 and 0.9  $[mg/m^3]$ , respectively [131]. In addition, there are specific limit values for some particular powders: for crystalline silica, the limit in the respirable fraction is 0.1  $[mg/m^3]$ , while for wheat flour, it is 0.5  $[mg/m^3]$  [132, 133]. In the case of wheat flour, a study from the Centers for Disease Control and Prevention showed that the actual exposure concentration was above the limit (between 1.03 and 8.21  $[mg/m^3]$ ) in the inhalable fraction [132]. Despite regulations, protective measures

can be insufficient to protect workers [133].

The first dustiness standard methods were published quite recently in 2006 (EN 15051). The first methods introduced were the rotating drum [154] and the continuous drop [155], which respectively simulate the dust emission of granulation and powder transfer unit operations. These two methods are used to measure the emitted dustiness mass fractions. In the rotating drum method, three fractions are measured—inhalable, thoracic, and respirable (EN 481:1993)—while the continuous drop method is only used to quantify the inhalable and the respirable fractions. In recent years, two other standard methods have been developed, the vortex shaker [161] and the small rotating drum [162], which both enable the respirable fraction to be measured along with the dust particles' size distribution and the number of particles emitted. Different methods to measure dustiness can be found in the scientific literature [146], such as the Andreasen single drop apparatus [147], the bench scale impact-type chamber [144], the UNC dustiness tester [151] and the vibrated fluidized bed [237]. Aside from the properties of the powder, the released dust depends on the device geometry and the mechanical solicitation—energy—supplied to the samples.

Several studies have focused on the dustiness of industrial samples. For instance, wood [142, 238], pharmaceutical active ingredients [25], nanostructured materials [239], carbon nanotubes/fibers, fumed oxides, metallic nanoparticles [240], betonite, organoclays [241], calcium carbonate nanopowder [242], powder mixtures of limestone ( $CaCO_3$ ) and codundum ( $Al_2O_3$ ) [243], among others [244]. Among powder properties, the influence of particles size distribution on dustiness has been extensively studied, but the conclusions are powder-related and no general conclusion can be drawn [134–137]. Some researchers show that smaller particles emit more dust than larger ones [134, 136] while others have found the opposite [135]. Plinke et al. [138] conclude that the impact of size was high for particles between 20 and 40  $\mu m$  and decreased for larger (insufficient amount of fine) and smaller (highly cohesive) particles. Particle shape has also been related to dustiness, with irregularly shaped particles being dustier than spherical particles [137, 235]. Some studies have focused on the effect of relative humidity (RH) on dustiness due to its well-known influence on powder handling. Air humidity can act as a binder or lubricant, changing capillary forces. Indeed capillary forces are one type of interparticle force that is stronger than van der Waals forces [47] and thus, it can be expected that high moisture content decreases dust generation due to the formation of liquid bridges. However, the scientific literature has shown that the behaviour of powders in relation to water changes according to the sample. Some authors have found a reduction in inhalable particles emission at high RH [142, 143] while others have found the opposite [138, 144, 145].

A few efforts have been made to model dust release. However, the prediction of these is complicated, and the proposed models either showed a lack-of-fit [243] or were only

a good fit for a limited number of materials [138, 245–247]. In the state of knowledge, fully understanding dustiness still needs experimental assessment to establish clear relationships between grain properties, bulk behaviour and dustiness.

Herein we focus on the effect of amorphous silica nanoparticles (S-NP) on powders' dustiness because nowadays powdered products are formulations constituted by several ingredients. In the vast majority of cases, S-NP are systematically added as flow-aids, 0.5 to 2% wt., as an easy way to ensure handling and process feasibility [51]. The effect of NP on powders has been widely studied, chiefly with regard to their flow-enhancement ability as a fundamental end-use property in industry [51, 77–79]. The effect of S-NP on powder flowability has been ascribed primarily to a reduction in interparticle forces such as van der Waals and capillary forces [81, 84, 188]. S-NP serve as spacers in these cases, reducing short-range forces. We recently showed that S-NP can cause physicochemical modifications on the grain's surface, influencing its surface energy [18].

Despite their widespread use, the toxicity of S-NP has not been clearly established and is even a controversial subject. For example, *in vitro* and *in vivo* studies have shown that S-NP causes acute toxic effects as well as being cytotoxic [23, 209–212]. At the same time, workers exposed to foundries (respirable silica) were found to die earlier from strokes than the general population [215]. The regulation entities (U.S. Food and Drug Administration and the European Food Safety Authority) allow the use of S-NP in food and pharmaceutical products, considering them non-toxic and non-irritant [208]. The limit amount of addition varies according to the purpose, but for some food categories for which the limit is defined as "quantum satis"—as much as needed [208].

This work aims to evaluate the impact of silica nanoparticles (SIPERNAT<sup>®</sup> D10) on the dustiness of four industrial powders widely used in the pharmaceutical, cosmetic (Avicel<sup>®</sup>PH-102), food (wheat flour), construction (joint filler) and road-marking (glass beads) industries. To the best of our knowledge, the dustiness of powder formulations containing S-NP has never been investigated. To represent different unit operations where dust can be emitted, the dustiness is evaluated using two standard methods the rotating drum (EN 15051-2) and the vortex shaker (EN 17199-5). Both devices supply different amounts of energy to the sample and provide further information about the emitted airborne particles.

This work introduces a new subject of study in the formulation field by showing the interest of dustiness as an end-use property, with a focus on the impact of nano ingredients.

## 2. Materials and methods

### 2.1. Materials

Four powders widely used in different industrial sectors were selected for this work: wheat flour (WF), microcrystalline cellulose (MCC), joint filler (JF), and glass beads (GB). WF is an artisan-made T45 WF, from the Poinsignon flour mill (Fouigny, France), commonly used in the food industry. In this work, Avicel<sup>®</sup> PH102 (A) is a MCC (FMC Biopolymer<sup>®</sup>), which is one of the principal excipients in pharmaceutical products and cosmetics because of its capacity to compact. In the construction industry, JF (MAPEI<sup>®</sup>) is employed to grout tiles and finish walls. Finally, GB from Potters<sup>®</sup> Industries LLC (Spheriglass<sup>®</sup> 3000-E) are used in highway safety marking. In granular physics, glass beads are used as "model materials" (spherical, smooth, hard particles) to model granular flows. SIPERNAT D10 (Evonik) are hydrophobic silica nano-aggregates with a porous sponge-like structure synthesized by precipitation. The fabricant suggests its use as a defoaming agent. In the scientific literature, their use as flow-aids has also been studied [51, 77].

In the following, powders are denoted as host particles (HP), while SIPERNAT<sup>®</sup> D10 guest particles (SD10).

### 2.2. Physical characterisation

HP particle size distribution was assessed by laser diffraction (PSD-LD) in liquid media (ethanol) using a Mastersizer 3000 (Malvern Instruments). Their morphology was characterised by scanning electron microscopy (SEM) using a Gemini 3 from Zeiss with a field-emission gun operating at 2 kV. Samples were placed on double-sided tape and then coated for 1 min with a gold-palladium layer using a Desk V - TSC from Denton Vacuum under air purge. SD10 were characterised using a 2100-F transmission electron microscope (TEM) from Jeol with a high tension of 200 kV. Images were recorded with a Gatan Orius SC 200 D camera. SD10 mean primary particle size was measured by randomly analysing ~100 particles selected, using ImageJ. The dust generated with the vortex shaker was characterised using an HT7700 TEM from HITACHI with a high tension of 200 kV.

Water sorption isotherms were obtained at 25°C in a dynamic vapour sorption (DVS-2) from Surface Measurement Systems (SMS), using a Cahn microbalance with a resolution of 5 mg. Before scanning, samples were vacuum dried for 60 minutes.

True powder density was determined in a Helium pycnometer (AccuPyc 1330, Micromeritics). All data presented are the average of ten measurements taken from a single powder sample.

### 2.3. Surface energy

Inverse Gas Chromatography in the infinity dilution region IGC-ID is based on the physical adsorption of gas molecules on a solid surface. Unlike analytical gas chromatography, in

IGC-ID, the studied solid is the stationary phase, and well-identified vapour molecules, called probes, are used to determine the interaction capacities of the material packed into the column (Fig.5.2). The retention time  $t_N$  results from the interaction between the solid's surface and the probe molecule's nature. If the probe molecules are n-alkanes and the adsorption takes place on a non-polar solid, the interaction forces are dominated by dispersive interactions (London type). Based on the Dorris-Gray model, by injecting a series of n-alkanes as probe molecules, their retention volume allows for determining the dispersive surface energy,  $\gamma_s^d$  from the following equation [176]:

$$\gamma_s^d = \frac{1}{\gamma_{CH_2}^d} \left[ -\frac{RT}{2N_a a_{CH_2}} \ln \frac{V_{N+1}}{V_N} \right]^2 \quad (5.1)$$

where  $V_N$  is the retention volume calculated from  $t_N$  by considering the pressure drop along the column during elution;  $N_a$  is the Avogadro number,  $a_{CH_2}$  is the surface area of  $CH_2$  molecule ( $6 \cdot 10^{-18} m^2$ ),  $\gamma_{CH_2}^d = 35.6 - 0.058(T - 20)$  is the surface energy of a methylene group,  $R$  is the perfect gas law constant and  $T$  is the column temperature.

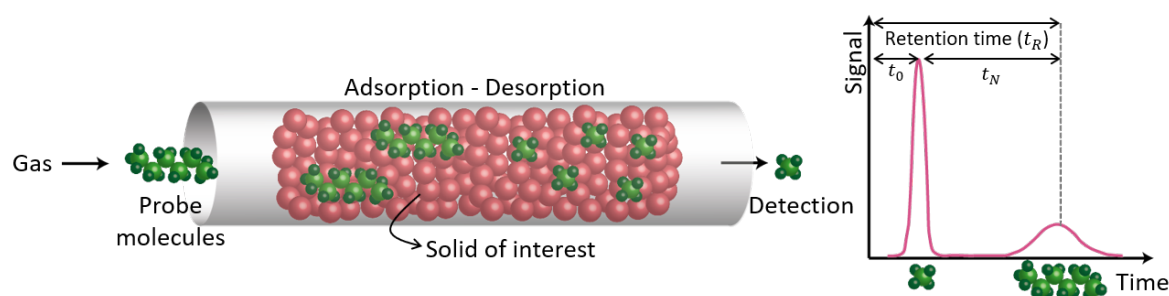


**Figure 5.2.** Inverse gas chromatography principle (adapted from [176]). The net retention time is given by  $t_N = t_R - t_0$  where  $t_R$  is the time spent for a probe molecule to pass through the powder column, and  $t_0$  corresponds to the time for a non-adsorbed molecule—methane—to do it.

The dispersive surface energies of the samples were measured by the NeuronIC inverse gas chromatography from Adscientis, France. Samples were placed into a stainless-steel column with a 100 mm length and 4 mm internal diameter. Before the analysis, each powder column was conditioned in-situ in the NeuronIC for 16 hours at a temperature of 25°C. Helium was used as carrier gas at a 10 mL/min flow rate. The retention times of methane and probe molecules were determined using a flame ionization detector (FID). The software Nucleus 3.2.4 was used to inject a homologous series of vapour n-alkanes (hexane, heptane, octane and nonane)—less than 5 nmoles per probe. The Solid 3.3.0 software, also from Adscientis, was used for the calculations.

#### 2.4. Preparation of mixtures

In this work, all mixtures were prepared to obtain a 40% surface coverage (SC). As previously described [18], the protocol involves mixing a known S-NP mass fraction, quantifying the SC from SEM micrographs using image treatment techniques, and

determining the proportional mass fraction needed to cover 40% of the HP surface. The mass fractions of the mixtures are given in table 5.1 and were experimentally validated using SEM imaging [18].

The samples were conditioned at fixed relative humidity (RH), 30% RH or 50% RH, as described previously [51]. The dustiness experiments airflow RH was also evaluated as a process parameter in order to study its influence on dustiness. Three samples/equipment airflow humidity configurations were tested: 30-30, 30-50 and 50-50.

**Table 5.1.** Mass fraction of SD10 needed to cover 40% of the HP surface.

Mixture	Host powder	SD10 [% wt.]
1	Avicel®PH-102	0.77
2	Wheat flour	1.55
3	Joint filler	1.60
4	Glass beads	0.37

## 2.5. Dustiness

Dust emission was quantified using two complementary devices: a rotating drum and a vortex shaker whose methodologies are described in the standards EN 15051-2 [154] and EN 17199-5 [161] respectively. The details of these two methodologies are described below.

### 2.5.1. The rotating drum (RD)

In this method, dust generation is created by the rotational movement of a drum (Fig.5.3). The protocol consists of adding 35 cm<sup>3</sup> of sample on a 300 mm diameter stainless-steel drum with eight longitudinal vanes that enable the sample's recollection and drop. The drum rotates at 4 rpm for 60 seconds. A particle-free airflow at 38 [L/min] transports the airborne particles to the drum outlet (TSI 3074B [153]). The dust is recovered in two metallic foams - 20 pores per inch (ppi) and 80 ppi - and a terminal filter made of glass fibres. The weighted samples on the selective foams and filter are used to determine the sample's inhalable (Eq.5.2), thoracic (Eq.5.3) and respirable (Eq.5.4) mass fractions.

$$w_I = \frac{\Delta m_{20} + \Delta m_{80} + \Delta m_f}{m_s} \quad (5.2)$$

$$w_T = \frac{\Delta m_{80} + \Delta m_f}{m_s} \quad (5.3)$$

$$w_R = \frac{\Delta m_f}{m_s} \quad (5.4)$$

with  $w_I$  the inhalable,  $w_T$  thoracic and  $w_R$  respirable indexes expressed in [mg/kg]. The subindexes 80, 20 and  $f$  design the foam filters and glass fibre filter mass recovered in

[mg], while  $m_s$  is the sample's mass in [kg]. The respirable fraction is only composed of particles  $\leq 10\mu m$  (mean diameter of  $4\mu m$ ).

The standard classifies dustiness according to four categories per fraction as shown in table 5.2. The airflow humidity during the test should be controlled at 50% RH according to the standard. However, to evaluate the influence of the airflow humidity on the samples' dustiness, experiments were also performed at 30% RH. Five samples of each powder were analysed, and the relative standard deviations obtained were less than 25%.

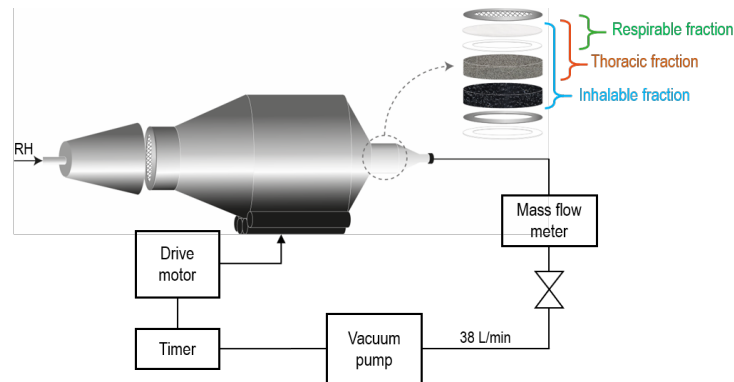


Figure 5.3. Rotating drum device (EN 15051-2 [154]).

Table 5.2. Dustiness classification for rotating drum standard EN 15051-2 [154].

Dustiness category	Mass fractions [mg/kg]		
	Inhalable, $w_I$	Thoracic, $w_T$	Respirable, $w_R$
Very low	<300	<80	<10
Low	300 - 650	80 - 300	10 - 60
Moderate	>650 - 3000	>300 - 1000	>60 - 210
High	>3000	>1000	>210

### 2.5.2. The vortex shaker (VS)

The VS device is composed of a stainless-steel cylindrical tube with an internal diameter of 31 mm and a volume of  $102\text{ cm}^3$ . A sample volume of  $0.5\text{ cm}^3$  is introduced, and the tube is mechanically agitated through orbital motions on the horizontal plane, with a displacement amplitude of 4 mm and a rotational speed of 1850 rpm. The airborne particles are transported to the sampling line using a filtered airflow of 4.2 [L/min] (TSI 3074B) and pre-selected by a GK2.69 cyclone [157] connected to a regulated pump (Gillian 5000, GilAir) to recover just the respirable fraction on the filter. The sampling line can be assembled in two configurations presented in figure 5.4. The first one (Fig.5.4a) consists of collecting the respirable mass fraction on a filter to determine  $w_R$  (Eq.5.4). In the second configuration (Fig.5.4b), the respirable fraction is divided using a flow splitter allowing two real-time measurements - CPC and ELPI- and the collection of the third part

of the aerosol on TEM grids - MPS.

The first real-time measurement is the number-based concentration measured by a condensation particle counter (CPC) Model 3007 from TSI® [153] operating at a flow rate of  $Q_{CPC} = 0.7$  [L/min], which detects airborne particles from about 10 nm to 1  $\mu\text{m}$ . The particles emitted are counted for 60 seconds, and then the number-based dustiness index is calculated as follows:

$$I_{VS} = \frac{1}{m_s} \times \sum_{t_1}^{t_1+60} C_{CPC}(t) \times Q_{VS} \times \Delta t_{CPC} \times \frac{10^3}{60} \quad (5.5)$$

where  $I_{VS}$  is the number-based dustiness in [ $\#/mg$ ],  $C_{CPC}$  is the particle number concentration measured by the CPC [ $1/\text{cm}^3$ ],  $\Delta t_{CPC}$  in the measuring step and  $Q_{VS}$  the flow rate within the stainless-steel cylinder in [L/min].

The second real-time measurement is a number-based PSD (PSD-ELPI) obtained using an electrical low-pressure impactor (ELPI®+ from Dekati [158]). This instrument charges the particles electrically and collects them into different impaction stages according to their aerodynamic diameter. The current measured at each impaction stage enables the number-based PSD-ELPI to be estimated. This instrument detects particles from 10 nm up to 10  $\mu\text{m}$ . The PSD-ELPI is calculated as follows:

$$f_n(d_i) = \frac{n_{i,VS}}{n_{tot,VS}} \times \frac{1}{\Delta \log(d_i)} \quad (5.6)$$

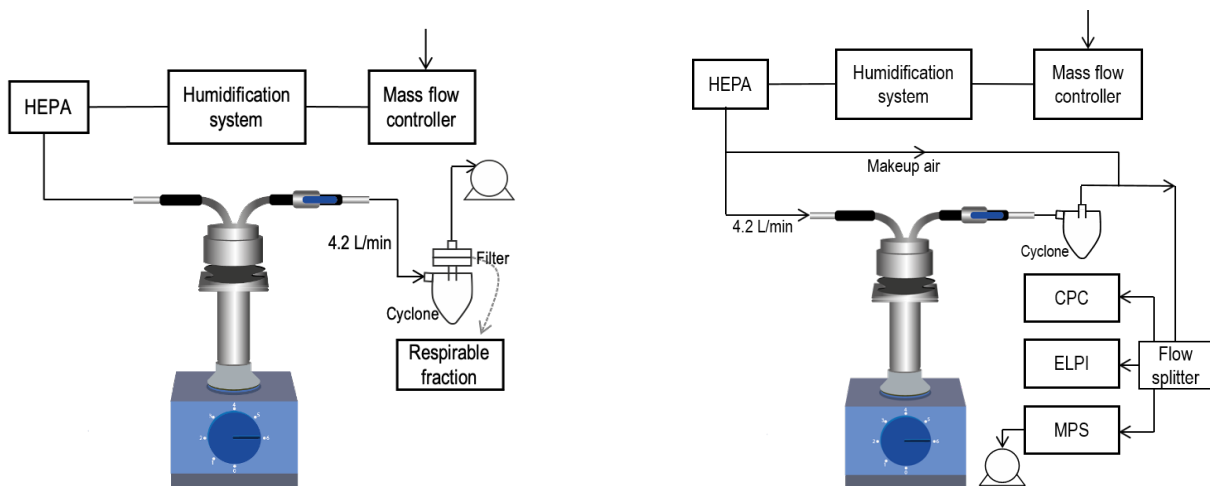
where  $i$  represents the channel in which the particles are counted,  $d_i$  represents the equivalent aerodynamic diameter of the  $i$ -channel,  $n_{i,VS}$  is the number of particles in the  $i$ -channel accumulated in 60 seconds,  $n_{tot,VS}$  is the total number of particles accumulated in all channels during the same 60 seconds, and  $\Delta \log(d_i)$  is the width of the  $i$ -channel of the ELPI®+ (15 channels). This technique differentiates the particles according to their size and does not provide information on their chemical composition.

Finally, the Mini Particle Sampler (MPS) from Ecomesure, France [160, 248] collects the airborne particles for 10 seconds at a flow rate of 1 [L/min] in a 400 Mesh TEM grid sampler equipped with a holey carbon layer.

For each sample, three replicates were performed, except for the collected aerosol on TEM grids. The relative standard deviation of the results was less than 36%.

These two methods of characterising the dustiness of powders - RD and VS - were selected because they enable different information to be obtained about the emitted airborne particles of each sample and the mixtures. From the RD, we can measure the three different mass fractions and classify them from low to high dustiness indices. In the VS method, only the mass respirable fraction is measured, which means the powders can be ranked

as well, but it does not have a classification scale (Table 5.2). The VS is known to transmit more energy per sample volume than the RD but also uses 70 times less sample volume. These differences in the energy supplied to the sample may lead to differences between the emitted dust and thus to differences in the respirable fraction values. VS also enables the measurement of number-based mass distribution and the collection of the emitted dust on TEM grids for further analysis.



(a) Respirable fraction sampling

(b) Real-time sampling: particle count, PSD-ELPI, and dust TEM collection

Figure 5.4. Vortex shaker method sampling configurations.

### 3. Results and discussion

#### 3.1. Physical characterisation

The volume-based size distribution PSD-LD of HP is presented in table 5.3. Avicel<sup>®</sup> PH-102 and wheat flour are composed of larger particles, while joint filler and glass beads present a similar PSD-LD with smaller particle sizes. The HP morphology is shown on the SEM micrographs in figures 5.5 and 5.6. Except for the glass beads, most HP are heterogeneous (size, shape and roughness). Avicel<sup>®</sup> PH-102 particles have an isometric rod shape with a rough surface. Wheat flour is composed of irregularly shaped gluten and starch which covers part of the gluten particles with a globule-like structure. The joint filler has an uneven shape with flat surfaces, while the glass beads are mostly spherical, with some irregularities on the surface. Figure 5.7 presents the physical aspect of SD10 with a cloud-like structure and a mean primary particle size of  $24 \pm 5$  nm evaluated from TEM images.

Table 5.3. Powder characteristics.

Powder	Particle size distribution $\approx 1$ [ $\mu\text{m}$ ]						Pycnometric density [ $\text{g}/\text{cm}^3$ ]
	$d_{10}$	$d_{50}$	$d_{90}$	$d_{32}$	$d_{43}$	$d_{50}^*$	
Avicel® PH-102	35	111	225	69	122	4.8	1.55
Wheat flour	17	83	177	25	91	0.7	1.46
Joint filler	2	18	72	6	29	0.7	2.81
Glass beads	4	24	60	8	29	0.6	2.66

\* Number size distribution

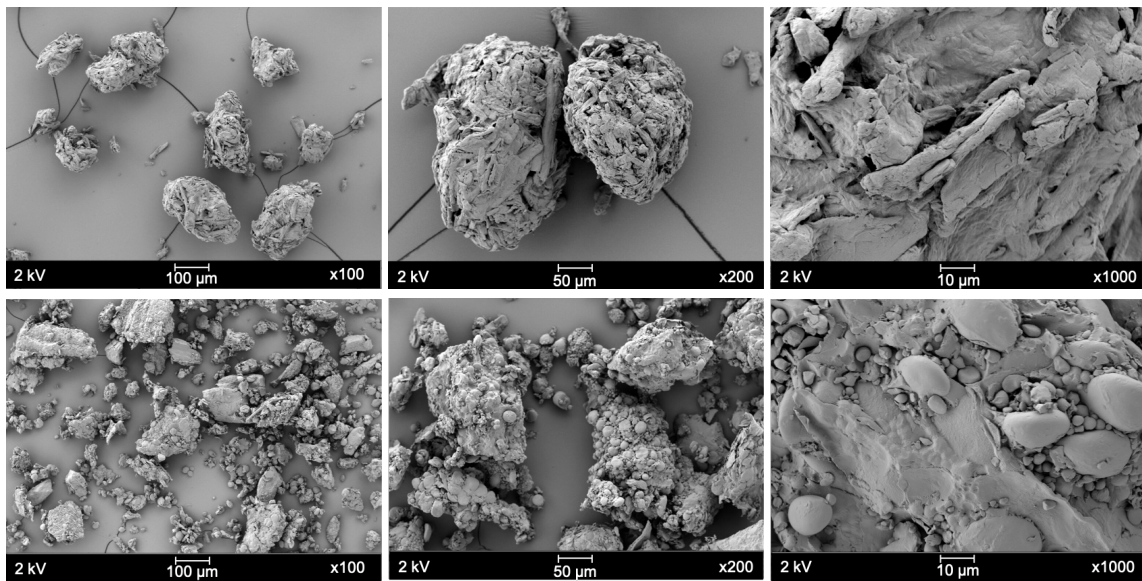


Figure 5.5. SEM micrographs of Avicel® PH-102 (first row) and Wheat flour (second row) at various magnifications (x100, x200 and x1000).

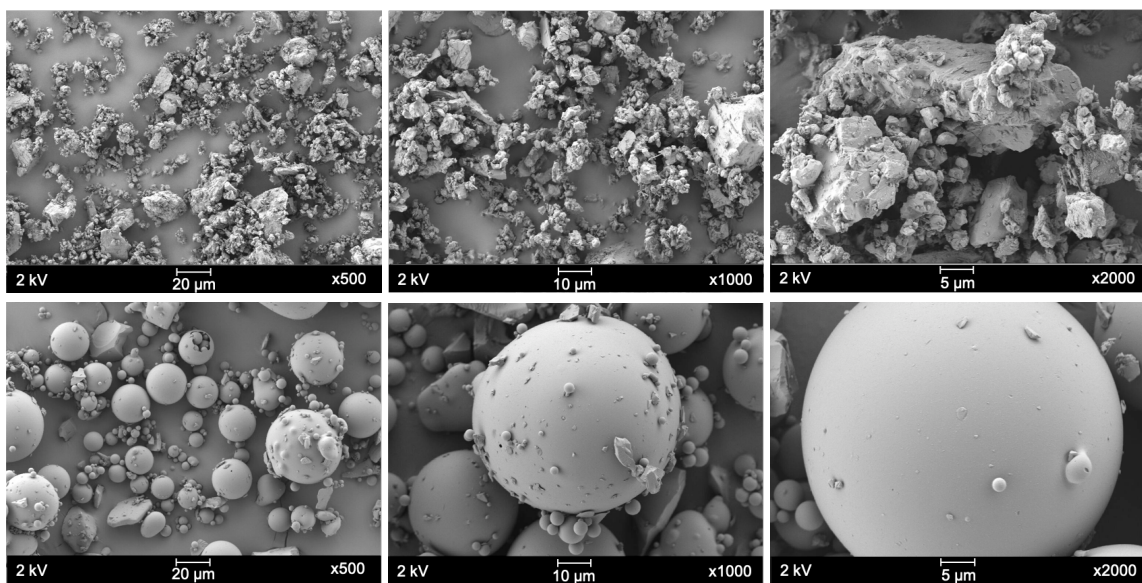
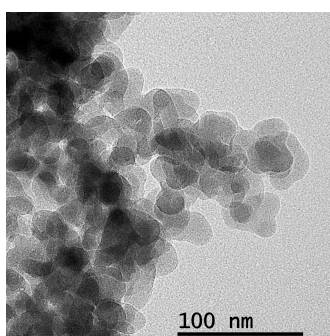
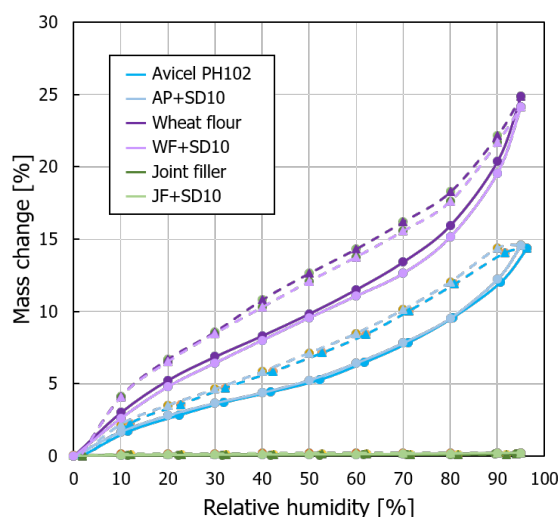


Figure 5.6. SEM micrographs of Joint filler (first row) and glass beads (second row) at various magnifications (x500, x1000 and x2000).



**Figure 5.7.** TEM micrographs SIPERNAT<sup>®</sup> D10.

The behaviour of the HP as regards water is presented in figure 5.8. The sorption isotherms showed that the HP that absorbs more water is the wheat flour, followed by Avicel<sup>®</sup> PH-102, and JF presented almost no water absorption. The isotherms obtained from the mixtures HP+SD10 showed no differences compared to HP alone.



**Figure 5.8.** Water sorption isotherms of HP at 25°C. Sorption curves are represented with a solid line, and desorption curves with a dashed line. Mixtures compositions are shown in table 5.1.

### 3.2. Dustiness of Host Powders and SIPERNAT D10

The dustiness indices of HP and SD10 for the VS and RD are presented in figure 5.9. According to the RD (Fig.5.9a), the dustiest HP are Avicel<sup>®</sup> PH-102 and glass beads with mass-based dustiness indices in the inhalable fraction of  $\sim 10^4$  [mg/kg] corresponding to "high" dustiness levels (see table 5.2). The same can be stated from the indices in the two other health-related fractions, i.e. thoracic and respirable. Wheat flour is the HP with the lowest dust generation, classified as "low" in the inhalable fraction, "very low" in the thoracic fraction while the respirable fraction is "lower than the limit of quantification" (Fig.5.9). The joint filler dustiness indices are all at a "moderate" level, even though it seems to be the dustier HP when handled. The dustiness indices of SD10 in the inhalable and thoracic fractions were higher than those of all HP but similar to the glass beads in the

respirable fraction. This result shows that SD10 emits more dust than the other samples and is potentially more harmful.

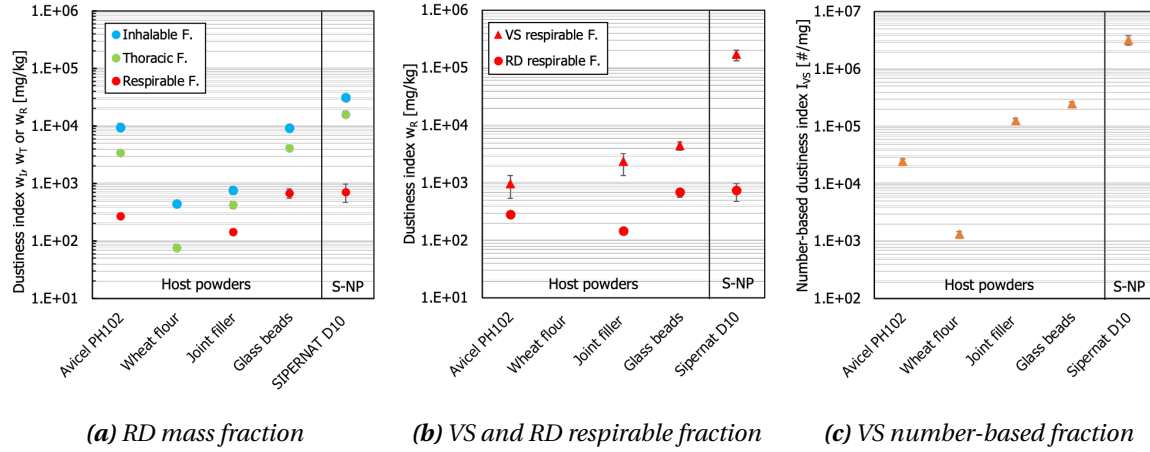


**Figure 5.9.** Dustiness characterisation of HP and SD10. RD data is presented with a circle marker and for the VS a triangle marker was used. The airflow and the sample conditioning RH are controlled at 30%.

According to the VS method, the dustiest HP are the glass beads with the second dustiest being joint filler as both have the smallest PSD-LD (table 5.3). For the SD10, the respirable fraction ( $w_R$ ) is at least two orders of magnitude greater than any HP, and it presented the highest  $I_{VS}$  ( $> 10^6$  [# / mg]). Both number and mass-based concentrations are similar, but there is a difference between the results of the  $w_R$  obtained with the VS or RD, being from 4 to 200 times larger for the VS (Fig.5.9b). These differences between methods can be explained by the energy transmitted to the sample (section 2.5.). Indeed, if we consider the adhesive forces between particles – cohesion - we find that the stronger the interaction is, the less the particles will be prompted to separate from each other. The energy required to overcome interparticle forces varies depending on the material. For instance, the bulk cohesion can be determined from plastic failure experiments [18, 111]. In previous works we have shown that the joint filler is the most cohesive powder ( $3.7 \pm 0.1$  [kPa]), followed by wheat flour ( $2.8 \pm 0.3$  [kPa]), Avicel® PH-102 ( $2.4 \pm 0.6$  [kPa]) and glass beads ( $1.3 \pm 0.5$  [kPa]). The dustiness results in figure 5.9 show that for the JF  $w_{R,VS} \sim 200 w_{R,RD}$  suggesting that when the energy transmitted to the sample increases, interparticle forces can be overcome, and more dust is emitted. The difference is lower for less cohesive powders, such as Avicel® PH-102 and the glass beads, probably because the energy required to overcome interparticle forces is already given to the sample by the RD. Then, supplying higher energies—like with the VS method—could allow airborne bigger/heavier particles.

### 3.3. Influence of relative humidity on the dustiness of HP

As RH influences powder handling and is rarely controlled during industrial processes, the influence of RH was studied by varying the conditioning of the samples and the experimental conditions (RH of the carrier gas). The results for the RD method are presented in figure 5.10.a. The dustiness of Avicel® PH-102 can be seen to decrease when

the conditioning and the experimental setup are at 50% RH, which is the expected behaviour due to the higher RH. The wheat flour, on the contrary, slightly increases its dust generation when the powder is conditioned at 30% and the carrier gas is at 50%, changing the dustiness classification of the inhalable fraction from "low" to "moderate" and the thoracic from "very low" to "low". However, when both conditions are at 50% RH, all dustiness fractions return to the same as at the 30% RH ones. For the joint filler, unexpectedly, when the RH increased, the dustiness also increased in the three fractions changing from "moderate" to "high" in the thoracic and respirable fractions. Wheat flour and joint filler's (Fig.5.10.a) counter-intuitive behaviour towards water are similar to those observed on clays in a continuous drop [145]. Lopez-Lilao et al. showed that dustiness rose with the increase of sample RH conditioning until reaching a critical point above which the dustiness started to decrease depending on the type of clay (carrier gas at 50% RH). In the case of our joint filler, which contains clay, the increase in dustiness indices might suggest that the critical moisture point of conditioning is not yet reached. Notwithstanding, no clear influence on samples' RH% was observed (Fig.5.8 - green isotherms). Finally, due probably to their hydrophobic nature, the RH of glass beads conditioning does not influence dustiness.

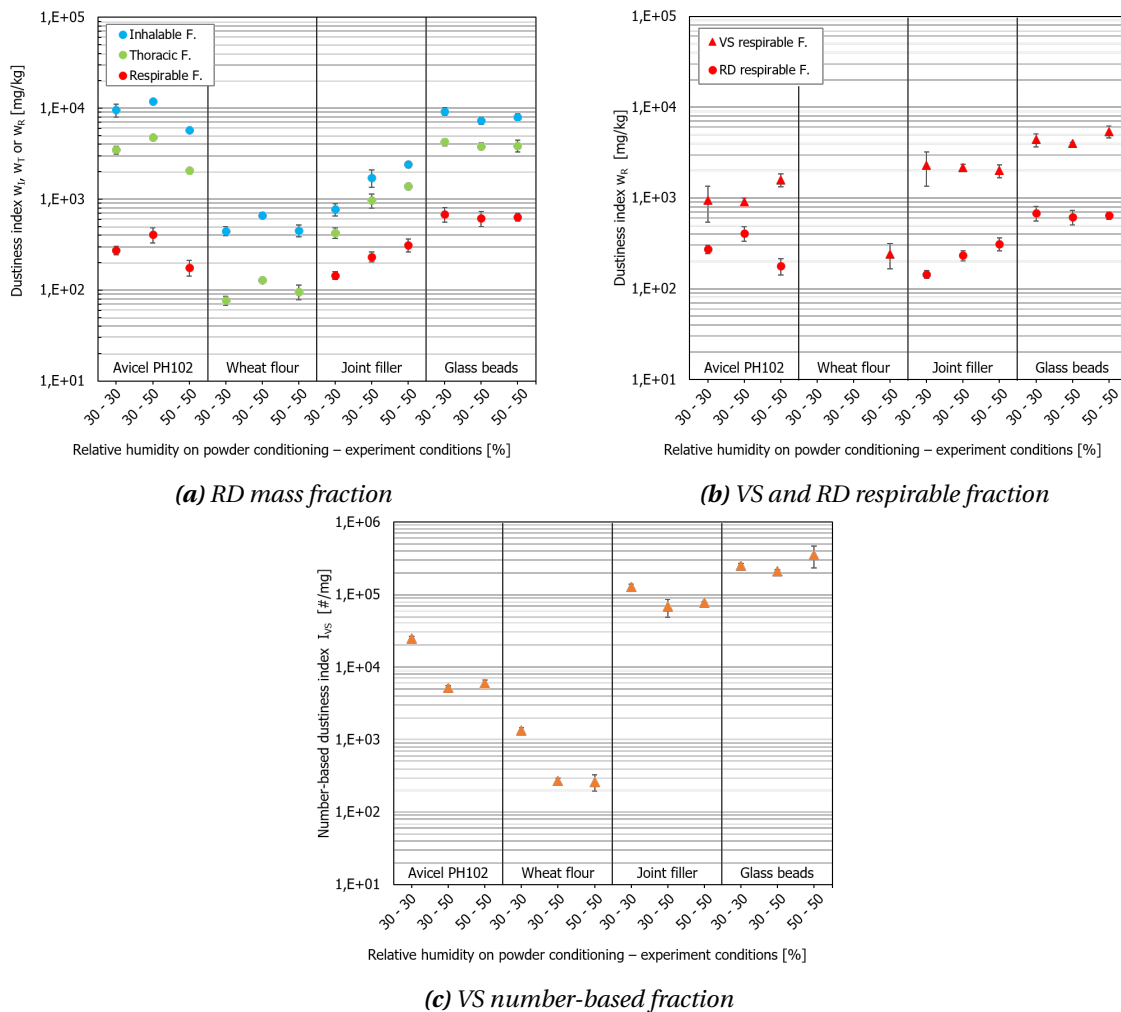


**Figure 5.10.** Influence of RH on the dustiness of HP. RD data is presented with a circle marker and for the VS a triangle marker was used. Three RH% configurations are represented for the powder conditioning - test airflow, 30-30, 30-50 and 50-50.

On the contrary, when using the VS method (Fig.5.10.b), the influence of RH on dustiness is not statistically significant except for the wheat flour, which unexpectedly increased its respirable fraction (see Fig.5.10.b 50-50). For conditions 30-30 and 30-50, the measure was below the quantification limit of balances (in both RD and VS). The  $I_{VS}$  did show the effect of the RH on the number of particles emitted, unlike the  $w_{R,VS}$ . Figure 5.10.c, presents that the  $I_{VS}$  decreased when RH increased, except for glass beads that were not sensitive to RH. The difference between the mass-based and number-based indices may be due to the fact that fewer particles are emitted, but with a higher weight, due to water adsorption/absorption. Sorption isotherms (Fig.5.8) showed that wheat flour is the HP that absorbs the most water when the RH is increased from 30% to 50%, which may explain the increase of the  $w_R$  at 50-50, as well as the slight increase on the  $w_{R,VS}$  for Avicel® PH-102 at the same RH configuration. The isotherms of HP+SD10 mixtures are superposed to those of the pure powders (Fig.5.8), showing no influence of SD10 on HP bulk behaviour towards water.

To sum up, in higher energy methods, like the VS, the influence of RH can be quantified as weaker, while for lower energy methods and hydrophilic samples, RH can be highly influential on dust generation, like in the RD method [249, 250]. Our results are similar to those of previous studies showing that the relationship between dustiness indices and air humidity – the sample conditioning and dustiness methodology - is complex and powder-dependent [138, 144, 145, 249, 250]. Indeed, even though the definition of dustiness has been well established, its assessment is device-related, both in terms of energy and geometry, and thus it is not an intrinsic property of powders. The sample/method RH should be related to the process conditions in order to reproduce the dust emission of the process studied as closely as possible.

### 3.4. Influence on dustiness when adding Sipernat D10

The effect of adding SD10 to HP on dustiness indices is presented in figure 5.11, where each graph allows the comparison between the mixture and the HP directly. As previously explained, the proportions of SD10 added were calculated to cover 40% of the HP surface (Table 5.1). The RD results (Fig.5.11.a) showed that the dustiness  $w_I$  and  $w_T$  indices increased when adding SD10. The  $w_{R,RD}$  index increased significantly for AP+SD10 and WF+SD10, remained constant for GB+SD10 and decreased slightly for JF+SD10. Surprisingly, the dustiness indices of HP+SD10 mixtures resemble those of SD10 except for JF+SD10. In contrast, dustiness quantification using the VS method (Fig.5.11.b) showed that the  $w_{R,VS}$  index did not increase by adding SD10, except for WF+SD10. In general, this might be due to the intensity of the energy transmitted to the samples. The  $I_{VS}$  (Fig.5.11.c) increased in most of the mixtures compared to HP alone, except for JF+SD10.

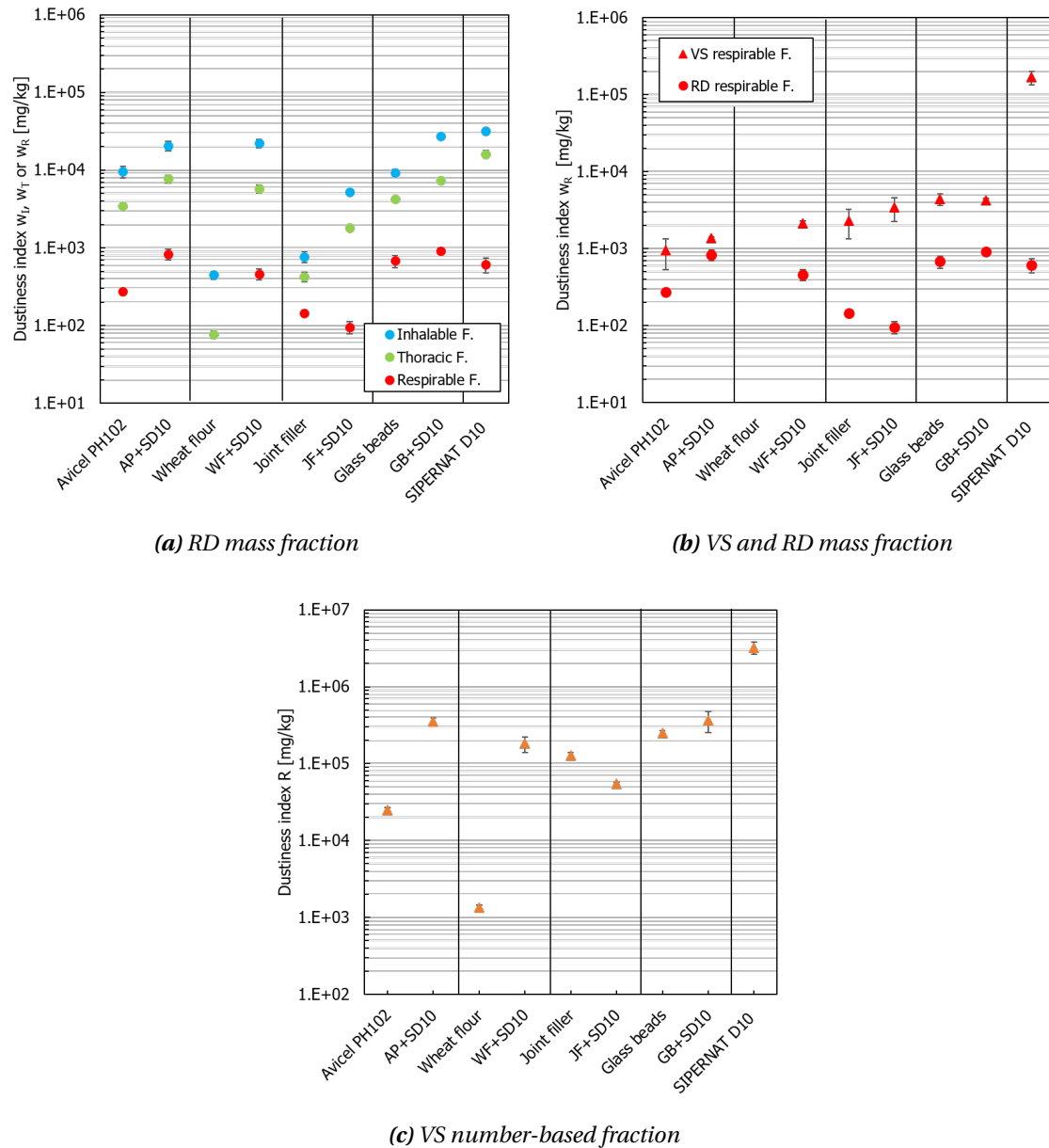


**Figure 5.11.** Dustiness indices of HP mixed with SD10 (40% SC). RD data is presented with a circle marker and for the VS a triangle marker was used. The airflow and the sample conditioning RH are controlled at 30%.

All these results from RD and VS methods suggest two things. Firstly, adding SD10 reduces HP interparticle forces, which has already been evidenced in previous work through bulk cohesion analysis:  $F_{AP+SD10} = 0.4$  [kPa],  $F_{WF+SD10} = 3.05$  [kPa],  $F_{JF+SD10} = 2.97$  [kPa] and  $F_{GB+SD10} = 0.8$  [kPa] [18]. Secondly, decreasing interparticle forces might increase dispersion, resulting in more airborne particles, mostly the lightest ones (WF and AP).

Thus, the influence of interparticle interactions on dispersion and the ability to emit airborne particles depends on both the device (energy supplied to the sample) and the particle's size and density. Notwithstanding, it is important to highlight that no linear—or easy—relationship has been found between the HP size distribution, shape, or density and

their dustiness.

### 3.5. Dustiness real-time analysis

The PSD-ELPI of airborne particles is presented in figure 5.12. Each graph contains three distributions: the one of the HP (dashed line), SD10 (dotted line) and the mixture HP+SD10 (solid line). The figure highlight that the airborne particles from mixtures APSD10, WF+SD10, and GB+SD10 have a wider size-distribution than those obtained from the HP alone. Furthermore, they presented nanosized particles or aggregates from 50 nm to 100 nm, which values are similar to those of SD10 alone. On the contrary, the JF and the mixture JF+SD10 mixture showed a similar PSD-ELPI suggesting a strong adhesive interaction between JF and SD10. All this indicates that SD10 particles can be detached from the HP and be released during mechanical treatment, which depends on HP/SD10 adhesive interaction.

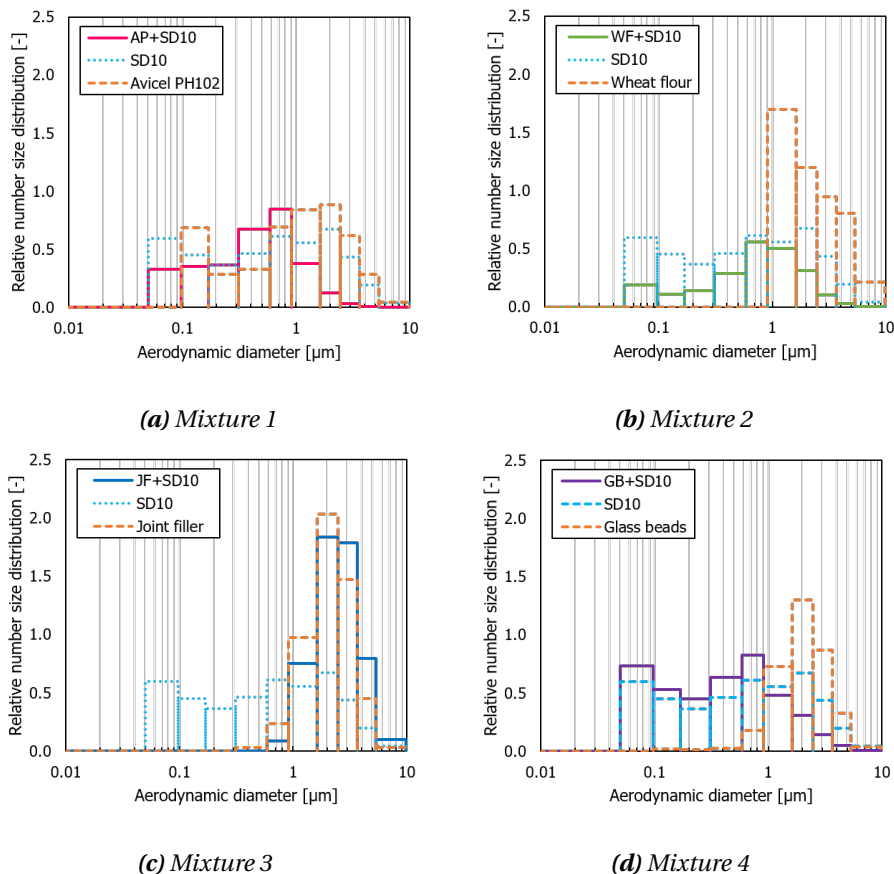
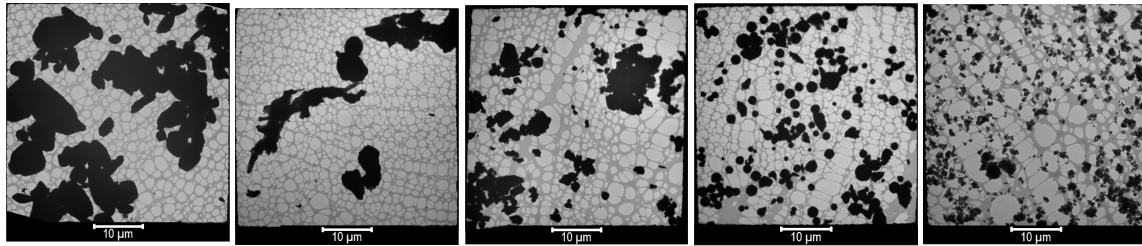


**Figure 5.12.** Number size distributions of aerosolized particles measured by ELPI<sup>®</sup> +.

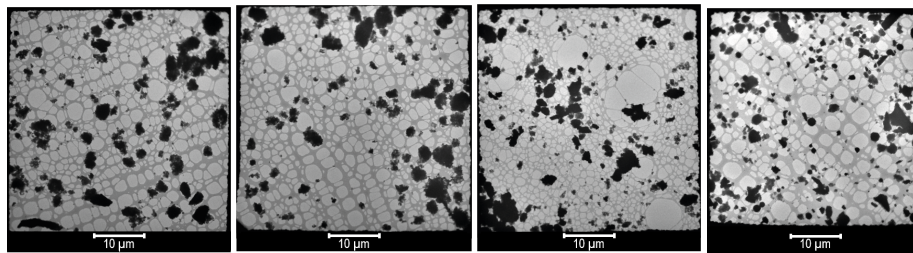
The aerosol produced in the VS method and collected directly on the TEM grids are shown in figures 5.13 and 5.14. Figure 5.13 shows that Avicel<sup>®</sup> PH-102 presents large particles in a cluster-like structure in which the different particles cannot be differentiated. Wheat flour emitted a few particles with different shapes. Joint filler and glass beads produce similar dust with some clusters. The SD10 micrographs show well-spread different-size

nanoaggregates. When the HP are mixed with SD10 (Fig.5.14), the particles collected are better dispersed on the TEM grid, and the dust seems more similar. For instance, the dusts that changed the most were Avicel® PH-102+SD10 and wheat flour+SD10, where the addition of SD10 emitted finer particles below 5  $\mu\text{m}$ . The smaller the dust particles, the farther they reach into the respiratory system. In the case of wheat flour, this increases the risk of Baker's asthma. It seems important to highlight that all HP+SD10 micrographs evidence the presence of isolated nanometric particles or aggregates.



(a) Avicel® PH-102 (b) Wheat flour (c) Joint filler (d) Glass beads (e) Sipernat D10

**Figure 5.13.** TEM micrographs of airborne particles of host powders and SD10.



(a) AP+SD10 (b) WF+SD10 (c) JF+SD10 (d) GB+SD10

**Figure 5.14.** TEM images of particles aerosolized from powder mixtures.

### 3.6. Surface energy analysis: Dustiness and interparticles forces

The experimental values of the HP and SD10 and the mixture HP/SD10 are shown in table 5.4. In the table, the last column corresponds to a theoretical calculation of the dispersive component  $\gamma_{s,SC}^d$  assuming a 40% SC ( $V_{N,SC} = V_{N,HP} \cdot 0.6 + V_{N,SD10} \cdot 0.4$ ).

**Table 5.4.** IGC data: specific retention volumes and dispersive surface energies.

Sample	Powder mass [mg]	$V_N[cm^3]$				$\gamma_s^d$ [mJ/m <sup>2</sup> ]	$\gamma_{s,SC}^d$ [mJ/m <sup>2</sup> ]
		Hexane	Heptane	Octane	Nonane		
Avicel <sup>®</sup> PH-102	785.1	1.17	4.31	15.79	61	57.8±0.7	-
Wheat flour	1190.3	2.15	6.63	20.69	-	42.8±0.2	-
Joint filler	2116.7	1.82	5.42	16.51		39.9±0.3	-
Glass beads	2573.3	0.49	1.59	5.14	17.33	47.2±0.4	-
SD10	103.5	66.93	170.64	436.81	-	29.3±0.1	-
AP+SD10	875.8	1.85	7.02	24.91	-	56.4±1.6	30.2
WF+SD10	1251.6	2.61	7.7	23.07	-	39.6±0.3	30.3
JF+SD10	2158.8	1.18	3.14	8.69	23.26	32.8±0.3	29.4
GB+SD10	2544.0	0.85	2.89	9.61	34.26	50.3±0.8	29.5

Dustiness measures in figure 5.11 show the dustiest powders are the APSD10 and WF+SD10. In both cases, the TEM grids showed S-NP detachment from the HP (Fig.5.14.a and b). For Avicel<sup>®</sup>PH-102, there is no significant surface energy differences before and after adding SD10,  $\gamma_{s,A}^d \approx \gamma_{s,APSD10}^d$ . By confronting these results with  $\gamma_{s,SC}^d$ , we conclude that the interaction forces between AP and SD10 are weak with SD10 acting as a spacer. In this case, it is like there was no real coverage, and the probe molecules interacted freely with AP's surface, which possesses more active sites,  $\gamma_{s,A}^d \gg \gamma_{s,SD10}^d$  (see Fig.5.15.a). Indeed, surface energetics in the infinite dilution region  $\gamma_s^d$  is highly influenced by the higher energy sites [176]. For wheat flour, there is a significant but small difference between  $\gamma_{s,WF}^d \sim \gamma_{s,WF+SD10}^d$ . Still  $\gamma_{s,WF+SD10}^d$  value is not close or similar to  $\gamma_{s,SC}^d$ . We conclude that the interaction force between WF and SD10 is weak and  $\gamma_{s,WF+SD10}^d$  is mostly a contribution of WF active sites (see Fig.5.15.a). The interaction Avicel<sup>®</sup>PH-102 and SD10 is probably weaker than the interaction of the wheat flour and SD10.

In the case of Joint filler and glass beads, adding SD10 has less impact on their dustiness (Fig.5.11). These results can also be explained through the strength of the interactions. For joint filler, there is a diminution of the surface energy when adding SD10,  $\gamma_{s,JF}^d < \gamma_{s,JF+SD10}^d$ . In these cases,  $\gamma_{s,SC}^d \sim \gamma_{s,JF+SD10}^d$ , which lead us to conclude that the interaction forces between JF and SD10 are strong, and the probe molecules see the mixture JF+SD10 as a different particle, a new surface (see Fig.5.15.b).

For the glass beads, surprisingly, when SD10 is added the dispersive surface energy increases,  $\gamma_{s,GB}^d < \gamma_{s,GB+SD10}^d$ . There are two probable explanations for this rise, and both point to a strong interaction between GB and S-NP. The first explanation is based on surface chemistry changes. Both glass beads and silica nanoparticles have many hydroxyl groups that readily participate in hydrogen bonding, reducing the number of hydroxyl groups available at the surface of GB. Because hydroxyl groups have the lowest surface energy, decreasing their number minimises their contribution to  $\gamma_{s,GB+SD10}^d$ . The other possible explanation is based on physical surface changes. The shape and roughness of particles can also influence the dispersive component of surface energy [221]. In this case,

adding SD10 increases the roughness of the glass beads, resulting in new, more active (high-energy) interaction sites (Fig.5.15.c). The strong adhesion between GB and SD10 explains the similarity in dust emissions between GB and GB+SD10.

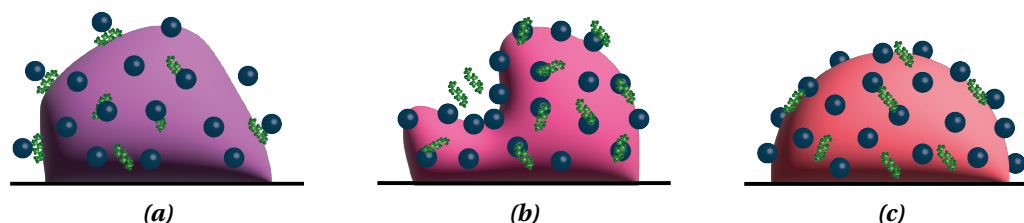


**Figure 5.15.** Interparticle interactions represented schematically using a surface energy analysis: a) Weak interaction: both HP and S-NP are seen as two different particles b) Strong interaction: the surface energy is modified by changing the surface chemistry—the mixture is "seen" as a new particle c) Strong interaction: the surface is physically modified by increasing HP roughness and creating new high energy sites.

All these results suggest that powder formulations containing silica nanoparticles, such as SD10, are more prompt to generate dust, increasing the potential for inhalation exposure. Still, the combined IGC-ID and dustiness analysis leads us to conclude that stronger HP/NP interactions result in less dust emission.

In terms of risk, it should be taken into account that adding silica nanoparticles produces dust clouds composed of primary particles, reducing the sample's minimum ignition energy and leading to a more significant explosion hazard [251, 252].

## 4. Conclusions

Dustiness is an important phenomenon occurring during industrial processing or handling, yet the systematic inclusion of silica nanoparticles in powder formulations has not previously been related to dustiness. This work focused on this lack of knowledge by studying the dustiness of four powders—Avicel® PH-102, wheat flour, joint filler and glass beads—when mixed with nanoscale silica (SD10). As dustiness is not an intrinsic property of powder because the airborne dust, quantity and nature, depends on the mechanical energy supplied to the sample two standard methods were used—the rotating drum (EN 15051-2) and the vortex shaker (EN 17199-5).

It is widely accepted that the physical properties of powder affect dustiness. However, in this study, particle size distribution, shape, and density were not directly or easily related to dustiness; no broad conclusions were made. Similarly, RH is well known to influence powder behaviour and the air RH is rarely controlled during processing and therefore we studied its influence over dustiness on samples and carrier gas: 30-30, 30-50 and 50-50% RH, respectively—standard methods quantify dustiness at 50% RH of the carrier gas. The effect of RH on dustiness seemed to be related to the samples' hygroscopicity but not in a trivial linear manner. For instance, wheat flour and joint filler dustiness increased with RH

until reaching a critical point, after which the dustiness decreased. From a technological point of view, the sample/method RH should be related to the actual process conditions to reproduce the dust emission of the process studied as closely as possible.

Surprisingly some HP+SD10 formulations exhibited high levels of dustiness found to be similar to the dust levels of the SD10 alone (RD), suggesting that part of the nanosilica detached from the HP surface during aerosolization. The TEM micrographs validate this statement by showing isolated SD10 nano-aggregates and better spread particles. This indicates that adding SD10 increases the potential for inhalation of airborne dust, which seems to contain SD10 nano-aggregates and the finest particles of the host powder. Our findings show that the amount and the nature of the dust is strongly related to interparticle forces, which must be overcome in order for particles to be airborne. Surface energy measurements were used to quantify and understand these interactions. For instance, Avicel<sup>®</sup> PH-102 and wheat flour mixed with SD10 were the dustiest samples, presenting the lowest adhesive interaction host particle/nano-additive. Instead, joint filler and glass beads showed the strongest HP/SD10 interaction, releasing less dust. Interparticle forces appear to be a crucial parameter linking grain properties, bulk behaviour, and dustiness.

In conclusion, we have highlighted the need for further research into the effects of nanoparticles on industrial dust emissions, which can be directly related to occupational safety. This work aims to promote the study of dustiness as an end-use property, particularly in nanoparticle-based formulations, due to their impact on humans and the environment.

## 5. Surface properties a deeper insight

In order to expand on the relationship between dustiness and surface properties, the BET specific surface,  $a_{BET}$ , of powders was determined. In Table 5.5 the experimental results are confronted with a theoretical estimation based on the physical mixture HP + SD10 (no changes of the HP surface) ( $a_{BET_{HP+SD10}} = a_{BET_{SD10}} \cdot X_{SD10} + a_{BET_{HP}} \cdot (1 - X_{SD10})$ ), where  $X_{SD10}$  is the mass fraction to achieve 40% SC.

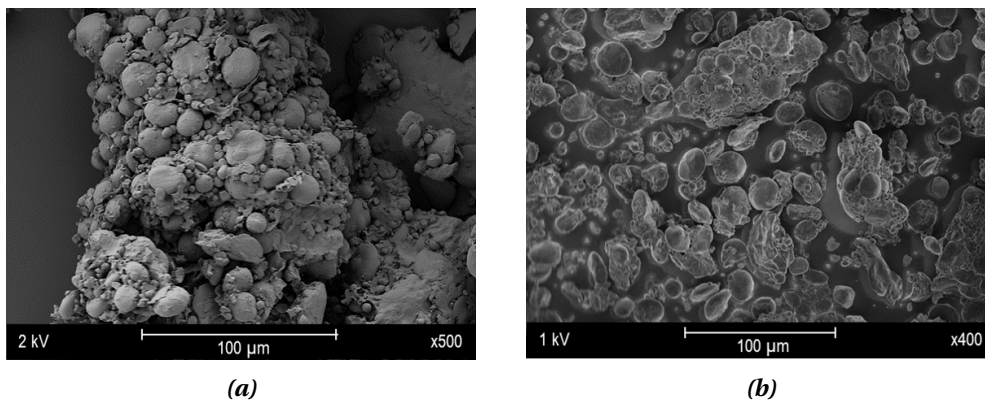
**Table 5.5.** Experimental and theoretical specific surface,  $a_{BET_{N_2}}$  of HP and HP+SD10 with 40% SC.

Formulation	Experimental $a_{BET}$ [ $m^2/g$ ]	Theoretical $a_{BET}$ [ $m^2/g$ ]
Avicel®PH-102	1.00±0.02	-
Wheat flour	0.31±0.01	-
Joint filler	1.12±0.02	-
Glass beads	-	-
AP+SD10	11.68±0.14	1.88
WF+SD10	4.88±0.09	2.1
JF+SD10	3.04±0.03	2.95
GB+SD10	-	-
SD10	115.5±0.92	-

The results in table 5.5 indicate that the mixture HP+SD10 has more surface available to interact with than HP alone. The AP+SD10 increased 11 times the pure AP value and the increase was 16 times greater for WF+SD10, while for JF, the  $a_{BET}$  almost tripled. The experimental  $a_{BET}$  were greater than the theoretical ones  $a_{BET}$  for AP and WF, while for JF was similar.

In the case of WF, the differences between experimental and theoretical values could be explained by a change in the porosity of the HP. Indeed WF is composed of gluten particles surrounded by starch (globules), as shown in Figure 5.16a. When S-NP are added the starch appears to be dispersed from the gluten particles—exposing gluten macropores—increasing the specific surface of the bulk (Fig 5.16b).

In the case of AP, the results are questionable and require further experimental work to verify their validity.

**Figure 5.16.** SEM micrographs of a) pure WF and b) WF mixed with 0.5%wt of SD10.

In an attempt to seek a relationship between surface properties and dustiness,  $\gamma_s^d$  and  $a_{BET}$  values were confronted to dust indices (Figs.5.17a and b). From the figures, it is shown that despite the importance of surface properties on dustiness the relationship between them is neither linear nor trivial. Still, it can be noted that the  $a_{BET}$ -dustiness relationship

exhibits a tendency-like. For further analysis, it would be interesting to evaluate this relationship using a larger number of experimental points.

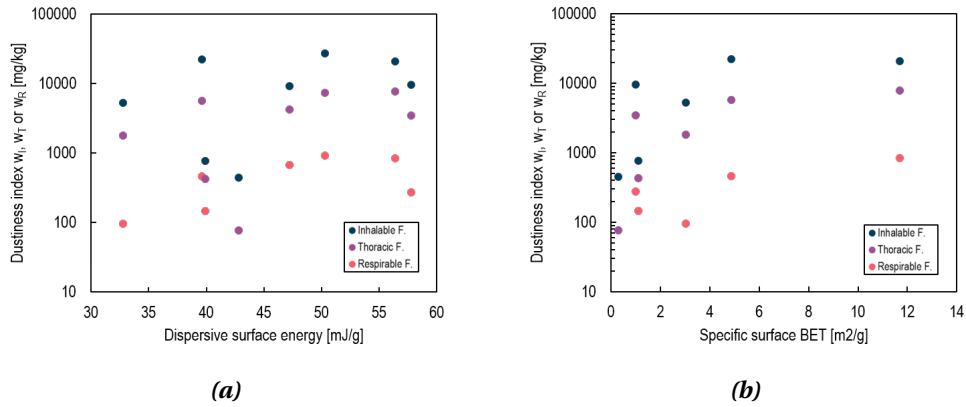


**Figure 5.17.** Relation between dustiness indices and the HP and HP+SD10 at 40%SC surface characterisation by a) dispersive surface energy,  $\gamma_s^d$ , and b) specific surface,  $a_{BET}$ .



# 6

## The relationship between flowability and dustiness

---

### 1. Introduction

Throughout this document, the primary objective of the thesis has been to establish a relation between the enhancement of powder flow behaviour and the dust emission. The results presented in Chapters 3 and 4 were focused on powder flowability improvement, while in Chapter 5, the dust emission of powders mixed with flow additives was discussed. Therefore, the current chapter attempts to establish a link between these two end-use properties, flowability and dustiness.

In this chapter, the results of flowability and dustiness of the HP and three HP+S-NP mixtures at different surface coverage (1%, 40%, and more than 40%) are presented and discussed. From these results in the last part of the chapter the relation between these two end-use properties is evaluated.

### 2. Experimental approach

Its shown in previous chapters, that S-NP/HP surface coverage and their interaction play an important role in the flowability and dustiness of powders. Therefore, in order to investigate these factors further, we considered four different S-NP/HP mixtures based on our previous results. The four formulations are presented in table 6.1 and consist of pure HP and HP+SD10 at three different surface coverage percentages: 1%, 40%, and more than 40%. By testing these four formulations per HP, we aimed to identify an optimal amount of S-NP that would enable good flow while minimizing dust production.

**Table 6.1.** SD10 mass fractions [%] to cover 0, 1, 40 and more than 40% of the HP surface.

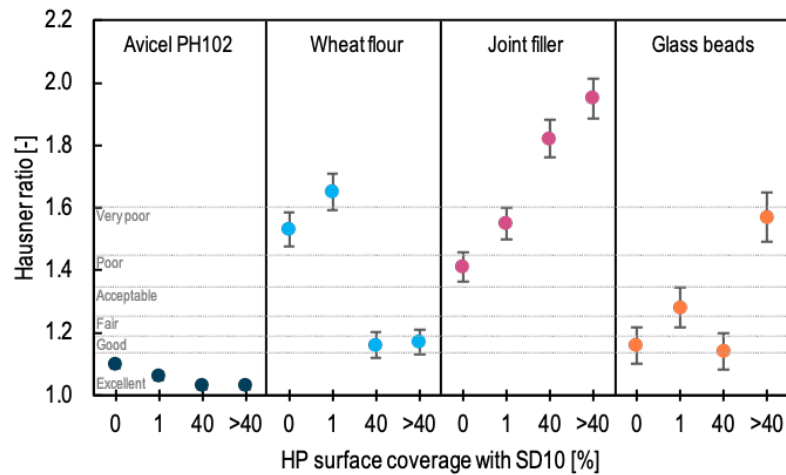
Surface coverage [%]	Avicel® PH-102	Wheat flour	Joint filler	Glass beads
0	-	-	-	-
1	0.02	0.04	0.04	0.03
40	0.77	1.55	1.60	0.37
>40	2.00	2.00	2.00	2.00

### 3. Flowability

The flow characteristics of the 16 formulations (refer to Table 6.1) were determined through three test with the aim to have a broad set of data that may allow to relate flowability to dustiness. The selected test, allows to compare two powder regime behaviours since the powder flow behaviour is evaluated the quasi-static and dynamic regimes. First, uniaxial compression was conducted to determine  $HR_c$  at 30 N, using the Instron press. Secondly, the shear test was performed with the FT4 rheometer at 6 kPa and 66 kPa, to measure  $ff$  and adhesion ( $c$ ). These two tests characterise the samples in a quasi-static regime. Lastly, our homemade flow-meter described in section 6.1.3. was used to characterise the formulations ability to flow through an orifice method.

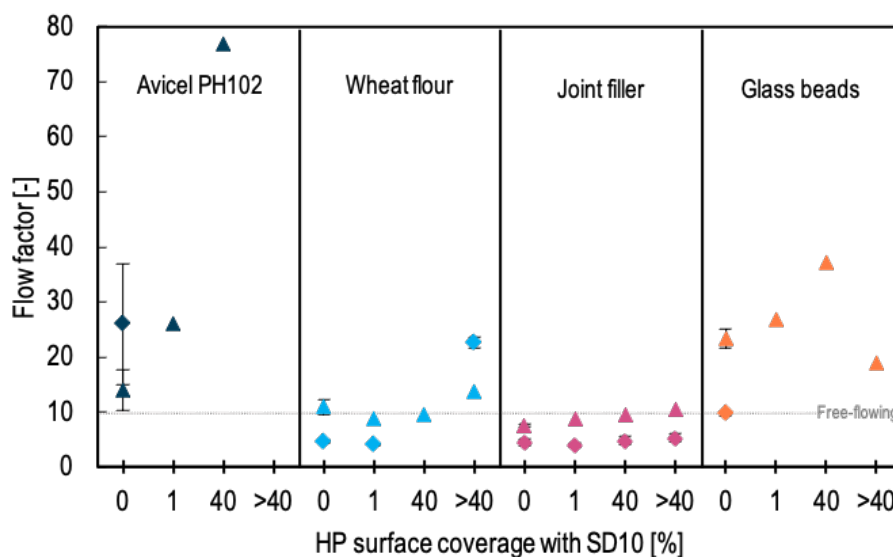
### 4. Quasi-static regime

Figure 6.1 displays the SD10 effect on the  $HR_c$ . Avicel® PH-102 (AP) and wheat flour (WF) exhibited a reduction in their  $HR_c$  as the SC increased. However, both powders showed no significant difference in  $HR_c$  between SC levels of 40% and >40%. This suggests that increasing the amount of SD10 may not further enhance their flowability, which is already excellent for AP and good for WF at 40% SC. In the case of joint filler (JF)  $HR_c$  increases with SC, while for the glass beads (GB), there is no significant variation of the  $HR_c$  until the SC exceeds 40%. Similarly to JF at SC over 40%. It can be highlighted that for JF formulations, the mass required to fill the 10 mL cell decreased when adding SD10 (i.e.  $m_{JF}=9.8$  g,  $m_{JF+1\%D10}=8.5$  g,  $m_{JF+40\%D10}=7.9$  g,  $m_{JF+>40\%D10}=7.8$  g) suggesting that the initial state of the formulations is more aerated and changing the initial compactness of the powder bed. In fact, the final compactness,  $\phi$ , did not change no matter the formulations. For instance, for AP and AP+SD10  $\phi = 0.27$ , for WF and WF+SD10  $\phi = 0.53$ , for the JF and JF+SD10  $\phi = 0.52$  and GB and GB+SD10  $\phi = 0.63$ . This shows the limit of HR as the ratio of two changing values.



**Figure 6.1.** Compression Hausner ratio,  $HR_c$ , measured using the Instron press at 30N of the HP with SD10 at 0%, 1%, 40% and >40% surface coverage.

The shear test results are presented in figures 6.2 (*ff*) and 6.4 (*c*). Two pressure levels, 6 kPa and 66 kPa, were used to evaluate the flow behaviour at low and high consolidations. 6 kPa was used as a classical value issued in shear tests analysis [179]. Besides, 66 kPa consolidation was selected to compare the results to the  $HR_c$ , measured at the same normal stress,  $66 \text{ kPa} \approx 30 \text{ N}$ . In the shear test measurement, the powder sample must undergo a plastic failure during testing to estimate the *ff* and the *c* (section 6.2.2.2.). However, powders with excellent flowability may not experience this plastic fracture and, instead, exhibit a slipping phenomenon. This behaviour is identified in the shear test results by negative adhesive values or significant variation between repetitions. The formulations that lack markers are those that appear to have excellent flow based on naked-eye evaluation (Figs. 6.2 and 6.4).



**Figure 6.2.** Flow factor, *ff*, of HP and HP+SD10 measured at 6 kPa (◆) and 66 kPa (▲) of pre-consolidation.

The  $ff$  results at low consolidation (6 kPa) show that the AP had an excellent flow behaviour, with a  $ff$  above 10 for the pure AP and lack of markers when SD10 is added. The  $ff$  values for the WF increased significantly from an easy-flowing regime to free-flowing from 40% SC. For the JF, the  $ff$  was around 5, no matter the SC. This behaviour was not expected since the naked-eye evaluation of the JF improved its aspect significantly by adding SD10, suggesting a flowability improvement compared with the pure JF (Fig.6.3 and Fig.4.10 in Chapter 4). Similar to AP, the GB also displayed excellent flow behaviour associated with the lack of markers.

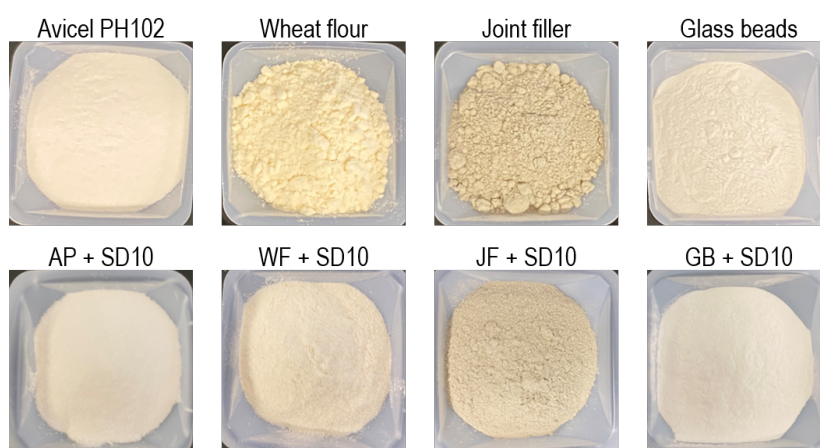


**Figure 6.3.** Qualitative flow behaviour visual assessment of HP (first row) and HP+SD10 at 40%SC (second row).

The results obtained at high consolidation (66 kPa) show that the  $ff$  increases with the SC for AP and WF. In contrast, JF showed little variation in the  $ff$  for all of the SC tested, which is consistent with the results obtained at 6 kPa. GB exhibited an increase in  $ff$  with SC, except for when the SC was >40%, which could be attributed to an excess of S-NP that increases adhesive forces and thus decreases  $ff$ . Nevertheless, the  $ff$  values indicated that GB displayed free-flowing behaviour in all cases. It is worth noting that free-flowing powders tend to slip rather than fracture. Then, the different  $ff$  above 10 do not classify powders' "free-flow" behaviour, which could be another reason why the  $ff$  of the GB formulation vary above 10.

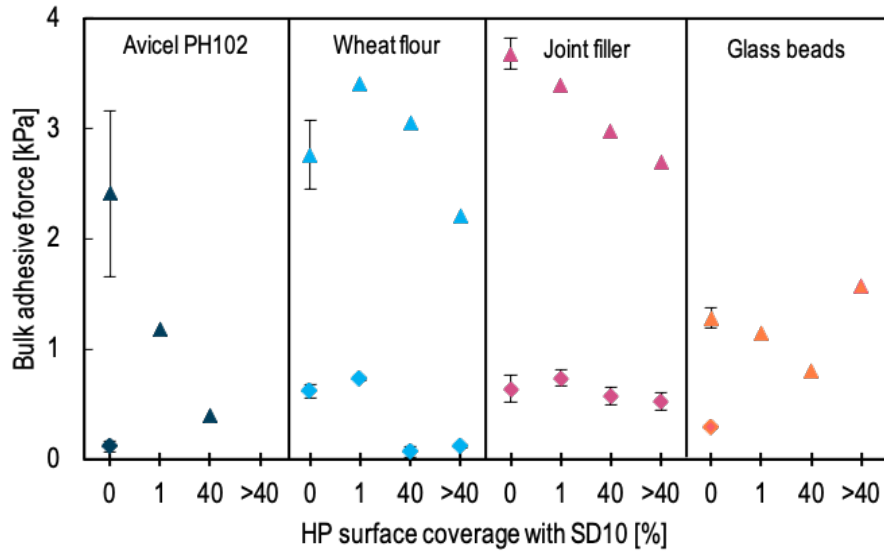


**Figure 6.4.** Bulk adhesive forces,  $c$ , of HP and HP+SD10 measured at 6 kPa (◆) and 66 kPa (▲) of pre-consolidation

The bulk adhesive interactions presented in figure 6.4 show the results of the shear test at low consolidation (6 kPa). AP was the powder with the least  $c$ . The WF decreased  $c$  with SC from 40% SC. For the JF, the addition of SD10 did not modify its  $c$ , as well as in the  $ff$ . GB showed similar behaviour to AP, with a very low  $c$  and a lack of marker of the HP+SD10 formulations. Compared to 6 kPa, at higher consolidation (66 kPa), the  $c$  values increase for all formulations. As the particles are closer to each other, the  $F_{vdW}$  might increase. The  $c$  of AP decrease with SC. For the WF, the  $c$  only decreases for the formulation with >40% SC. The  $c$  of the JF formulations decreases with SC. In the case of GB, the  $c$  decreased until 40% SC and then increased. When comparing  $ff$  to  $c$ , it is possible to observe that in most cases, when the  $ff$  increases,  $c$  decreases. Only for the JF, the  $ff$  did not change significantly when adding SD10 (6 and 66 kPa), but the  $c$  at 66 kPa decreased with the SC. Nevertheless, according to the qualitative visual assessment (Fig.6.3), the JF seems to improve its flowability by the addition of S-NP. These qualitative observations and the shear test results might indicate that very cohesive powders, like the JF, might not be well described on quasi-static regime techniques [111].

## 5. Dynamic regime

The powder flow rate is described by the Beverloo correlation (Eq.6.1) [112], explained in section 6.2.3.1..

$$W = C_{BV} \rho_b g^{1/2} D_o^{5/2} \quad (6.1)$$

where  $W$  is the flow rate [kg/s],  $g$  is the gravity acceleration [ $m/s^2$ ],  $D_o$  is the diameter of the orifice [m] and  $\rho_b$  is the bulk density [ $kg/m^3$ ].  $C_{BV}$  is a dimensionless function of friction, which is estimated by fitting the model to the experimental data.

This test is typically employed in the design of silos and funnels to ensure material flow, still there is no classification that relate the powder flow through an orifice to flowability. Figure 6.5 displays the results of the 16 formulation flow rates. Table 6.2 presents the value of the parameter  $C_{BV}$ , the  $R^2$  of the model, and the critical diameter, which is the diameter of the last orifice through which the powder flows.

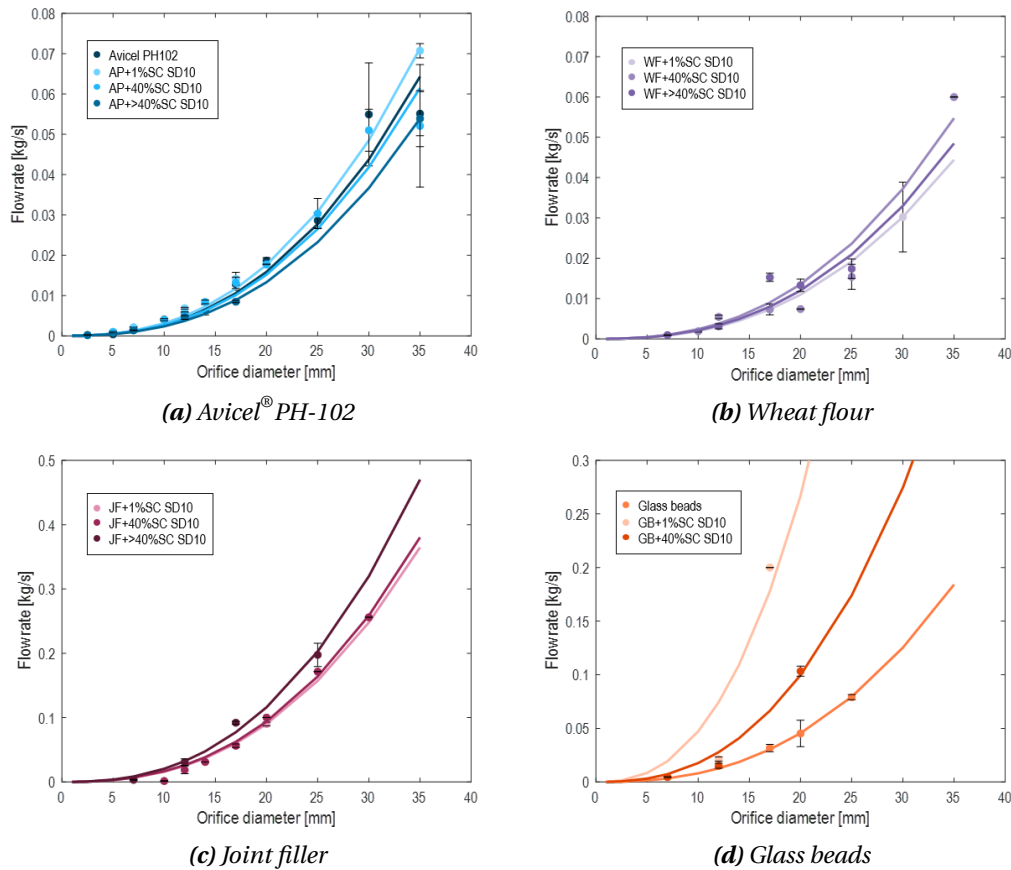


**Figure 6.5.** HP and HP+SD10 with 1%, 40% and >40% SC flow rates through different orifices (2.5 - 35 mm) fitted with the Beverloo model (Eq.6.1), represented by the solid line. a) Avicel PH102, b) wheat flour, c) joint filler and d) glass beads.

Figure 6.5 presents the flow rate of the HP and HP+S-NP. It is worth noting that the results are presented in separate graph per HP to avoid the direct comparison of the flow rates them. The flow rate value is dependant on the density of the powder, then it is expected that the more dense powders present a greater flow rate independent of their flow behaviour. For instance, JF and GB, presented the highest flow rate values, being the HP with the highest densities.

From the results on figure 6.5, the first evident result is that the pure JF and WF are not presented in figures 6.5b and c because they were not able to flow though any of the orifices. This result, exhibit the poor flow behaviour of the JF and WF in comparison to the AP and GB, that were able to flow through multiple orifices.

In figure 6.5a it is shown that the addition of SD10 did not improve the AP flow rate since there are not significant differences between formulations. For the case of WF and JF (Figs.6.5b and c) the addition of SD10 improved the flow behaviour compared to the pure HP, since the HP+SD10 achieve to flow through some of the orifices, no matter the SC. The GB formulations (Fig.6.5d) displayed the most significant changes, with the curves distinctly separated.

Beverloo [112] stated that  $C_{BV}$  varies according to the particle shape for divided solids with particle sizes between 0.045-0.17 cm. Some authors reported a value of 0.58 for  $C_{BV}$  [27, 36], but this value does not fit all powders experimental data, as Nedderman [4] suggested that  $C_{BV}$  is highly influenced by particle size. Baserinia and Sinka [52] suggested that  $C_{BV}$  was material-dependent, and their results showed that the parameter is effectively related to particle properties of pharmaceutical powders with particle size between 50 and 180  $\mu\text{m}$ .

The  $C_{BV}$  is estimated from the fit of the experimental data and the equation 6.1. The  $R^2$  on the 6.2 shows that most of the experimental data exhibited an excellent fit, allowing to estimate  $C_{BV}$ . Based on the  $C_{BV}$  results (Table 6.2), it is observed that the formulations with the best flow characteristics (AP) had a  $C_{BV}$  value of approximately 0.26. However, for AP+SD10 at >40% SC, the  $C_{BV}$  value decreased to 0.16. Therefore, no relation between flow behaviour and Beverloo model constant  $C_{BV}$  value was found. While it may be tempting to conclude that a lower  $C_{BV}$  value indicates a better flowability, it should be noted that when comparing  $C_{BV}$  values, we observed random variations that did not provide any meaningful information about the powder flowability.

From the results in table 6.2, the critical diameters show that the more flowing formulations are the AP ones, where the flow was enhanced from 40% SC, decreasing the critical diameter from 5 mm to 2.5 mm. For the WF, the JF and GB the critical diameter decreased when the SC was increased. This result exhibit that higher SC, 40% and >40%, improved the flowability on all of the HP since their critical diameter decrease in comparison to pure HP.

**Table 6.2.** Flow through an orifice results: critical diameter and model parameter  $C_{BV}$  and  $R^2$  of the Beverloo model fitting (Eq.6.1) of HP and HP+SD10 with 1%, 40% and >40% surface coverage.

Formulation	Critical diameter [mm]	$C_{BV}$ [-]	$R^2$
Avicel <sup>®</sup> PH-102	5	0.26	0.943
AP+1%SC D10	5	0.26	0.997
AP+40%SC D10	2.5	0.25	0.944
AP+>40%SC D10	2.5	0.16	1.000
Wheat flour	-	-	-
WF+1%SC D10	30	0.12	*
WF+40%SC D10	10	0.14	0.942
WF+>40%SC D10	7	0.10	0.699
Joint filler	-	-	-
JF+1%SC D10	20	0.52	*
JF+40%SC D10	10	0.66	0.991
JF+>40%SC D10	7	0.73	0.988
Glass beads	17	0.19	0.998
BV+1%SC D10	12	1.04	0.793
BV+40%SC D10	7	0.40	0.969

\*Just one point to trace the model then no  $R^2$

As a general conclusion, the three test methods used to assess the flowability of powders allow to show that the dynamic test is more sensitive to flowability enhancement for cohesive powders in comparison to tests on the quasi-static regime. In addition, the results of the flowability characterisation allowed to point out, that the addition of SD10 improved the flow behaviour of all the HP.

For Avicel<sup>®</sup> PH-102, which already exhibit good flowability based on  $HR_c$ ,  $ff$ ,  $c$  and critical diameter. Including S-NP further improves these flowability indicators starting from a 1% SC concentration. This indicates that, even with a small amount of flow additives, the flow behaviour of the powder can significantly improve.

The wheat flour flowability improvement was different in each characterisation device. Based on quasi-static regime tests, wheat flour flow is enhanced from 40% SC while in the dynamic tester, adding SD10 for 1% SC was enough to improve its flow by modifying the critical diameter and flow rate. According to this results, WF flowability is improved by adding 0.04-1.55% wt. of SD10.

The joint filler is a highly cohesive fine powder that dynamic tests may better describe compared to quasi-static regime testers (FT4, Densitap), which may not accurately represent flowability at elevated cohesion levels. This is supported by the results of  $HR_c$  and  $ff$ , where JF samples did not change their flowability or even worsen it. The flow behaviour through orifices of the JF improved from 1% SC, allowing the sample to flow

through smaller orifices. Besides, adding S-NP drastically changes the powder's physical bulk aspect (Fig.4.10), suggesting a flow behaviour modification. Consequently, the required amount of S-NP may vary depending on the handling operation. This powder may require assistance in some operations, while in others, it would have good flow with low quantities of flow additives (1% SC), such as transfer, transport, flow through a silo, etc.

The GB exhibit improved flow from 1% SC, based on the  $ff$  and critical diameter. However, according to  $HR_c$ , there is no improvement, and flow behaviour worsens at >40% SC. This sample does not require flow additives since its flowability is already excellent, similar to AP.

From a two-component (S-NP+HP) simplified formulation perspective, evaluating the required amount of flow additives considering each sample individually might reduce the unnecessary use of S-NP. For instance, our results showed that AP, WF and GB improved their flowability with 1%SC, corresponding to 0.02, 0.04 and 0.03%wt. of SD10, respectively. All of these mass fractions are below the industrial "standard" amount (0.5 - 2% wt.), which could suggest that some industrial powders might not require the amount of S-NP that are being added.

## 6. Dustiness

The dustiness results for HP, SD10 and HP+SD10 at different SC are presented in figure 6.6. The dust emission ( $w_I, w_T$  and  $w_R$ ) of pure AP doubled when SD10 was added, regardless of the SC. No differences were observed in dustiness indices values between surface coverages. Moreover, the dustiness indices of the AP+SD10 at all SC are similar to the SD10, which suggests a release of the S-NP during aerosolisation. For WF, the dustiness depends on the SC. Indeed, at 1% SC, the  $w_I$  doubled and the  $w_T$  tripled compared to pure WF, while the collected dust on the  $w_R$  was out of the measurement limit. WF+SD10 covered at 40% and over 40%, increased the  $w_I$  by 50 times and the  $w_T$  by 75 times compared to pure WF. At these SC (40% and >40%), a high level of respirable particles was also measured. Compared to AP and WF, JF and GB did not showed an increase in dust emission across all SC. The JF and GB dustiness remained the same at 1% SC. For JF at 40% SC,  $w_I$  increased by 7 times and the  $w_T$  by 4 times, while  $w_R$  slightly decreased. GB exhibited different behaviour, its dust emission doubled with GB+SD10 at 40% SC, but dustiness decreased over 40% SC. This latter result might be attributed to excess SD10 that aggregates itself.

The samples that increased the most their dust emission were AP and WF compared to JF and GB. As well as presented in Chapter 5, the HP which have a stronger interaction with the S-NP tends to emit less dust, which is the case of the JF and GB, according to the surface energy. Nevertheless, for the HP with weak interactions with the SD10, AP and WF,

the dustiness indices do not increase more when the amount of SD10 was increase, from 1%SC to >40%SC. The  $w_I$  and  $w_R$  of the AP+SD10 and WF+SD10 are similar to the emitted pure SD10.

In general, adding flow additives increased the dust emission for all HP, being greater for the S-NP/HP with weaker interactions compared to those with stronger interactions.

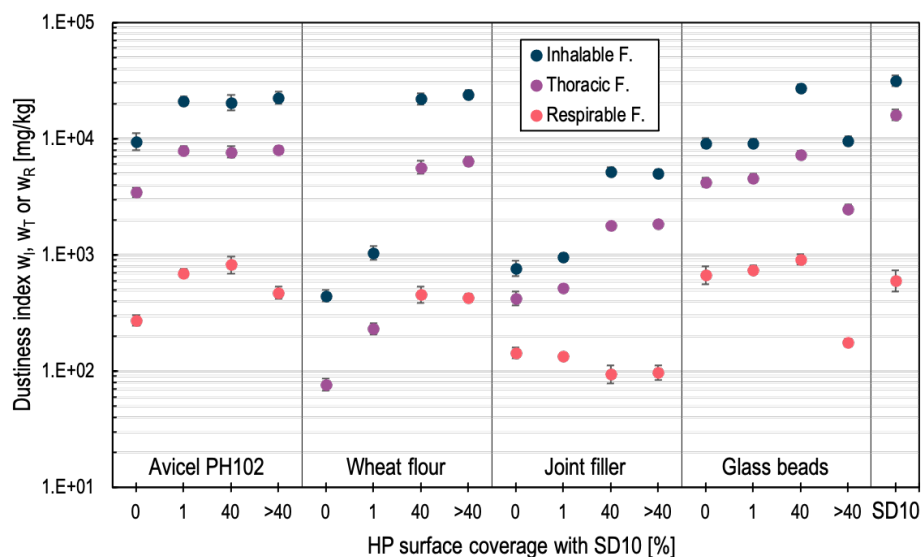


**Figure 6.6.** Inhalable ( $w_I$ ), thoracic ( $w_T$ ) and respirable ( $w_R$ ) indices of HP and 1%, 40% and >40% surface coverage, and SIPERNAT<sup>®</sup> D10 measured in the rotating drum.

## 7. Are flowability and dustiness related?

In this section, the relationship between flowability and dustiness is discussed. First, the relationship between these properties is evidenced by the behaviour of the pure HP. Powders that generate more dust tend to flow better, as observed in AP and GB, which have good flowability and high dustiness indices. Some authors relate dustiness to particle size since smaller particles are easier to suspend in the air [134, 135, 139]. However, the capacity of a particle to be suspended in the air is also influenced by its density. For instance, our results showed that the dustier HP, AP, presents the larger particle size ( $d_{50} = 69\mu\text{m}$ ) and a low density ( $\rho = 1.5\text{g}/\text{cm}^3$ ) in comparison to the JF, which presents a moderate dustiness level, a much more smaller size ( $d_{50} = 6\mu\text{m}$ ) and greater density ( $\rho = 2.8\text{g}/\text{cm}^3$ ).

When flow additives are added to HP, both flowability and dustiness are modified. In cases where flow behaviour is improved, dust generation also tend to increase. In addition, in some cases, dustiness did not change or change slightly, as observed in JF and GB + 1% SC SD10. This behaviour is explained by the S-NP/HP strong adhesion interactions, as described in the previous section and in Chapter 5. In contrast, for weak

interactions, an increase in flowability systematically increase dust emission, even at low S-NP concentrations. This suggests that the relationship between flow and dust in HP+S-NP mixtures depends on interparticle interaction.

To look for potential correlations between powder flow behaviour and dust generation, the flow and dust indicators were plotted as shown in Figure 6.7. The pink markers on the graph represent instances where the correlation had an  $R^2$  value of 0.8 or higher. Even if an  $R^2$  of 0.8 do not represent a good fit, this analysis seeks to identify the best possible tendencies that relate dustiness and flowability. Out of the correlations identified, five were solely linked to flowability indicators, and six indicated a relationship between flowability and dustiness.

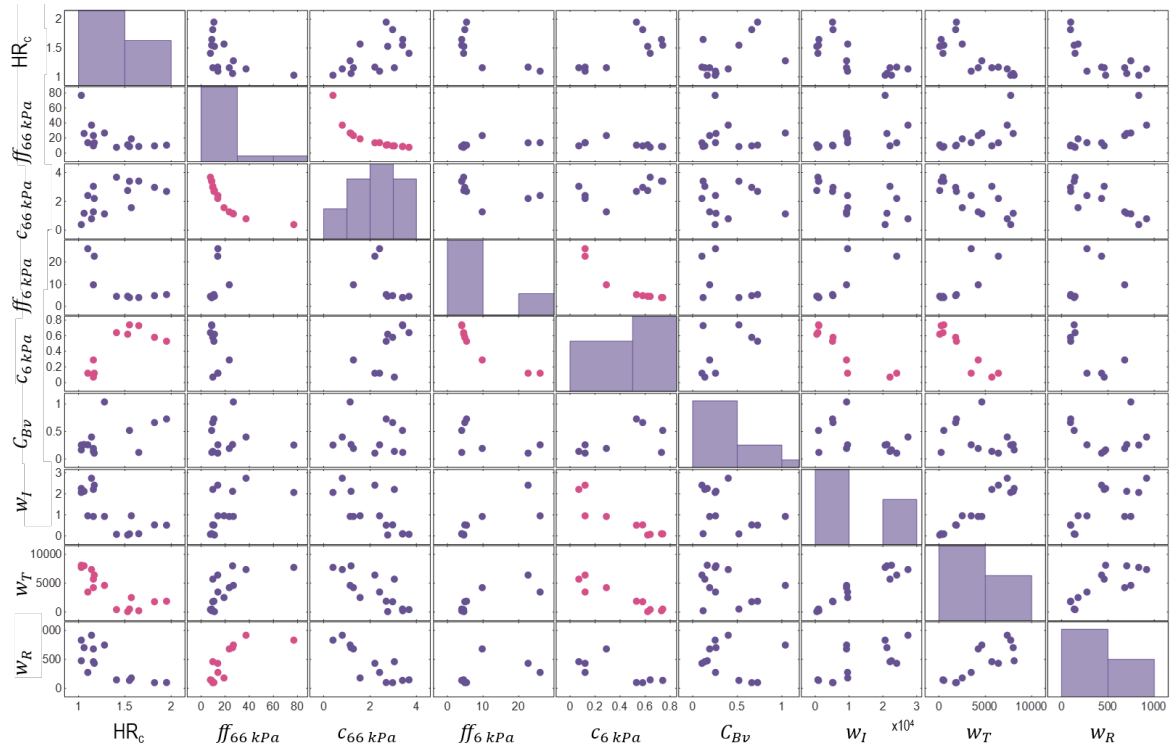


**Figure 6.7.** Flowability indicators plotted against dustiness indicators of HP and HP+SD10 with 1%, 40% and >40% surface coverage. The pink markers indicate a correlation with a  $R^2$  of at least 0.8.

The relationship between flowability characterisation has been narrowed down to only two factors, as four of them are the  $ff$ - $c$  relation (Fig.6.8). This correlation was first proposed by Cares-Pacheco and Falk [111] as discussed in chapter 4. Figure 6.8a illustrates the excellent fit of our experimental data to their findings. Additionally, figure 6.8b depicts the relationship between  $HR_c$  and  $c$ . This relation shows that a powder with high  $HR_c$  presents strong adhesive interactions until a  $HR_c = 1.7$ . The flowability section of this chapter concluded that highly cohesive powders, like JF, might not be well described by the quasi-static regime test. Therefore, the  $HR_c$ - $c$  relation is limited for powders with a maximal  $HR_c$  of 1.7.

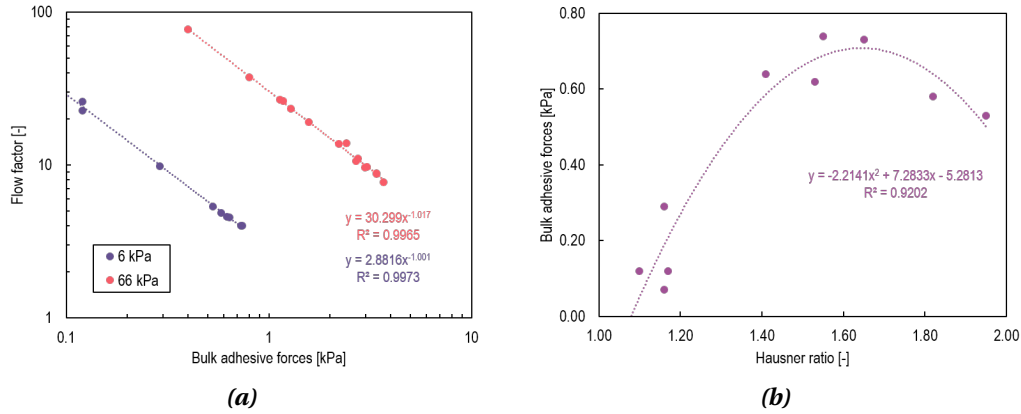


**Figure 6.8.** Flowability relations between a) the flow factor,  $ff$  (6 and 66 kPa) and the bulk adhesive forces,  $c$  measured in the FT4 and b) Compressive Hausner ratio,  $HR_c$  and the bulk adhesive forces,  $c$ .

The six flowability-dustiness relations identified in figure 6.7, are narrowed to four. The first two relate  $w_T$  and  $w_R$  to  $HR_c$  and  $ff$ , respectively. The other two, relate  $w_T$  and  $w_I$  to  $c$ .

Based on the relationships depicted in figure 6.7,  $w_T$  and  $w_R$  seems linked to  $HR_c$  and  $ff$ , respectively (Fig.6.9). Both relations follow a second-degree polynomial model (Eqs. 6.2 and 6.3) with an  $R^2$  value of around 0.8, which suggests a moderate fit.

$$w_T = 17878HR_c^2 - 59570HR_c + 50335 \quad 1.03 < HR_c < 1.95 \quad (6.2)$$

$$w_R = -0.3924ff^2 + 43.675ff - 199.02 \quad 8 < ff < 77 \quad (6.3)$$

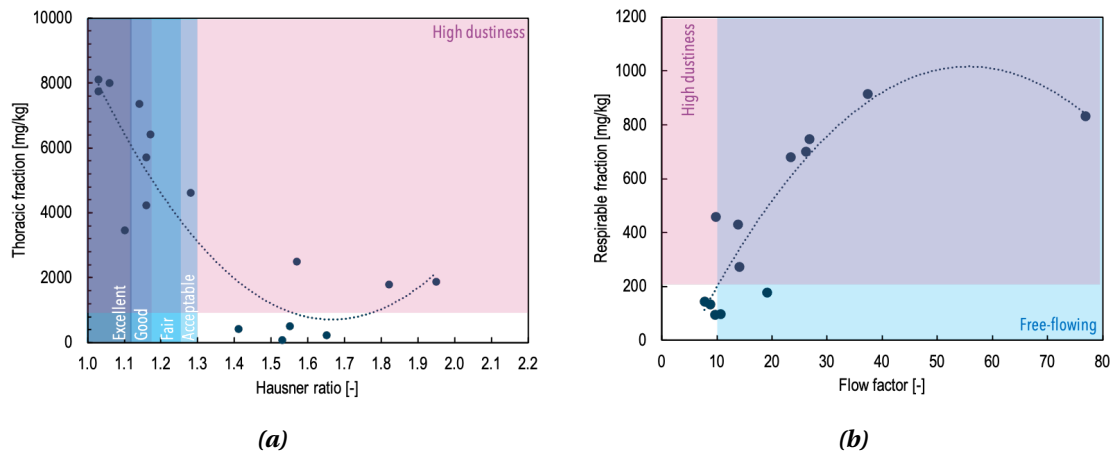


**Figure 6.9.** Correlations of a) the thoracic fraction,  $w_T$ , and the compressive Hausner ratio,  $HR_c$ , at 30N, and b) the respirable fraction,  $w_R$ , and the flow factor,  $ff$ , measured at a pre-consolidation of 66 kPa. The pink region indicates where the dust emission level is classified as high. The blue regions precise the flowability according to Hausner ratio and flow factor.

The tendencies (Fig.6.9) showed that better flowability results in higher dustiness levels in the  $w_T$  and  $w_R$  fractions. For instance, good flow behaviour (low  $HR_c$  and high  $ff$ ) correspond to higher  $w_T$  and  $w_R$  values. Given that flowability characterisation is more

common in industry than dustiness characterisation, the equations extracted from the tendency were employed to predict the dustiness indices using  $HR_c$  and  $ff$ . The results of this analysis are presented in table 6.3. The predicted dustiness values are not entirely accurate. However, the model predicted the dust classification (high, moderate, low, very low) in most cases. The predictions estimate a higher dustiness classification than the actual measured classification, except for the GB+>40%SC and the WF+40%SC.

**Table 6.3.** Comparison of the experimental ( $w_{T,E}$  and  $w_{R,E}$ ) and predicted ( $w_{T,P}$  and  $w_{R,P}$ ) thoracic and respirable values [mg/kg] and dustiness classification level of HP and HP+SD10, using Eqs.6.2 and 6.3. The values in pink highlights the cases in which the dustiness classification is not well predicted.

Formulation	$w_{T,E}$	$w_{T,E}$ level	$w_{T,P}$	$w_{T,P}$ level	$w_{R,E}$	$w_{R,E}$ level	$w_{R,P}$	$w_{R,P}$ level
AP	3473	High	6440	High	273	High	332	High
AP+1%SC	8007	High	7279	High	703	High	673	High
AP+40%SC	7736	High	7945	High	832	High	840	High
AP+ <40%SC	8110	High	7945	High	475	High	-	-
WF	77	Very low	1044	High	-	-	-	-
WF+1%SC	233	Low	717	Moderate	-	-	-	-
WF+40%SC	5704	High	5290	High	459	High	187	Moderate
WF+<40%SC	6409	High	5111	High	431	High	327	High
JF	428	Moderate	1885	High	145	Moderate	114	Moderate
JF+1%SC	520	Moderate	953	Moderate	135	Moderate	152	Moderate
JF+40%SC	1795	High	1137	High	96	Moderate	184	Moderate
JF+<40%SC	1880	High	2155	High	98	Moderate	220	High
GB	4233	High	5290	High	680	High	606	High
GB+1%SC	4621	High	3377	High	747	High	688	High
GB+40%SC	7364	High	5659	High	917	High	883	High
GB+<40%SC	2512	High	878	Moderate	177	High	488	High

Figure 6.10 shows the relationships between bulk adhesive forces at low consolidation (6 kPa) and the  $w_T$  and  $w_I$  fractions. The  $w_T$ - $c$  relation is described by the linear equation 6.4 with an  $R^2$  value of 0.88. The  $w_I$ - $c$  experimental data is represented by a second-degree polynomial equation (Eq.6.5) with an  $R^2$  value of 0.81. As with the previous models, the  $R^2$  indicates a moderate fit, which can be described more as a tendency than a model. While these models do not provide accurate predictions of dustiness indices value, they could be useful for predicting dustiness classification in most cases (Table 6.4).

$$w_T = -8246c + 6136.4 \quad 0.07 < c < 0.74 \quad (6.4)$$

$$w_I = 35291c^2 - 57253c + 24058 \quad 0.07 < c < 0.74 \quad (6.5)$$

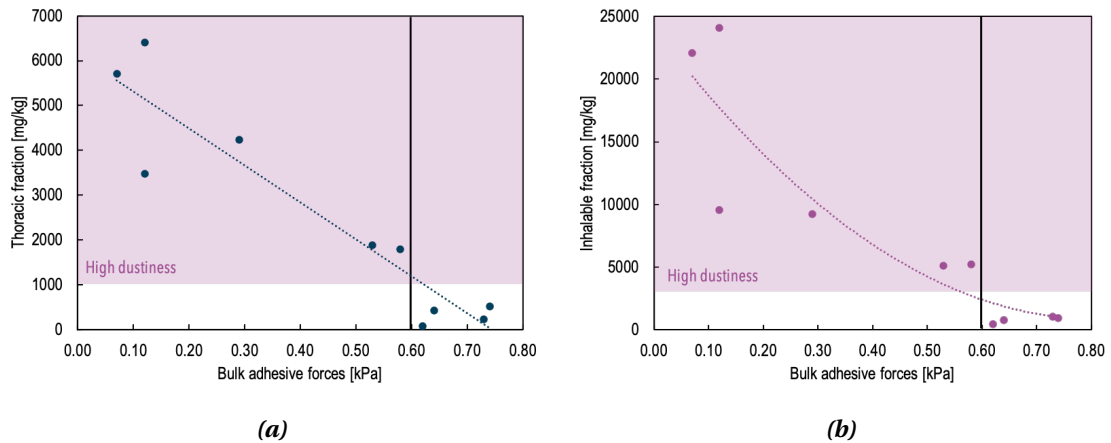


**Figure 6.10.** Correlations of a) the thoracic fraction,  $w_T$ , and b) the inhalable,  $w_I$ , fraction with the bulk adhesive forces,  $c$ , measured at 6kPa of pre-consolidation in the FT4. The pink region indicates where the dust emission level is classified as high.

The relations between the bulk adhesive forces and the dustiness indices show that both the  $w_T$  and the  $w_I$  fractions increase when the bulk adhesive forces are low. This behaviour agrees with the dispersive surface energy characterisations that indicate that the interparticle interactions influence the dust release. For instance, at higher interparticle interaction, less dust is emitted (Fig.6.10).

**Table 6.4.** Comparison of the experimental ( $w_{T,E}$  and  $w_{I,E}$ ) and the predicted ( $w_{T,P}$  and  $w_{I,P}$ ) thoracic and inhalable values [mg/kg] and dustiness classification level of HP and HP+SD10, using Eqs. 6.4 and 6.5. The values in pink highlights the cases in which the dustiness classification is not well predicted.

Formulation	$w_{T,E}$	$w_{T,E}$ level	$w_{T,P}$	$w_{T,P}$ level	$w_{I,E}$	$w_{I,E}$ level	$w_{I,P}$	$w_{I,P}$ level
AP	3473	High	5147	High	9539	High	17696	High
WF	77	Very low	1024	High	447	Low	2127	Moderate
WF+1%SC	233	Low	117	Low	1046	Moderate	1070	Moderate
WF+40%SC	5704	High	5559	High	22074	High	20223	High
WF+>40%SC	6409	High	5147	High	24075	High	17696	High
JF	428	Moderate	859	Moderate	771	Moderate	1871	Moderate
JF+1%SC	520	Moderate	34	Very low	960	Moderate	1016	Moderate
JF+40%SC	1795	High	1354	High	5232	High	2723	Moderate
JF+>40%SC	1880	High	1766	High	5100	High	3627	High
GB	4233	High	3745	High	9231	High	10423	High

Some authors [135, 144] have studied the relationship between flowability and dustiness. Most of them just focused on the fact that better flowability results in higher dustiness. Our results agree with this statement since the results presented in this section show that better-flowing powders/formulations tend to emit more dust than those with poor flow. All of the quasi-static regime flowability indicators ( $HR_c$ ,  $ff$  and  $c$ ) show that the dustiness fractions increase when they indicate good flow.

In contrast, Dazon [249] conducted tests to investigate the relationship between the  $HR$ , using a tapping device (4500 taps) and the  $w_R$  emitted in a Vortex Shaker (VS) of

nanometric powders. However, the results of this study were inconclusive as  $HR$  was not a reliable indicator for dustiness. In contrast, our study finds a correlation between  $HR_c$  and the  $w_T$  measured using the rotating drum. The differences between our findings and Dazon's study arise from several factors. First, the dustiness characterisation device used in our study, the RD, differs from the VS. The VS applies more energy to a smaller sample size than the RD, resulting in higher  $w_R$  emissions measured in the VS. In Chapter 5, we have discussed the energy difference between these two devices showing that the VS always emit more  $w_R$  than the RD. Secondly, the  $HR$  measurement protocols are different, between Dazon, using a tapping device ( $HR$ ), and us, using an uniaxial compression tester ( $HR_c$ ). In Chapter 3, we have compared the energy levels between a tapping device and an uniaxial compression tester, showing that the tapping device is more energetic and that  $HR$  depends on the protocol. All of the Dazon samples, were characterized with the same tapping protocol, consisting of 4500 taps, which do not guarantee that the samples achieve their maximal compaction.

Further research is needed to evaluate the correlation between  $HR$  and dustiness in other dustiness devices, such as the VS, to determine whether the tendencies observed in our study can be extrapolated to other devices.

## 8. Conclusion

This chapter presents new findings that suggest a relationship between these two end-use properties. Specifically, it is observed that powders with better flowability tend to have higher dust emissions. Four predictive models are developed to assess this relationship, which show that free-flowing powders have higher dust emissions than poor-flowing powders. Although these models cannot accurately predict dustiness indices, they provide a good classification (high, moderate, low and very low) of dustiness in most cases.

We study a set of powders and formulations consisting of four host powders (HP) and HP mixed with flow additives to achieve different surface coverages. The addition of flow additives enhance flowability, with the extent of improvement depending on the surface area covered by the additives. Optimal flow behaviour may require more than the common industry amount of 0.5% wt. of flow additives when the product is highly cohesive. However, the amount of flow additives needed is not standardised, and proper characterisation of the required amount for each material can reduce or even eliminate the need for flow additives.

The results show that dust emission depend on the surface coverage and the interaction between S-NP/HP. Weak interparticle interactions (AP+SD10 and WF+SD10) result in greater dust emission than strong interactions (JF+SD10 and GB+SD10).

In conclusion, this chapter presents new insights into the relationship between flowability and dustiness, providing useful tendencies that might help predict dustiness fractions from flowability characterisation techniques. These findings can be valuable in industries where dustiness characterisation is not usually performed. However, further research is needed to validate the accuracy and the possible generalisation of these findings to other types of powder.

# Conclusions and perspectives

---

The present study aimed to deepen the understanding of two key end-use properties of powders flowability and dustiness. The complexity of the study lies in the absence of well-established laws that describe the flow behaviour and dust emission of powders. Although powders are ubiquitous in many products as an ingredient or final product, their handling present several complications. Most of this issues are attributed to poor flowability, which results in product blockages, ratholing or bridging. In addition, operations that requires transfer of powders tend to generate dust, which leads to occupational exposure to various hazards (inhalation, fire and explosion). Therefore, a better comprehension of these two end-use properties and its relationship could facilitate the conception of safer and performing powder products.

The main objective of this research was to understand the underlying phenomena that contribute to improve flowability, when nano-additives are use, and how it affects dust emission. Additionally, the study also aimed to develop methodologies that may help reach the target of good powder handling with minimal dust emission.

## Main findings and contributions

This thesis focuses on two primary topics: flowability and dustiness relationship. The following discussion present the main findings and contributions.

### Flowability

Characterising powder flowability is a complex task because it is not an intrinsic property of the powder itself an thus it is influenced by the device used methodology. Chapter 3 addressed this challenge by considering the impact of the supplied energy on flowability measurements using two densification devices methodologies - the Densitap and the uniaxial compression test (FT4 and Instron press). The comparison of results from these two devices highlights the need to ensure that the same amount of energy -under the same conditions- is supplied to the powder to compare flowability data accurately from densification methodologies. Nevertheless, quantifying the amount of energy supplied to a powder is challenging due to the powder's highly dissipative nature. Then, if a comparison of powders is performed on the same equipment, it is essential that the samples are in a steady state at the supplied energy, which may differ from one sample to another. For example, in the Densitap, comparing the volume variation at the

same number of taps (e.g., 500) may not accurately characterise the samples. Instead, it is recommended to perform the measurement with a number of taps that ensures that the sample volume no longer changes and achieve a steady state. In confined systems, such as compression cells, it is also recommended to add a relaxation time to each force applied to the powder before proceeding to the next force step to reach a steady state. By following these recommendations, we can obtain more reliable and comparable results for the flowability of different powders in uniaxial compression testers.

The effect of adding S-NP to powder flowability was evaluated using the FT4. The first results show that hydrophilic and hydrophobic S-NP improved the flow behaviour of pharmaceutical powders. Besides, S-NP modified the flow behaviour of powders towards water since at high RH, the HP worsened its flowability, but with the addition of S-NP, the flow behaviour was always improved regardless of the RH condition. Typically, S-NP are added to pharmaceutical formulations at amounts ranging from 0.5-2% wt. However, our results showed no significant differences in flow behaviour between the pharmaceutical powders when the S-NP amount is increased from 0.5 to 2% wt.

From these preliminary results, the study was oriented towards understanding of mechanisms of action of S-NP on powder flow behaviour, assessed through an experimental design. The results show that the powder itself is the main factor that dictates powder flow behaviour, as powder flowability is extremely sensitive to grain interaction. In addition, the bulk friction modification by the S-NP does not seem to affect flow behaviour. In contrast, our results suggest that powders surface modification is an important mechanism by which S-NP act on powder flowability. The more cohesive powders tend to require more S-NP surface coverage to improve their flow. The surface modification of HP was quantified by surface energy ( $\gamma_s^d$ ) measurements. All of this results, questioned the amount S-NP used in formulations (0.5-2%wt.). The methodology presented in frame 1 proposes a protocol to determine an optimal amount of S-NP, intending to reduce their use while maintaining flow behaviour.

### Frame 1

Determination of the optimal amount of S-NP to improve powder flowability.

1. Prepare a mixture with a known amount of S-NP (e.g. 0.5% wt.).
2. characterise the surface coverage percentage of S-NP on the sample using SEM imaging (refer to section 4. for the image treatment protocol).
3. Estimate the required amount of S-NP for achieving surface coverage of 1%, 20% and 40%.
4. Evaluate the flowability of the sample using a device that best describes the industrial operation (e.g. shear test for silos).
5. Choose the optimal surface coverage that yields the best flow performance.

## Dustiness

To the best of my knowledge, no studies evaluate the effect of adding flow additives to dust generation. All of my results, showed that adding S-NP increases dustiness and the particles' emitted concentration. We initially expected the S-NP remained attached to the surface of the HP due to their strong adhesive interactions. However, dustiness methods results indicated that S-NP detached from HP in both measuring devices. In the rotating drum, HP+S-NP emitted dustiness similar to S-NP alone, while in the VS, the detachment of S-NP is mainly evidenced in TEM micrographs and dust size distribution measured by an (ELPI+).

The strength of the interactions between HP and S-NP play a role in dust emission, with stronger interactions resulting in fewer dust particles and a maintained respirable fraction regardless of SC. The dispersive surface energy,  $\gamma_s^d$ , was with dustiness results allowing to distinguishing between weak and strong interactions. Powders/S-NP stronger interactions emit fewer particles than those with weaker interactions.

Additionally, surface coverage affects dust emissions. Lower SC give rise to lower dust emissions even when interactions HP/S-NP were weak suggesting that dust emission can be controlled by formulating products according to the particles SC.

## Flowability and Dustiness, what have we learned

Our results have shown that powders with excellent flow behaviour tend to emit more dust. Our findings suggest that the thoracic and respirable fraction levels could be predicted by relating them to the compressive  $HR_c$  at 30N and the flow factor (66 kPa), respectively. In addition, the bulk adhesive forces at low consolidation (6 kPa) are related to thoracic and respirable fractions. The three established equations seem to predict dust levels with a quite good accuracy, except when the experimental fraction is very low. In that specific case, the predicted value overestimates the experimental value. It is worth noting that the limited number of data points used to develop the models do not allow them to have the best fit. Nevertheless, our study marks a starting point for relating flowability and dustiness, an avenue that, to our knowledge, has not been explored before.

The relevance of this finding lies in the fact that flowability and dustiness are two properties needed to be known to conduct industrial operations handling powders. From an industrial perspective, the flowability-dustiness tendencies may provide a starting point for safer processes and performing powder formulations. First, this work shows that the required amount of flow additives must be optimised to reduce dust emissions. Then, dust emission levels could be estimated using the proposed equations based on the flowability parameters,  $HR_c$  and/or  $ff$ .

From an economic point of view, this "formulation starting point" is more expensive than adding a standard amount of flow additives to improve powder flowability. However and more important, it also aims to reduce the use of flow additives to reduce occupational exposure to powders and flow additives, which are often nanomaterials.

From a scientific perspective, this work contributes to understanding the relation of two essential end-use properties of powder -flowability and dustiness- that are not generally related. It highlights the importance and utility of continuing to study them together to better understand granular materials' behaviour and industrialisation.

## Perspectives

One important consideration that should be included in almost any experimental study on the granular matter is the need to validate all findings with a larger sample size with the aim to state broad conclusions, for the use in multiple industries. As demonstrated in our present work, we studied four main powders, each exhibiting unique flowability and dustiness behaviour.

Regarding dustiness, the rotating drum measurements could be completed using a sampling line similar to the VS to provide real-time measurements in less energetic devices. Additionally, it would be interesting to incorporate a dustiness sampling line into flowability measurements where dust is emitted, such as tapping devices, rotating drums, and flow-through orifices, among others. Such measurements may provide insight into the dustiness generation during the industrial operations these devices aim to simulate. Besides it would be interesting to develop a dustiness measuring device that allow to modify the energy supplied to the sample, with the objective to study the adhesion interactions between the powder and the flow additives.

The understanding of adhesive interactions between flow additives and powders requires further research, which could be evaluated through atomic force microscopy characterisations. Indeed, we have shown that weak and strong interactions influence the dust emission levels. Therefore, by comprehending these interactions, the industry could benefit from a more accurate, effective, and safe use of flow additives. Moreover, in order to facilitate the selection of flow additives, it would be beneficial to deepen our analysis of S-NP/HP adhesive interactions by evaluating multiple combinations which may ease the choice of S-NP/HP combination.

From a broader perspective, evaluating the relationship between flowability and dustiness in complex formulations containing multiple ingredients would be valuable. This could enable finding tendencies/models that can guide the conception of high-performance and safe products across various industries.

# Nomenclature

---

## Acronyms

---

NM	Nanomaterial
NP	Nanoparticles
HP	Host powders
S-NP	Silica nanoparticles
FDA	United States Food and Drug Administration
EFSA	European Food Safety Authority
PSD	Particle size distribution
RD	Rotating drum
SRD	Small rotating drum
VS	Vortex shaker
CD	Continous drop
CPC	Condensation particle counter
ELPI	Electrical low-pressure impactor
MPS	Mini particle sampler
TEM	Transmission electron microscopy
SEM	Scanning electron microscopy
MCC	Microcrystalline cellulose
AP	Avicel <sup>®</sup> PH-102
WF	Wheat flour
JF	Joint filler
GB	Glass beads
R	Retalac
IGC	Inverse gas chromatography
UCT	Uniaxial compression testers

---

## Symbols

VSSA	Specific surface area by volume	$\text{m}^2/\text{cm}^3$
$F_{vdW}$	Forces de van der Waals	N
$F_{cap}$	Capillary forces	N
$F_{elec}$	Electrostatic forces	N
A	Hamaker constant	J
RH	Relative humidity	%
AoR	Angle of repose	°
CI	Carr index	-
HR	Hausner ratio	-
$HR_c$	Compressive Hausner ratio	-
$ff$	Flow factor	-
$c$	Bulk adhesive interactions	kPa
$w_I$	Inhalable fraction	mg/kg
$w_T$	Thoracic fraction	mg/kg
$w_R$	Respirable fraction	mg/kg
$I_{VS}$	Number-based dustiness index	#/mg
$PSD_{ELPI}$	Number-based particle size distribution	$\mu\text{m}$
SC	Surface coverage	%
$a_w$	Water activity	-
$a_{BET}$	Specific surface	$\text{m}^2/\text{g}$
$N_a$	Avogadro number	-

## Greek symbols

$\rho$	Pycnometric density	$\text{g}/\text{cm}^3$
$\rho_b$	Bulk density	$\text{g}/\text{cm}^3$
$\rho_t$	Tapped density	$\text{g}/\text{cm}^3$
$\sigma_1$	Major principal stress	kPa
$\sigma_c$	Unconfined yield strength	kPa
$\gamma_s^d$	Dispersive surface energy	$\text{mJ}/\text{m}^2$

# List of Figures

1	Granular materials production in France (40 million tons/year)[5–13]. . . . .	7
2	Powder handling clumsy and dangerous operations due to poor flowability and dustiness. . . . .	8
1.1	Richards and Brown bulk solids definition [27]. . . . .	12
1.2	Powders behaviour regimes solid, liquid and gas. . . . .	13
1.3	Solid, liquid and gas powder regimes co-existing in an industrial process. . . . .	14
1.4	Liquid bridge between two spherical particles [41]. . . . .	16
1.5	Synthesis of several flowability characterisation techniques. . . . .	20
1.6	Angle of repose variation. a) $\theta$ refers to the maximum angle of the pile before avalanche and b) $\alpha$ , the angle produced after avalanche. h represents the height and r the radii of the pile. . . . .	21
1.7	Forces acting on a particle on a pile of powder. $F_N$ is the normal force, $m$ is the mass of the particle, $\mu$ is the friction coefficient, $g$ is the gravitational acceleration and $\theta$ is the angle of repose. . . . .	21
1.8	Angle of repose measuring techniques. $\theta$ refers to the angle of repose . . . . .	23
1.9	Densification of granular materials. . . . .	23
1.10	Densification devices. . . . .	25
1.11	Powder rigid plastic failure: pre-shear normal stress, $\sigma_{ps}$ , and shear normal to failure stress, $\sigma_c$ . . . . .	26
1.12	Shear test graphical representations. The left plot illustrates the shear stress ( $\tau$ ) applied overtime during the shear test. The $\tau$ values are associated with the right graph to construct the Mohr circles, with the normal stress ( $\sigma$ ), through the failure points. The intersection of the yield locus with the y-axis represents the adhesive interactions ( $c$ ). The minor and major Mohr circle intersections with the x-axis represent the maximum compressive stress ( $\sigma_c$ ) and major principal stress ( $\sigma_1$ ). . . . .	26
1.13	Flowability classification according to the flow function. . . . .	27
1.14	Shear test cells. . . . .	27
1.15	Flow behaviour through different orifices diameters. . . . .	28
1.16	Dynamic angle measurement. . . . .	29
1.17	Geldart powder classification according to their fluidisation [118]. $\rho_s$ is the particle density, $\rho_f$ is the fluidisation fluid density. . . . .	30
1.18	Dustiness fractions. . . . .	32
1.19	Forces acting on the sedimentation of an airborne particle [141]. . . . .	33
1.20	Synthesis of the standard dustiness characterisation methods. . . . .	36
1.21	Rotating drum device (EN 15051-2 [154]). . . . .	37
1.22	Continuous drop device (EN 15051-2 [155]). . . . .	38
1.23	Real-time measuring devices. . . . .	40
1.24	Mini particle sampler. . . . .	40
1.25	Vortex shaker method sampling configurations. . . . .	41

2.1	Surface coverage evaluation treatment. . . . .	48
2.2	SEM micrographs of powders mixed with 0.5% wt of AEROSIL R972 (first row), AEROSIL 300 (second row), SIPERNAT <sup>®</sup> D10 (third row) and SIPERNAT <sup>®</sup> 500LS (fourth row) . . . . .	49
2.3	SEM micrographs of Avicel <sup>®</sup> PH-102 + S-NP mixtures for an estimated surface coverage of 40%. . . . .	50
2.4	SEM micrographs of powder mixtures with different S-NP surface coverages	50
2.5	SEM micrographs of powders . . . . .	51
2.6	TEM micrographs of silica nanoparticles . . . . .	52
2.7	Powders particle size distribution. . . . .	52
2.8	Specific surface BET calculation method, values obtained from Avicel <sup>®</sup> PH-102.	53
2.9	Water sorption isotherms of host powders at 25°C. The sorption curves are represented with a solid line, and desorption curves with a dashed line. . . .	56
2.10	Inverse gas chromatography principle (adapted from [176]). The net retention time is given by $t_N = t_R - t_0$ where $t_R$ is the time spent for a probe molecule to pass through the powder column, and $t_0$ corresponds to the time for a non-adsorbed molecule—methane—to do it. . . . .	57
2.11	Uniaxial compression densification testers. . . . .	59
2.12	FT4 shear test steps described in the standard ASTM D7891-15 [179]. . . . .	60
2.13	Home-made flow tester. . . . .	61
3.1	Force sensor signal measurement of the tapping vibrations of a Densitap. . .	65
3.2	Apparatus description from [107]. . . . .	72
3.3	FT4 rheometer compressibility test, from conditioning to compaction. . .	73
3.4	Example of FT4 compaction test data treatment. Applied normal stress increments of 10 N until 40 N. . . . .	74
3.5	SEM micrographs of Avicel <sup>®</sup> PH-102, at different magnifications. . . . .	75
3.6	SEM micrographs of Retalac <sup>®</sup> , at different magnifications. . . . .	75
3.7	Water sorption isotherms of Avicel <sup>®</sup> PH-102 (cyan) and Retalac <sup>®</sup> (blue), at 20°C. Sorption curves are represented with a solid line, and desorption curves with a dashed line. . . . .	75
3.8	Study of the dynamic of compaction in Densitap <sup>®</sup> samples conditioned at 30% RH. . . . .	77
3.9	Dynamic of compaction as function of the powder moisture content using Densitap <sup>®</sup> . . . . .	77
3.10	Chicago Model obtained from iterative minimization using Densitap data (500 taps). Samples conditioned at 30% RH. . . . .	78
3.11	KWW model obtained from iterative minimization using DensiTap data (500 taps). Samples conditioned at 30% RH. . . . .	78
3.12	FT4 compaction test at different force ramps with Avicel <sup>®</sup> PH-102 at 60% RH.	79
3.13	Compactness and flowability assessment as a function of the specific energy supplied to the system. Samples conditioned at 30% and 60% RH. . . . .	80
3.14	Flowability assessment as function of the specific energy supplied to the granular media using FT4 (circles) and Densitap (triangles) devices. . . . .	81
3.15	Flow influence of NPs for RetaLac using FT4. Force ramp from 0 to 40 N using a 2 N step. . . . .	82
3.16	Flowability influence of NPs for Avicel <sup>®</sup> PH-102 using FT4. Force ramp from 0 to 40N using a 2N step. . . . .	82

3.17 Influence of Sipernats D10 and 500LS in the flowability of Avicel® PH-102. Mixtures prepared with 0.5% w/w of S-NPs and conditioned in different moisture environments. . . . .	83
3.18 SEM micrographs of Avicel® PH-102 with 0.5% w/w of 50S, conditioned at 30% RH. . . . .	84
3.19 SEM micrographs of Avicel® PH-102 with 0.5% w/w of 500LS, conditioned at 30% RH. . . . .	84
3.20 SEM micrographs of Avicel® PH-102 with 0.5% w/w of D10, conditioned at 30% RH. . . . .	84
3.21 SEM micrographs of Avicel® PH-102 with 0.5% w/w of D17, conditioned at 30% RH. . . . .	85
3.22 Granular densification expressed by HR of Avicel® PH-102, wheat flour, joint filler, glass beads and Retalac® assessed with a Densitap. . . . .	88
3.23 Powders flowability behaviour at 30% and 60% RH measured by FT4 compression test, $HR_c$ . . . . .	89
4.1 Mechanisms of action of flow agents. . . . .	96
4.2 Design of experiments: responses, factors and levels. . . . .	97
4.3 SEM micrographs of powders mixed with 0.5% wt of ®R972 (first row), ®300 (second row), SIPERNAT® D10 (third row) and SIPERNAT® 500LS (fourth row)	99
4.4 SEM micrographs of Avicel® PH-102 (first row) and Wheat flour (second row) at various magnifications (x100, x200 and x1000). . . . .	102
4.5 SEM micrographs of Joint filler (first row) and glass beads (second row) at various magnifications (x500, x1000 and x2000) . . . . .	103
4.6 TEM micrographs of silica nanoparticles . . . . .	103
4.7 SEM micrographs of Avicel® PH-102 + S-NP mixtures for a theoretical surface coverage of 40%. . . . .	105
4.8 S-NP number distribution for Avicel® PH-102 at 40% of surface coverage. . . . .	105
4.9 SEM micrographs of powder mixtures with different theoretical S-NP surface coverages . . . . .	105
4.10 Visual assessment of sample images to determine flow. The first column presents pure host particles. Columns 2 and 3 correspond to runs where flow behaviour was not improved. Columns 4 and 5 show runs where flow was enhanced for the mixtures. The numbers in the images indicate the number of the run on the DoE matrix (see supporting information file in section 5., table 4.4) . . . . .	106
4.11 Influence of the nature of the granular media studied on responses measured in the DoE: a) adhesion force, b) friction coefficient, c) flow factor, and d) Hausner ratio . . . . .	107
4.12 Moisture conditioning, mixing protocol, and glidant added significantly affect DoE Responses: a) adhesion force, b) flow factor, and c) Hausner ratio	108
4.13 Adhesive force as a function of glidant radius. A and H were taken as $10^{-19} J$ and 0.4 nm, respectively. . . . .	110
4.14 Avicel® PH-102 covered with 40% SC . . . . .	111
4.15 Physical aspect of powder mixtures of the experimental design runs. . . . .	115
4.16 Model fitting between the experimental flow factor, at high and low consolidations, and the predicted flow factor (Eq.4.6) using the fitting parameters: ● $\alpha =14.8$ and $\beta =0.28$ [55] , ● $\alpha =204$ and $\beta =0.29$ [71], ● $\alpha =89.5$ and $\beta =0.54$ [58]. . . . .	117

4.17	Cares-Pacheco and Falk model (Eq.4.10) evaluated with the 51 DoE points at 66 kPa, the four HP and the HP+SD10 formulation at 40% SC measured at 6 kPa and 66 kPa. . . . .	118
4.18	Flow factor prediction according to eq.4.13 for HP measured at 6 and 66 kPa. . . . .	119
5.1	Schematic of health-related aerosol fractions. . . . .	123
5.2	Inverse gas chromatography principle (adapted from [176]). The net retention time is given by $t_N = t_R - t_0$ where $t_R$ is the time spent for a probe molecule to pass through the powder column, and $t_0$ corresponds to the time for a non-adsorbed molecule—methane—to do it. . . . .	127
5.3	Rotating drum device (EN 15051-2 [154]). . . . .	129
5.4	Vortex shaker method sampling configurations. . . . .	131
5.5	SEM micrographs of Avicel <sup>®</sup> PH-102 (first row) and Wheat flour (second row) at various magnifications (x100, x200 and x1000). . . . .	132
5.6	SEM micrographs of Joint filler (first row) and glass beads (second row) at various magnifications (x500, x1000 and x2000). . . . .	132
5.7	TEM micrographs SIPERNAT <sup>®</sup> D10. . . . .	133
5.8	Water sorption isotherms of HP at 25°C. Sorption curves are represented with a solid line, and desorption curves with a dashed line. Mixtures compositions are shown in table 5.1. . . . .	133
5.9	Dustiness characterisation of HP and SD10. RD data is presented with a circle marker and for the VS a triangle marker was used. The airflow and the sample conditioning RH are controlled at 30%. . . . .	134
5.10	Influence of RH on the dustiness of HP. RD data is presented with a circle marker and for the VS a triangle marker was used. Three RH% configurations are represented for the powder conditioning - test airflow, 30-30, 30-50 and 50-50. . . . .	136
5.11	Dustiness indices of HP mixed with SD10 (40% SC). RD data is presented with a circle marker and for the VS a triangle marker was used. The airflow and the sample conditioning RH are controlled at 30%. . . . .	138
5.12	Number size distributions of aerosolized particles measured by ELPI <sup>®</sup> +. . . . .	139
5.13	TEM micrographs of airborne particles of host powders and SD10. . . . .	140
5.14	TEM images of particles aerosolized from powder mixtures. . . . .	140
5.15	Interparticle interactions represented schematically using a surface energy analysis: a) Weak interaction: both HP and S-NP are seen as two different particles b) Strong interaction: the surface energy is modified by changing the surface chemistry—the mixture is "seen" as a new particle c) Strong interaction: the surface is physically modified by increasing HP roughness and creating new high energy sites. . . . .	142
5.16	SEM micrographs of a) pure WF and b) WF mixed with 0.5%wt of SD10. . . . .	144
5.17	Relation between dustiness indices and the HP and HP+SD10 at 40%SC surface characterisation by a) dispersive surface energy, $\gamma_s^d$ , and b) specific surface, $a_{BET}$ . . . . .	145
6.1	Compression Hausner ratio, $HR_c$ , measured using the Instron press at 30N of the HP with SD10 at 0%, 1%, 40% and >40% surface coverage. . . . .	149
6.2	Flow factor, $ff$ , of HP and HP+SD10 measured at 6 kPa (◆) and 66 kPa (▲) of pre-consolidation. . . . .	149
6.3	Qualitative flow behaviour visual assessment of HP (first row) and HP+SD10 at 40%SC (second row). . . . .	150

6.4	Bulk adhesive forces, $c$ , of HP and HP+SD10 measured at 6 kPa (◆) and 66 kPa (▲) of pre-consolidation . . . . .	151
6.5	HP and HP+SD10 with 1%, 40% and >40% SC flow rates through different orifices (2.5 - 35 mm) fitted with the Beverloo model (Eq.6.1), represented by the solid line. a) Avicel PH102, b) wheat flour, c) joint filler and d) glass beads. . . . .	152
6.6	Inhalable ( $w_I$ ), thoracic ( $w_T$ ) and respirable ( $w_R$ ) indices of HP and 1%, 40% and >40% surface coverage, and SIPERNAT <sup>®</sup> D10 measured in the rotating drum. . . . .	156
6.7	Flowability indicators plotted against dustiness indicators of HP and HP+SD10 with 1%, 40% and >40% surface coverage. The pink markers indicate a correlation with a $R^2$ of at least 0.8. . . . .	157
6.8	Flowability relations between a) the flow factor, $ff$ (6 and 66 kPa) and the bulk adhesive forces, $c$ measured in the FT4 and b) Compressive Hausner ratio, $HR_c$ and the bulk adhesive forces, $c$ . . . . .	158
6.9	Correlations of a) the thoracic fraction, $w_T$ , and the compressive Hausner ratio, $HR_c$ , at 30N, and b) the respirable fraction, $w_R$ , and the flow factor, $ff$ , measured at a pre-consolidation of 66 kPa. The pink region indicates were the dust emission level is classified as high. The blue regions precise the flowability according to Hausner ratio and flow factor. . . . .	158
6.10	Correlations of a) the thoracic fraction, $w_T$ , and b) the inhalable, $w_I$ , fraction with the bulk adhesive forces, $c$ , measured at 6kPa of pre-consolidation in the FT4. The pink region indicates were the dust emission level is classified as high. . . . .	160
7.1	Production de matériaux granulaires en France [5–13]. . . . .	196
7.2	Opérations maladroites et dangereuses lors de la manipulation des poudres à cause d'une mauvaise coulabilité et la émission de poussière. . . . .	196



# List of Tables

1.1	Angle of repose flowability classification [48]	22
1.2	Densification flowability classifications [48]	24
1.3	Dynamic shape factor of aerosol particles (taken from [141]).	34
1.4	Dustiness classification for rotating drum standard EN 15051-2 [154].	37
1.5	Dustiness classification for continuous drop standard EN 15051-3 [155].	38
2.1	Surface coverage percentage of mixtures with 0.5% wt. of S-NP [%]	49
2.2	Samples nanomaterial classification according to VSSA.	55
2.3	Surface energy of host powders and SD10.	57
3.1	Devices characteristics	74
3.2	Excipients as host particles	75
3.3	Physical characteristics of silica nanoparticles	76
3.4	ImageJ software Analysis of SEM micrographs of Avicel® PH-102 surface in binary mixtures of 0.5% (w/w).	86
4.1	Powder characteristics.	102
4.2	Nanoparticles characteristics	103
4.3	Flow behaviour parameters of host powders	104
4.4	D-Optimal experimental design matrix and experiments results, p-value=0.05.	114
4.5	HP and HP+40%SC SD10 sauter diameter, $d_{32}$ , pycnometric density, $\rho$ and the dispersive surface energy, $\gamma_s^d$ used to estimate the Hamaker constant, A, the Bond number, $B_{og}$ , the cohesion/adhesion force, $F_{vdW}$ . The experimental values of $ff$ measured at 66 kPa, $ff_{66kPa}$ , and at 6 kPa, $ff_{6kPa}$ .	117
5.1	Mass fraction of SD10 needed to cover 40% of the HP surface.	128
5.2	Dustiness classification for rotating drum standard EN 15051-2 [154].	129
5.3	Powder characteristics.	132
5.4	IGC data: specific retention volumes and dispersive surface energies.	141
5.5	Experimental and theoretical specific surface, $a_{BET_{N_2}}$ of HP and HP+SD10 with 40% SC.	144
6.1	SD10 mass fractions [%] to cover 0, 1, 40 and more than 40% of the HP surface.	148
6.2	Flow through an orifice results: critical diameter and model parameter $C_{BV}$ and $R^2$ of the Beverloo model fitting (Eq.6.1) of HP and HP+SD10 with 1%, 40% and >40% surface coverage.	154
6.3	Comparison of the experimental ( $w_{T,E}$ and $w_{R,E}$ ) and predicted ( $w_{T,P}$ and $w_{R,P}$ ) thoracic and respirable values [mg/kg] and dustiness classification level of HP and HP+SD10, using Eqs.6.2 and 6.3. The values in pink highlights the cases in which the dustiness classification is not well predicted.	159

- 6.4 Comparison of the experimental ( $w_{T,E}$  and  $w_{I,E}$ ) and the predicted ( $w_{T,P}$  and  $w_{I,P}$ ) thoracic and inhalable values [mg/kg] and dustiness classification level of HP and HP+SD10, using Eqs. 6.4 and 6.5. The values in pink highlights the cases in which the dustiness classification is not well predicted. 160

# Bibliography

- [1] E. Hayes, “What was ground?: a functional analysis of grinding stones from madjedbebe and lake mungo, australia,” *University of Wollongong Thesis Collection 1954-2016*, 2015.
- [2] A. Revedin, B. Aranguren, R. Becattini, L. Longo, E. Marconi, M. M. Lippi, N. Skakun, A. Sinitsyn, E. Spiridonova, and J. Svoboda, “Thirty thousand-year-old evidence of plant food processing,” *Proc Natl Acad Sci U S A*, vol. 107, no. 44, pp. 18815–18819, 2010.
- [3] P. G. de Gennes, “Granular matter: a tentative view,” *Rev. Mod. Phys.*, vol. 71, no. 2, pp. S374–S382, 1999.
- [4] R. M. Nedderman, *Statics and Kinematics of Granular Materials*. Cambridge University Press, 1992.
- [5] Syndicat Français de l’Industrie Cimentière published by Statista, “Production volume of cement in france from 2011 to 2020,” 2022.
- [6] US Geological Survey published by Statista, “Mica production worldwide in 2022, by country,” 2023.
- [7] MRFR published by Statista, “Global copper powder market research report: Forecast to 2030,” 2021.
- [8] FranceAgriMer published by Statista, “Evolution of the volume of various types of powdered milks produced in france between 2008 to 2021,” 2022.
- [9] FranceAgriMer published by Statista, “Volume of flour produced in france from 2010 to 2020,” 2021.
- [10] SNFS published by Statista, “Production of beet sugar in france from 2012 to 2017,” 2019.
- [11] US Geological Survey published by Statista, “Major countries in industrial sand and gravel production worldwide in 2022,” 2023.
- [12] SNFS published by Statista, “Production of cane sugar in france from 2012 to 2017,” 2019.
- [13] FranceAgriMer published by Statista, “Volume of products derived from grain in france from 2010 to 2020, by product category,” 2021.
- [14] Prescott, James K. and Barnum, Roger A., “On powder flowability,” *Pharmaceutical technology*, vol. 24, no. 10, pp. 60–84, 2000.

- 
- [15] B. Liu, L. He, X. Zhao, Q. Qin, and Y. Guo, "Design and characteristic analysis of vibration feeding system for coal-gas dust-removal medium," *Clean Energy*, vol. 4, pp. 372–378, Dec. 2020.
- [16] J. Hristov, "Magnetically assisted gas–solid fluidization in a tapered vessel: Part II: Dimensionless bed expansion scaling," *Particuology*, vol. 7, pp. 183–192, June 2009.
- [17] Y. Zhou and J. Zhu, "Group c+ particles: Enhanced flow and fluidization of fine powders with nano-modulation," *Chemical Engineering Science*, vol. 207, pp. 653–662, 2019.
- [18] M.-C. Jiménez Garavito, M.-G. Cares Pacheco, F. Gerardin, and V. Falk, "Silica nanoparticles as glidants for industrial processing: A statistical approach," *Ind. Eng. Chem. Res.*, vol. 61, no. 44, pp. 16517–16528, 2022.
- [19] U. S. Food and Drug Administration, "CFR - code of federal regulations title 21," 2022.
- [20] European Commission, "COMMISSION REGULATION (EU) 2017/1271: amending annex III to regulation (EC) no 1333/2008 of the european parliament and of the council as regards the use of use of silicon dioxide (e 551) in potassium nitrate (e 252)," 2017.
- [21] J. G. Croissant, K. S. Butler, J. I. Zink, and C. J. Brinker, "Synthetic amorphous silica nanoparticles: toxicity, biomedical and environmental implications," *Nat Rev Mater*, vol. 5, no. 12, pp. 886–909, 2020.
- [22] V. Marques Da Silva, M. Benjdir, P. Montagne, J.-C. Pairon, S. Lanone, and P. Andujar, "Pulmonary toxicity of silica linked to its micro- or nanometric particle size and crystal structure: A review," *Nanomaterials*, vol. 12, no. 14, p. 2392, 2022.
- [23] S. Murugadoss, D. Lison, L. Godderis, S. Van Den Brule, J. Mast, F. Brassinne, N. Sebaihi, and P. H. Hoet, "Toxicology of silica nanoparticles: an upyear," *Arch Toxicol*, vol. 91, no. 9, pp. 2967–3010, 2017.
- [24] G. V. Research, "Market volume of nanosilica in the united states from 2014 to 2025," 2019.
- [25] C. Champmartin and F. Clerc, "Inhalable dust measurements as a first approach to assessing occupational exposure in the pharmaceutical industry," *Journal of Occupational and Environmental Hygiene*, vol. 11, no. 2, pp. 85–92, 2014.
- [26] J. Duran, *Sands, Powders, and Grains: An Introduction to the Physics of Granular Materials*. Partially Ordered Systems, Springer-Verlag, 2000.
- [27] R. L. Brown and J. C. Richards, *Principles of Powder Mechanics: Essays on the Packing and Flow of Powders and Bulk Solids*. Pergamon Press, 1970.
- [28] A. Castellanos, "The relationship between attractive interparticle forces and bulk behaviour in dry and uncharged fine powders," *Advances in Physics*, vol. 54, no. 4, pp. 263–376, 2005.
- [29] D. McGlinchey, *Characterisation of Bulk Solids*. John Wiley & Sons, 2005.

- 
- [30] ISO/TC 229, "Nanotechnology - nanoparticles in powder form - characteristics and measurements - ISO 17200:2020," 2020.
- [31] AFNOR X457, "Nanotechnologies - vocabulary - part 1 : core terms - XP CEN ISO/TS 80004-1," 2015.
- [32] European Commission, "Commission recommendation of 10 June 2022 on the definition of nanomaterial - (2022/c 229/01)," 2022.
- [33] European Commission, "Commission recommendation of 18 October 2011 on the definition of nanomaterial (2011/969/EU)," 2011.
- [34] H. M. Jaeger, S. R. Nagel, and R. P. Behringer, "The Physics of Granular Materials," *Physics Today*, vol. 49, no. 4, pp. 32–38, 1996.
- [35] H. M. Jaeger, "Sand, jams and jets," *Phys. World*, vol. 18, pp. 34–39, Dec. 2005.
- [36] B. Andreotti, Y. Forterre, and O. Pouliquen, *Les Milieux Granulaires Entre Fluide Et Solide*. EDP Sciences, Feb. 2011.
- [37] H. Masuda, K. Higashitani, and H. Yoshida, *Powder Technology: Handling and Operations, Process Instrumentation, and Working Hazards*. Taylor & Francis Group, 2006.
- [38] H. Wadell, "Volume, shape, and roundness of quartz particles," *The Journal of Geology*, vol. 43, no. 3, pp. 250–280, 1935.
- [39] J. N. Israelachvili, *Intermolecular and Surface Forces Ed. 3*. Elsevier Science, 2011.
- [40] H. C. Hamaker, "The London—van der Waals attraction between spherical particles," *Physica*, vol. 4, no. 10, pp. 1058–1072, 1937.
- [41] J. Seville, U. Tüzün, and R. Clift, *Processing of Particulate Solids*. Springer Netherlands, 1997.
- [42] C. Coulomb, *Histoire de l'Academie royale des sciences*. De l'imprimerie royale, 1785.
- [43] L. Zhang, X. Bi, and J. R. Grace, "Measurements of electrostatic charging of powder mixtures in a free-fall test device," *Procedia Engineering*, vol. 102, pp. 295–304, 2015.
- [44] H. Grosshans and S. Jantač, "Recent progress in cfd modeling of powder flow charging during pneumatic conveying," *Chemical Engineering Journal*, vol. 455, p. 140918, 2023.
- [45] ISO/TC 173, "Aides pour absorption d'urine - méthodes d'essai pour caractériser les matériaux absorbants à base de polymères - partie 9: Détermination gravimétrique de la masse volumique ISO 17190-9:2020," 2020.
- [46] AFNOR A95E, "Métallurgie des poudres - vocabulaire ISO 3252," 2019.
- [47] D. Schulze, "Flow properties of bulk solids," in *Powders and Bulk Solids: Behavior, Characterization, Storage and Flow* (D. Schulze, ed.), pp. 57–100, Springer International Publishing, 2021.
- [48] R. L. Carr, "Evaluating flow properties of solids," *Chemical Engineering*, no. 72, pp. 163–168, 1965.

- 
- [49] AFNOR X34B, "Biocombustibles solides - vocabulaire ISO 16559," 2022.
- [50] A. Saker, M. G. Cares-Pacheco, P. Marchal, and V. Falk, "Powders flowability assessment in granular compaction: What about the consistency of hausner ratio?," *Powder Technology*, vol. 354, pp. 52–63, 2019.
- [51] M. G. Cares Pacheco, M. C. Jiménez Garavito, A. Ober, F. Gerardin, E. Silvente, and V. Falk, "Effects of humidity and glidants on the flowability of pharmaceutical excipients. an experimental energetical approach during granular compaction," *International Journal of Pharmaceutics*, vol. 604, p. 120747, 2021.
- [52] R. Baserinia and I. C. Sinka, "Mass flow rate of fine and cohesive powders under differential air pressure," *Powder Technology*, vol. 334, pp. 173–182, July 2018.
- [53] J. Bouillard, F. Henry, and P. Marchal, "Rheology of powders and nanopowders through the use of a couette four-bladed vane rheometer: flowability, cohesion energy, agglomerates and dustiness," *J Nanopart Res*, vol. 16, no. 8, p. 2558, 2014.
- [54] M. Capece, R. Ho, J. Strong, and P. Gao, "Prediction of powder flow performance using a multi-component granular bond number," *Powder Technology*, vol. 286, pp. 561–571, 2015.
- [55] M. Capece, K. R. Silva, D. Sunkara, J. Strong, and P. Gao, "On the relationship of inter-particle cohesiveness and bulk powder behavior: Flowability of pharmaceutical powders," *International Journal of Pharmaceutics*, vol. 511, no. 1, pp. 178–189, 2016.
- [56] Y. Chen, J. Yang, R. N. Dave, and R. Pfeffer, "Fluidization of coated group c powders," *AIChE Journal*, vol. 54, no. 1, pp. 104–121, 2008.
- [57] X. Fu, D. Huck, L. Makein, B. Armstrong, U. Willen, and T. Freeman, "Effect of particle shape and size on flow properties of lactose powders," *Particuology*, vol. 10, no. 2, pp. 203–208, 2012.
- [58] M. Giraud, *Analyse du comportement rhéologique des poudres à partir des propriétés des grains, application à l'étude d'un procédé de broyage/mélange pour la préparation du combustible nucléaire MOX*. thesis, Ecole nationale des Mines d'Albi-Carmaux, 2020.
- [59] H. P. Goh, P. W. S. Heng, and C. V. Liew, "Comparative evaluation of powder flow parameters with reference to particle size and shape," *International Journal of Pharmaceutics*, vol. 547, no. 1, pp. 133–141, 2018.
- [60] S. Koynov, B. Glasser, and F. Muzzio, "Comparison of three rotational shear cell testers: Powder flowability and bulk density," *Powder Technology*, vol. 283, pp. 103–112, 2015.
- [61] M. Krantz, H. Zhang, and J. Zhu, "Characterization of powder flow: Static and dynamic testing," *Powder Technology*, vol. 194, no. 3, pp. 239–245, 2009.
- [62] L. X. Liu, I. Marziano, A. C. Bentham, J. D. Litster, E.T.White, and T. Howes, "Effect of particle properties on the flowability of ibuprofen powders," *International Journal of Pharmaceutics*, vol. 362, no. 1, pp. 109–117, 2008.

- [63] G. Xu, P. Lu, M. Li, C. Liang, P. Xu, D. Liu, and X. Chen, "Investigation on characterization of powder flowability using different testing methods," *Experimental Thermal and Fluid Science*, vol. 92, pp. 390–401, 2018.
- [64] S. E. Brika and V. Brailovski, "Influence of powder particle morphology on the static and fatigue properties of laser powder bed-fused ti-6al-4v components," *Journal of Manufacturing and Materials Processing*, vol. 4, no. 4, p. 107, 2020.
- [65] J. J. Fitzpatrick, S. A. Barringer, and T. Iqbal, "Flow property measurement of food powders and sensitivity of jenike's hopper design methodology to the measured values," *Journal of Food Engineering*, vol. 61, no. 3, pp. 399–405, 2004.
- [66] G. Lumay, K. Traina, F. Boschini, V. Delaval, A. Rescaglio, R. Cloots, and N. Vandewalle, "Effect of relative air humidity on the flowability of lactose powders," *Journal of Drug Delivery Science and Technology*, vol. 35, pp. 207–212, 2016.
- [67] C. S. Omar, R. M. Dhenge, S. Palzer, M. J. Hounslow, and A. D. Salman, "Roller compaction: Effect of relative humidity of lactose powder," *European Journal of Pharmaceutics and Biopharmaceutics*, vol. 106, pp. 26–37, 2016.
- [68] X.-Y. Lu, L. Chen, C.-Y. Wu, H.-K. Chan, and T. Freeman, "The effects of relative humidity on the flowability and dispersion performance of lactose mixtures," *Materials*, vol. 10, no. 6, p. 592, 2017.
- [69] E. Juarez-Enriquez, G. I. Olivas, P. B. Zamudio-Flores, E. Ortega-Rivas, S. Perez-Vega, and D. R. Sepulveda, "Effect of water content on the flowability of hygroscopic powders," *Journal of Food Engineering*, vol. 205, pp. 12–17, 2017.
- [70] E. Teunou, J. J. Fitzpatrick, and E. C. Synnott, "Characterisation of food powder flowability," *Journal of Food Engineering*, vol. 39, no. 1, pp. 31–37, 1999.
- [71] G. Bernard-Granger, M. Giraud, E. Pascal, L. Mailhan, T. Larsson, C. Valot, C. Ablitzer, C. Gatumel, and H. Berthiaux, "Rheological properties of alumina powder mixtures investigated using shear tests," *Powder Technology*, vol. 345, pp. 300–310, 2019.
- [72] M. Beretta, T. R. Hörmann, P. Hainz, W. K. Hsiao, and A. Paudel, "Investigation into powder tribo-charging of pharmaceuticals. part II: Sensitivity to relative humidity," *International Journal of Pharmaceutics*, vol. 591, p. 120015, 2020.
- [73] M. Capece, C. Borchardt, and A. Jayaraman, "Improving the effectiveness of the comil as a dry-coating process: Enabling direct compaction for high drug loading formulations," *Powder Technology*, vol. 379, pp. 617–629, 2021.
- [74] R. Chirone, D. Barletta, P. Lettieri, and M. Poletto, "Bulk flow properties of sieved samples of a ceramic powder at ambient and high temperature," *Powder Technology*, vol. 288, pp. 379–387, 2016.
- [75] R. Freeman, "Measuring the flow properties of consolidated, conditioned and aerated powders — a comparative study using a powder rheometer and a rotational shear cell," *Powder Technology*, vol. 174, no. 1, pp. 25–33, 2007.
- [76] P. York, "Application of powder failure testing equipment in assessing effect of glidants on flowability of cohesive pharmaceutical powders," *Journal of Pharmaceutical Sciences*, vol. 64, no. 7, pp. 1216–1221, 1975.

- [77] A.-K. Müller, J. Ruppel, C.-P. Drexel, and I. Zimmermann, "Precipitated silica as flow regulator," *European Journal of Pharmaceutical Sciences*, vol. 34, no. 4, pp. 303–308, 2008.
- [78] J. Yang, A. Sliva, A. Banerjee, R. N. Dave, and R. Pfeffer, "Dry particle coating for improving the flowability of cohesive powders," *Powder Technology*, vol. 158, no. 1, pp. 21–33, 2005.
- [79] S. Jonat, S. Hasenzahl, M. Drechsler, P. Albers, K. G. Wagner, and P. C. Schmidt, "Investigation of compacted hydrophilic and hydrophobic colloidal silicon dioxides as glidants for pharmaceutical excipients," *Powder Technology*, vol. 141, no. 1, pp. 31–43, 2004.
- [80] Q. Zhou, L. Shi, S. Chatteraj, and C. C. Sun, "Preparation and characterization of surface-engineered coarse microcrystalline cellulose through dry coating with silica nanoparticles," *Journal of Pharmaceutical Sciences*, vol. 101, no. 11, pp. 4258–4266, 2012.
- [81] A. F. B. Ruzaidi, U. K. Mandal, and B. Chatterjee, "Glidant effect of hydrophobic and hydrophilic nanosilica on a cohesive powder: Comparison of different flow characterization techniques," *Particuology*, vol. 31, pp. 69–79, 2017.
- [82] B. Ma, Q. Jiang, J. Huang, X. Wang, and J. Leng, "Effect of different silica particles on flowability of gypsum powder for 3d powder printing," *Construction and Building Materials*, vol. 217, pp. 394–402, 2019.
- [83] D. Majerová, L. Kulaviak, M. Růžička, F. Štěpánek, and P. Zámotný, "Effect of colloidal silica on rheological properties of common pharmaceutical excipients," *European Journal of Pharmaceutics and Biopharmaceutics*, vol. 106, pp. 2–8, 2016.
- [84] H. Rumpf, "Die wissenschaft des agglomerierens," *Chemie ingenieur technik*, vol. 46, no. 1, pp. 1–11, 1974.
- [85] K. Dixit, V. Karde, A. Jauhari, S. C. Bhattacharyya, and C. Ghoroi, "Flow improvement of fine oxidizer using nano-additives," *Advanced Powder Technology*, vol. 33, p. 103711, Aug. 2022.
- [86] D. Bao, L. Sang, J. Xie, H. Zhang, H. Zhang, and J. Zhu, "Experimental and Computational Study on Effects of Flow Additive on Flowability of Fine Coating Particles," *Processes*, vol. 11, p. 2, Jan. 2023.
- [87] T. Kojima and J. A. Elliott, "Effect of silica nanoparticles on the bulk flow properties of fine cohesive powders," *Chemical Engineering Science*, vol. 101, pp. 315–328, 2013.
- [88] R. Gannoun, J. M. P. Ebrí, A. T. Pérez, M. J. Espín, F. J. Durán-Olivencia, and J. M. Valverde, "Nanosilica to improve the flowability of fine limestone powders in thermochemical storage units," *Chemical Engineering Journal*, vol. 426, p. 131789, 2021.
- [89] I. Tomasetta, D. Barletta, and M. Poletto, "Correlation of powder flow properties to interparticle interactions at ambient and high temperatures," *Particuology*, vol. 12, pp. 90–99, 2014.

- [90] D. Macrì, M. Poletto, D. Barletta, S. Sutcliffe, and P. Lettieri, "Analysis of industrial reactive powders flow properties at high temperature," *Powder Technology*, vol. 316, pp. 131–138, 2017.
- [91] J. Schwedes, "Review on testers for measuring flow properties of bulk solids," *GM*, vol. 5, no. 1, pp. 1–43, 2003.
- [92] M. Krantz, H. Zhang, and J. Zhu, "Characterization of powder flow: Static and dynamic testing," *Powder Technology*, vol. 194, no. 3, pp. 239–245, 2009.
- [93] M. Leturia, M. Benali, S. Lagarde, I. Ronga, and K. Saleh, "Characterization of flow properties of cohesive powders: A comparative study of traditional and new testing methods," *Powder Technology*, vol. 253, pp. 406–423, 2014.
- [94] G. Tan, *Examining the mechanisms of how surface modification alters the flow of fine powders*. phdthesis, Monash University, 2021.
- [95] A. Saker, *Etude critique de quelques techniques expérimentales d'évaluation de la coulabilité des poudres*. PhD thesis, Université de Lorraine, 2018.
- [96] GDR MiDi, "On dense granular flows," *Eur. Phys. J. E*, vol. 14, no. 4, pp. 341–365, 2004.
- [97] I. M. F. Wouters and D. Geldart, "Characterising semi-cohesive powders using angle of repose," *Part. Part. Syst. Charact.*, vol. 13, no. 4, pp. 254–259, 1996.
- [98] O. Macho, K. Demkova, L. Gabrisova, M. Cierny, J. Musikova, P. Galbava, Z. Niznaska, J. Blasko, P. Peciar, R. Fekete, and P. Marian, "Analysis of static angle of repose with respect to powder material properties," *Acta Polytechnica*, vol. 60, no. 1, pp. 73–80, 2020.
- [99] R. Condotta, *Coulabilité des poudres cohésives : mesures aux faibles contraintes, granulaires humides et application à une poudre industrielle*. PhD thesis, Institut national polytechnique de Toulouse, 2005.
- [100] Z. Berk, *Food Process Engineering and Technology Ed. 2*. Elsevier Science, 2013.
- [101] H. M. Beakawi Al-Hashemi and O. S. Baghabra Al-Amoudi, "A review on the angle of repose of granular materials," *Powder Technology*, vol. 330, 2018.
- [102] M. Antequera, A. Ruiz, M. Perales, N. Munoz, and M.-C. Ballesteros, "Evaluation of an adequate method of estimating flowability according to powder characteristics," *International Journal of Pharmaceutics*, vol. 103, pp. 155–161, Mar. 1994.
- [103] H. H. Hausner, "Friction conditions in a mass of metal powder," *Int. J. Powder Met.*, 3: No. 4, 7-13(Oct. 1967)., 1967.
- [104] AFNOR, "Engrais - détermination de la masse volumique après tassement NF 1237," 1995.
- [105] ASTM, "Standard test method for mechanically tapped density of activated carbon (powdered and fine mesh) ASTM D8176-18," 2018.
- [106] ASTM, "Standard test method for mechanically tapped packing density of formed catalyst and catalyst carriers ASTM D4164-13," 2018.
- [107] U. Pharmacopeia, "Bulk density and tapped density of powders," 2015.

- 
- [108] A. Suaza-Montalvo, M. G. Cares-Pacheco, and V. Falk, "Time-dependent behaviour of industrial granular materials under vibration: Modelling and phenomenology," *Chemical Engineering Science*, vol. 271, p. 118571, 2023.
- [109] C. A. Coulomb, *Essai sur une application des règles de maximis & minimis à quelques problèmes de statique, relatifs à l'architecture*. De l'Imprimerie Royale, 1776.
- [110] A. W. Jenike, *Gravity flow of bulk solids*. University of Utah, 1961.
- [111] M. G. Cares-Pacheco and V. Falk, "A phenomenological law for complex granular materials from mohr-coulomb theory," *Advanced Powder Technology*, vol. 34, no. 1, p. 103888, 2023.
- [112] W. A. Beverloo, H. A. Leniger, and J. van de Velde, "The flow of granular solids through orifices," *Chemical Engineering Science*, vol. 15, pp. 260–269, Sept. 1961.
- [113] ISO, "Céramiques techniques. détermination de l'aptitude à l'écoulement des poudres céramiques ISO 14629-2016," 2016.
- [114] AFNOR X43C, "Poudres métalliques - détermination du temps d'écoulement au moyen d'un entonnoir calibré (appareil de hall) ISO 4490:2018," 2018.
- [115] AFNOR A95E, "Poudres métalliques - détermination du temps d'écoulement au moyen d'un entonnoir calibré (cône d'écoulement de gustavsson) ISO 13517," 2020.
- [116] X. Y. Liu, E. Specht, and J. Mellmann, "Experimental study of the lower and upper angles of repose of granular materials in rotating drums," *Powder Technology*, vol. 154, no. 2, pp. 125–131, 2005.
- [117] X. Zhu, Q. Zhang, Y. Wang, and F. Wei, "Review on the nanoparticle fluidization science and technology," *Chinese Journal of Chemical Engineering*, vol. 24, pp. 9–22, Jan. 2016.
- [118] D. Geldart, "Types of gas fluidization," *Powder Technology*, vol. 7, pp. 285–292, May 1973.
- [119] World Health Organization. Occupational and Environmental Health Team, "Hazard prevention and control in the work environment: : airborne dust," 1999.
- [120] ISO/TC 119, "Exposition sur les lieux de travail - terminologie NF EN 1540," 2018.
- [121] A. Renoux and D. Boulaud, *Les aérosols: physique et métrologie*. Tec & Doc Lavoisier, 1998.
- [122] T. Schneider, D. H. Brouwer, I. K. Koponen, K. A. Jensen, W. Fransman, B. Van Duuren-Stuurman, M. Van Tongeren, and E. Tielemans, "Conceptual model for assessment of inhalation exposure to manufactured nanoparticles," *J Expo Sci Environ Epidemiol*, vol. 21, no. 5, pp. 450–463, 2011.
- [123] AFNOR X43C, "Atmosphères des lieux de travail - définition des fractions de taille pour le mesurage des particules en suspension dans l'air - NF 481," 1993.
- [124] M. Ricaud, E. Belut, L. Fina, A. Janes, V. Marquenie, F. Moreau, and R. Worehrly, "Mise en œuvre de matériaux pulvérulents," 2021.

- [125] C. Breton, "Prévention des allergies respiratoires professionnelles en boulangerie-pâtisserie, "le souffle des boulangers, un enjeu de santé au travail", 2002.
- [126] M. Wiszniewska and J. Walusiak-Skorupa, "Diagnosis and frequency of work-exacerbated asthma among bakers," *Ann Allergy Asthma Immunol*, vol. 111, no. 5, pp. 370–375, 2013.
- [127] C. C. Leung, I. T. S. Yu, and W. Chen, "Silicosis," *The Lancet*, vol. 379, no. 9830, pp. 2008–2018, 2012.
- [128] H. Kakooei, A. Gholami, M. Ghasemkhani, M. Hosseini, D. Panahi, and G. Pouryaghoub, "Dust exposure and respiratory health effects in cement production," *Acta Medica Iranica*, pp. 122–126, 2012.
- [129] J. M. James and J. F. Crespo, "Allergic reactions to foods by inhalation," *Curr Allergy Asthma Rep*, vol. 7, no. 3, pp. 167–174, 2007.
- [130] A. Stobnicka and R. L. Górny, "Exposure to flour dust in the occupational environment," *International Journal of Occupational Safety and Ergonomics*, vol. 21, no. 3, pp. 241–249, 2015.
- [131] B. Courtois, S. Binet, E. Langlois, G. Mater, Rousset, and O. Witschger, "Valeurs limites d'exposition professionnelle," 2022.
- [132] E. Page, C. Dowell, C. Mueller, and R. Biagini, "Evaluation of sensitization and exposure to flour dust, spices, and other ingredients among poultry breeding workers," 2013.
- [133] A. Martinelli, F. Salamon, M. L. Scapellato, A. Trevisan, L. Vianello, R. Bizzotto, M. A. Crivellaro, and M. Carrieri, "Occupational exposure to flour dust. exposure assessment and effectiveness of control measures," *Int J Environ Res Public Health*, vol. 17, no. 14, p. 5182, 2020.
- [134] C. Pujara and D. Kildsig, "Effect of Individual Particle Characteristics on Airborne Emissions," in *Containment in the Pharmaceutical Industry*, pp. 29–53, CRC Press, 2000.
- [135] A. López-Lilao, V. S. Forner, G. M. Gasch, and E. M. Gimeno, "Particle size distribution: A key factor in estimating powder dustiness," *Journal of Occupational and Environmental Hygiene*, vol. 14, no. 12, pp. 975–985, 2017.
- [136] I. Pensis, J. Mareels, D. Dahmann, and D. Mark, "Comparative Evaluation of the Dustiness of Industrial Minerals According to European Standard EN 15051, 2006," *The Annals of Occupational Hygiene*, vol. 54, pp. 204–216, Mar. 2010.
- [137] S. Chakravarty, M. Fischer, O. L. Bihan, and M. Morgeneyer, "Towards a theoretical understanding of dustiness," *Granular Matter*, vol. 21, no. 4, p. 97, 2019.
- [138] M. A. Plinke, D. Leith, M. G. Boundy, and F. Löffler, "Dust generation from handling powders in industry," *American Industrial Hygiene Association Journal*, vol. 56, no. 3, pp. 251–257, 1995.
- [139] O. Behrens, C. Hamberg, and E. Tveten, "Effects of morphology on alumina strength and dustiness," in *Volume: 6 th Alumina Quality Workshop*, Sept. 2002.

- 
- [140] K. Hjemsted and T. Schneider, "Dustiness from powder materials," *Journal of Aerosol Science*, vol. 27, pp. S485–S486, Sept. 1996.
- [141] J. H. Vincent, *Aerosol Science for Industrial Hygienists*. Elsevier Science & Technology, 1995.
- [142] U. Alwis, J. Mandryk, A. D. Hocking, J. Lee, T. Mayhew, and W. Baker, "Dust exposures in the wood processing industry," *Am Ind Hyg Assoc J*, vol. 60, no. 5, pp. 641–646, 1999.
- [143] M. A. Plinke, D. Leith, D. B. Holstein, and M. G. Boundy, "Experimental examination of factors that affect dust generation," *American Industrial Hygiene Association Journal*, vol. 52, no. 12, pp. 521–528, 1991.
- [144] C. Cowherd, M. Grelinger, P. Englehart, R. Kent, and K. Wong, "An apparatus and methodology for predicting the dustiness of materials," *American Industrial Hygiene Association Journal*, vol. 50, no. 3, pp. 123–130, 1989.
- [145] A. López-Lilao, M. P. Gómez-Tena, G. Mallol, and E. Monfort, "Clay hydration mechanisms and their effect on dustiness," *Applied Clay Science*, vol. 144, pp. 157–164, Aug. 2017.
- [146] F. Hamelmann and E. Schmidt, "Methods of estimating the dustiness of industrial powders – a review," *KONA Powder and Particle Journal*, vol. 21, pp. 7–18, 2003.
- [147] N. R. A.H.M. Andreasen, H. Hofman-Bang, "Über das staubungsvermögenger stoffe," *Kolloid-Zeitschrift*, vol. 86, no. 1, pp. 70–77, 1939.
- [148] ASTM, "Test method for index of dustiness of coal and coke - ASTM D547-41," 1941.
- [149] J. Cooke, J. Perkins, and N. F. Getchell, "Controlling dust in agricultural products with additives," *Cereal foods world*, vol. 9, pp. 271–277, 1979.
- [150] G. J. Burdett, *Development of a method for dustiness testing: annexes to SMT4-CT96-2074*. Sheffield: Health & Safety Laboratory, 2000.
- [151] M. Boundy, D. Leith, and T. Polton, "Method to evaluate the dustiness of pharmaceutical powders," *Ann Occup Hyg*, vol. 50, no. 5, pp. 453–458, 2006.
- [152] K. Saleh, M.-T. Moufarej Abou Jaoude, M. Morgeneyer, E. Lefrancois, O. Le Bihan, and J. Bouillard, "Dust generation from powders: A characterization test based on stirred fluidization," *Powder Technology*, vol. 255, pp. 141–148, 2014.
- [153] G. Mordas, H. E. Manninen, T. Petäjä, P. P. Aalto, K. Hämeri, and M. Kulmala, "On operation of the ultra-fine water-based CPC TSI 3786 and comparison with other TSI models (TSI 3776, TSI 3772, TSI 3025, TSI 3010, TSI 3007)," *Aerosol Science and Technology*, vol. 42, no. 2, pp. 152–158, 2008.
- [154] AFNOR, "Workplace exposure - measurement of the dustiness of bulk materials - part 2: Rotating drum method - NF EN 15051-2+A1," 2017.
- [155] AFNOR, "Workplace exposure - measurement of the dustiness of bulk materials - part 3: Continuous drop method - NF EN 15051-3," 2014.

- [156] AFNOR, "Workplace exposure - measurement of dustiness of bulk materials that contain or release respirable NOAA or other respirable particles - part 1: requirements and choice of test methods - EN 17199-1," 2019.
- [157] T. Lee, S. W. Kim, W. P. Chisholm, J. Slaven, and M. Harper, "Performance of high flow rate samplers for respirable particle collection," *Ann Occup Hyg*, vol. 54, no. 6, pp. 697–709, 2010.
- [158] J. Yli-Ojanperä, J. Kannosto, M. Marjamäki, and J. Keskinen, "Improving the nanoparticle resolution of the ELPI," *Aerosol Air Qual. Res.*, vol. 10, no. 4, pp. 360–366, 2010.
- [159] B. R'Mili, O. L. Bihan, C. Dutouquet, O. Aguerre-Chariol, and E. Frejafon, "Particle Sampling by TEM Grid Filtration," *Aerosol Science and Technology*, vol. 47, no. 7, p. 767, 2013.
- [160] M. Xiang, *Aerosol sampling and characterization technique using TEM porous grids*. These de doctorat, Compiègne, 2021.
- [161] AFNOR, "Workplace exposure - measurement of dustiness of bulk materials that contain or release respirable NOAA or other respirable particles - part 5: Vortex shaker method - EN 17199-5," 2019.
- [162] AFNOR, "Workplace exposure - measurement of dustiness of bulk materials that contain or release respirable NOAA or other respirable particles - part 4: small rotating drum method - EN 17199-4," 2019.
- [163] AFNOR, "Workplace exposure - measurement of dustiness of bulk materials that contain or release respirable NOAA or other respirable particles - part 2: rotating drum method - EN 17199-2," 2019.
- [164] AFNOR, "Workplace exposure - measurement of dustiness of bulk materials that contain or release respirable NOAA or other respirable particles - part 3: continuous drop method - EN 17199-3," 2019.
- [165] M. Authier-Martin, "Alumina Handling Dustiness," in *Essential Readings in Light Metals: Volume 1 Alumina and Bauxite* (D. Donaldson and B. E. Raahauge, eds.), pp. 774–782, Cham: Springer International Publishing, 1989.
- [166] IMARC Group, "Microcrystalline cellulose market: Global industry trends, share, size, growth, opportunity and forecast 2022-2027," 2021.
- [167] H. Zhao, C. Shi, L. Zhao, Y. Wang, and L. Shen, "Influences of different microcrystalline cellulose (MCC) grades on tablet quality and compression behavior of MCC-lactose binary mixtures," *Journal of Drug Delivery Science and Technology*, vol. 77, p. 103893, Nov. 2022.
- [168] J. Nsor-Atindana, M. Chen, H. D. Goff, F. Zhong, H. R. Sharif, and Y. Li, "Functionality and nutritional aspects of microcrystalline cellulose in food," *Carbohydrate Polymers*, vol. 172, pp. 159–174, Sept. 2017.
- [169] M. Lynch, "Decorative skin and hair cosmetics containing microcrystalline cellulose as enhancing agent - US20040156811A1," 2004.

- 
- [170] IMARC Group, "Wheat flour market: Global industry trends, share, size, growth, opportunity and forecast 2023-2028," 2022.
- [171] Future market insights , "Joint compound market by product type, end use, application and region – forecast 2021 - 2031," 2021.
- [172] MarketsandMarkets, "Retro-reflective materials market by technology, product type, application and region – global forecast to 2023," 2018.
- [173] ResearchNester, "Global lactose market size, forecast, and trend highlights over 2023 - 2033," 2023.
- [174] Evonik industries, "AEROSIL® – fumed silica technical overview," 2015.
- [175] S. Brunauer, P. H. Emmett, and E. Teller, "Adsorption of gases in multimolecular layers," *Journal of the American Chemical Society*, vol. 60, no. 2, pp. 309–319, 1938.
- [176] M. G. Cares-Pacheco, G. Vaca-Medina, R. Calvet, F. Espitalier, J. Letourneau, A. Rouilly, and E. Rodier, "Physicochemical characterization of d-mannitol polymorphs: The challenging surface energy determination by inverse gas chromatography in the infinite dilution region," *International Journal of Pharmaceutics*, vol. 475, no. 1, pp. 69–81, 2014.
- [177] G. M. Dorris and D. G. Gray, "Adsorption of n-alkanes at zero surface coverage on cellulose paper and wood fibers," *Journal of Colloid and Interface Science*, vol. 77, no. 2, pp. 353–362, 1980.
- [178] M. Peleg, "Flowability of food powders and methods for its evaluation — a review," *Journal of Food Process Engineering*, vol. 1, no. 4, pp. 303–328, 1977.
- [179] D18 Committee, "Test method for shear testing of powders using the freeman technology FT4 powder rheometer shear cell," 2016.
- [180] A. B. Yu and J. S. Hall, "Packing of fine powders subjected to tapping," *Powder Technology*, vol. 78, no. 3, pp. 247–256, 1994.
- [181] E. Rondet, M. Delalonde, S. Chuetor, and T. Ruiz, "Modeling of granular material's packing: Equivalence between vibrated solicitations and consolidation," *Powder Technology*, vol. 310, pp. 287–294, 2017.
- [182] J. B. Knight, C. G. Fandrich, C. N. Lau, H. M. Jaeger, and S. R. Nagel, "Density relaxation in a vibrated granular material," *Phys Rev E Stat Phys Plasmas Fluids Relat Interdiscip Topics*, vol. 51, no. 5, pp. 3957–3963, 1995.
- [183] D. A. Head, "Phenomenological glass model for vibratory granular compaction," *Phys. Rev. E*, vol. 62, no. 2, pp. 2439–2449, 2000.
- [184] P. Ribière, P. Philippe, P. Richard, R. Delannay, and D. Bideau, "Slow compaction of granular systems," *Journal of Physics: Condensed Matter*, vol. 17, no. 24, pp. 2743–2754, 2005.
- [185] J. M. Valverde Millán, "The use of additives to control powder flow. mechanical properties of fine powder beds," in *Fluidization of Fine Powders: Cohesive versus Dynamical Aggregation* (J. M. Valverde Millán, ed.), Particle Technology Series, pp. 99–120, Springer Netherlands, 2013.

- [186] M. Ricaud, "Le point des connaissances sur... les silices amorphes," *Brochure ED 6441 - INRS*, 2007.
- [187] M. a. S. Quintanilla, J. M. Valverde, and A. Castellanos, "Adhesion force between fine particles with controlled surface properties," *AIChE Journal*, vol. 52, no. 5, pp. 1715–1728, 2006.
- [188] F. Fulchini, U. Zafar, C. Hare, M. Ghadiri, H. Tantawy, H. Ahmadian, and M. Poletto, "Relationship between surface area coverage of flow-aids and flowability of cohesive particles," *Powder Technology*, vol. 322, pp. 417–427, 2017.
- [189] K. Traina, R. Cloots, S. Bontempi, G. Lumay, N. Vandewalle, and F. Boschini, "Flow abilities of powders and granular materials evidenced from dynamical tap density measurement," *Powder Technology*, vol. 235, pp. 842–852, 2013.
- [190] I. Zimmermann, M. Eber, and K. Meyer, "Nanomaterials as flow regulators in dry powders," *Zeitschrift für Physikalische Chemie*, vol. 218, no. 1, pp. 51–102, 2004.
- [191] T. Kojima and J. A. Elliott, "Incipient flow properties of two-component fine powder systems and their relationships with bulk density and particle contacts," *Powder Technology*, vol. 228, pp. 359–370, 2012.
- [192] X. Zhu, Q. Zhang, C. Huang, Y. Wang, C. Yang, and F. Wei, "Validation of surface coating with nanoparticles to improve the flowability of fine cohesive powders," *Particuology*, vol. 30, pp. 53–61, 2017.
- [193] Janés, Agnès and Chaineaux, Jacques, "Explosions de poussières dans les lieux de travail, recensement et analyse," 2010.
- [194] Janés, Agnès and Vignes, Alexis, "Incendie, explosion : Attention au phénomène d'auto-échauffement des solides divisés," 2018.
- [195] P. Jop, Y. Forterre, and O. Pouliquen, "A constitutive law for dense granular flows," *Nature*, vol. 441, no. 7094, pp. 727–730, 2000.
- [196] P. Marchal, *Viscoélasticité des milieux granulaires denses*. thesis, Université de Lorraine (Nancy), 2013.
- [197] S. Kim and K. Kamrin, "Power-law scaling in granular rheology across flow geometries," *Phys. Rev. Lett.*, vol. 125, no. 8, p. 088002, 2020.
- [198] F. Raganati, R. Chirone, and P. Ammendola, "Gas–solid fluidization of cohesive powders," *Chemical Engineering Research and Design*, vol. 133, pp. 347–387, 2018.
- [199] J. Shabaniyan, R. Jafari, and J. Chaouki, "Fluidization of ultrafine powders," *Materials Science, Chemistry*, vol. 4, no. 1, p. 35, 2012.
- [200] T. P. Vinod and R. Jelinek, "Inorganic nanoparticles in cosmetics," in *Nanocosmetics: From Ideas to Products* (J. Cornier, C. M. Keck, and M. Van de Voorde, eds.), pp. 29–46, Springer International Publishing, 2019.
- [201] M. A. Robles-García, F. Rodríguez-Félix, E. Márquez-Ríos, J. A. Aguilar, A. Barrera-Rodríguez, J. Aguilar, S. Ruiz-Cruz, and C. L. Del-Toro-Sánchez, "Applications of nanotechnology in the agriculture, food, and pharmaceuticals," *Journal of Nanoscience and Nanotechnology*, vol. 16, no. 8, pp. 8188–8207, 2016.

- 
- [202] H. Haynes and R. Asmatulu, "Chapter 7 - nanotechnology safety in the aerospace industry," in *Nanotechnology Safety* (R. Asmatulu, ed.), pp. 85–97, Elsevier, 2013.
- [203] COMMISSION EUROPEENNE, "Recommandation n° 2011/696/UE du 18/10/11 relative à la définition des nanomatériaux," 2011.
- [204] European Commission, "COMMUNICATION FROM THE COMMISSION TO THE EUROPEAN PARLIAMENT, THE COUNCIL AND THE EUROPEAN ECONOMIC AND SOCIAL COMMITTEE second regulatory review on nanomaterials," 2012.
- [205] R. C. Rowe, P. Sheskey, and M. Quinn, *Handbook of Pharmaceutical excipients*. Libros Digitales - Pharmaceutical Press, 2009.
- [206] Evonik, "Aerosil and Sipernat, Silica products for personal care applications."
- [207] Center for Food Safety and Applied, "Food additive status list," *FDA*, 2021.
- [208] M. Younes, P. Aggett, F. Aguilar, R. Crebelli, B. Dusemund, M. Filipič, M. J. Frutos, P. Galtier, D. Gott, U. Gundert-Remy, G. G. Kuhnle, J.-C. Leblanc, I. T. Lillegaard, P. Moldeus, A. Mortensen, A. Oskarsson, I. Stankovic, I. Waalkens-Berendsen, R. A. Woutersen, M. Wright, P. Boon, D. Chrysafidis, R. Gürtler, P. Mosesso, D. Parent-Massin, P. Tobback, N. Kovalkovicova, A. M. Rincon, A. Tard, and C. Lambré, "Re-evaluation of silicon dioxide (e 551) as a food additive," *EFSA Journal*, vol. 16, no. 1, p. e05088, 2018.
- [209] Y. Gichard and A. Kirsch, "Toxicité des silices amorphes synthétiques - article de revue - INRS," 2022.
- [210] E. E. Fröhlich and E. Fröhlich, "Cytotoxicity of nanoparticles contained in food on intestinal cells and the gut microbiota," *Int J Mol Sci*, vol. 17, no. 4, p. 509, 2016.
- [211] C. Hempt, J.-P. Kaiser, O. Scholder, T. Buerki-Thurnherr, H. Hofmann, A. Rippl, T. B. Schuster, P. Wick, and C. Hirsch, "The impact of synthetic amorphous silica (e 551) on differentiated caco-2 cells, a model for the human intestinal epithelium," *Toxicology in Vitro*, vol. 67, p. 104903, 2020.
- [212] S. Ivanov, S. Zhuravsky, G. Yukina, V. Tomson, D. Korolev, and M. Galagudza, "In vivo toxicity of intravenously administered silica and silicon nanoparticles," *Materials*, vol. 5, no. 10, pp. 1873–1889, 2012.
- [213] J. C. Lai, G. Ananthakrishnan, S. Jandhyam, V. V. Dukhande, A. Bhushan, M. Gokhale, C. K. Daniels, and S. W. Leung, "Treatment of human astrocytoma u87 cells with silicon dioxide nanoparticles lowers their survival and alters their expression of mitochondrial and cell signaling proteins," *Int J Nanomedicine*, vol. 5, pp. 715–723, 2010.
- [214] R. Villota, J. G. Hawkes, and H. Cochrane, "Food applications and the toxicological and nutritional implications of amorphous silicon dioxide," *C R C Critical Reviews in Food Science and Nutrition*, vol. 23, no. 4, pp. 289–321, 1986.
- [215] C. Fan, P. Graff, P. Vihlborg, I.-L. Bryngelsson, and L. Andersson, "Silica exposure increases the risk of stroke but not myocardial infarction—a retrospective cohort study," *PLOS ONE*, vol. 13, no. 2, p. e0192840, 2018.

- [216] N. Sharma and S. Jha, "Amorphous nanosilica induced toxicity, inflammation and innate immune responses: A critical review," *Toxicology*, vol. 441, p. 152519, 2020.
- [217] D. J. McClements and H. Xiao, "Is nano safe in foods? establishing the factors impacting the gastrointestinal fate and toxicity of organic and inorganic food-grade nanoparticles," *npj Sci Food*, vol. 1, no. 1, p. 6, 2017.
- [218] A. A. Keller, S. McFerran, A. Lazareva, and S. Suh, "Global life cycle releases of engineered nanomaterials," *J Nanopart Res*, vol. 15, no. 6, p. 1692, 2013.
- [219] A. Ale, M. F. Gutierrez, A. S. Rossi, C. Bacchetta, M. F. Desimone, and J. Cazenave, "Ecotoxicity of silica nanoparticles in aquatic organisms: An upyeard review," *Environmental Toxicology and Pharmacology*, vol. 87, p. 103689, 2021.
- [220] A. Gans, O. Poulliquen, and M. Nicolas, "Cohesion-controlled granular material," *Phys. Rev. E*, vol. 101, no. 3, p. 032904, 2020.
- [221] M. G. Cares-Pacheco, R. Calvet, G. Vaca-Medina, A. Rouilly, and F. Espitalier, "Inverse gas chromatography a tool to follow physicochemical modifications of pharmaceutical solids: Crystal habit and particles size surface effects," *International Journal of Pharmaceutics*, vol. 494, no. 1, pp. 113–126, 2015.
- [222] S. C. Das, Q. Zhou, D. A. V. Morton, I. Larson, and P. J. Stewart, "Use of surface energy distributions by inverse gas chromatography to understand mechanofusion processing and functionality of lactose coated with magnesium stearate," *European Journal of Pharmaceutical Sciences*, vol. 43, no. 4, pp. 325–333, 2011.
- [223] L. M. Sander, "Diffusion-limited aggregation: A kinetic critical phenomenon?," *Contemporary Physics*, vol. 41, no. 4, pp. 203–218, 2000.
- [224] O. A. Odeku, S. Weber, and I. Zimmermann, "Efficiency of nanoscaled flow regulators," *Chemical Engineering & Technology*, vol. 34, no. 1, pp. 69–74, 2011.
- [225] S. Comte, R. Calvet, J. A. Dodds, and H. Balard, "Surface properties of low specific surface powders using inverse gas chromatography," *Powder Technology*, vol. 157, no. 1, pp. 39–47, 2005.
- [226] European Commission. Joint Research Centre., *An overview of concepts and terms used in the European Commission's definition of nanomaterial*. Publications Office, 2019.
- [227] J. M. Valverde, A. Ramos, A. Castellanos, and P. Keith Watson, "The tensile strength of cohesive powders and its relationship to consolidation, free volume and cohesivity," *Powder Technology*, vol. 97, no. 3, pp. 237–245, 1998.
- [228] S. Mandal, M. Nicolas, and O. Poulliquen, "Insights into the rheology of cohesive granular media," *Proc Natl Acad Sci U S A*, vol. 117, no. 15, pp. 8366–8373, 2020.
- [229] Krupp H, *Particle adhesion theory and experiment*. Elsevier, 1967.
- [230] Z. Huang, "Flow and bulk density enhancements of pharmaceutical powders using a conical screen mill\_ a continuous dry coating device," *Chemical Engineering Science*, p. 16, 2015.

- [231] G. LIDÉN, “Dustiness testing of materials handled at workplaces,” *The Annals of Occupational Hygiene*, vol. 50, no. 5, pp. 437–439, 2006.
- [232] “International standard - ISO 4225: Air quality - General aspects - Vocabulary,” May 2020.
- [233] S. Bach and E. Schmidt, “Determining the dustiness of powders—a comparison of three measuring devices,” *Ann Occup Hyg*, vol. 52, no. 8, pp. 717–725, 2008.
- [234] F. Hamelmann and E. Schmidt, “Methods for characterizing the dustiness estimation of powders,” *Chemical Engineering & Technology*, vol. 27, no. 8, pp. 844–847, 2004.
- [235] K. Hjemsted and T. Schneider, “Documentation of a dustiness drum test,” *The Annals of Occupational Hygiene*, vol. 40, no. 6, pp. 627–643, 1996.
- [236] A. Santandrea, S. Pacault, S. Bau, Y. Oudart, A. Vignes, L. Perrin, and O. Dufaud, “Safer and stronger together? effects of the agglomeration on nanopowders explosion,” *Journal of Loss Prevention in the Process Industries*, vol. 69, p. 104348, 2021.
- [237] H. Salehi, D. Barletta, and M. Poletto, “A comparison between powder flow property testers,” *Particuology*, vol. 32, pp. 10–20, 2017.
- [238] Shandilya, N., Kuijpers, E., Tuinman, I., and Fransman, W., “Powder intrinsic properties as dustiness predictor for an efficient exposure assessment,” *Annals of Work Exposures and Health*, 2019.
- [239] D. Dahmann and C. Monz, “Determination of dustiness of nanostructured materials,” *Gefahrstoffe Reinhaltung der Luft*, vol. 71, 2011.
- [240] D. E. Evans, L. A. Turkevich, C. T. Roettgers, G. J. Deye, and P. A. Baron, “Dustiness of fine and nanoscale powders,” *Ann Occup Hyg*, vol. 57, no. 2, pp. 261–277, 2013.
- [241] K. A. Jensen, I. K. Koponen, P. A. Clausen, and T. Schneider, “Dustiness behaviour of loose and compacted bentonite and organoclay powders: What is the difference in exposure risk?,” *J Nanopart Res*, vol. 11, no. 1, pp. 133–146, 2009.
- [242] G. Burdett, D. Bard, A. Kelly, and A. Thorpe, “The effect of surface coatings on the dustiness of a calcium carbonate nanopowder,” *J Nanopart Res*, vol. 15, no. 1, p. 1311, 2012.
- [243] M. Parey and E. Schmidt, “A model to evaluate the dustiness of powders and binary powder mixtures,” *Chemical Engineering & Technology*, vol. 41, no. 1, pp. 35–43, 2018.
- [244] M. Morgeneyer, O. Le Bihan, A. Ustache, and O. Aguerre-Chariol, “Experimental study of the aerosolization of fine alumina particles from bulk by a vortex shaker,” *Powder Technology*, vol. 246, pp. 583–589, 2013.
- [245] J. S. Lanning, M. G. Boundy, and D. Leith, “Validating a model for the prediction of dust generation,” *Particulate Science and Technology*, vol. 13, no. 2, pp. 105–116, 1995.

- 
- [246] N. O. Breum, "The rotating drum dustiness tester: Variability in dustiness in relation to sample mass, testing time, and surface adhesion," *The Annals of Occupational Hygiene*, vol. 43, no. 8, pp. 557–566, 1999.
- [247] S. Chakravarty, O. L. Bihan, M. Fischer, and M. Morgeneuer, "Dust generation in powders: Effect of particle size distribution," *EPJ Web Conf.*, vol. 140, p. 13018, 2017.
- [248] M. Xiang, M. Morgeneuer, O. Aguerre-Chariol, F. Philippe, and C. Bressot, "Airborne nanoparticle collection efficiency of a TEM grid-equipped sampling system," *Aerosol Science and Technology*, vol. 55, no. 5, pp. 526–538, 2021.
- [249] C. Dazon, *Expositions professionnelles aux nanomatériaux lors de la manipulation de poudres : relations entre les propriétés des poudres et les caractéristiques des aérosols émis*. thesis, Aix-Marseille, 2019.
- [250] C. Ribalta, M. Viana, A. López-Lilao, S. Estupiñá, M. Minguillón, J. Mendoza, J. Díaz, D. Dahmann, and E. Monfort, "On the relationship between exposure to particles and dustiness during handling of powders in industrial settings," *Annals of Work Exposures and Health*, vol. 63, no. 1, pp. 107–123, 2019.
- [251] Y. Bu, A. Addo, P. Amyotte, C. Yuan, C. Li, and X. Hou, "Insight into the dust explosion hazard of pharmaceutical powders in the presence of flow aids," *Journal of Loss Prevention in the Process Industries*, vol. 74, p. 104655, 2022.
- [252] K. Groos-Gerardin, L. Perrin, V. Falk, and O. Dufaud, "Combining product engineering and inherent safety to improve the powder impregnation process," *Journal of Loss Prevention in the Process Industries*, vol. 38, p. 1, 2015.



# 7

## Résumé en français des travaux menés et des résultats obtenus

---

### 1. Contexte

De nos jours, les matériaux granulaires sont omniprésents dans la vie quotidienne, qu'ils soient transformés ou qu'ils fassent partie de l'environnement naturel (par exemple: les graines, le sable et le pollen). D'après les outils archéologiques, la production de poudres alimentaires a été développée il y a environ 50 000 ans (Paléolithique supérieur) en broyant des graines, des plantes et des noix entre des meules [1, 2]. Depuis, la fabrication et l'utilisation de poudres sont apparues et se sont développées, devenant la deuxième matière la plus manipulée après l'eau [3]. Les poudres sont utilisées et manipulées dans de nombreuses industries, telles que la construction, la pharmacie, l'alimentation et les cosmétiques. Il est difficile d'estimer la quantité de poudre produite et consommée dans le monde. Toutefois, on estime que la moitié des produits finis et les trois quarts des matières premières de l'industrie chimique se présentent sous forme de solides divisés [4]. Afin de quantifier la quantité de poudres brutes produites en France, une étude de marché des poudres provenant de diverses industries a été réalisée. Les résultats de cette étude ont révélé que la production de masse de poudres dépasse 40 millions de tonnes par an (Fig. 1). Toutefois, il s'agit probablement d'une sous-estimation de la quantité réelle, car les données des industries pharmaceutiques, cosmétiques et autres ne sont pas accessibles au public. Cette statistique donne un aperçu de l'ampleur réelle de la manipulation des poudres et des défis associés auxquels sont confrontées les innombrables personnes qui travaillent quotidiennement avec ces matériaux.

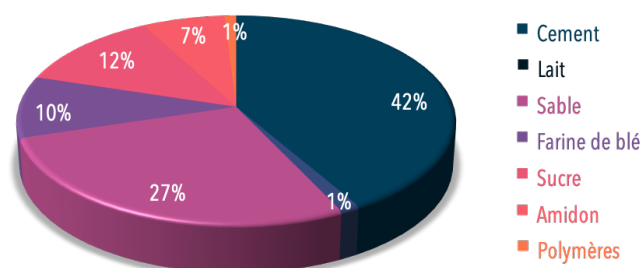


Figure 7.1. Production de matériaux granulaires en France [5–13].

Même si les poudres sont largement utilisées, leur traitement présente encore plusieurs complications (Fig.2). Par exemple, le stockage dans des trémies, des silos et des bacs pose des problèmes de blocage, de voûte, de trous et de ségrégation [14]. Ces problèmes entraînent des difficultés lors du transfert des poudres, ce qui oblige à ramasser maladroitement les poudres à la main ou à marteler les équipements de stockage, ce qui est dangereux pour les travailleurs et endommage les installations. Le compactage des poudres peut entraîner certaines complications lors des opérations de transfert. De plus, des opérations spécifiques telles que le dosage donnent des résultats incohérents, ce qui est problématique pour tous les types de produits, comme les produits pharmaceutiques qui nécessitent une quantité précise de principes actifs.



Figure 7.2. Opérations maladroites et dangereuses lors de la manipulation des poudres à cause d'une mauvaise coulabilité et la émission de poussière.

Tous ces problèmes sont généralement dus à la mauvaise coulabilité des poudres. La coulabilité des poudres peut être améliorée par les moyens suivants :

1. Modification de l'installation, par exemple en ajoutant des alimentateurs vibrants largement utilisés pour les engrais [15]. Toutefois, il s'agit rarement d'une solution universelle, car le comportement de l'écoulement peut s'aggraver pour les poudres plus fines.

2. La fluidisation des poudres, dont il a été démontré qu'elle améliorerait le comportement d'écoulement des poudres contenant de grosses particules. Néanmoins, pour les poudres pharmaceutiques plus fines, ce processus nécessite l'ajout d'autres mécanismes, tels que l'assistance magnétique [16], ce qui augmente la complexité du processus et les coûts [17].
3. L'ajout d'additifs de flux, qui est considéré comme la solution la plus efficace avec le meilleur rapport bénéfice/coût et la solution la plus fréquemment adoptée dans les industries. Sur la base d'essais et d'erreurs - "*savoir-faire*" industriel - la quantité d'additifs d'écoulement ajoutée aux formulations est d'environ 0.5-2% wt. [18].

Les nanoparticules de silice amorphe (S-NP) sont l'un des additifs d'écoulement les plus utilisés. Cet ingrédient de formulation est généralement reconnu comme sûr (GRAS) par la Food and Drug Administration (FDA) des États-Unis, ce qui limite son utilisation à 2 % m/m dans les produits alimentaires. La FDA suggère toutefois d'ajouter une "quantité n'excédant pas la quantité raisonnablement nécessaire pour produire un effet anti-agglomérant" [19]. En revanche, l'Autorité européenne de sécurité des aliments (EFSA) a fixé une dose journalière admissible "non spécifiée", ce qui implique que le S-NP ne présente aucun risque pour la santé [20]. Même si les deux organismes de réglementation, la FDA et l'EFSA, considèrent que le S-NP est sûr pour l'alimentation, sa toxicité reste controversée. Ces entités réglementaires concentrent leurs résolutions sur les effets toxiques de l'ingestion de S-NP, où il a été démontré que des doses élevées sont tolérées [21]. Cependant, il est surprenant de constater que l'exposition professionnelle par inhalation n'est pas prise en compte. Une étude récente a révélé qu'à des niveaux d'exposition élevés, la silice cristalline et la silice amorphe avaient des effets toxiques similaires, à l'exception de la silicose, qui n'est attribuée qu'à la forme cristalline [22]. En outre, des études *in vitro* et *in vivo* ont montré une augmentation des réponses pro-inflammatoires lors d'une exposition à la silice nanométrique par rapport à une exposition micrométrique [21, 23]. Bien que certaines études suggèrent qu'il pourrait y avoir une toxicité potentielle associée à l'utilisation du S-NP, celle-ci n'est pas encore bien établie. Les organismes de réglementation ne fonctionnent pas toujours selon le principe de précaution, ce qui peut être associé à l'augmentation de l'utilisation du S-NP dans l'industrie malgré les risques potentiels [24].

En plus des complications liées à un mauvais écoulement, les opérations mécaniques telles que le tamisage, le transport et la granulation, ainsi que les opérations manuelles telles que le versement et le pesage, sont promptes à émettre des nuages de poussière. L'émission de poussières peut causer des problèmes lors du traitement des poudres, entraînant une contamination croisée, le colmatage des filtres et des pertes de produits, ainsi qu'un risque accru d'inhalation, d'explosions et d'incendies [25] (Fig.2). Les émissions de poussières ont été fortement liées aux risques professionnels en raison de leurs conséquences dangereuses. Au fil des ans, les études se sont principalement

concentrées sur la caractérisation des poudres pures, en testant une grande variété de matériaux à l'aide de différentes méthodes d'essai. Toutefois, en se concentrant sur les poudres pures, on néglige les émissions de poussières de la plupart des produits en poudre, qui sont composés de plusieurs ingrédients.

Cette thèse a été effectuée entre le Laboratoire de Réactions et Génie Chimique (LRGP) et l'Institut National de Recherche et de Sécurité (INRS), l'organisme de référence en matière de sécurité et de prévention des risques professionnels en France. Cette collaboration visait à relier la **coulabilité** des poudres à la **poussière**. De nos jours, les S-NP sont systématiquement ajoutés aux produits en poudre pour garantir la faisabilité du processus et une bonne coulabilité. Étonnamment, à notre connaissance, la relation entre la coulabilité et la pulvérulence n'a jamais été directement étudiée. C'est pourquoi ce travail vise à évaluer les effets de l'ajout de S-NP sur l'émission de poussières. La compréhension du mécanisme d'action du S-NP sur la coulabilité pourrait fournir un guide pour réduire leur utilisation et l'exposition professionnelle.

Ce manuscrit se compose de six chapitres, qui présentent le contexte du travail de recherche et les résultats, qui sont rapportés dans trois publications et un chapitre final sur les résultats. Chaque publication-chapitre comprend une synthèse des résultats les plus significatifs, suivie de résultats supplémentaires qui n'ont pas été inclus dans le travail publié.

Le **premier chapitre** explore l'intérêt de l'étude des poudres, en fournissant des définitions pertinentes et en présentant le comportement complexe des poudres et leurs propriétés. En outre, la coulabilité et la pulvérulence des poudres sont présentées, ainsi que leurs méthodes de caractérisation respectives. Enfin, les premiers aperçus de la corrélation entre la coulabilité et la pulvérulence sont présentés.

Le **deuxième chapitre** se concentre sur le matériel et les méthodes utilisés dans l'étude. Le raisonnement qui sous-tend la sélection des échantillons de poudre est expliqué en détail, de même que les méthodes. La première partie présente la sélection des poudres, des additifs d'écoulement et le protocole de formulation, suivis de la caractérisation physicochimique des poudres et des formulations. Les techniques de caractérisation de la coulabilité et de la pulvérulence sont également décrites en détail.

Les résultats de ces travaux sont présentés du chapitre 3 au chapitre 6. Les chapitres 3 et 4 se concentrent sur les résultats de coulabilité, tandis que le chapitre 5 présente les résultats de pulvérulence. Enfin, le chapitre 6 examine la relation entre ces deux propriétés d'utilisation finale.

Dans le **troisième chapitre**, les premières conclusions sur la coulabilité sont examinées.

Ce chapitre vise à identifier un dispositif de mesure de la coulabilité approprié en fonction de la quantité d'énergie appliquée à l'échantillon. En outre, ce chapitre présente l'impact des additifs d'écoulement sur les excipients pharmaceutiques.

**Publication I:** Effects of humidity and glidants on the flowability of pharmaceutical excipients. An experimental energetical approach during granular compaction. M.-G. Cares Pacheco, M.-C. Jiménez Garavito, A. Ober, F. Gerardin, E. Silvente and V. Falk. Int.J.Pharm. 2021. DOI: [10.1016/j.ijpharm.2021.120747](https://doi.org/10.1016/j.ijpharm.2021.120747)

Dans le **quatrième chapitre**, la discussion des résultats de coulabilité est poursuivie avec un accent plus profond sur la compréhension des facteurs qui contribuent au comportement d'écoulement des poudres. En outre, cette section évalue le mécanisme d'action des additifs d'écoulement sur la coulabilité des poudres.

**Publication II:** Silica nanoparticles as glidants for industrial processing: a statistical approach. M.-C. Jiménez Garavito, M.-G. Cares Pacheco, F. Gerardin and V. Falk. 2022. DOI: [10.1021/acs.iecr.2c02455](https://doi.org/10.1021/acs.iecr.2c02455)

Le **chapitre cinq** présente les résultats de l'influence de l'ajout d'additifs de flux sur l'émission de poussières par les poudres. Ces résultats montrent l'importance des interactions adhésives entre les poudres et les nano-additifs, ce qui permet d'approfondir la compréhension de la propension à émettre des poussières.

**Publication III:** The effect of silica nanoparticles on the dustiness of industrial powders. M.-C. Jiménez Garavito, M.-G. Cares Pacheco, F. Gerardin, S. Bau, O. Witschger and V. Falk. Submitted to *Adv. Powder Technol. special issue*

Le dernier chapitre du manuscrit, **chapitre six**, explore la relation entre la coulabilité et la pulvérulence. La première partie présente les résultats des tests de coulabilité réalisés à l'aide de différents dispositifs pour évaluer les effets des différentes formulations. Ensuite, les résultats de l'émission de poussières sont présentés, suivis d'une analyse des différents comportements de génération de poussières en fonction de l'échantillon et de la formulation. Enfin, la corrélation entre la coulabilité et la pulvérulence est évaluée, en cherchant à trouver des modèles qui pourraient permettre la prédiction de ces deux propriétés d'utilisation finale.

Enfin, une **conclusion** générale est présentée, soulignant les principaux résultats et contributions de cette étude. En outre, quelques travaux futurs **perspectives** sont proposés.

## 2. Principaux résultats obtenus

Cette thèse se concentre sur deux sujets principaux : la coulabilité et la relation avec la pulvérulence. La discussion suivante présente les principales conclusions et contributions.

## 2.1. Coulabilité

La caractérisation de la coulabilité des poudres est une tâche complexe car il ne s'agit pas d'une propriété intrinsèque de la poudre elle-même et elle est donc influencée par la méthodologie de l'appareil utilisé. Le chapitre 3 a relevé ce défi en examinant l'impact de l'énergie fournie sur les mesures de coulabilité à l'aide de deux méthodologies d'appareils de densification - le Densitap et l'essai de compression uniaxiale (FT4 et Instron press). La comparaison des résultats obtenus avec ces deux appareils met en évidence la nécessité de veiller à ce que la même quantité d'énergie - dans les mêmes conditions - soit fournie à la poudre afin de comparer avec précision les données de coulabilité issues des méthodologies de densification. Néanmoins, la quantification de la quantité d'énergie fournie à une poudre est difficile en raison de la nature hautement dissipative de la poudre. Ensuite, si une comparaison des poudres est effectuée sur le même équipement, il est essentiel que les échantillons soient dans un état stable à l'énergie fournie, qui peut différer d'un échantillon à l'autre. Par exemple, dans le Densitap, la comparaison de la variation de volume pour le même nombre de coups (par exemple, 500) peut ne pas caractériser les échantillons avec précision. Il est plutôt recommandé d'effectuer la mesure avec un nombre de robinets qui garantit que le volume de l'échantillon ne change plus et d'atteindre un état stable. Dans les systèmes confinés, tels que les cellules de compression, il est également recommandé d'ajouter un temps de relaxation à chaque force appliquée à la poudre avant de passer à l'étape de force suivante pour atteindre un état stable. En suivant ces recommandations, nous pouvons obtenir des résultats fiables et comparables pour la coulabilité de différentes poudres dans les testeurs de compression uniaxiale.

L'effet de l'ajout de S-NP sur la coulabilité des poudres a été évalué à l'aide du FT4. Les premiers résultats montrent que le S-NP hydrophile et hydrophobe améliore le comportement d'écoulement des poudres pharmaceutiques. En outre, le S-NP a modifié le comportement d'écoulement des poudres vers l'eau, car à une HR élevée, la coulabilité de l'HP s'est détériorée, mais avec l'ajout de S-NP, le comportement d'écoulement s'est toujours amélioré, quelle que soit la condition d'HR. Généralement, les S-NP sont ajoutés aux formulations pharmaceutiques à des quantités allant de 0.5 à 2 % wt. Cependant, nos résultats n'ont pas montré de différences significatives dans le comportement d'écoulement entre les poudres pharmaceutiques lorsque la quantité de S-NP est augmentée de 0.5 à 2 % wt.

À partir de ces résultats préliminaires, l'étude a été orientée vers la compréhension des mécanismes d'action du S-NP sur le comportement de l'écoulement des poudres, évalués au moyen d'un plan expérimental. Les résultats montrent que la poudre elle-même est le principal facteur qui dicte le comportement de l'écoulement de la poudre, car la coulabilité de la poudre est extrêmement sensible à l'interaction des grains. En outre, la modification du frottement global par le S-NP ne semble pas affecter le comportement

de l'écoulement. En revanche, nos résultats suggèrent que la modification de la surface des poudres est un mécanisme important par lequel le S-NP agit sur la coulabilité des poudres. Les poudres les plus cohésives ont tendance à nécessiter une plus grande couverture de surface par le S-NP pour améliorer leur écoulement. La modification de la surface des HP a été quantifiée par des mesures de l'énergie de surface ( $\gamma_s^d$ ). Tous ces résultats ont remis en question la quantité de S-NP utilisée dans les formulations (0.5 à 2 % wt.). La méthodologie présentée dans le cadre 1 propose un protocole pour déterminer une quantité optimale de S-NP, dans l'intention de réduire leur utilisation tout en maintenant le comportement d'écoulement.

### Cadre 1

Cette méthodologie vise à déterminer la quantité optimale de S-NP nécessaire pour améliorer l'écoulement, tout en évitant l'utilisation excessive de S-NP.

1. Préparer un mélange avec une quantité connue de S-NP (par exemple 0.5% en masse).
2. Caractériser le pourcentage taux de recouvrement du S-NP sur l'échantillon en utilisant des images MEB (se référer à la section 4. pour le protocole de traitement d'image).
3. Estimer la quantité de S-NP nécessaire pour obtenir un taux de recouvrement de 1%, 20% et 40%.
4. Évaluer la coulabilité de l'échantillon à l'aide de la technique que décrit le mieux l'opération industrielle (par exemple, test de cisaillement pour les silos).
5. Choisir le taux de recouvrement optimale qui donne la meilleure performance d'écoulement.

## 2.2. Pulvéulence

À ma connaissance, aucune étude n'évalue l'effet de l'ajout d'additifs de flux sur la génération de poussière. Tous mes résultats montrent que l'ajout de S-NP augmente la pulvéulence et la concentration des particules émises. Nous nous attendions initialement à ce que le S-NP reste attaché à la surface du HP en raison de leurs fortes interactions adhésives. Cependant, les résultats des méthodes de mesure de la pulvéulence ont indiqué que le S-NP s'est détaché du HP dans les deux dispositifs de mesure. Dans le tambour rotatif, le HP+S-NP émet une pulvéulence similaire à celle du S-NP seul, tandis que dans le VS, le détachement du S-NP est principalement mis en évidence dans les micrographies TEM et la distribution de la taille des poussières mesurée par un (ELPI+).

La force des interactions entre HP et S-NP joue un rôle dans l'émission de poussières, des interactions plus fortes entraînant moins de particules de poussière et une fraction respirable maintenue indépendamment du SC. L'énergie de surface dispersive,  $\gamma_s^d$ , a été avec les résultats de pulvéulence permettant de distinguer entre les interactions faibles et fortes. Les poudres/S-NP ayant des interactions plus fortes émettent moins de particules que celles ayant des interactions plus faibles. En outre, la couverture de la surface influe sur les émissions de poussière. Une couverture de surface plus faible donne lieu à des émissions de poussières plus faibles même lorsque les interactions HP/S-NP sont faibles, ce qui suggère que les émissions de poussières peuvent être contrôlées en formulant les

produits en fonction de la couverture de surface des particules.

La couverture de surface est également un facteur important dans la réduction des émissions de poussières.

### 2.3. Relation coulabilité-pulvéulence

Nos résultats ont montré que les poudres ayant un excellent comportement d'écoulement tendent à émettre plus de poussière. Nos résultats suggèrent que les niveaux de fraction thoracique et respirable pourraient être prédits en les reliant au  $HR_c$  de compression à 30N et au facteur d'écoulement (66 kPa), respectivement. En outre, les forces d'adhésion en vrac à faible consolidation (6 kPa) sont liées aux fractions thoraciques et respirables. Les trois équations établies semblent prédire les niveaux de poussière avec une assez bonne précision, sauf lorsque la fraction expérimentale est très faible. Dans ce cas précis, la valeur prédite surestime la valeur expérimentale. Il convient de noter que le nombre limité de points de données utilisés pour développer les modèles ne leur permet pas d'avoir la meilleure adéquation possible. Néanmoins, notre étude marque un point de départ pour la mise en relation de la coulabilité et de la pulvéulence, une voie qui, à notre connaissance, n'a pas été explorée auparavant.

L'intérêt de cette découverte réside dans le fait que la coulabilité et la pulvéulence sont deux propriétés qu'il est nécessaire de connaître pour mener à bien les opérations industrielles de manipulation des poudres. D'un point de vue industriel, les tendances en matière de coulabilité et de pulvéulence peuvent constituer un point de départ pour des processus plus sûrs et des formulations de poudres plus performantes. Tout d'abord, ce travail montre que la quantité requise d'additifs d'écoulement doit être optimisée pour réduire les émissions de poussières. Ensuite, les niveaux d'émission de poussières pourraient être estimés à l'aide des équations proposées basées sur les paramètres de coulabilité,  $HR_c$  et/ou  $ff$ .

D'un point de vue économique, ce "point de départ de la formulation" est plus coûteux que l'ajout d'une quantité standard d'additifs d'écoulement pour améliorer la coulabilité de la poudre. Cependant, et c'est plus important, il vise également à réduire l'utilisation d'additifs d'écoulement afin de réduire l'exposition professionnelle aux poudres et aux additifs d'écoulement, qui sont souvent des nanomatériaux.

D'un point de vue scientifique, ce travail contribue à la compréhension de la relation entre deux propriétés essentielles de l'utilisation finale des poudres - la coulabilité et la pulvéulence - qui ne sont généralement pas liées. Il souligne l'importance et l'utilité de continuer à les étudier ensemble pour mieux comprendre le comportement et l'industrialisation des matériaux granulaires.

### **3. Perspectives**

Une considération importante qui devrait être incluse dans presque toutes les études expérimentales sur la matière granulaire est la nécessité de valider tous les résultats avec un échantillon plus important dans le but d'énoncer des conclusions générales, pour l'utilisation dans de multiples industries. Comme le montre le présent travail, nous avons étudié quatre poudres principales, chacune présentant une coulabilité et une pulvérulence uniques.

En ce qui concerne la pulvérulence, les mesures sur les tambours rotatifs pourraient être effectuées à l'aide d'une ligne d'échantillonnage similaire au VS afin de fournir des mesures en temps réel dans des dispositifs moins énergiques. En outre, il serait intéressant d'incorporer une ligne d'échantillonnage de la pulvérulence dans les mesures de coulabilité où de la poussière est émise, telles que les dispositifs de taraudage, les tambours rotatifs et les orifices d'écoulement, entre autres. Ces mesures peuvent donner une idée de la pulvérulence générée au cours des opérations industrielles que ces dispositifs visent à simuler. En outre, il serait intéressant de développer un dispositif de mesure de la pulvérulence qui permette de modifier l'énergie fournie à l'échantillon, dans le but d'étudier les interactions d'adhésion entre la poudre et les additifs d'écoulement.

La compréhension des interactions adhésives entre les additifs d'écoulement et les poudres nécessite des recherches supplémentaires, qui pourraient être évaluées au moyen de caractérisations par microscopie à force atomique. Par conséquent, en comprenant ces interactions, l'industrie pourrait bénéficier d'une utilisation plus précise, plus efficace et plus sûre des additifs d'écoulement. En outre, afin de faciliter la sélection des additifs d'écoulement, il serait utile d'approfondir notre analyse des interactions adhésives S-NP/HP en évaluant de multiples combinaisons et en créant une base de données qui facilite le choix de la combinaison S-NP/HP.

Dans une perspective plus large, il serait utile d'évaluer la relation entre la coulabilité et la pulvérulence dans des formulations complexes contenant de multiples ingrédients. Cela pourrait permettre de trouver des tendances/modèles susceptibles de guider la conception de produits performants et sûrs dans diverses industries.

## Abstract

Granular matter is ubiquitous in daily life and industry. After water, it is the second most frequently manipulated material form. However, even today, handling grains entails some sloppy and/or dangerous operations due to poor flowability and dust emission. Although flow additives such as silica nanoparticles (S-NP) are commonly used to improve flow behaviour, dust emission is often overlooked from a formulation perspective. Therefore, this work evaluates the effects of the addition of S-NP on dust emission. The understanding of the S-NP mechanism of action on flowability might provide a guide to reduce their use and occupational exposure. To achieve this goal, experimental tests were carried out to improve the flowability of four industrial powders using S-NP with varying surface coverage (SC). The results indicated that S-NP main action mechanism for flow improvement is related to surface modification, which was quantified by surface energy measurements. However, dustiness results showed that increasing flowability resulted in increased dust emissions. Moreover, the propensity of a powder to release dust appears to be related to its adhesive interaction with S-NP, which was associated with surface energy modifications. Based on the experimental characterisation of the samples' flowability and dustiness, two equations are proposed to estimate dust emissions levels from two flowability indicators, the Hausner ratio and the flow factor. This work contributes to understanding the relation of powder flowability and dustiness and proposes a methodology to optimise the use of S-NP, reducing their use in enhancing powder flow while minimising dust emission.

## Résumé

Les matières granulaires sont omniprésentes dans la vie quotidienne et dans l'industrie. Après l'eau, c'est la forme de matériau la plus fréquemment manipulée. Cependant, même aujourd'hui, la manipulation des grains implique certaines opérations bâclées et/ou dangereuses en raison d'une mauvaise coulabilité et de l'émission de poussières. Bien que les additifs d'écoulement tels que les nanoparticules de silice (S-NP) soient couramment utilisés pour améliorer le comportement de l'écoulement, l'émission de poussières est souvent négligée du point de vue de la formulation. C'est pourquoi ce travail vise à évaluer les effets de l'ajout de S-NP sur l'émission de poussières. La compréhension du mécanisme d'action du S-NP sur la coulabilité pourrait permettre de réduire son utilisation et l'exposition professionnelle. Pour atteindre cet objectif, des tests expérimentaux ont été réalisés pour améliorer la coulabilité de quatre poudres industrielles en utilisant du S-NP avec une couverture de surface (SC) variable. Les résultats indiquent que le principal mécanisme d'action du S-NP pour l'amélioration de l'écoulement est lié à la modification de la surface, qui a été quantifiée par des mesures de l'énergie de surface. Cependant, les résultats relatifs à la pulvérulence ont montré que l'augmentation de la coulabilité se traduisait par une augmentation des émissions de poussières. En outre, la propension d'une poudre à libérer de la poussière semble être liée à son interaction adhésive avec le S-NP, qui a été associée à des modifications de l'énergie de surface. Sur la base de la caractérisation expérimentale de la coulabilité et de la pulvérulence des échantillons, deux équations sont proposées pour estimer les niveaux d'émissions de poussières à partir de deux indicateurs de coulabilité, le rapport de Hausner et le facteur de fluidité. Ce travail contribue à la compréhension de la relation entre la coulabilité et la pulvérulence des poudres et propose une méthodologie pour optimiser l'utilisation des S-NP, en réduisant leur utilisation pour améliorer l'écoulement des poudres tout en minimisant l'émission de poussières.